Effect of Reservoir Boundaries on the Seismic Response of Gravity Dams

By

KIANOOSH HATAMI

A Thesis

Submitted to the School of Graduate Studies

in Partial Fulfillment of the Requirements

for the Degree

Doctor of Philosophy

McMaster University

January 1997

TO MY PARENTS

DOCTOR OF PHILOSOPHY (1996) McMASTER UNIVERSITY
(Civil Engineering) Hamilton, Ontario

TITLE: Effect of Reservoir Boundaries on the Seismic Response of Gravity Dams

AUTHOR: Kianoosh Hatami, M.Sc. (1991) (Civil Engineering),
Sharif University of Technology, Tehran - IRAN

SUPERVISOR: Dr. A. Ghobarah

NUMBER OF PAGES: xxvii, 267

ABSTRACT

Dam safety is an important issue of current interest. In seismic regions, dynamic forces on the dam may be significant and may lead to crack initiation and propagation in the dam. A significant component of the dynamic forces is due to the hydrodynamic effects of the impounded water in the reservoir. The developed hydrodynamic force on the dam is highly dependent on the physical characteristics of the boundaries surrounding the reservoir including the reservoir bottom and sides.

In this study, the effects of the reservoir boundary conditions on the seismic response of the dam are investigated. This study consists of four components. First, a mathematical model is proposed to account for the absorption effect of a sedimented reservoir bottom on the seismic response of the dam-reservoir system. Secondly, a study is conducted to examine the possibility of reducing the earthquake response of concrete gravity dams using hydrodynamic isolation at the dam-reservoir boundary. Thirdly, an analytical procedure is developed to compute the response of the hydrodynamic pressure and the seismic response of the dam impounding a reservoir of general shape and boundary conditions. Finally, The earthquake response of the dam was studied with special attention to the stresses in the dam. An index for the evaluation of the overall state of stress in the dam subjected to different load combinations is proposed. The dynamic component of stress and the proposed index in the dam are computed when the dam-reservoir system is subjected to different ground motion records.

The effect of the reflected waves from underlying reservoir foundation rock on the calculated response of the dam when subjected to earthquake ground motion was found to be very important. It is concluded that the effect of the stiffness of a semi-infinite reservoir foundation on the reduction of the dam seismic response is more significant as compared to the dissipation effect of the sedimentation layer. It is shown that the isolation layer needs to be very soft and with sufficient thickness so as to effectively reduce the hydrodynamic pressure acting on the dam. The effects of the reservoir length and the type of boundary condition at the truncated reservoir boundary on the calculated response of hydrodynamic pressure were found significant. The proposed index for the stress in the dam (Stress Factor) was shown to have an acceptable correlation with the intensity of the input ground motion and can be used as a complementary design factor for seismic design of concrete gravity dams.

ACKNOWLEDGEMENTS

The author wishes to express his sincere appreciation to his supervisor, Dr. A. Ghobarah for his continuous encouragement and guidance throughout the research program. His invaluable suggestions and advice are gratefully acknowledged.

The financial support of McMaster University and the Ministry of Culture and Higher Education of the I.R. of Iran are highly appreciated.

The author also wishes to take the opportunity to extend his most sincere gratitude to his family for their priceless support and confidence in him without which he would never see this moment. I hereby would like to express my love and deep appreciation to my mother, Dr. Soudabeh Ghavami, my late father, Dr. Mohammad Hossein Hatami and my dear sister Dr. Azin Hatami for every single day that they did not have me beside them but encouraged me in my endeavour.

TABLE OF CONTENTS

LIST OF FIGURES

CHAPTER 3

CHAPTER 4

CHAPTER 5

LIST OF TABLES

CHAPTER 3

CHAPTER 4

CHAPTER 5

LIST OF NOTATION

A_j	area of finite element j
A_T	total area of monolith
a	size of finite element mesh
b	attenuation constant of the sediment material
$C(\omega)$	frequency-dependent compliance function of the reservoir bottom
C_c, C_f, C_l, C_s, C_w	travel speed of longitudinal waves in the dam concrete, foundation rock, isolation layer, sediments and water, respectively
$D(\omega)$	refraction function of the reservoir boundary
d_s	thickness of the sediment layer
E_c, E_f, E_l, E_s	modulus of elasticity of concrete, foundation rock, isolation layer and sediment, respectively
F_{dyn}, F_{st}	dynamic and static components of the force on the dam from the impounded water
$\mathcal{F}_n$	a complex-valued function
f	frequency
f_{as}, f_{ad}, f_{ps}, f_{pd}	actual static, actual dynamic, apparent static and apparent dynamic tensile strength of mass concrete, respectively
f_c	compressive strength of mass concrete

f_l	viscosity parameter of the isolation layer
f_r	tensile strength of concrete
g	acceleration of gravity
H	reservoir depth
H_s	height of dam
I_{0n}, I_{1n}	integral definitions
$I_E(\xi)$	Arias Intensity of earthquake
$I_{EQ}(\xi)$	modified earthquake intensity
$\hat{I}_\sigma$	L_1-norm of principal tensile stress
i	$(-1)^{1/2}$
j	index for Ritz vectors in the dam model
K_n	an auxiliary variable related to the nth eigenvalue of the impounded water
k_f, k_s, k_w	wave number in the foundation rock, sediment material and water, respectively
L	reservoir length
L_e	the excited part of the reservoir length
L_p-norm ($\|\cdot\|_p$)	Lebesgue norm
m	exponent of the attenuation-frequency relationship
N	total number of finite elements in the dam model
NRTZ	total number of Ritz vectors in the dam model
n	index for the eigenvalues of the impounded water and mode shapes of the isolation layer

n	inward normal to the reservoir
P	complex frequency response function of the hydrodynamic pressure
P^{x}_{0}, P^{y}_{0}, P^{f}_{f}	response of hydrodynamic pressure due to rigid body motions of the reservoir boundaries in horizontal and vertical directions and flexible vibration of the dam, respectively
P_{dyn} , P_{st}	dynamic and static components of the pressure on the dam from the impounded water
P_{iw} , P_{0iw}	the steady-state response function and the amplitude (equal to one) of the incidental pressure wave to the reservoir bottom, respectively
P_{rw} , P_{0rw}	the steady-state response function and the amplitude of the reflected pressure wave from the reservoir bottom, respectively
P_{rs} , P_{0rs}	the steady-state response function and the amplitude of the reflected pressure wave in the sediment material, respectively
P_{tr} , P_{0tr}	the steady-state response function and the amplitude of the transmitted pressure wave in the foundation rock, respectively
P_{ts} , P_{0ts}	the steady-state response function and the amplitude of the transmitted pressure wave in the sediment material,

	respectively
PGA	peak ground acceleration of the recorded earthquake
PGV	peak ground velocity of the recorded earthquake
p	order of Lebesgue norm
q_f, q_l, q_u	damping coefficients of the reservoir foundation, the isolation layer and the upstream far-end boundary, respectively
q_{hl}	complex frequency response function of the horizontal displacement at the surface of the isolation layer
R_f	frequency ratio
S_I	pseudo-impact
$S_v(\xi,T)$	pseudo-relative velocity of the structure
SF	Stress Factor of the dam
SI	spectral intensity
s	local coordinate along the reservoir solid boundary
T, T_d	undamped and damped periods of the single degree of freedom analogy of the dam, respectively
TR	Transmissibility ratio
t	time
t_d	duration time of the response analysis
t_l	thickness of the isolation layer
t_S	duration of strong ground motion
t_T	total duration of recorded earthquake

$u(x,t)$	longitudinal displacement
$\bar{u}(x,\omega)$	steady-state displacement response
$\ddot{u}_g(t)$	recorded ground acceleration
$\ddot{u}_n(s)$	normal acceleration of the reservoir boundary
v_f, v_s, v_s	complex frequency response functions for the vertical displacement in the foundation rock, the sediment material and total displacement at the surface of the reservoir bottom, respectively
v_{0rs}	amplitude of the reflected waves in the sediment layer
v_{0tr}, v_{0ts}	amplitudes of the transmitted waves in the foundation rock and the sediment layer, respectively
$w(\tau)$	an arbitrary function of τ
x,y	Cartesian coordinates
$\ddot{Y}_j(t)$	second derivative of the jth generalized coordinate
$\ddot{Y}_j(\omega)$	Fourier transform of $\ddot{Y}_j(t)$
$\alpha_b(\omega)$	frequency-dependent wave reflection coefficient of the reservoir bottom
α_b, α_d, α_l, α_u	constant wave reflection coefficients of the reservoir bottom, dam, isolation layer and upstream far-end boundary, respectively
$\beta_b(\omega)$	frequency-dependent overall relative impedance of the reservoir bottom and water

β	damped relative impedance of the foundation rock and sediment material
β', β_{sw}	damped and undamped relative impedance of the sediment material and water, respectively.
β_c	undamped relative impedance of concrete and water
β_{sf}	undamped relative impedance of the sediment material and foundation rock
Γ_l	compliance function of the isolation layer
γ_l , γ_s	complex-valued, damped wave numbers in the isolation and sediment materials, respectively
δ_{xl} ,δ_{yl} , l=x,y	Kronecker delta
ζ_n	nth eigenvalue of the reservoir
η_l , η_s	coefficients of longitudinal viscosity of the isolation and sediment materials, respectively
η_{lc}	critical layer viscosity
θ (ω)	an auxiliary parameter
κ_1 (ω)	a frequency-dependent function of the reservoir first eigenvalue
Λ_n	the nth eigenfunction of the impounded water
λ	wavelength
λ_s	a non-dimensionalized parameter of the sediment material
μ_s	attenuation coefficient of the sediment material
ξ	modal viscous damping ratio of the dam

ρ_c, ρ_f, ρ_l, ρ_s and ρ_w	density of concrete, foundation rock, isolation material, sediment and water, respectively
σ^t_1 (t)	time history of principal tensile stress
σ_{max}	maximum tensile stress
σ_{min}	maximum compressive stress
$\bar{\sigma}(0,\omega)$	steady-state complex frequency response of the transmitted pressure acting on the face of the isolated dam
Ψ_j	the jth mode shape of the dam
Ω_r	reservoir-to-monolith frequency ratio
ω	circular frequency
ω^1_c	coupled fundamental frequency of the dam-reservoir system on rigid foundation
ω_l	first free vibration frequency of the isolation layer
ω^1_r	fundamental frequency of the reservoir
ω^1_s	fundamental frequency of the dam-foundation system with empty reservoir
$\tilde{\omega}$	non-zero frequency corresponding to unit transmissibility ratio

CHAPTER 1

INTRODUCTION

1.1 BACKGROUND

There is a large number of concrete dams worldwide. Some of the dams are in seismically active areas. Dam safety during and after an earthquake is an area of current concern. The failure of a dam during an earthquake may be catastrophic in terms of loss of life and financial loss. The analysis of dams is a complex problem due to the dam-reservoir and dam-foundation interaction. In addition to the static water pressure, the dam is subjected to dynamic forces from the reservoir when the system is subjected to earthquake ground motion. The magnitude of this additional hydrodynamic force is quite significant and may lead to crack initiation and propagation in the dam even under a moderately strong seismic event (Hall 1986, Hall *et al.* 1992). The developed hydrodynamic force on the dam is dependent on the physical characteristics of the boundaries surrounding the reservoir including the reservoir bottom and sides. In general, maximum values of the dam structure response are dominated by the amount of the damping present in the dam-reservoir-foundation system. Concrete dams do not possess high structural damping as compared to other civil engineering structures. Due to the effect of the adjacent reservoir, however, there are other sources of damping present in a dam-reservoir-foundation system. The *added damping* due to the radiation of waves in the unbounded upstream direction of the reservoir and due to the absorption of incidental waves at the reservoir bottom may result in significant

reduction in the response of a concrete dam under earthquake excitation. In addition to the radiation of refracted waves from the bottom of the reservoir, the foundation of the dam allows for the radiation of energy waves from the vibrating dam to the far field.

There are a number of techniques to calculate the hydrodynamic force on a gravity dam impounding a reservoir of arbitrary shape when subjected to the ground motion (Hall and Chopra 1980, Tsai and Lee 1989 and Tsai and Lee 1992). Current numerical techniques are also capable of providing the desired degree of refinement and accuracy in the solution for the structural response of the dam subjected to seismic excitation (Fenves and Chopra 1984a, Tsai *et al.* 1992 and Galindo *et al.* 1992). However, regardless of the degree of refinement incorporated in the structural model of a dam-foundation system, reliable results can not be achieved without a consistent level of accuracy in evaluating the effects of reservoir boundaries on the developed hydrodynamic pressure. For example, the absorption effect of the reservoir bottom is included by selecting an approximate wave reflection coefficient for this boundary. It has been shown by Fenves and Chopra (1983, 1984a and 1985) that depending on the selected value for the wave reflection coefficient, the hydrodynamic pressure and the response of the dam can vary significantly. There are no available guidelines for the selection of an appropriate value for the reflection coefficient based on the physical characteristics of the reservoir bottom. Consequently, maximum values of the dam response including crest displacement and developed stresses are not necessarily reliable values for a given set of input ground motion and reservoir characteristics. Structural damage to some existing concrete dams that have experienced severe ground motions (Chopra and Chakrabarti 1972, Ahmadi *et al.* 1992, Leger and Tinawi 1994, Pekau *et al.* 1995) illustrates the importance of a realistic analysis and design. In such a design, the appropriate physical parameters of the dam-reservoir system should be selected.

In the following sections, the relevant research available in the literature is reviewed. Following the survey of the literature, the objectives of the present study are defined and the overall scope of the work is outlined.

1.2 LITERATURE SURVEY

1.2.1 General

In seismic response analysis of concrete dams, the effects of various sections of the reservoir surrounding boundary have been individually addressed. These sections include the reservoir bottom, the reservoir far end, the water surface and the dam-reservoir interface.

The effect of the reservoir bottom absorption of hydrodynamic pressure waves has been extensively studied. However, the associated amount of structural response reduction still needs to be predicted more reliably using a realistic and efficient approach.

The effect of the truncated upstream boundary of the reservoir model on the resulting hydrodynamic response has been the subject of several recent studies. As a result, appropriate boundary conditions to account for the effect of the truncated far field on the hydrodynamic pressure on the dam under horizontal ground motion are available. No such model is available for the case of vertical excitation of the reservoir model.

According to the results of the studies on the seismic response of a finite-length reservoir with a solid upstream boundary, the hydrodynamic loading on the dam varies significantly depending on the assumptions made in the mathematical model including the differential excitation of the reservoir end boundaries as well as the aspect ratio of the reservoir model.

The effect of water surface waves on the hydrodynamic loading on the dam has been shown to be negligible. This is due to the size and dynamic characteristics of common dam-reservoir systems and the characteristics of the seismic ground motions.

In most of the studies of the seismic response analysis of concrete dams, the dam-reservoir interface is considered as completely reflective. Results of some investigations, however, indicate the possibility of reducing the hydrodynamic force on the dam by

attaching an isolating soft layer.

Different approaches for dealing with the fluid domain in the response analysis of dam-reservoir systems vary from continuum solutions to various numerical methods. In this investigation, the hydrodynamic response analysis is based on both a closed-form solution and the finite element approach. The closed-form solution is applied in the case of a simple geometry and boundary conditions whereas the finite element method is applied in the more general case of geometry and boundary conditions of the reservoir model.

In the following sections, a survey of some numerical solutions of the reservoir hydrodynamic response with special emphasis on the two dimensional finite element approach in the frequency domain, is presented. The available studies addressing the individual parts of the reservoir boundary are reviewed.

1.2.2 Numerical solutions of the hydrodynamic response

Chopra *et al.* (1969) examined the applicability of the finite element method as a numerical technique for the response calculations of a dam-reservoir system. They studied the response of the hydrodynamic force on a dam impounding a finite-length reservoir with the aspect ratio (reservoir length to water height) of L/H=1 under horizontal excitation. For the case of a rigid dam and far boundary under unit step function, good agreement between the results of the finite element technique and the closed-form solution was obtained. However, there was a modest frequency shift of the hydrodynamic response based on the finite element approach compared with the theoretical solution. Chopra *et al.* found a significant discrepancy in the results of the two solutions for the response of the hydrodynamic force under earthquake type of excitation. They attributed the source of error to the chosen time step in the analysis. They concluded that the Finite element method is

potentially a versatile approach for the seismic response analysis of the dam-reservoir systems with arbitrary geometry and material properties.

Nath (1971) studied the response of the hydrodynamic force on a gravity dam. He used the finite difference method to solve the coupled equations of motion in the frequency domain. Nath argued that the reservoirs of many existing dams are limited at the far end. On this basis, he assumed the reservoir model to have a finite length. The reservoir aspect ratio was taken as L/H=4.5. In the absence of pressure wave radiation at the far boundary and viscosity of water, the only source of damping was taken to be the structural damping of the dam. Nath's model did not include the refraction of the impinging pressure waves at the reservoir boundaries. The dam structure was approximated as a cantilever beam and the system excitation was limited to the harmonic horizontal ground motion. Nath presented a simplified formulation for the evaluation of the fundamental coupled frequency of the dam-reservoir system which was shown to give more satisfactory results than the traditional added mass approach.

Wylie (1975) utilized an approach based on latticework of pipelines analogy to solve the two-dimensional wave equation in the reservoir. The wave equation in the two-dimensional space was replaced by one dimensional transient flow equations in two orthogonal directions. The principles of identical pressure heads and mass conservation at internal nodes were applied to obtain the time-variation of the hydrodynamic pressure in the reservoir. The method of characteristics was used to solve the resulting equations. Both cases of rigid as well as flexible dams were included in the analysis. In the case of the flexible dam, a one-dimensional shear beam analogy was made for the structural response. Wylie obtained a satisfactory agreement between the theoretical and the pipeline network analogy solutions for the transient hydrodynamic response under unit step excitation function. The

results showed good agreement in both the amplitudes and the phase of the response. Both cases of finite and infinite length reservoirs were included in the analysis. The response of the hydrodynamic pressure on the rigid dam subjected to the horizontal component of a typical earthquake excitation for the case of L/H=2 was found to be larger than the response in the case of L/H=1. Wylie attributed the reason for the observed anomaly to the frequency content of the input ground motion in relation to the natural frequencies of the reservoir in the above two cases. The results of the hydrodynamic response in both cases were overestimated because no absorption of pressure waves was allowed in the reservoir model.

Zienkiewicz and Bettess (1978) categorized the solution of coupled fluid-structure systems, neglecting the large scale flow, into two general approaches. The first approach is called *Lagrangian* approach in which the fluid is treated as a *solid* with a negligible amount of shear resistance. The fluid motion is described by its displacements similar to a solid structure. Accordingly, it is possible to use identical discretizations for both the fluid and structure domains. Besides, this method has the advantage of obtaining banded matrices in the global algebraic equations of motion of the dam-reservoir system. In the second approach, called the *Eulerian* approach, the fluid is identified by the nodal pressure as a single unknown quantity. In this approach, the coupling of the fluid and the structure is achieved through the equilibrium of the interface forces. The advantage of the Eulerian approach over the Lagrangian method is in the much smaller number of unknowns for the fluid domain. The Eulerian method has been more extensively used in the seismic analysis of dam-reservoir systems than the Lagrangian approach.

Hall and Chopra (1980) analyzed the case of a uniform channel of infinite length attached to a near-field reservoir of an irregular shape. The irregular part of the reservoir was modelled by the finite element method. The infinite-length channel, solved as a one-

dimensional finite element model in depth, was combined with a theoretical solution in the streamwise direction. The model formed the basis for numerous studies by Chopra and his co-workers (Hall and Chopra 1982a and 1982b, Fenves and Chopra 1984a and Hall 1986) as well as by other researchers (Jablonski 1990).

Lotfi *et al.* (1987) used the so-called hyperelements to model different solid and fluid parts of the dam-reservoir-foundation model in its response analysis when subjected to earthquake ground motion. Their hyperelement approach included the finite element discretization in depth together with the continuum solution in the horizontal direction for the regions away from the dam.

1.2.3 Reservoir Bottom Boundary

The influence of the reservoir bottom absorption on the seismic response of concrete dams has been the subject of some recent studies. Different models for the interaction of the reservoir water with its foundation may be categorized as follows:

Rigid Reservoir Foundation

In the early studies of the seismic response of concrete dams, the foundation of the reservoir was assumed as completely reflective (Bustamente and Flores 1966, Chopra 1967 and 1970, Chopra *et al.* 1969). Since a rigid foundation does not allow for the radiation of the impinging pressure waves away from the reservoir, the hydrodynamic pressure and the resulting structural response of the dam are generally overestimated. The overestimation of the dam response was found to be especially significant in the case of vertical excitation of the dam-reservoir system (Chopra 1967, Chakrabarti and Chopra 1973, Fenves and Chopra 1984a and 1985). With the assumption of completely reflective reservoir bottom, the

frequency response function of the dam at the natural frequencies of the reservoir is unbounded for vertical input ground motion. In this case, the interaction effects due to the vertical excitation form a significant part of the total hydrodynamic force on the concrete dam as compared to the contribution of the horizontal ground motion.

Partially Absorptive Foundation (with no sediment layer)

In recent studies (Hall and Chopra 1980, Fenves and Chopra 1983, Antes and Von Estroff 1987, Chandrashaker and Humar 1993), a flexible reservoir foundation was considered in the analysis which allows for the radiation of incidental pressure waves to lower depths. This results in bounded peaks with generally lower values for the response of the dam. Chandrashaker and Humar (1993) compared the results of the analysis based on the one-dimensional wave propagation model with the results obtained using a rigorous model utilizing the boundary element method for the foundation underneath the dam-reservoir system. They evaluated the reflectivity of the reservoir bottom on the basis of the characteristics of the foundation while the effects of the overlying sediment layer were not included. Chandrashaker and Humar concluded that the simplified one-dimensional representation of the fluid-foundation interaction is reasonably accurate in evaluating the displacement response as well as the stresses in the dam due to an actual earthquake.

Partially Absorptive Foundation (neglecting the effect of the foundation rock)

According to Fenves and Chopra (1984a and 1985), the interaction of the reservoir water with its foundation is dominated by the energy dissipation and hysteretic behaviour of the overlying sediment layer. The impinging pressure waves to the reservoir bottom are assumed to be dissipated before they reach the underlying foundation rock and therefore only

the material properties of the sediment layer are used to evaluate the reflectivity of the boundary. In the model, however, the thickness of the layer is not explicitly included. Therefore, the effect of the proximity of the underlying rock to the surface on the equivalent reflection coefficient of the reservoir bottom is not included in the representation of the boundary. Consequently, their simplified approach excluding the influence of the reservoir foundation rock leads to overestimation of the reduction of the dam response due to the absorption effects of the reservoir bottom.

Partially Absorptive Foundation (including the sediment layer)

In more rigorous investigations (Zuoxin 1987, Lotfi *et al.* 1987, Cheng 1987, Medina *et al.* 1990, Bougacha and Tassoulas 1991a and 1991b, Valliappan *et al.* 1991), the effect of the sediment layer is explicitly included in the model of the dam-reservoir-foundation system. Zuoxin (1987) examined the effect of a sediment layer with a constant thickness over a semi-infinite foundation on the response of the hydrodynamic pressure on the dam based on the solution of the one dimensional wave equation. In that study, however, the attenuation of the refracted waves across the sediment layer was not included. The reduction effect of the sediment layer was obtained in the form of a trigonometric function of the layer thickness with no damping effect of the sediment material. Accordingly, little reduction was obtained for a typical value of the sediment layer thickness at the reservoir bottom. Moreover, the study was limited to the case of a rigid dam subjected to the horizontal ground motion.

Lotfi *et al.* (1987) developed a finite element formulation for the linear, viscoelastic layered foundation. It was found that the effect of sediments in reducing the dynamic response of the dam is considerably less than that suggested by Fenves and Chopra (1985) using the one dimensional wave reflection coefficient approach. Their evaluation of the

performance of the one dimensional wave reflection coefficient model is claimed to be inaccurate due to the inconsistency of the selected material properties used in their comparison (Chandrashaker and Humar 1993). Medina *et al.* (1990) found that their results utilizing the boundary element method are in good agreement with the results of Fenves and Chopra (1984a) for the case of a time-harmonic vertical excitation. However, Medina *et al.* concluded that the approach of Fenves and Chopra results in an underestimation of the acceleration response of the dam to the horizontal ground motion for an identical equivalent reflection coefficient of the reservoir bottom based on the properties of the foundation rock. In spite of the above discrepancies in the results of different approaches, all the above studies share in common that the reduction effect of the sediment layer at the reservoir bottom is most significant for the case where the underlying foundation rock is assumed as rigid.

Bougacha and Tassoulas (1991a) and Cheng (1987) modelled the sediment material as a poroelastic continuum. The results were presented for both fully and partially saturated sediments. Bougacha and Tassoulas (1991b) found that fully saturated sediments lead to little decrease in the response of the hydrodynamic force as well as the maximum acceleration of the dam. The amount of response reduction was found to be highly dependent on the degree of saturation of the sediment material when subjected to horizontal excitation. No significant reduction was observed due to the absorption effect of the sediment layer under vertical ground motion regardless of the degree of saturation. This conclusion is inconsistent with the results of other related studies (Hall and Chopra 1980, Fenves and Chopra 1984a and 1985). The model by Cheng (1987) was incorporated into the solution of the one-dimensional Helmholz equation for the hydrodynamic pressure in the reservoir. The one-dimensional Helmholz equation along the depth of the reservoir does not include the variations of the boundary conditions along the reservoir end boundaries.

The rigorous poroelastic model for the sediment material requires consistently accurate information on the layer characteristics such as the material grain size, porosity, degree of saturation and hydraulic conductivity. Such detailed data for the reservoirs of the existing dams is not readily available. Besides, the rigorous poroelastic modelling of the reservoir bottom sediments is less attractive from computational point of view than the simplified viscoelastic approach which is simpler and requires less data for the analysis.

Valliappan *et al.* (1991) modelled the reservoir foundation and the overlying sediment layer using finite and infinite elements. The sediment layer was assumed to be of constant thickness. They examined the response of a dam subjected to horizontal ground motion for three different cases; namely, full reservoir with sedimentation, full reservoir without sedimentation and empty reservoir. Valliappan *et al.* found that the displacement response of the dam in the case of full reservoir with sedimentation at the bottom was larger than in the case of no sedimentation. The thickness of the sediment layer in a 100 m deep reservoir model was assumed to be 20 m. The acceleration response at the top of a dam subjected to an earthquake ground motion including the effect of the sediment layer was unrealistically larger than the case of no sedimentation. The maximum acceleration including the sediment layer in the model was found to be four times the acceleration peak for the case of no sedimentation. The above observation is in contradiction with the trend of results obtained by other investigators (Fenves and Chopra 1984a and 1985, Lotfi *et al.* 1987, Cheng 1987, Medina *et al.* 1990, Bougacha and Tassoulas 1991b). Valliappan *et al.* found that the fundamental frequency of the dam-reservoir system varies noticeably for the cases of including the sedimentation and no sedimentation in the reservoir model. They attributed the amplifying effect of the sediment layer to the proximity of the predominant frequency of the input ground motion to the fundamental frequency of the dam-reservoir system including the

sediment layer. This argument is not credible because the contradictory effect of the sediment layer was also observed for the frequency response function of the dam displacement which is independent of a given transient input. No damping effect was included in the sediment model. Accordingly, the sediment model did not result in a realistic response evaluation of the dam-reservoir system subjected to the seismic input.

The above review indicates that there are no practical guidelines for a reliable evaluation of the absorption coefficient of the reservoir bottom in the analysis of the hydrodynamic response for different reservoir bottom conditions.

1.2.4 Reservoir Far Boundary

The applied boundary condition at the upstream end of a two dimensional reservoir model primarily depends on its geometrical configuration. For a sufficiently long reservoir in the streamwise direction, the effect of reflected waves from the far boundary on the imposed hydrodynamic pressure on the dam is negligible. Accordingly, a radiation condition is applied at the far boundary of the finite-length discretization of the reservoir model. For a finite reservoir, the reflected waves from the upstream end are no longer negligible and may result in significant increase in developed hydrodynamic pressure in the impounded water. This is the case where there is a bend in the river or where the dam is built parallel to the course of the river with the far bank of the river serving as the upstream boundary. Another example is the case where the reservoir has a steep slope of its bottom ending at a shallow river on the upstream side.

For the case of an infinite-length reservoir, the applied radiation condition and its location to account for the outgoing pressure waves in a limited-length numerical model of the reservoir is important. The proper boundary condition to account for an infinite domain

at a truncated boundary has been the subject of many studies in various areas of continuum mechanics (Smith 1974, Hanson and Petschek 1976, Engquist and Majda 1977, Clayton and Engquist 1977, White et al. 1977, Kausel and Tassoulas 1981). A review of the studies with specific application to the modelling of dam-reservoir systems is presented.

In early studies of the hydrodynamic pressure on dams based on the analytical solution, the governing wave equation was solved subject to the boundary conditions including a radiation condition at the far side of the infinite-length reservoir (Westergaard 1933, Chopra 1967). The theoretical solution is possible for simple reservoir geometry. For more complex geometries, the hydrodynamic wave equation has to be solved numerically with appropriately discretized reservoir domain. From the computational point of view, the extent of the discretized model representing an infinitely long channel of the reservoir is limited such that the response computation can be made in a reasonable time. The infinite characteristic of the reservoir should be represented by adopting an appropriate numerical model at the truncated boundary to account for the absence of the reflected waves towards the dam. Various techniques which have been used in numerical models of the reservoir are briefly reviewed with emphasis on the two-dimensional analysis of the concrete gravity dams in the frequency domain.

Zienkiewicz *et al.* (1977) examined the basic formulation of infinity conditions in the solution of pressure wave equation in the reservoir. They concluded that Sommerfeld boundary condition is appropriate for a sufficiently large reservoir model and can be easily incorporated in the finite element discretization of the fluid domain. According to Zienkiewicz *et al.*, utilization of Sommerfeld boundary condition prevents any reflection of the striking pressure waves at the curtailed boundary in the normal direction. The assumption of normal incidence of the waves to the far boundary is valid for sufficiently far distance

from the disturbance. According to Lysmer and Kuhlemeyer (1969), almost no reflection was observed even for obliquely impinging waves for the angle of incidence of up to $\pm 60^\circ$ from the normal. Zienkiewicz *et al.* proposed a similar form of boundary condition for radiation of gravity waves at the surface of the reservoir. In that boundary condition, however, the wave propagation velocity is a function of frequency. According to Zienkiewicz *et al.*, the proposed boundary condition can not be applied simultaneously with the Sommerfeld radiation condition for short reservoir models with truncated boundaries. However, Zienkiewicz *et al.* argued that since the important depth ranges of the dilatational waves and surface waves as well as their decaying rates with distance from the disturbance are practically separated, the simultaneous application of the two boundary conditions is possible. However, they did not clarify the range of reservoir length to depth ratio for which the application of such a boundary condition is recommended.

Bettess (1977) introduced infinite elements with the shape functions in a form similar to Lagrange polynomials including an exponential decay term. He illustrated the success of the method in problems involving viscous flows. Bettess concluded that for a satisfactory result, the unknown quantity in the field problem should vanish at the far field. Moreover, the decay rate parameter should be carefully selected. Bettess also concluded that the infinite element approach models the effect of the far field on the near field of the reservoir rather than give a true indication of the model behaviour at infinity.

Saini *et al.* (1978) and Saini (1982) used infinite elements to model the radiation damping at the truncated upstream boundary in a two-dimensional model of the dam-reservoir system. Saini *et al.* showed that modelling radiation damping using infinite elements required a shorter length for the reservoir model than the length required when utilizing the conventional radiation boundary condition.

Hall and Chopra (1982a and 1982b) studied the hydrodynamic effects of the impounded reservoir on the seismic response of concrete gravity dams. They utilized approximate one-dimensional boundary conditions for the radiation of the outgoing waves from the reservoir and the refraction of the waves at the reservoir bottom. The only restriction imposed on the boundary condition at the far end was the assumption of a constant depth for the semi-infinite channel attached to the reservoir near field. The dam and reservoir subdomains were discretized based on the finite element method. They found the finite element approach to be successful in seismic response analysis of the dam-reservoir systems including dam flexibility and water compressibility in the model. Hall and Chopra (1982b) found that when the compressibility of the impounded water is neglected, the hydrodynamic force on a rigid gravity dam when subjected to horizontal ground motion is slightly dependent on the shape of the fluid domain. Under vertical excitation the hydrodynamic force was found to be virtually independent of the reservoir shape.

Humar and Roufaiel (1983) proposed a modified Sommerfeld boundary condition in the frequency domain for the truncated boundary of a finite-length representation of an infinitely long reservoir channel. The performance of the proposed boundary condition was superior to the classical Sommerfeld condition (Zienkiewicz *et al.* 1977) in the frequency range between the first and the second natural frequencies of the reservoir channel. In the above frequency range, the increase in the length of the reservoir model using Sommerfeld boundary condition did not result in any improvement in the accuracy (Hanna and Humar 1982, Humar and Roufaiel 1983, Sharan 1984 and Humar 1984).

Humar (1984) argued that the discrepancy between the Sommerfeld boundary condition in the finite element model of the reservoir and the theoretical solution for the hydrodynamic response can be better illustrated by the distribution of the pressure along the

dam height. Humar demonstrated that the total hydrodynamic force on the dam may be accurate, however, the results of the pressure distribution can be substantially different.

Sharan (1985a) proposed a radiation boundary condition for the truncated boundary of the reservoir model. His proposed boundary was based on the closed-form solution for the hydrodynamic pressure in the reservoir in the frequency domain under horizontal excitation. Water was treated as incompressible and the dam was assumed rigid in the analysis of both cases of having vertical and inclined upstream face of the dam. Sharan obtained reasonably good agreement with the available theoretical solutions in each case for considerably short reservoir lengths in the model.

Sharan (1985b) extended the proposed boundary condition for a compressible model of the impounded water. The reservoir bottom was assumed horizontal and completely reflective. The reservoir model was subjected to harmonic horizontal input ground motion. Sharan showed the Sommerfeld boundary condition and the modified boundary condition proposed by Humar and Roufaiel (1983) to be special cases of his proposed boundary condition. He further showed that for excitation frequencies lower than the fundamental frequency of the reservoir, satisfactory results for the hydrodynamic response are not obtained using Sommerfeld boundary condition unless the truncated boundary is located sufficiently far away from the dam. He also demonstrated that for higher excitation frequencies, the numerical approach using the Sommerfeld boundary condition does not converge to the exact solution by increasing the length of the reservoir model. Rather, it oscillates about the result corresponding to the case of infinite reservoir as the length of the reservoir model is increased. However, the pressure amplitudes are generally lower for higher excitation frequencies. Accordingly, the resulting errors are insignificant in the excitation frequency range that is higher than the second natural frequency of the reservoir

and the use of the simpler Sommerfeld boundary condition is recommended.

The radiation condition proposed by Sharan (1985b) is limited to the case where the fluid domain is unbounded in the direction of the structural motion. Sharan (1986) extended his proposed radiation boundary condition for the analysis of a submerged structure with truncated surrounding fluid boundary in all directions in a two-dimensional model.

For the near field of a reservoir of arbitrary geometry, Sharan (1987a) proposed a modified radiation condition. The reservoir far-field was limited to a constant-depth, semi-infinite channel with a horizontal rigid bottom. The dam was assumed deformable with an arbitrary shape. Satisfactory results were obtained with a short length of the reservoir model for frequencies lower than the second natural frequency of the uniform channel.

Sharan (1987b) modelled the radiation damping in the two-dimensional finite element analysis of hydrodynamic pressure in the time-domain. Water was assumed compressible. The expression for the proposed radiation condition was independent of the excitation frequency. For this reason, the expression was appropriate for the time-domain analysis of dam-reservoir systems. However, the effectiveness of the proposed boundary condition was dependent on the excitation frequency and showed a slight discrepancy with the theoretical solution in the vicinity of the fundamental frequency of the fluid domain. Sharan showed that the proposed boundary condition performed better than the traditional Sommerfeld boundary condition when the dam upstream face was inclined. However, the boundary condition was derived based on the assumption that the upstream face for the dam is vertical.

In later studies, Sharan (1991 and 1992) included the influence of an absorptive reservoir bottom in the proposed radiation condition. He observed some discrepancies with the theoretical solutions near the second and third natural frequencies of the reservoir channel. However, Sharan concluded that the proposed boundary condition leads to more

accurate results as compared to the Sommerfeld boundary condition for shorter length of the reservoir model. The proposed model was still limited to the case of a semi-infinite horizontal far-field attached to the near-field of arbitrary geometry.

Jablonski (1990) studied the effect of the location of a transmitting boundary on developed hydrodynamic pressure in the reservoir. Based on a two-dimensional model for the dam-reservoir-foundation system, the effect of the location of the transmitting boundary due to the change of geometry of the near-field part of the reservoir was investigated. In this aspect, Jablonski's study was different from those made by Sharan (1991 and 1992) where the location of the truncated boundary did not affect the geometry of the reservoir near-field. Jablonski used the radiation condition proposed by Hall and Chopra (1980) at the truncated boundary. He found that the slope of the reservoir bottom had a significant effect on the resulting hydrodynamic force on the dam. He also concluded that for the case of a completely reflective bottom, the length of transmitting boundary elements should be less than a tenth of the shortest wave length in the reservoir so that the radiation effect can be properly represented. Jablonski's conclusion is comparable with the condition proposed by Lysmer and Kuhlemeyer (1969) suggesting a ratio of one-twelfth between the size of the largest element and the minimum wave length propagating in the domain of analysis.

In the present study, both finite and infinite length reservoirs are included in the analysis. The finite-length reservoir is limited to a solid far boundary. In the numerical solution of the hydrodynamic response, one-dimensional boundary elements are included along the reservoir solid boundaries to account for partial absorption of impinging waves. For the cases where the solutions of the finite-length discretization of the reservoir model are compared with those of the semi-infinite case, the corresponding reflection coefficient of the elements at the far boundary are set to zero to model the case of complete absorption.

1.2.5 Water Surface

Since the first studies of the seismic response of dam-reservoir systems, the effects of surface waves have traditionally been neglected (Bakhmeteff 1933 and Chopra 1967). There are two main reasons behind this assumption: First, the excitation frequency associated with the gravity waves are well separated from the resonant frequencies of the typical dam-reservoir systems. It is quite unlikely that the low-frequency sloshing modes of the impounded water are significantly excited for the common depths of the concrete dam reservoirs. Secondly, developed hydrodynamic pressure due to the effects of surface waves vanishes rapidly with the depth of the water leaving the imposed hydrodynamic pressure on the dam due to the compressive waves virtually unchanged.

Bustamente *et al.* (Newmark and Rosenblueth 1971) showed that for the ratio of reservoir depth to the dominant period of disturbance exceeding 75 m/s, neglecting water surface waves as compared to the more accurate Poisson boundary condition leads to insignificant errors in the total hydrodynamic force on the dam. The margin of error was found to be not more than 5 to 20% depending on the above ratio. The error margin was considered to be conservative (Newmark and Rosenblueth 1971). Based on practical values of the depth to dominant period parameter, the actual errors are likely to be much smaller. The dam in the study by Bustamente *et al.* was assumed with vertical upstream face impounding an infinitely long reservoir.

Nath (1969) examined the effect of water surface waves using Poisson boundary condition. In a case study, he compared the pressure coefficient at water surface based on Poisson's linear condition with the case where the surface waves were neglected. The difference between the results was insignificant except for very low excitation frequencies. Nath concluded that for the frequency range of interest in seismic analysis of concrete dams

where the compressibility effects are important, the effect of gravity waves is negligible.

Eatock Taylor (1981) studied the effect of surface waves on the response of the hydrodynamic force in a two-dimensional model of a gravity dam. In his model, The deflection of the dam with a vertical upstream face was approximated using the fundamental vibration mode of the structure. Eatock Taylor concluded that the effect of reservoir surface waves is negligible for the case of deep reservoirs and rigid dam structures. The associated error margin based on an error estimation proposed by Bustamente *et al.* (Eatock Taylor 1981) was found to be 5%. Eatock Taylor compared the range of frequencies where the conditions for neglecting the surface waves and including the compressibility of the impounded water are valid. Based on his analysis, the above two conditions overlap when the depth of the reservoir is over 1890 m. This is beyond the practical reservoir depths in existing dams. Accordingly, there is no significant interactive effect of the surface waves and compressibility of water in the modification of the hydrodynamic response. This is consistent with the common assumption of neglecting the effects of surface waves and including the water compressibility in hydrodynamic response analysis of dam reservoirs.

The most serious effect of the earthquake-induced gravity waves is the possibility of overtopping. This phenomenon is of major concern in earth- and rockfill dams for its potential threat to the downstream side and should be accurately calculated for the proper design of the freeboard.

Based on the results of the above studies, the influence of the surface waves on the earthquake response of the dam is neglected throughout the course of the present study.

1.2.6 Dam-Reservoir Boundary

In past studies of the hydrodynamic pressure in the reservoir, the upstream face of the

concrete dam has been traditionally considered as completely reflective. Few studies in the available literature address the effects of a partially absorptive boundary at the upstream face of the dam. These studies examine the possibility of reducing the imposed hydrodynamic pressure on dams by means of *hydrodynamic isolation*. The investigated hydrodynamic isolation systems are limited to those utilizing air as the intermediate layer between the dam and the reservoir.

Lombardo *et al.* (1987) proposed the idea of an *air curtain* as an aseismic provision for the reduction of seismic loading on concrete dams. Hall and El-Aidi (1989) examined the possibility of reducing the hydrodynamic pressure by considering two practical alternatives for providing the air curtain at the upstream face of the dam: a) anchored air balloons and b) injected gas bubbles. Neither of these two methods achieved significant reduction in the dynamic response of the dam-reservoir system mainly due to the violation of the assumption of the linear variation of the air pressure along the depth of the curtain in addition to the excitation of extra modes associated with the oscillation of the gas domain. Hall *et al.* (1991 and 1992) studied the effect of a soft material attached to the upstream face of the concrete dam on the reduction of the dam response. However, the compressibility of the material was assumed to be that of a perfect gas with a simplified one-dimensional behaviour. With this model for the soft layer, Hall *et al.* did not obtain significant reduction in the response of the concrete dam.

The idea of reduction of hydrodynamic pressure on the dam by using an air curtain at the upstream side of the dam has also been examined by Sheinin (1992). He considered the air curtain in the forms of air bubbles and air vessels. The air bubble scheme did not seem practical due to the large quantity of air needed for providing a secure air-layer. There is also a prohibitive amount of expense associated with the air bubble scheme as an *active* type of

isolation. In this scheme of isolation, an on-line system of supply and surveillance is needed to obtain a reliable isolation curtain. The air containers provided a more practical type of permanent air curtains. Sheinin measured a significant reduction in the hydrodynamic pressure on Krivoporozhsk dam in Karelia, Russia, isolated from its reservoir with air containers.

Savinov *et al.* (1992) conducted theoretical studies on the effectiveness of the air curtains on the hydrodynamic isolation of dams. They assumed a linear mechanical behaviour along the depth of the curtain. Assuming the water as incompressible, Savinov *et al.* concluded that when the vibration frequency of the added mass of water acting on the air curtain is less than a third of the fundamental frequency of the dam, hydrodynamic pressure is reduced by a factor of 5 to 10. Savinov *et al.* suggested that compressibility of water increases the effectiveness of the air curtain scheme of isolation, however, little substantiation was provided.

As'kov *et al.* (1992) and Gellis *et al.* (1992) examined the idea of hydrodynamic isolation by laboratory model tests as well as measurements of the dam prototypes equipped with air curtain. They reported promising reductions of the hydrodynamic force exerted on the dam due to the effect of the isolation layer.

The effectiveness of the isolation in reducing the hydrodynamic pressure on the dam is decreased if the specific volume of the air in the curtain is reduced. This may happen due to leakage of the air out of the containers with time under the effects of the temperature variations, bio-organisms and vibrations of the dam and the isolation system due to the seismic events. Consequently, the air curtain scheme of isolation necessitates additional expenditure and maintenance for its long term reliability.

1.3 OBJECTIVES AND SCOPE

The main objective of the present study is to examine the effects of the reservoir boundaries on the seismic response of the concrete gravity dam. Special emphasis of the study is on the effects of the reservoir bottom absorption and the effects of a partially absorptive boundary at the interface of the dam and reservoir. The far end boundary of a finite-length reservoir is considered as a partially absorptive, stationary boundary in the analysis. For an infinitely long uniform reservoir channel, Sommerfeld radiation condition was used for the theoretical solution. A measure of the dynamic stress response of the dam is proposed and applied in the evaluation of the response of a dam with different reservoir characteristics when subjected to various earthquake ground motions. A theoretical investigation of the case of a partially absorptive boundary condition at the dam-reservoir interface is conducted. Because of the potential for important practical application, this study was extended to investigate the response and design of an isolating layer to protect the dam against the hydrodynamic loading.

To achieve the above objectives, an analytical study was conducted. The investigation of different parts of the reservoir boundary are presented in different chapters. Chapter 2 is devoted to the examination of the absorption effects of the reservoir bottom on seismic response of the dam. A theoretical model is proposed to effectively account for the absorption effect of the hydrodynamic pressure waves impinging on the boundary. Results of the dependence of the equivalent reflection coefficient and the structural response of the dam on the thickness and mechanical properties of the sediment layer are presented.

The dam-reservoir boundary is addressed in Chapter 3. The effect of the current assumption of a completely reflective dam-reservoir interface on the dam response is compared with the case where this boundary is assumed as partially reflective. The practical

application of such assumption is the case where a layer made of a soft material is installed at the upstream side of the concrete dam. An analysis was conducted to examine the isolation effects of various soft materials with proper thickness and dissipation characteristics on the structural response of a dam subjected to earthquake ground motion. The effects of the material parameters on the amount of response reduction are investigated.

Chapter 4 includes a general case of the reservoir boundary-value problem which is solved using the finite element method. When the dam-reservoir system is subjected to vertical excitation, the boundary-value problem of the reservoir with absorptive boundaries needs to be solved numerically. The two-dimensional model of the reservoir is discretized using finite elements with hydrodynamic pressure as the unknown nodal parameter. The computed nodal pressures evaluated at the dam-reservoir interface replace the analytical values currently used to obtain the hydrodynamic terms in the general frequency-domain equations. The developed procedure is applied to verify the analytical results for horizontal excitation as well as to study the effects of the reservoir length-to-depth ratio and the effects of an absorptive far boundary with an arbitrary reflection coefficient on the dam response.

Chapter 5 contains the stress analysis of the dam when subjected to selected horizontal and vertical input ground motions. A global parameter to include the stress time-history response as well as the overall state of stress over the cross section of the dam monolith is proposed. The proposed parameter, (the *Stress Factor*) is verified and used to express the state of stress in the dam subjected to different ground motions. Subsequently, the effects of reservoir boundary conditions on variation of the stress factor are investigated.

The conclusions resulting from the investigations in this thesis are presented in Chapter 6. The major assumptions through the course of the study are underlined which provides the basis for the recommendations for further studies on the subject.

CHAPTER 2

RESERVOIR BOTTOM BOUNDARY

2.1 INTRODUCTION

In this chapter, a model is proposed to include the absorption effects of the reservoir bottom in earthquake analysis of dams. The model utilizes the wave reflection coefficient approach which was used by Hall and Chopra (1980). The proposed model is based on the solution of the wave equation in a sediment layer of viscoelastic material with a constant thickness overlying an elastic semi-infinite foundation rock. Expressions for the equivalent reflection coefficient of the reservoir bottom are derived using two alternative approaches. In the first approach, the compliance function is first obtained from the material properties of the reservoir bottom. The function is subsequently used to calculate the wave reflection coefficient of the boundary. In the second approach, the impedance of the reservoir bottom is used to calculte the equivalent wave reflection coefficient.

Numerical studies were conducted to evaluate the effects of the sediment layer thickness and material properties as well as characteristics of the underlying rock on the response of the dam. In addition, the criteria for the significance of the absorption effects at the reservoir bottom for a given set of mechanical characteristics and the thickness of the sediment layer are presented.

2.2 THE PROPOSED MODEL

The foundation of the dam-reservoir system which is assumed as a semi-infinte space with an overlying layer of sediment materials of constant thickness in the reservoir is schematically shown in Fig. 2.1. The compliance function, $C(\omega)$, and the equivalent wave reflection coefficient, $\alpha_b(\omega)$, of the reservoir bottom are calculated based on the properties of both the foundation rock and the overlying sediment layer of assumed thickness.

Two separate approaches are presented to evaluate the absorption effect of the reservoir foundation. In the first approach, the compliance function, $C(\omega)$, is obtained for the water-sediment-foundation rock system. Based on the compliance function, the wave reflection coefficient, $\alpha_b(\omega)$, is calculated. In the second approach, the expression for the equivalent wave reflection coefficient is derived based on the impedance of the reservoir bottom which is subsequently incorporated in the corresponding boundary condition.

2.2.1 The Compliance Function Approach

The boundary condition for the reservoir-foundation interaction in a two-dimensional model of the reservoir in the frequency domain is expressed as (Fig. 2.2):

$$\frac{\partial P}{\partial y}(x,0;\omega) - \rho_w \omega^2 v_t(x;\omega) = -\rho_w \tag{2.1}$$

where

$P(x,y;\omega)$ is the complex frequency response function of the hydrodynamic pressure

$v_t(x;\omega)$ is the frequency response function of the total vertical displacement at the surface of the reservoir bottom due to the water-foundation interaction

ρ_w is the density of water

ω is the frequency of excitation

The continuous function, $v_t(x;\omega)$, is related to the hydrodynamic pressure at the reservoir bottom by the expression:

$$v_t(x;\omega) = -C(\omega) P(x,0;\omega) \tag{2.2}$$

The compliance function, $C(\omega)$, is obtained through the solution of Helmholz equation representing the steady-state vibration of the sediment material and the foundation rock:

$$\frac{d^2 v_s(y;\omega)}{dy^2} + \gamma_s^2(\omega) v_s(y;\omega) = 0 \qquad (0 \le y \le d_s)$$

$$\frac{d^2 v_f(y;\omega)}{dy^2} + \frac{\omega^2}{C_f^2} v_f(y;\omega) = 0 \qquad (y \ge d_s) \tag{2.3}$$

where d_s is the thickness of the sediment layer and $v_s(y;\omega)$ and $v_f(y;\omega)$ are the frequency response functions for the vertical displacements of the sediment layer and the foundation rock, respectively. The travel speed of longitudinal waves in the foundation rock is C_f, and $\gamma_s(\omega)$ is defined as:

$$\gamma_s(\omega) = \frac{\omega/C_s}{\sqrt{1 + i\omega\eta_s/E_s}} \tag{2.4}$$

where η_s, E_s and C_s are the coefficient of longitudinal viscosity, elastic modulus and the equivalent travel speed of longitudinal waves in the sediment material, respectively. In Eq. 2.3, the sediment material is considered as viscoelastic overlying an elastic foundation rock with no material damping. The complex function, $\gamma_s(\omega)$, can be expressed as:

$$\gamma_s(\omega) = k_s - i\mu_s \tag{2.5}$$

where k_s is the wave number in sediment material and μ_s is the attenuation coefficient. The wave propagation parameters k_s and μ_s are functions of frequency and can be found by equating Eqs. 2.4 and 2.5 which yields:

$$\mu_s(\omega) = \frac{[1 + \rho_s^2 \lambda_s^2(\omega).\omega^4]^{1/2} - 1}{2E_s[1 + \lambda_s^2(\omega)]} \tag{2.6}$$

and

$$k_s(\omega) = \frac{\rho_s \omega^2 \lambda_s(\omega)}{2E_s[1 + \lambda_s^2(\omega)]}.[\mu_s(\omega)]^{-1/2} \tag{2.7}$$

where ρ_s is the density of the sediment material and:

$$\lambda_s(\omega) = \frac{\eta_s \omega}{E} \tag{2.8}$$

For a given frequency of excitation, the wave propagation parameters k_s and μ_s are known based on the mechanical characteristics of the sediment material. The response function $v_s(y;\omega)$ for the sediment layer can be expressed as:

$$v_s(y;\omega) = v_{0rs}(\omega).\exp(-\mu_s d_s).\exp[i(k_s - i\mu_s)y]$$

$$+ v_{0ts}(\omega).\exp[-i(k_s - i\mu_s)y] \tag{2.9}$$

where $v_{0rs}(\omega)$ and $v_{0ts}(\omega)$ are the amplitudes of the reflected and transmitted waves in the sediment layer, respectively. The proposed wave function $v_s(y;\omega)$ is obtained based on the assumption of an exponential attenuation of the transmitted and reflected waves in the sediment layer as shown in Fig. 2.2. It can be readily shown that $v_s(y;\omega)$ satisfies Eq. 2.3. The response function, $v_f(y;\omega)$, for a semi-infinite, elastic foundation is written as:

$$v_f(y;\omega) = v_{0tf}(\omega).\exp(-ik_f y) \tag{2.10}$$

where $v_{0tf}(\omega)$ is the amplitude of the transmitted wave in the foundation rock and k_f is the wave number of the travelling pressure wave in the foundation rock. The amplitudes of the dilatational waves in the sediment layer and the foundation rock are obtained by applying the conditions of force equilibrium and displacement compatibility at the reservoir bottom and sediment - foundation boundaries using the response functions of Eqs. 2.9 and 2.10. The compliance function for the reservoir bottom is obtained as:

$$C(\omega) = v_s(0;\omega)$$

$$= \frac{i}{E_c(k_c + i\mu_c)} \cdot \frac{(\beta+1)\exp(\mu_s + ik_s)d_s - (\beta-1)\exp[-(\mu_s + ik_s)d_s]}{(\beta+1)\exp(\mu_c + ik_c)d_c + (\beta-1)\exp[-(\mu_c + ik_c)d_c]} \tag{2.11}$$

where:

$$\beta = \frac{E_f k_f}{E_s(k_s - i\mu_s)} \tag{2.12}$$

and E_f is the elastic modulus of the foundation rock.

From the general expression for the compliance function, the following special cases

are discussed:

a) Neglecting the viscosity of the sediment layer (attenuation coefficient μ_s =0), Eq. 2.11 reduces to:

$$C(\omega)\big|_{\mu_s=0} = \frac{-1}{\rho_s C_s \omega}\left[\frac{\beta\cos k_s d_s - i\sin k_s d_s}{\beta\sin k_s d_s + i\cos k_s d_s}\right] \tag{2.13}$$

b) The compliance function for the sediment layer on a rigid foundation rock ($E_f \to \infty$) is:

$$C(\omega)\big|_{\beta\to\infty} = \frac{i}{E_s(k_s + i\mu_s)} \cdot \frac{\exp(\mu_s + ik_s)d_s - \exp[-(\mu_s + ik_s)d_s]}{\exp(\mu_s + ik_s)d_s + \exp[-(\mu_s + ik_s)d_s]} \tag{2.14}$$

c) For an inviscid sediment layer on a rigid foundation ($\mu_s = 0$, $E_f \to \infty$):

$$C(\omega) = \frac{-1}{\rho_s C_s \omega} \tan k_s d_s \tag{2.15}$$

The equivalent wave reflection coefficient, $\alpha_b(\omega)$, of the reservoir bottom with rigid foundation can be obtained using Eq. 2.14 as:

$$\alpha_b(\omega) = \frac{1 + i\rho_w C_w \omega C(\omega)}{1 - i\rho_w C_w \omega C(\omega)} \tag{2.16}$$

which results in:

$$\alpha_b(\omega)\big|_{\beta\to\infty} = \left|\frac{\beta\,(\exp(\mu_s + ik_s)d_s + \exp[-(\mu_s + ik_s)d_s]) - (\exp(\mu_s + ik_s)d_s - \exp[-(\mu_s + ik_s)d_s])}{\beta\,(\exp(\mu_s + ik_s)d_s + \exp[-(\mu_s + ik_s)d_s]) + (\exp(\mu_s + ik_s)d_s - \exp[-(\mu_s + ik_s)d_s])}\right| \tag{2.17}$$

where

$$\beta' = \beta_{sw}(1 - \frac{i\mu_s C_s}{\omega}) \tag{2.18a}$$

and

$$\beta_{sw} = \frac{\rho_s C_s}{\rho_w C_w} \tag{2.18b}$$

where C_w is the traveling speed of waves in water. For an inviscid layer, Eq. 2.17 reduces to:

$$\alpha_b(\omega)\,|_{\mu_s = 0, \beta \to \infty} = \left| \frac{\beta_{sw}\cos k_s d_s - i\sin k_s d_s}{\beta_{sw}\cos k_s d_s + i\sin k_s d_s} \right| \tag{2.19}$$

2.2.2 The Wave reflection coefficient approach

An equivalent method may be used to evaluate the absorption characteristics of the reservoir bottom. The boundary condition at the water-foundation interface can be written in the form:

$$\left[\frac{\partial P}{\partial y} + \frac{i\omega}{\beta_{sw} C_w} P\right]\Big|_{(x,0;\omega)} = -\rho_w \tag{2.20}$$

where β_{sw} is based on the material properties of the sediment layer and neglecting the effect of reflected waves from the foundation rock. For a sediment layer overlying the foundation rock, β_{sw} is replaced by the frequency dependent equivalent relative impedance, $\beta_b(\omega)$, in the boundary condition at the reservoir bottom, where:

$$\beta_b(\omega) = \frac{1 + \alpha_b(\omega)}{1 - \alpha_b(\omega)} \tag{2.21}$$

In Eq. 2.21, $\alpha_b(\omega)$ is the overall reflection coefficient of the reservoir bottom which can be directly obtained from the impedance of the reservoir bottom defined as the ratio of the acting pressure to the particle velocity at the surface of the boundary. The steady-state response functions for the incidental, transmitted and reflected pressure waves shown in Fig. 2.2 can be expressed as:

$$P_{iw} = \exp(-ik_w y)$$

$$P_{rw} = P_{0rw}\exp(ik_w y) \qquad (y \le 0)$$

$$P_{ts} = P_{0ts}\exp[-(\mu_s + ik_s)y]$$

$$P_{rs} = P_{0rs}\exp[-\mu_s(d_s - y) + ik_s y] \qquad (0 \le y \le d_s)$$

$$P_{tf} = P_{0tf}\exp(-ik_f y) \qquad (y \ge d_s) \tag{2.22}$$

where indices *i*, *t* and *r* are used for incidental, transmitted and reflected waves and indices *w*, *s* and *f* denote water, the sediment material and foundation rock, respectively. $k_j, j=w,s,f$ are the wave number of traveling pressure waves in water, the sediment layer and the foundation, respectively. The response functions of pressure amplitudes are obtained using the conditions for continuity of pressure and particle velocities across the boundaries as:

at $y = 0$:

$$1 + P_{0rw} = P_{0ts} + P_{0rs}.\exp(-\mu_s d_s)$$

$$\frac{1}{\rho_w C_w} - \frac{P_{0rw}}{\rho_w C_w} = \frac{P_{0ts}}{\rho_s C_s} - \frac{P_{0rs}.\exp(-\mu_s d_s)}{\rho_s C_s}$$

at $y = d_s$:

$$P_{0ts}.\exp[-(\mu_s + ik_s)d_s] + P_{0rs}.\exp(ik_s d_s) = P_{0tf}.\exp(-ik_f d_s)$$

$$P_{0ts}.\exp[-(\mu_s + ik_s)d_s] - P_{0rs}.\exp(ik_s d_s) = \beta_{sr} P_{0tf}.\exp(-ik_f d_s) \qquad (2.23)$$

where

$$\beta_{sf} = \frac{\rho_s C_s}{\rho_f C_f} \qquad (2.24)$$

and ρ_f is the density of the foundation rock. By definition, the wave reflection coefficient, $\alpha_b(\omega)$, is obtained from the solution of the Eqs. 2.23 in the form of (Hatami 1996):

$$\alpha_b(\omega) = |P_{0rw}| \qquad (2.25)$$

For the case of a rigid foundation rock, Eq. 2.25 yields:

$$\alpha_b(\omega) = \left| \frac{\beta_{sw}(\exp(\mu_s + ik_s)d_s + \exp[-(\mu_s + ik_s)d_s]) - (\exp(\mu_s + ik_s)d_s - \exp[-(\mu_s + ik_s)d_s])}{\beta_{sw}(\exp(\mu_s + ik_s)d_s + \exp[-(\mu_s + ik_s)d_s]) + (\exp(\mu_s + ik_s)d_s - \exp[-(\mu_s + ik_s)d_s])} \right|$$

(2.26)

Eq. 2.26 is identical to Eq. 2.19 for $\mu_s = 0$. For the case of $\mu_s \neq 0$, Eq. 2.26 is equivalent to

Eq. 2.17 provided that:

$$\frac{\mu_s C_s}{\omega} \ll 1 \tag{2.27}$$

The condition of Eq. 2.27 can be examined based on the available data on the attenuation coefficient, μ_s, of the underwater sediments. Since $_s\mu$ is a function of frequency, the dominant coupled frequency of the dam-reservoir system, ω'_c, is selected to be used in Eq. 2.27. A typical cross section of a gravity dam with 91.44 m (300 ft) height and the downstream slope of 0.78:1 is considered in the present study. The fundamental peak of the crest response at full reservoir condition occurs in the vicinity of $\omega = 20$ rad/s as shown in Fig. 2.3 which hereafter is referred to as the coupled fundamental frequency of the dam-reservoir system on a rigid foundation, ω'_c. On the basis of the attenuation coefficient obtained for natural saturated sediments (Hamilton 1972), the attenuation coefficient of the sediment material for the fundamental frequency of the dam-reservoir system is calculated to be: $\mu_s = 6\times10^{-5}$ m^{-1} (2×10^{-5} ft^{-1}). The speed of dilatational waves in the sediments can also be estimated based on the available measurements (Shumway 1960). For C_s=1500 m/s (5000 fps), $\mu_s C_s/\omega = 4.5\times10^{-3} \ll 1$ which satisfies condition 2.27.

2.3 NUMERICAL STUDIES

The results of several numerical solutions for specific cases are presented in two parts. In the first part, the effect of the sediment layer and the foundation rock characteristics on the equivalent reflection coefficient is examined. These characteristics include the layer thickness, the modulus of elasticity and the attenuation coefficient of the sediment material as well as the modulus of elasticity of the foundation rock. In the second part of the study, the effect of the sediment and rock characteristics on the dam response is evaluated.

A typical two-dimensional model of a concrete gravity dam monolith with vertical upstream face, is considered. The dam impounds an infinite-length reservoir of rectangular shape. With smooth contraction joints, the monolith is assumed to be in plane stress condition. The height of the monolith is taken to be 91.44 m (300 ft) with the overall downstream slope of 0.78:1. The modulus of elasticity of the concrete is assumed to be 21500 MPa (3125 ksi) with the Poisson's ratio of 0.2. The hysteretic damping factor of the dam concrete is assumed constant for all modes and is taken as 0.1. Only dynamic forces are considered in the analysis and the effect of the static loads is excluded. Water level in the reservoir is assumed at the crest level of the dam. The recorded S69E component of the Kern County earthquake, California at Taft Lincoln School Tunnel on July 21, 1952 was selected as the free field ground acceleration for the analysis. The same accelerogram input ground motion was applied in both horizontal and vertical directions.

The analysis was made in the frequency domain using the substructuring technique with Ritz vectors for the dam substructure together with a continuum solution for the reservoir. The first ten mode shapes are included for the dam substructure.

Results from experimental measurements on underwater sediments indicate that the traveling speed of the dilatational waves varies in the range of 1400-1800 m/s (4500-6000

fps) (Hamilton 1972). Available measured data also indicate that the attenuation, μ_s, is a first-order function of the frequency:

$$\mu_s = bf^m \tag{2.28}$$

where f is the frequency in kHz and b is a constant. The measured values of the exponent of the frequency, m, in the natural sediments over some widely scattered geographic areas, various water depths and over a wide frequency range were found to be very close to one (Hamilton 1972). The constant b, on the other hand, varies considerably according to the sediment material and its mechanical characteristics such as grain size and porosity. It is also a function of frequency. Reported measurements on the attenuation characteristics of marine sediments in the seismic frequency range of excitation suggest that the value of b is in the range of 0.035 to 0.35.

For the present study, the density of the sediment material was taken as twice the value for the water. Accordingly, with the speed of dilatational waves equal to C_s = 1500 m/s (5000 fps), the equivalent modulus of elasticity for the sediments are obtained as: $E_s = \rho_s C_s^2$ = 4500 MPa (653 ksi). The constant b in Eq. 2.28 was assigned the values of 0.05, 0.25 and 0.50. The depth of the sediment layer was varied between 0.9 m (3 ft) (d_s /H = 0.01) and 4.5 m (15 ft) (d_s/H = 0.05). The modulus of elasticity of the flexible foundation was taken as 23000 MPa (3333 ksi).

2.4 RESULTS

2.4.1 Equivalent Reflection Coefficient

The variation of the reflection coefficient of the reservoir bottom, $\alpha_b(\omega)$, with the characteristics of the sediment layer and the foundation rock are presented in Figs. 2.4 to 2.8. The effect of the change in the attenuation constant, *b*, on the variation of the wave reflection coefficient $\alpha_b(\omega)$ with the thickness of the sediment layer normalized to the depth of the impounded water, H is shown in Fig. 2.4. The elastic modulus of the material is taken as E_s = 4500 MPa (653 ksi) overlying a rigid and a flexible foundation rock, respectively. The results are shown for the excitation frequency $\omega = \omega^1_r$. It is shown that the reflectivity of the reservoir bottom is reduced with the increase in the thickness of the sediment layer. The rate and extent of reduction are higher for the case of a rigid foundation. As would be expected, the overall value of $\alpha_b(\omega)$ is lower for the case of a more dissipative soil.

The variation of $\alpha_b(\omega)$ with frequency for selected values of sediment layer thickness of d_s/H=0.01 and d_s/H = 0.05 overlying a flexible foundation is plotted in Fig. 2.5. The frequency is normalized with respect to the fundamental frequency of the reservoir, ω^1_r. The reflection coefficient of the reservoir bottom decreases for higher frequencies of excitation and is generally lower for a larger attenuation constant. According to Fig. 2.5, the effect of the attenuation constant is more significant for a deeper layer of sediment.

The effects of the thickness and the attenuation constant of the sediment layer on the variation of $\alpha_b(\omega)$ with respect to frequency for the case of a rigid foundation rock are shown in Fig. 2.6. For low values of the attenuation constant, b, the reflection coefficient of a rigid reservoir bottom covered with natural underwater sediments remains slightly below unity over the dominant range of characteristic frequencies of the dam-reservoir system. This conclusion is in agreement with the results obtained by Bougacha and Tassoulas (1991b) for

a fully-saturated poroelastic model for the sediments. On the other hand, for a large value of the attenuation constant, a noticeable reduction is obtained for sufficiently large thickness of the layer. The value of the attenuation constant of $b = 0.50$ is unrealistically high. In this case, the significant part of reduction in the equivalent reflection coefficient, $\alpha_b(\omega)$, is at the higher range of frequencies which is beyond the dominant characteristic frequencies of the dam-reservoir system.

The effect of the foundation rock flexibility on the variation of $\alpha_b(\omega)$ is shown in Fig. 2.7 for a wide range of rock modulus of elasticity. For a given set of typical sediment layer characteristics E_s, μ_s and ρ_s and for a given frequency of excitation, the equivalent reflection coefficient of the reservoir bottom increases with the increase of the elastic modulus of the rock, E_f. The value of $\alpha_b(\omega)$ is more sensitive to the variation of the elastic modulus of rock for lower values of E_f/E_s ratio (Fig. 2.7). The value of $\alpha_b(\omega)$ is lower for a larger attenuation constant of the sediment material. The variation of $\alpha_b(\omega)$ with E_f is less sensitive to the attenuation constant of the sediment when the underlying rock is closer to the surface as shown in Fig. 2.7. The effect of the softness of the sediment material, characterized by its modulus of elasticity, on $\alpha_b(\omega)$ is presented in Fig. 2.8. The overall reflection coefficient at the boundary increases slightly with the increase in the modulus of elasticity of the sediment material. The effect of the attenuation constant on variations of $\alpha_b(\omega)$ with respect to E_s and E_f is more significant for a lower value of E_s/E_f and a larger thickness of the sediment layer. From Figs. 2.7 and 2.8 it is also concluded that for the case of a stiff sedimentation, the value of $\alpha_b(\omega)$ is not significantly affected by the thickness of the sediment layer.

2.4.2 Structural Response

Fig. 2.9 shows a plot of the crest acceleration response versus the non-dimensionalized frequency ω/ω^1_s where ω^1_s is the fundamental frequency of the dam on a rigid foundation rock with empty reservoir. In the figure, the response function of the dam crest acceleration for the case of a constant value for α_b based on the properties of the sediment material (α_b = 0.35) is compared with the cases where $\alpha_b(\omega)$ is obtained according to the proposed model for various thicknesses of the layer. The difference in the magnitude of response between the various cases is quite significant. The difference in the crest acceleration response even for the high value of $b = 0.5$ for the attenuation constant may amount to one order of magnitude. The responses shown in Fig. 2.9 represent the case of a rigid foundation rock. For a flexible foundation rock, the value of the reflection coefficient is generally lower than for the rigid case and the effect of variation of the sediment characteristics is less significant (Fig. 2.10). For low values of the attenuation coefficient of the sediment material the response of the dam is dominated by the characteristics of the underlying rock.

Based on the available measurements of the sediment characteristics, neglecting the effects of foundation rock underneath the reservoir may significantly underestimate the reflectivity of the reservoir bottom which results in an unconservative estimate of the structural response of the dam.

The effect of the modulus of elasticity of the sediment material for selected values that correspond to typical soft, medium and dense type of soils (Bowles 1984) on the structural response of the dam was examined. The effects of layer characteristics on the structural response of the dam are presented in Figs. 2.11 and 2.12 for horizontal and vertical excitation of the dam-reservoir system, respectively. To restrict the study to the effect of sediment layer characteristics on the amount of response reduction, the foundation rock underneath the dam

and the reservoir is assumed to be rigid. The maximum principal tensile stress at the heel of the dam is selected for the purpose of comparison between various cases. The reduction in the structural response is represented in terms of the response of the dam for a completely reflective reservoir bottom (α_b = 1.0). Comparing the results presented in Figs. 2.11 and 2.12 indicates that the percentage of response reduction is larger for the case of vertical ground motion as compared to horizontal excitation of the system. The difference is significantly reduced with the increase in the modulus of elasticity of the sediment material. This observation is specially important in the analysis of the response of the concrete dam to vertical ground motion. The effect of dam - reservoir interaction is reduced when the bottom of the reservoir is assumed absorptive. The realistic representation of the absorption effect of the reservoir bottom is important. Based on the results of the present study, the relative significance of the vertical excitation in the overall seismic response of the concrete dam is underestimated without the proper attention to the reflected waves from the reservoir foundation rock.

2.5 CONCLUSIONS

The wave reflection coefficient approach is modified to model reservoir bottom absorption effects in the earthquake analysis of concrete dams. The proposed model explicitly accounts for the effects of wave attenuation in the sediment layer as well as reflection of waves from the underlying foundation rock. The above effects are in addition to the radiation of the refracted waves into the foundation which is the only effect that is normally considered to account for the absorption of pressure waves at the reservoir bottom. The proposed model provides a representation for the reservoir - foundation boundary that is consistent with the recent approach for modelling dam-foundation system. Besides, the proposed method utilizes the mechanical parameters of the layer and the foundation rock that are more readily available compared with the ones needed in more sophisticated poroelastic models for the sediment material.

From the analysis presented in this chapter, the following conclusions are arrived at:

1- The overall reflection coefficient of the reservoir bottom increases with the increase of the modulii of elasticity of the sediment material and the foundation rock. The dependence of the reflection coefficient, $\alpha_b(\omega)$, on the elastic modulus of the underlying rock, E_f, is more significant when the sediment material is stiff with a high modulus of elasticity, E_s, and a low coefficient of attenuation, μ_s. The reflection coefficient, $\alpha_b(\omega)$, becomes more significantly dependent of E_s in the case of a very soft and dissipative sediment and a stiffer underlying rock. The reflection coefficient decreases for higher frequencies of excitation, larger thickness of the sediment layer and for higher values of the attenuation constant of the sediment material. The effect of the sedimentation attenuation constant on $\alpha_b(\omega)$ is more significant for a deeper layer of sediment. The value of $\alpha_b(\omega)$ is not significantly altered with the thickness of the sediment layer for

the case of a stiff sedimentation.

2- If the wave reflection coefficient at the reservoir bottom is evaluated based on the characteristics of the sediment material alone while neglecting the effect of reflected waves from the underlying rock, a significant underestimation of the seismic response of the concrete dam will result.

3- Due to the unexpectedly high modulus of elasticity and low attenuation coefficient of the typical underwater sediments, it is concluded that the response of the dam is not significantly reduced by the absorption effect of a thin sediment layer, overlying a rigid foundation rock, compared with the case of a completely reflective boundary. Accordingly, radiation of refracted waves to the foundation of the reservoir plays a more important role in the reduction of the dam response than the absorption of the wave energy within the sediment layer. The above argument is valid with minor differences for both horizontal and vertical components of the input ground motion. If the absorption effect of the reservoir bottom is evaluated based on the properties of the sediment material only, the relative significance of the vertical excitation in the overall response is underestimated.

4- The presented observations and conclusions are based on the response analysis of a specific dam to a single record of ground motion. All the conclusions that are case specific may not apply to all concrete gravity dams and all ground motions. For example, the dam-reservoir interaction and reservoir-foundation boundary absorption depends to a certain extent on the specific dam and ground motion selected. However, the broad conclusions remain applicable to many cases.

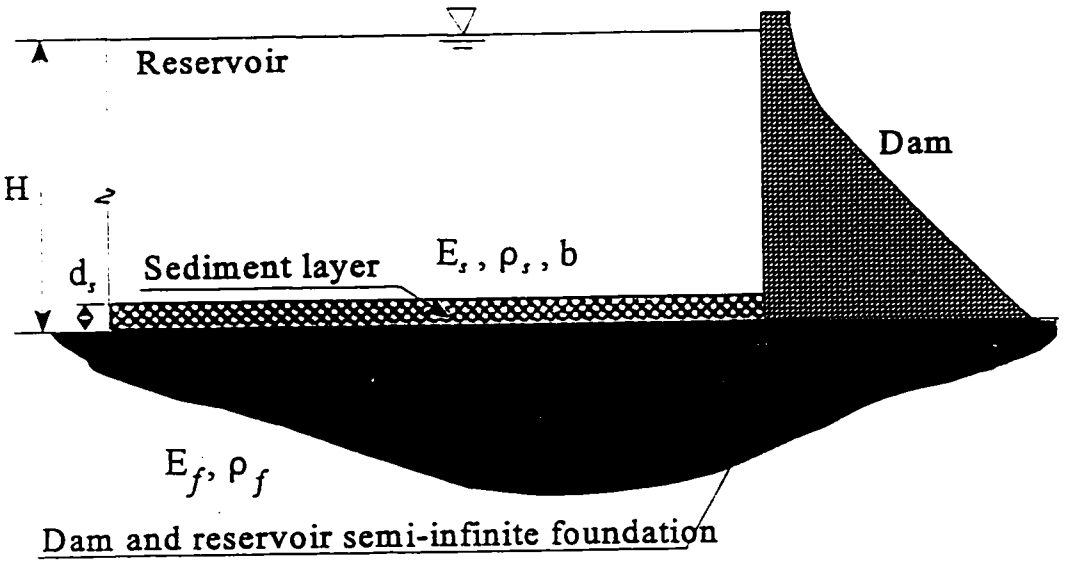

Fig. 2.1 Dam-reservoir-foundation and sediment layer model

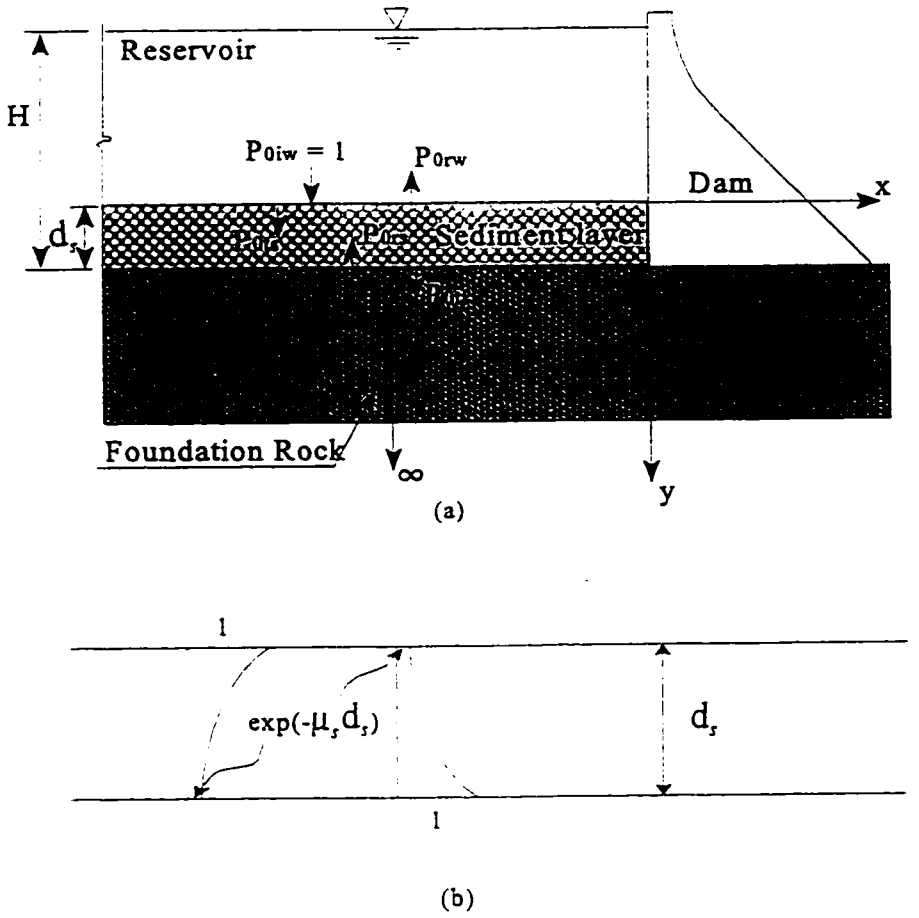

Fig. 2.2 Wave transmission to the foundation: (a) refraction and reflection of impinging waves; (b) attenuation in the sediment layer

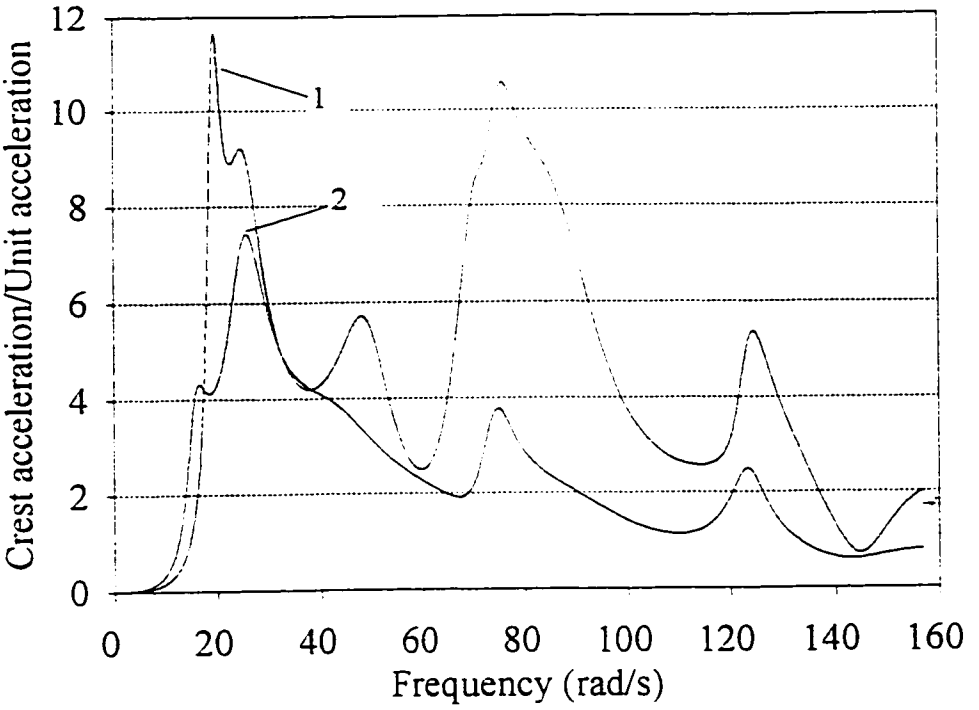

Fig. 2.3 Crest acceleration response of the dam subjected to unit harmonic vertical acceleration for the cases of rigid and flexible dam foundation ($\alpha_b = 0.68$)

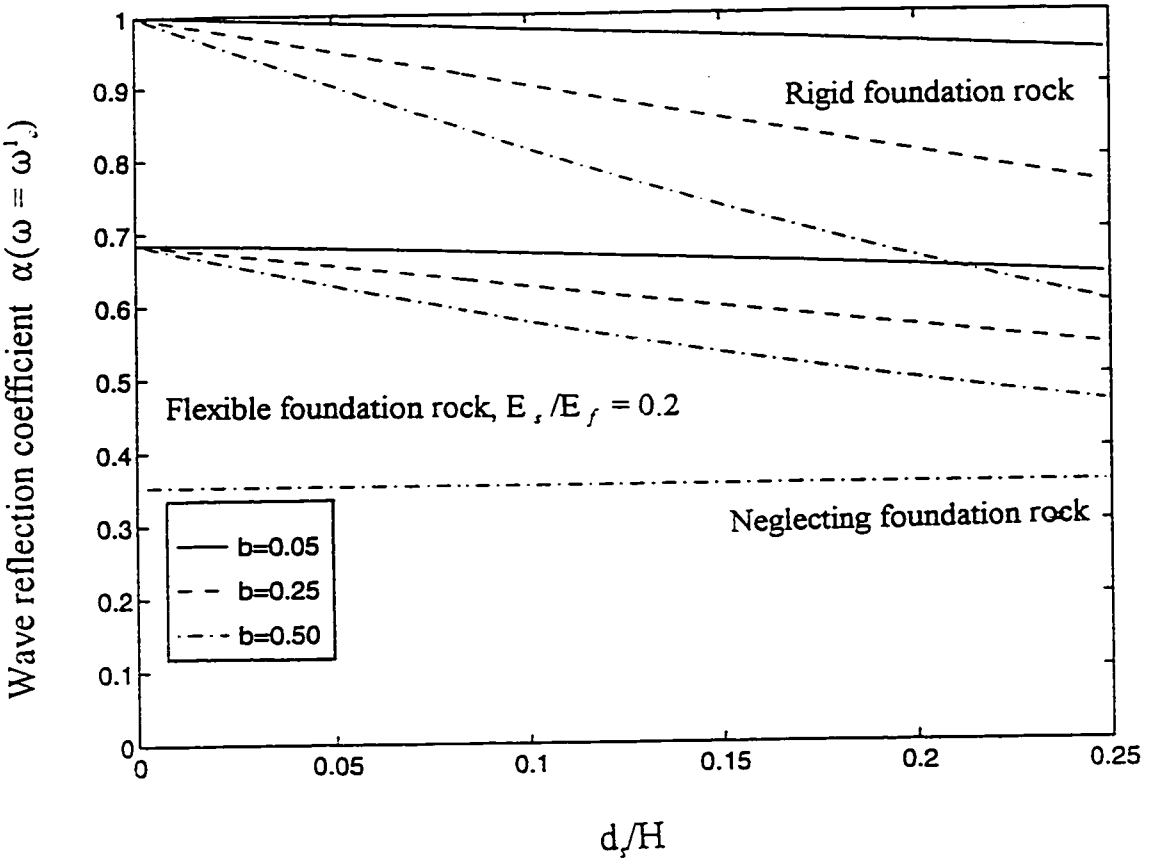

Fig. 2.4 Effect of the attenuation constant and foundation rigidity on the variation of the reflection coefficient with the thickness of the sediment layer

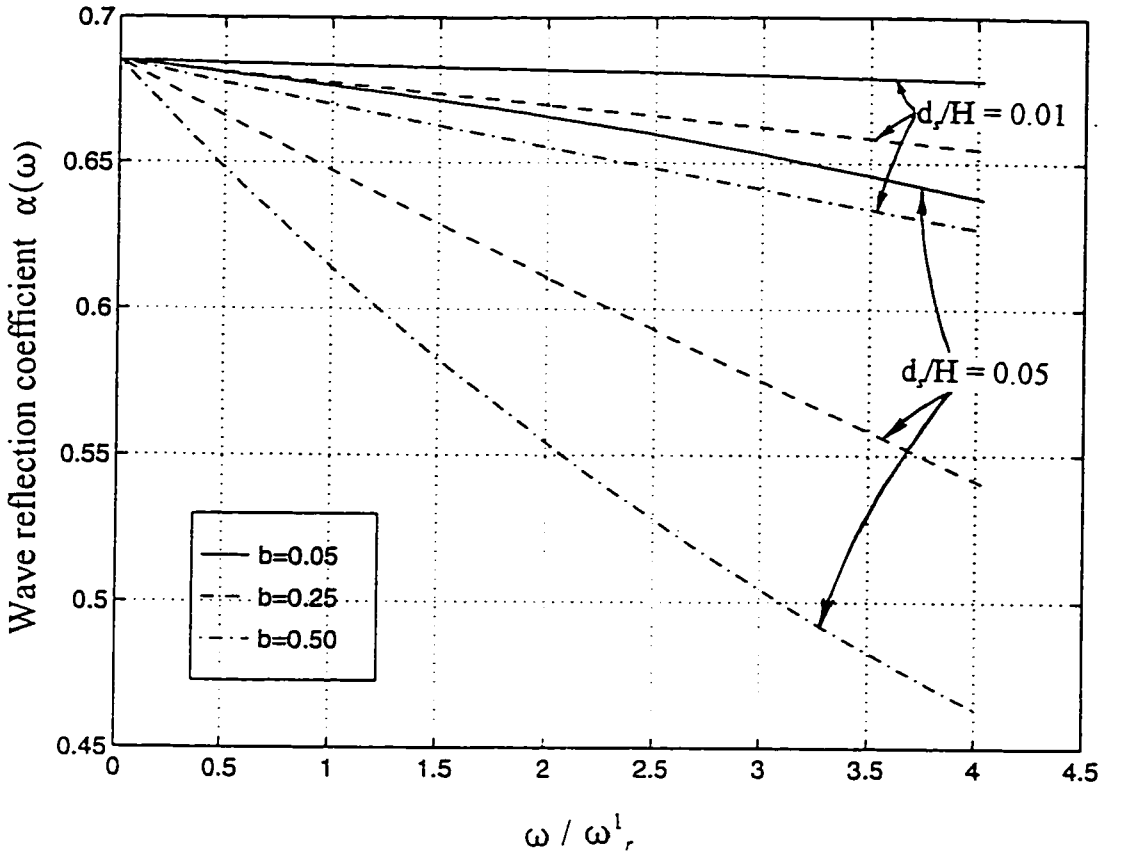

Fig. 2.5 Effect of the attenuation constant and the thickness of the sediment layer overlying a flexible foundation on the variation of the wave reflection coefficient with frequency (E_r = 23000 MPa, E_s/E_r=0.2)

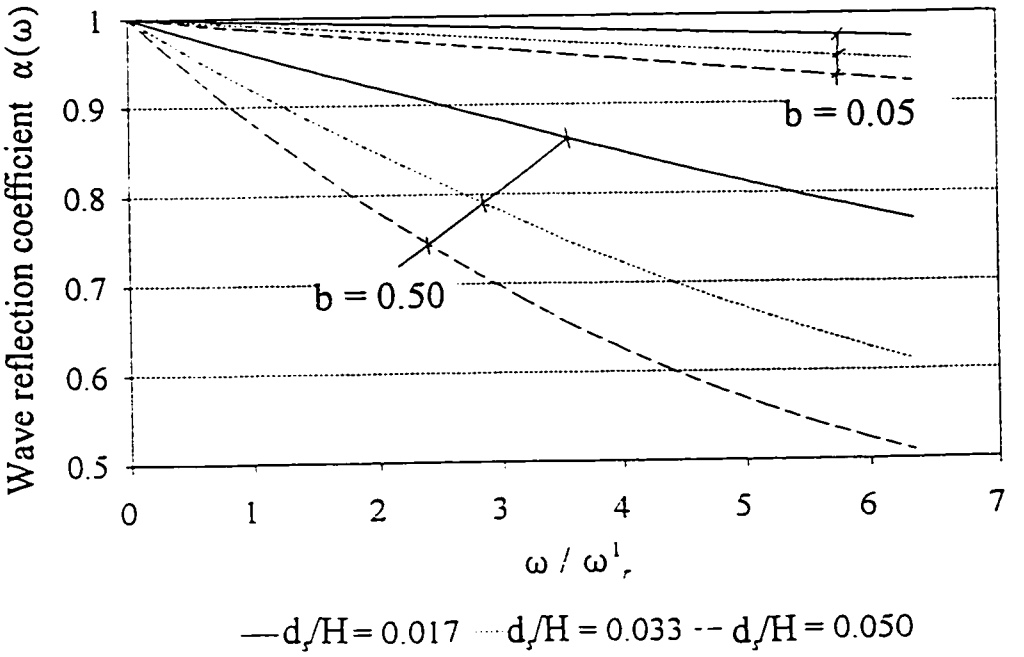

Fig. 2.6 Effect of the attenuation constant and the thickness of the sediment layer overlying a rigid foundation rock on the variation of the wave reflection coefficient with frequency (E_s = 4500 MPa)

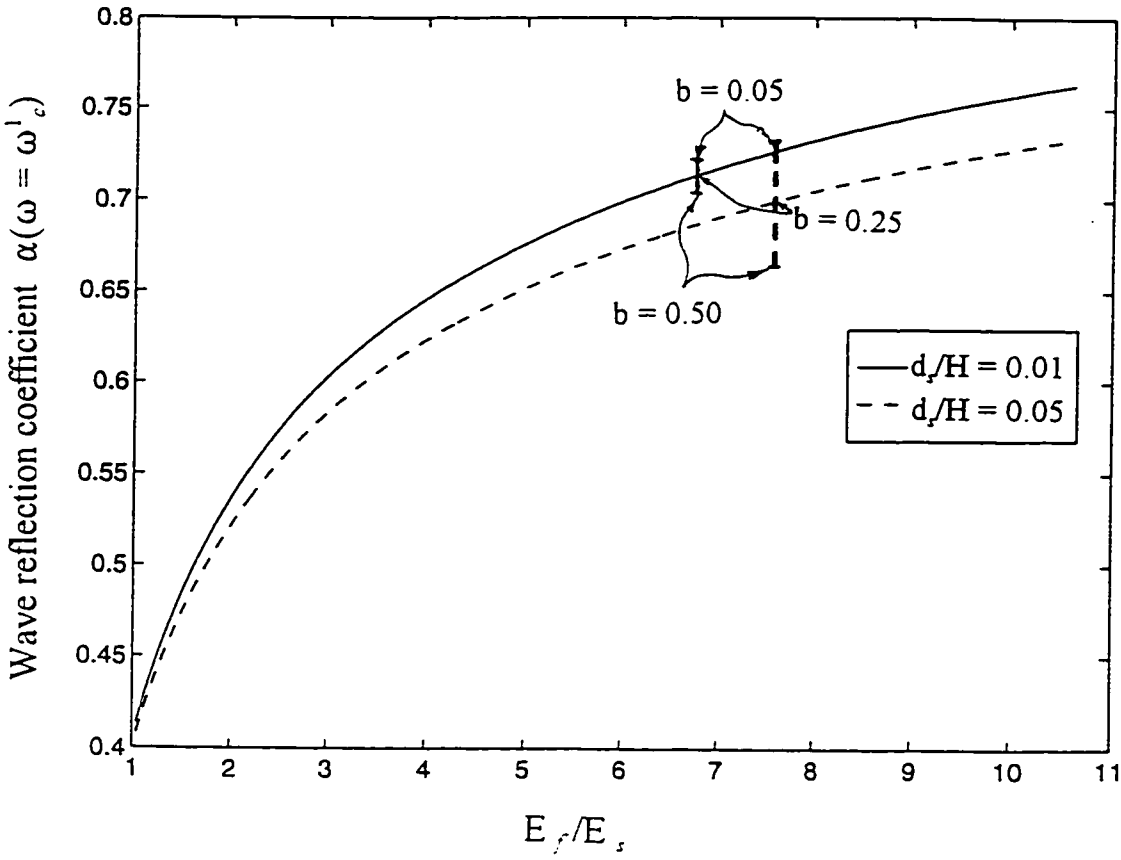

Fig. 2.7 Variation of the reflection coefficient of the reservoir bottom with the modulus of elasticity of the underlying foundation rock (E_s = 4500 MPa)

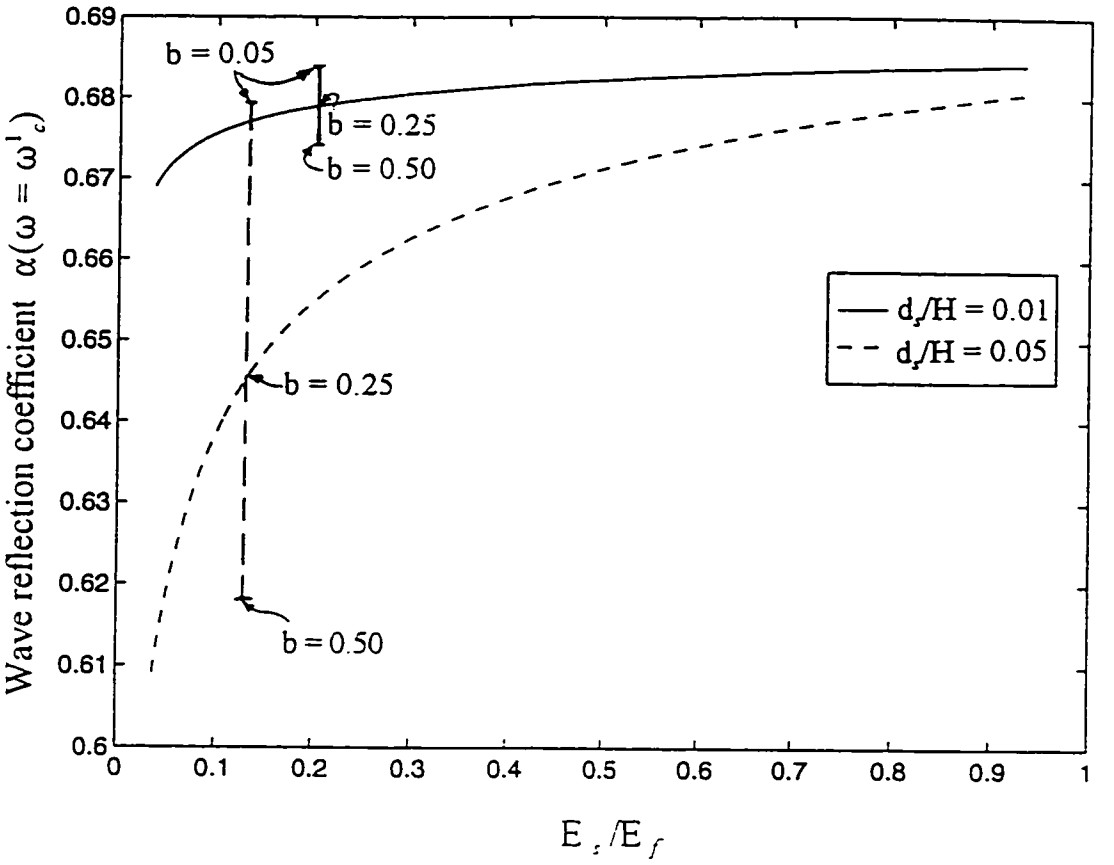

Fig. 2.8 Variation of the reflection coefficient of the reservoir bottom with the modulus of elasticity of the sediment material (E_f = 23000 MPa)

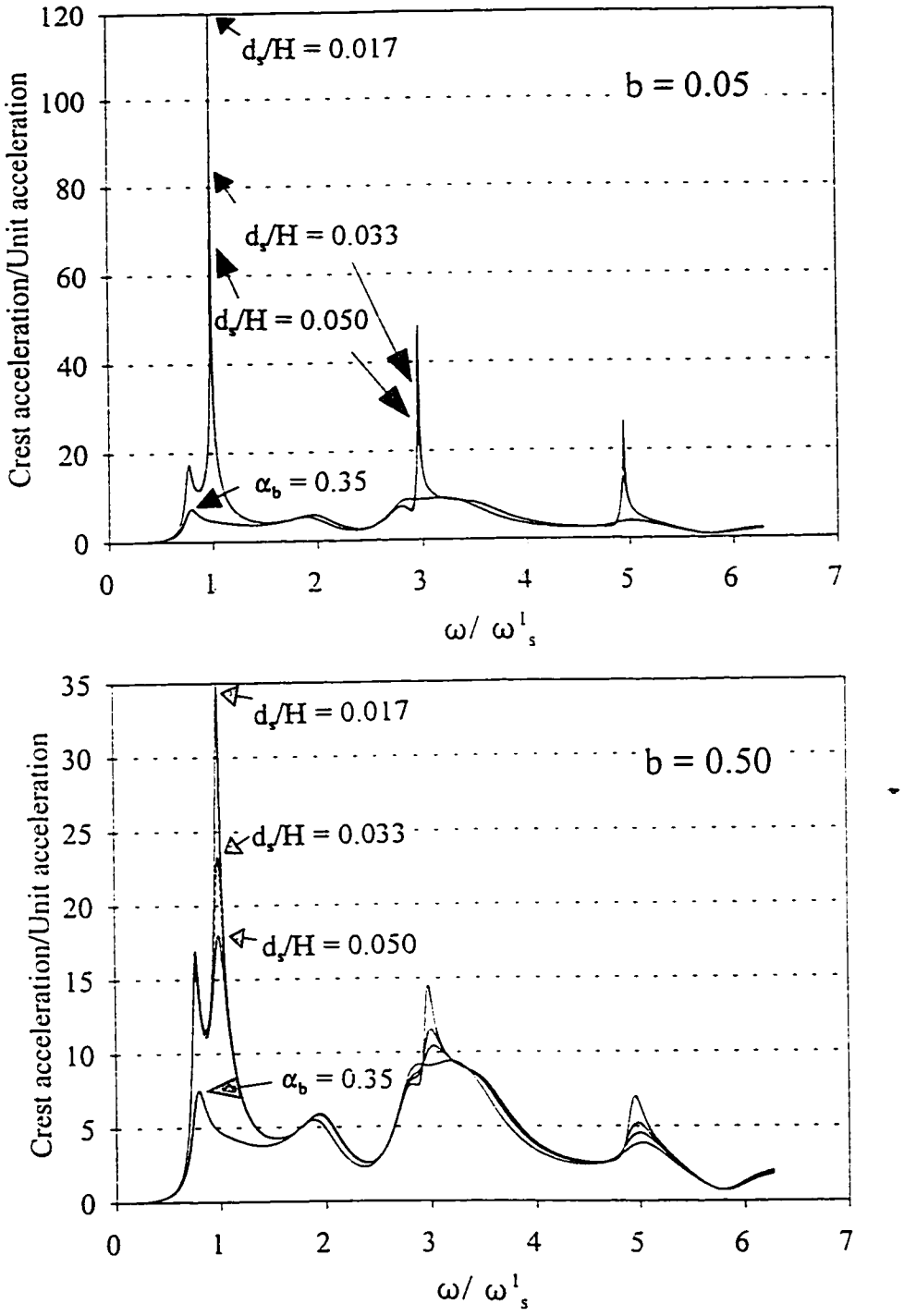

Fig. 2.9 Effect of the layer thickness on the crest acceleration response of the dam on rigid foundation subject to vertical excitation (E_s= 4500 MPa)

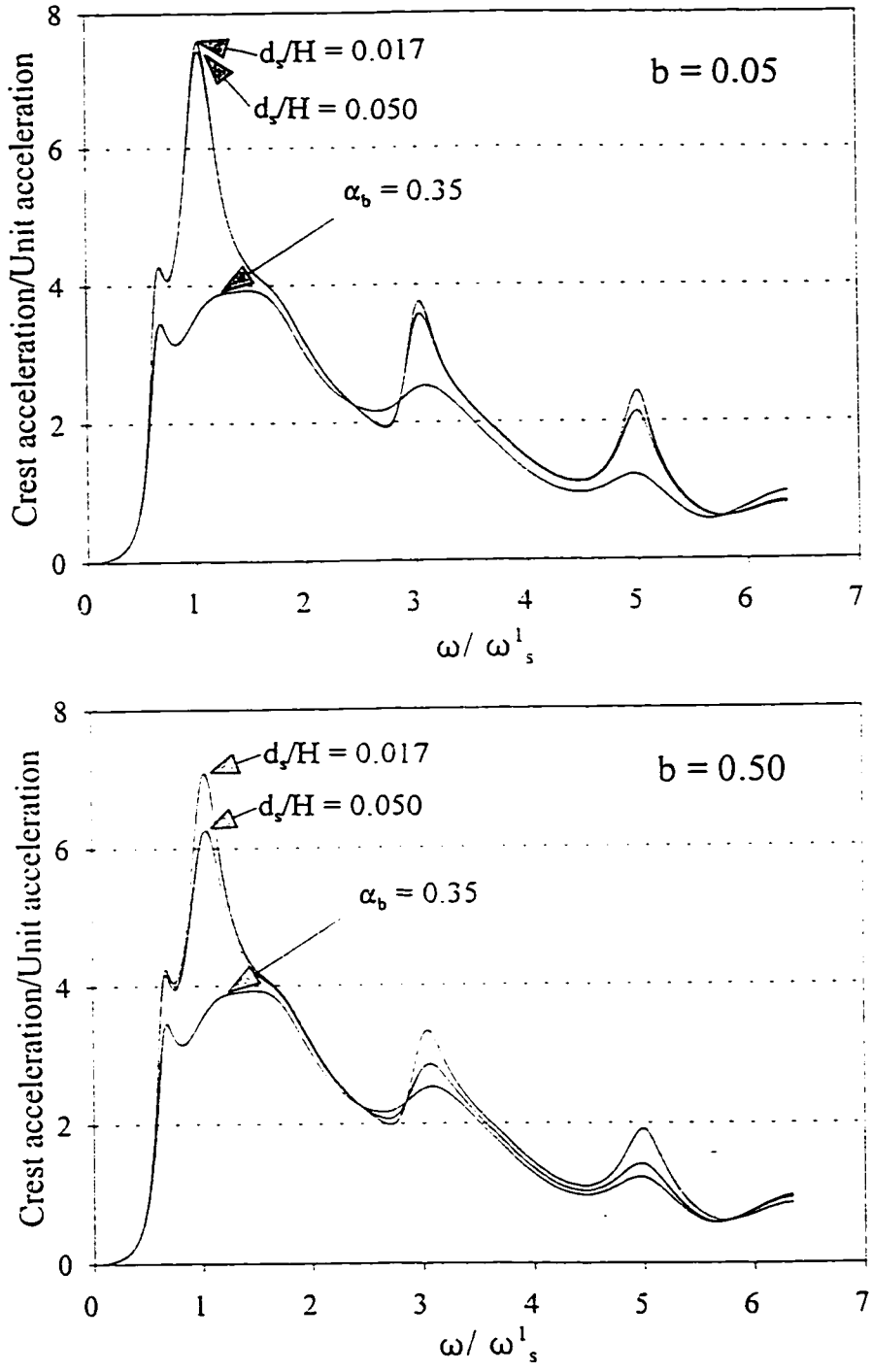

Fig. 2.10 Effect of the layer thickness on the crest acceleration response of the dam on flexible foundation subject to vertical excitation (E_f= 23000 MPa,E_s/E_f= 0.2)

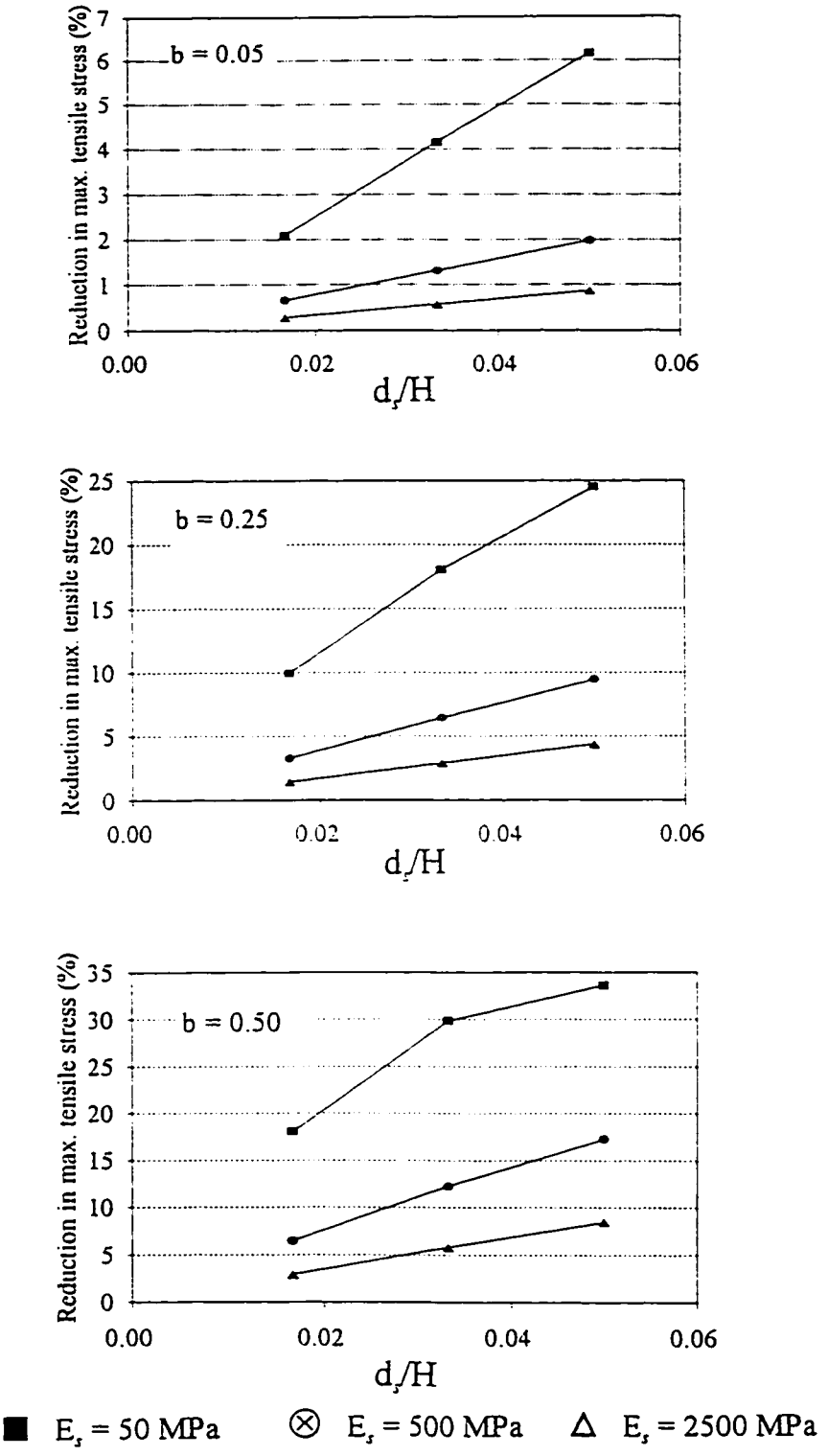

Fig. 2.11 Effect of the thickness and modulus of elasticity of the sediment layer on the structural response reduction of the dam on rigid foundation subject to horizontal excitation

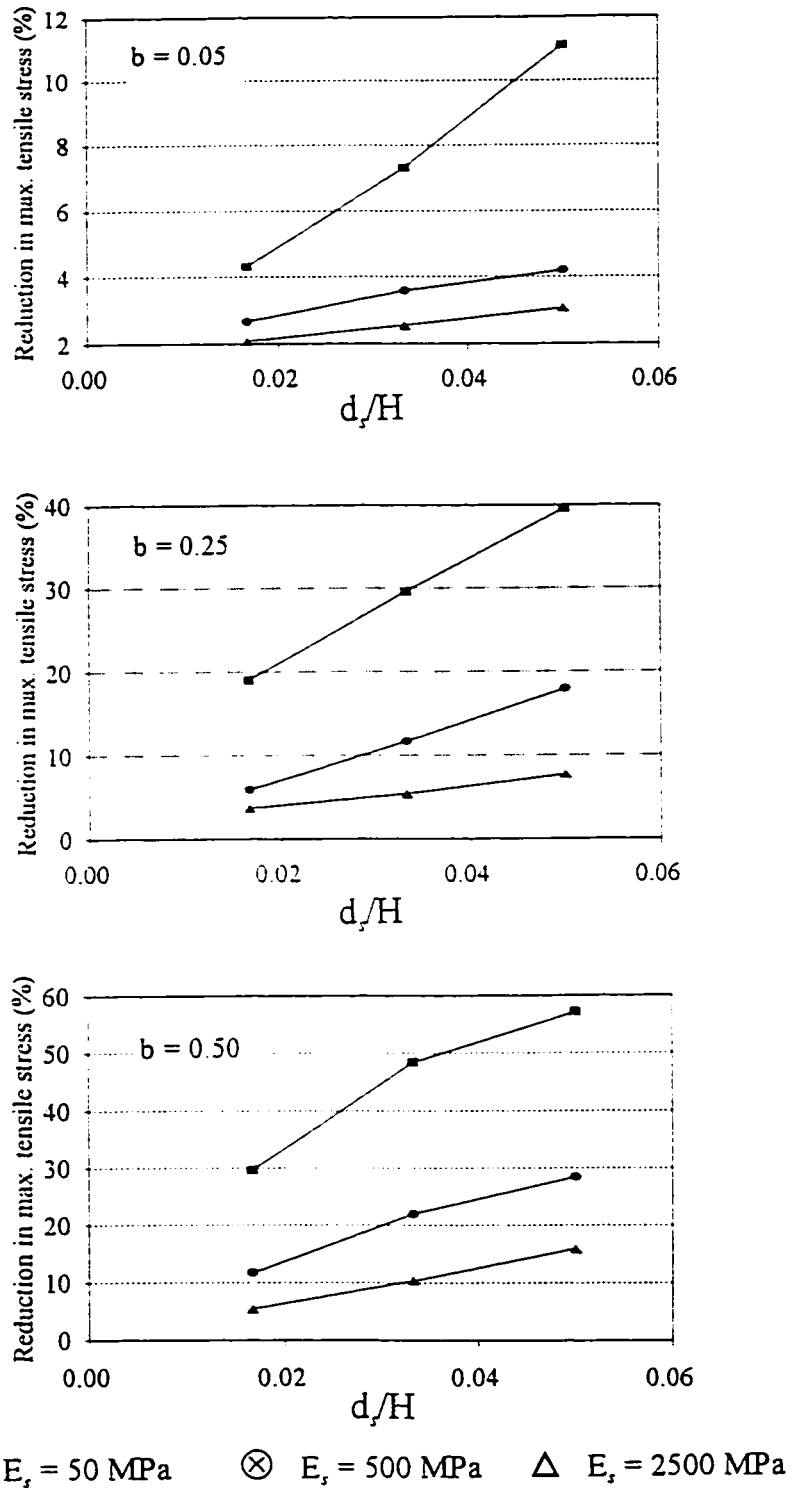

Fig. 2.12 Effect of the thickness and modulus of elasticity of the sediment layer on the structural response reduction of the dam on a rigid foundation subject to vertical excitation

CHAPTER 3

DAM-RESERVOIR BOUNDARY

3.1 INTRODUCTION

The interface of the dam with the impounded water is an important boundary where the static and hydrodynamic forces are applied to the dam structure. Theses forces provide a significant contribution to the seismic response analysis and design of the dam. The maximum hydrodynamic pressure on the dam when subjected to a moderately strong earthquake ground motion may reach the magnitude of the hydrostatic pressure (Chopra 1967, Hanna and Humar 1983, Tsai and Lee 1989). Current approaches to the seismic analysis of dams assume a completely reflective boundary at the dam-reservoir interface. This assumption may not be realistic since a partially absorptive surface is a closer representation of the physical characteristics of the dam face boundary.

In this chapter, an analysis of the earthquake response of a concrete dam with a general boundary condition at its interface with the reservoir is conducted. The commonly used condition of a completely reflective boundary is replaced with a more general form of a partially absorptive surface. The resulting boundary value problem is solved and implemented in the analysis to examine the effect of boundary absorption on the seismic response of the concrete dam. The analysis is applied to both cases of an infinite reservoir and a finite-length reservoir subject to horizontal and vertical excitations.

The introduction of an artificial absorptive boundary at the dam-reservoir interface

represents an attempt for hydrodynamic isolation. The function of the isolation material is to reduce the hydrodynamic forces transmitted to the dam structure from the reservoir during an earthquake. Due to its important application in seismic response reduction of the concrete dam, the effects of the thickness and material properties of the isolation layer on the structural response reduction are investigated. Practical considerations concerning the design and installation of the isolation layer are presented followed by the overall conclusions based on the results of the analysis.

3.2 EFFECT OF A PARTIALLY REFLECTIVE DAM-RESERVOIR INTERFACE

3.2.1 Theoretical formulation

Infinite-Length Reservoir

The analysis is carried out in the frequency domain using a two dimensional model of the concrete dam (Fig. 3.1). The substructure method is applied using modal analysis for the dam structure together with a closed form solution for the infinite-length reservoir continuum (Fenves and Chopra 1984a). The hydrodynamic pressure in the reservoir is evaluated by solving the governing pressure wave equation in the frequency domain together with the appropriate boundary conditions. With the assumption of linearly compressible and non-viscous water, the small amplitude irrotational vibration of the reservoir is governed by Helmholtz equation:

$$\frac{\partial^2 P}{\partial x^2} + \frac{\partial^2 P}{\partial y^2} + \frac{\omega^2}{C_w^2} P = 0 \tag{3.1}$$

where $P(x,y,\omega)$ is the complex-valued frequency response function for the hydrodynamic pressure, C_w is the travelling speed of pressure wave in water and ω is the frequency of excitation.

In past studies of the hydrodynamic pressure in the reservoir, the upstream surface of the concrete dam has been assumed to be completely reflective. However, it is possible to evaluate the equivalent wave reflection coefficient of this boundary based on the physical properties of concrete. For typical values of the modulus of elasticity and the specific density of concrete, $E_c = 2.24\times10^4$ MPa and $\rho_c = 2.48\times10^3$ kg/m^3, the traveling speed of dilatational waves in concrete, C_c, is equal to $(E_c/\rho_c)^{1/2} = 3005$ m/s. It is assumed that the specific density and the travelling speed of pressure waves in water are $\rho_w = 1000$ kg/m^3

and C_w = 1440 m/s, respectively. The relative acoustic impedance of concrete with respect to that of water, β_c, can be obtained as: $\beta_c = \rho_c C_c / \rho_w C_w = 5.175$. The wave reflection coefficient, α_d, which is defined as the relative amplitude of the reflected wave to the amplitude of the incidental wave normal to the dam-water interface, can be computed using the relative impedance, β_c, as: $\alpha_d = (\beta_c - 1)/(\beta_c + 1) = 0.676$. The relative impedance, β_c, is calculated based on the assumption that the effect of reflected waves from the downstream face of the dam on the hydrodynamic pressure at the dam-reservoir boundary is negligible. Therefore, the magnitude of the wave reflection coefficient, α_d, of the concrete dam with finite thickness is expected to be slightly higher than the calculated value of 0.676. Traditionally, in studies of the effect of reservoir bottom sediments on the hydrodynamic pressure, the wave reflection coefficient is normally assigned values in the range of 0.68-0.85 (Chopra and Chakrabarti 1981, Hall and Chopra 1982, Hall 1986, Staurdi and Prato 1990). These values are higher than the equivalent wave reflection coefficient of the concrete dam face.

In the present study, a soft layer is assumed to be attached to the upstream face of the dam. This layer which partially absorbs the incident pressure waves from the reservoir is referred to as the *isolation layer*. Due to the finite thickness and geometry of the concrete dam, the reflected waves from the downstream face of the dam and the dam-layer interface may slightly alter the equivalent value of the wave reflection coefficient at the upstream face of the dam. However, the effect of waves reflected back to the reservoir is neglected. It is assumed that the reflected waves from the layer-dam interface and the downstream side of the dam are dissipated within the soft layer before re-entering the reservoir. The boundary condition for the partially reflective surface of the dam covered with a soft layer is written as:

$$\frac{\partial P}{\partial x}(0,y,\omega) = -\rho_w [\, 1 - \omega^2 q_{hl}(y,\omega) + \sum_{j=1}^{NRTZ} \psi_j(y)\ \ddot{Y}_j(\omega)\,] \qquad (3.2)$$

where

$\psi_j(y)$ is a continuous function representing the jth mode shape of the dam

NRTZ is the number of Ritz vectors in the dam-foundation system

$\ddot{Y}_j(\omega)$ is the complex frequency response function of the generalized coordinate $\ddot{Y}_j(t)$ with the dots representing time derivatives

$q_{hl}(y,\omega)$ is the frequency response function for the horizontal displacement of the dam-reservoir interface due to the interaction between the impounded water and the soft layer attached to the upstream face of the dam

The three different terms on the right hand side of Eq. 3.2 correspond to the free-field ground motion (rigid-body vibration of the dam in horizontal direction), the acceleration of the solid particle at the surface of the dam due to the effect of the impinging waves from the reservoir and the acceleration of the boundary due to the flexible structural response of the dam, respectively. The response of a solid boundary to the incidental water pressure waves depends not only on the overall response of the dam structure but also on the soft layer's acoustic impedance $\rho_l C_l$ where ρ_l is the density of the material and C_l is the speed of travelling dilatational waves in the material. In the case where the soft isolation layer is so supported that flexible vibrational mode shapes are insignificant, the developed hydrodynamic pressure in the reservoir is still dependent on the impedance of the wall material.

The dam-reservoir interface is treated as an absorptive boundary in a similar fashion to the analysis of reservoir bottom sediments (Fenves and Chopra 1984a). An approximate one-dimensional model for the absorption of water pressure waves at the surface of the dam

is considered. In this approximation, the dam is assumed to consist of hypothetically independent horizontal layers which receive the impinging pressure waves at right angles to the dam-reservoir interface. The ratio of the intensities of the reflected and incidental waves from a solid boundary remains virtually unchanged for incidental angle up to about 15° (Brekhovskikh and Maksimovich 1991). Accordingly, a small angle of inclination for the incident waves is assumed not to introduce significant errors in the results.

The frequency response function $q_{hl}(y,\omega)$ can be related to the hydrodynamic pressure at the upstream face of the dam through the compliance function $\Gamma_l(\omega)$:

$$q_{hl}(y,\omega) = -\Gamma_l(\omega) \cdot P(0,y,\omega) \tag{3.3}$$

The function $\Gamma_l(\omega)$ is obtained from the solution of the wave equation in the isolation layer subject to the appropriate boundary conditions as:

$$\Gamma_l(\omega) = \frac{1}{\rho_l C_l \omega} i \tag{3.4}$$

where $i=\sqrt{-1}$ and $C_l = (E_l/\rho_l)^{1/2}$. With the substitution of Eqs. 3.3 and 3.4 into Eq. 3.2, the boundary condition at the reservoir-isolation layer interface is written as:

$$[\frac{\partial}{\partial x} + i\omega q_l]\, P(0,y,\omega) = -\rho_w [\, 1 + \sum_{j=1}^{NRTZ} \psi_j(y)\ \ddot{Y}_j(\omega)\,] \tag{3.5}$$

where $q_l = \rho_w/\rho_l C_l$. For the streamwise horizontal ground motion, the boundary conditions at the reservoir bottom and reservoir free surface are:

$$[\frac{\partial}{\partial y} - i\omega q_f]\, P(x,0,\omega) = 0 \tag{3.6}$$

$$P(x,H,\omega) = 0 \tag{3.7}$$

In Eq. 3.6, $q_f = \rho_w / \rho_f C_f$ where ρ_f and C_f are the mass density and the travelling speed of dilatational waves in the reservoir foundation, respectively. The frequency response function $P(x,y,\omega)$ for the hydrodynamic pressure in the reservoir of depth H, is the solution of Eq. 3.1 subject to the boundary conditions 3.5 to 3.7 together with the radiation condition at the upstream boundary of the reservoir. The frequency response function for the hydrodynamic pressure can be written as:

$$P(x,y,\omega) = P_0^x(x,y,\omega) + \sum_{j=1}^{NRTZ} \ddot{Y}_j(\omega).P_j^f(x,y,\omega) \tag{3.8}$$

where $P^x{}_o(x,y,\omega)$ is the frequency response function due to the horizontal acceleration of a rigid dam and $P_j^f(x,y,\omega)$ is the frequency response function due to the horizontal acceleration of the deflected dam associated with the jth Ritz vector. The solutions of the boundary value problem for the hydrodynamic pressure due to rigid body motion and flexible response of the dam are:

$$P_o^x(x,y,\omega) = -2\rho_w H \sum_{n=1}^{\infty} \frac{\zeta_n^2(\omega)}{H[\zeta_n^2(\omega) - (\omega q_f)^2] + i\omega q_f} . \frac{I_{on}(\omega)}{K_n + i\omega q_l} . e^{K_n x} . \Lambda_n(y,\omega) \tag{3.9}$$

$$P_j^f(x,y,\omega) = -2\rho_w H \sum_{n=1}^{\infty} \frac{\zeta_n^2(\omega)}{H[\zeta_n^2(\omega)-(\omega q_f)^2]+i\omega q_f} \cdot \frac{I_{jn}(\omega)}{K_n+i\omega q_l} \cdot e^{K_n x} \cdot \Lambda_n(y,\omega) \qquad (3.10)$$

where

$K_n = [\zeta_n{}^2(\omega) - \omega^2/C_w{}^2]^{1/2}$

$\zeta_n(\omega)$ is the nth eigenvalue of the impounded water

$\Lambda_n(y,\omega)$ is the nth eigenfunction of the impounded water given by:

$$\Lambda_n(y,\omega) = \frac{1}{2\zeta_n(\omega)}\{[\zeta_n(\omega)+\omega q_f]e^{i\zeta_n(\omega)y}+[\zeta_n(\omega)-\omega q_f]e^{-i\zeta_n(\omega)y}\} \qquad (3.11)$$

$I_{0n}(\omega)$ and $I_{jn}(\omega)$ are defined as:

$$I_{0n}(\omega) = \frac{1}{H}\int_0^H \Lambda_n(y,\omega)\,dy \qquad (3.12)$$

$$I_{jn}(\omega) = \frac{1}{H}\int_0^H \psi_j(y)\Lambda_n(y,\omega)\,dy \qquad (3.13)$$

Although Eqs. 3.9 and 3.10 account for the contribution of an infinite number of modes in the hydrodynamic response, the number of significant modes is limited by the highest frequency of excitation considered in the analysis.

Effect of the Reservoir Length

In the case of a reservoir of finite length, L, a partially absorptive boundary condition replaces the radiation condition of the infinite reservoir at the far side. The presence of a reflective boundary at the far end of the reservoir introduces horizontal modes in the solution

of the hydrodynamic pressure in the reservoir. For a complete solution, the single summations in expressions 3.9 and 3.10 should be replaced by sets of double summations over the reservoir eigenvectors in both horizontal and vertical directions. Such a theoretical solution for a general case of reservoir shape and boundary conditions is not available. In analogy with Eqs. 3.9 and 3.10, however, one may express the solution for the hydrodynamic pressure in the reservoir of rectangular shape in the form (Hatami and Ghobarah 1995):

$$P_j^f(x,y,\omega) = -2\rho_w H \sum_{n=1}^{\infty} \frac{\mu_n^2(\omega)}{H[\mu_n^2(\omega)-(\omega q_f)^2]+i\omega q_f} \cdot \frac{I_{jn}(\omega)}{K_n - i\omega q_l} \cdot \frac{e^{K_n x}\frac{K_n+i\omega q_u}{K_n-i\omega q_u} + e^{-2K_n L} e^{-K_n x}}{\frac{K_n+i\omega q_l}{K_n-i\omega q_l}\cdot\frac{K_n+i\omega q_u}{K_n-i\omega q_u} - e^{-2K_n L}} \cdot \Lambda_n(y,\omega) \tag{3.14}$$

where $I_{jn}(\omega)$ is given by Eq. 3.13 when the effect of ground motion at the far boundary is neglected. In the case of the rigid body motion of the dam, $I_{0n}(\omega)$ given by Eq. 3.12 replaces $I_{jn}(\omega)$ in Eq. 3.14. Damping coefficients of dam upstream surface, reservoir foundation and reservoir far boundary are denoted by q_l, q_f and q_u, respectively.

For the case of an infinite-length reservoir ($L \rightarrow \infty$), Eq. 3.14 reduces to the expression for the hydrodynamic pressure given by Eq. 3.10. In the case of a finite-length reservoir confined within solid boundaries, it is expected that the response reduction due to the partially absorptive dam boundary is more significant than for the case of the reservoir of infinite length.

The distribution of hydrodynamic pressure in the reservoir of finite length subject to the horizontal ground motion is represented by Eq. 3.14. A major assumption in deriving Eq. 3.14 is to neglect the interaction effect of off-diagonal reservoir modes in the horizontal and vertical directions; i.e., only the diagonal terms in the summations are kept in the series

expansion of the solution. The problem is also solved using the finite element method introduced in Chapter 4. The results of the structural response based on the two approaches are compared to examine the margin of error involved in the approximate closed-form solution given in Eq. 3.14.

For uniform vertical excitation of the reservoir, the solution for the hydrodynamic pressure is independent of the horizontal coordinate (Fenves and Chopra 1984a). Such a solution is not capable of including the variations of boundary conditions along the reservoir sides; namely, partial absorption of pressure waves into the boundaries. Moreover, the boundary value problem of the reservoir with general boundary conditions at the sides when the reservoir is subjected to vertical excitation does not form a separable homogeneous Sturm-Liouville problem due to the excitation of the reservoir bottom. Accordingly, the latter problem was tackled numerically using the finite element procedure described in Chapter 4.

3.2.2 Numerical Example

To evaluate the effect of a partially absorptive dam-reservoir interface on the dam response, a numerical example is analyzed. A typical cross section of a 91.44 m high concrete dam with a downstream slope of 0.8:1.0, is considered. The upstream face of the dam is assumed to be vertical. The modulus of elasticity of concrete is taken to be 21,500 MPa and Poisson's ratio is taken to be 0.2. Water is assumed compressible with the travelling speed of the acoustic wave C_w = 1440 m/s. The ground motion used in the analysis is the S69E component recorded at Taft Lincoln School Tunnel during 1952 Kern County earthquake. This earthquake record has been extensively used in the analysis of dams because the record's predominant frequency coincides with that of many dams.

The dam foundation rock is assumed rigid and the reservoir bottom is assumed to be

completely reflective. In the case of the finite reservoir, the far boundary is assumed as totally reflective, Eqs. 3.9 and 3.10 were used to obtain the frequency response of the dam with a partially reflective upstream surface impounding a reservoir of infinite length. For the case of the finite-length reservoir, Eq. 3.14 as the simplified closed-form solution together with the finite element procedure introduced in Chapter 4 were used. A simplified procedure was applied using the first two mode shapes of the dam in the analysis (Baumber and Ghobarah 1995). The accuracy of the procedure was shown to be satisfactory provided that the dominant frequencies of excitation are smaller than the frequency of the second mode of the dam monolith. Since this is normally the case for many concrete gravity dams, the analysis is considered to be valid for a wide range of practical applications.

Infinite reservoir

The isolation layer contributes to the hydrodynamic pressure reduction as a low reflection coefficient material. This effect can be isolated by neglecting the effect of the layer thickness. In the case of a full reservoir with an infinite-length, the main contribution to the dam response is due to the fundamental mode of vibration of the dam-reservoir system as shown in Fig. 3.2. With the reflection coefficient $\alpha_d = 2/3$, a 40% reduction of response at the fundamental frequency of the system is obtained. In practical terms, it appears possible to design an attached soft layer with reflection coefficient $\alpha_d = 2/3$. In terms of stresses, Figs. 3.3b and 3.3c show a range of 30-40% reduction which brings the maximum developed stresses below the allowable tensile stress of concrete and reduces the risk of crack initiation and propagation in the dam monolith.

Effect of the reservoir length

The effect of a partially absorptive boundary at the dam face on response reduction is more appreciable for a reservoir of finite length. For a short reservoir length of L/H = 1 with $\alpha_d = 2/3$ for the absorptive layer, the reduction in response at the fundamental frequency of the dam-reservoir system is approximately 57% (Figs. 3.4 and 3.5). The amount of reduction decreases for higher values of L/H and remains nearly constant for L/H > 2. Figure 3.5 shows the relationship between the L/H ratio and the amount of response reduction at the fundamental frequency of the dam-reservoir system.

The structural response of the dam monolith with a finite-length reservoir shown in Fig. 3.4 is obtained using the approximate closed-form solution given by Eq. 3.14. The closed-form solution captures the higher frequency peaks due to the effect of reflected waves from the far boundary. The corresponding finite element solution, however, indicates larger number of reponse peaks due to the additional horizontal modes (Fig. 3.6). Comparison of Figs. 3.4 and 3.6 reveals that the additional peaks are secondary to the principal higher frequency peaks and do not introduce significant modifications to the monolith response. The general trend of the monolith frequency response obtained with the finite element procedure shows a good agreement with the results based on the closed-form solution (Figs. 3.4 and 3.6). The fundamental peak of the crest acceleration response is somewhat (about 20%) overestimated based on the closed-form expression and does not include the singularity of response at $\omega = \omega'_s$ as is captured by the finite element approach (Fig. 3.6). For the case of $\alpha_d < 1.0$, the aforementioned differences between the two approaches are significantly reduced.

The monolith response when subjected to vertical ground motion is shown in Fig. 3.7. The reservoir bottom and far boundary are assumed as completely reflective which is the

cause of the singular peaks of the response in the figure. The dam boundary is considered with different reflectivity conditions as shown. From Fig. 3.7, it is concluded that the effect of an absorptive dam boundary on the reduction of the monolith response becomes more significant as the L/H ratio is decreased. This conclusion is in accordance with the effect of a partially absorptive dam boundary subject to horizontal excitation.

Comparison of Figs. 3.6 and 3.7 reveals that the effect of reservoir's finite length on the monolith response when subjected to horizontal and uniform vertical ground motions are different. In the case of horizontal ground motion, a longer reservoir with a reflective far end introduces a larger number of peaks in the structural response of the dam but has little effect on the magnitude of the fundamental peak of the response (Fig. 3.6). In the case of the uniform vertical excitation of the reservoir, the longer reservoir has a more noticeable effect on the fundamental peak of the monolith response compared to the horizontal excitation but has little effect on the number of frequency response peaks of the dam (Fig. 3.7). The results shown in Fig. 3.7 also reveal the dependence of the monolith response on the boundary condition of the dam-reservoir interface when the system is subjected to uniform vertical excitation. The latter effect as well as the reservoir length effects are not captured by the special case theoretical solution for the hydrodynamic pressure currently available in the EAGD-84 program (Fenves and Chopra 1984b).

Compared with the infinite case, higher modes of reservoir vibration are present in a limited-length reservoir; a soft dam boundary reduces the response of the dam at higher frequencies considerably. As the ratio of L/H increases, the number of resonant peaks increases accordingly; yet, all the amplitudes of the response peaks are reduced due to the absorption effect of the upstream layer.

3.3 HYDRODYNAMIC ISOLATION

3.3.1 Introduction

During an earthquake, the contribution of the hydrodynamic pressure to the seismic response of a concrete gravity dam is significant. The resulting stresses may lead to crack initiation and propagation inside the dam during a moderately strong seismic event. The direct approach for response reduction of a concrete dam is to increase its structural damping to a desired high value. However, due to the nature of the dam structure and the concrete material properties there is little that can be done on the structural damping aspect of response reduction. The idea of reducing the hydrodynamic loading on the dam appears to be a promising approach for seismic response reduction of concrete dams.

In this part of the study, the possibility of reducing the hydrodynamic pressure on the dam is investigated. An absorptive layer attached to the upstream face of the dam is considered. The resulting boundary value problem for the hydrodynamic pressure is solved for the cases of infinite and finite-length, rectangular shaped reservoirs. The response of an isolated dam is compared with the response of an unisolated dam. The effect of the thickness and material properties of the isolation layer on the extent of response reduction is evaluated. A set of criteria is developed for the design of the isolation layer material.

The isolation layer is assumed attached to the upstream face of the dam as shown in Fig. 3.8. The layer reduces the dam response due to the hydrodynamic effect of the reservoir in essentially two different ways:

a) The layer serves as a boundary for the reservoir with a low reflection coefficient which results in reduction in the developed hydrodynamic pressure in the reservoir compared with the case of a completely reflective boundary. This effect was addressed in the previous part of the theoretical solution excluding the layer's isolation effects.

b) The isolation of the dam from the hydrodynamic pressure is the result of the layer thickness as well as its material properties which alter the amplitude of the transmitted pressure wave across the layer.

3.3.2 Mathematical Model

The compliance function $\Gamma_l(\omega)$ in Eq. 3.4 depends only on the characteristics of the upstream surface of the layer without any explicit reference to its thickness and the associated dissipation of the incident waves across the layer. However, in practical terms, a thick layer introduces an additional decaying effect towards reducing the influence of the reservoir loading on the dam. With the assumption of a homogeneous and viscoelastic material for the upstream layer, the one-dimensional wave equation including the material damping is written as:

$$\frac{\partial^2 u}{\partial t^2} - \frac{\eta_l}{\rho_l}\cdot\frac{\partial^3 u}{\partial t \partial x^2} - \frac{E_l}{\rho_l}\cdot\frac{\partial^2 u}{\partial x^2} = 0 \qquad (3.15)$$

where

$u(x,t)$ is the longitudinal displacement, t is time

η_l is the viscosity coefficient of the isolation layer

ρ_l is the mass density of the layer material

E_l is the Young's modulus of elasticity

x is the spatial coordinate in streamwise direction with the origin at the upstream face of the dam

Introducing $u(x,t) = \bar{u}(x,\omega)\, e^{i\omega t}$ in Eq. 3.15 for the steady-state response, the Helmholz equation is obtained in the form:

$$\frac{\partial^2 \bar{u}(x,\omega)}{\partial x^2} + \gamma_l^2 \bar{u}(x,\omega) = 0 \tag{3.16}$$

where

$$\gamma_l = \frac{\omega}{C_l\left(1 + \frac{i\eta_l\omega}{E_l}\right)^{1/2}} \tag{3.17}$$

The equilibrium condition at the surface of the layer ($x = -t_l$) is:

$$E_l \frac{\partial \bar{u}}{\partial x}\Big|_{(-t_l,\omega)} = 1 \tag{3.18}$$

With the soft layer attached to the upstream face of the dam, the kinematic boundary condition at the dam-layer interface is $\bar{u}(0,\omega) = 0$. The solution of Eq. 3.16 subject to the above boundary conditions is:

$$\bar{u}(x,\omega) = \frac{1}{E_l \gamma_l} \cdot \frac{Sin(\gamma_l x)}{Cos(\gamma_l t_l)} \tag{3.19}$$

The resulting pressure on the upstream face of the dam ($x = 0$) is obtained as:

$$\bar{\sigma}(0,\omega) = \frac{1}{Cos\,[\theta(\omega)]} \tag{3.20}$$

where:

$$\theta(\omega) = \frac{\omega t_l}{C_l\left(1 + \frac{i\eta_l\omega}{E_l}\right)^{1/2}} \tag{3.21}$$

The modulus of the complex-valued pressure, $\bar{\sigma}(0,\omega)$, represents the fraction of the unit amplitude hydrodynamic pressure transmitted to the upstream face of the dam at the frequency of ω and hereafter is referred to as the *transmissibility ratio, TR* . Accordingly, the hydrodynamic terms in the global system of equations for the solution of the generalized coordinates (Fenves and Chopra 1984a) are multiplied by $|\bar{\sigma}(0;\omega)|$.

The effectiveness of the isolation is strongly dependent on the characteristics of the upstream layer as shown by Eqs. 3.20 and 3.21. A typical variation of the transmissibility ratio with respect to the frequency of excitation for different values of the layer viscosity is shown in Fig. 3.9. The *viscosity parameter,* f_l, is defined in terms of the viscosity coefficient of the layer, η_l and other mechanical properties as:

$$f_l = \frac{\eta_l}{\rho_l C_l t_l} \tag{3.22}$$

Due to the significance of the vibration of the reservoir at its fundamental mode, the frequency is normalized to the fundamental frequency of the impounded water, ω^1_r. Alternatively, the coupled frequency of the dam-reservoir system at the fundamental mode, ω^1_c , may be used. The frequency range of interest in hydrodynamic isolation is in the vicinity of $\omega/\omega^1_r=1$ or $\omega/\omega^1_c=1$. In the present analysis, the ratio ω/ω^1_r is used. The nth natural frequency of a reservoir of depth H is:

$$\omega^n_r = (2n-1)\frac{\pi C_w}{2H} \tag{3.23}$$

Depending on the relative natural frequencies of the isolation layer and the reservoir, the hydrodynamic loading on the dam may be reduced or magnified. The isolation layer reduces

the hydrodynamic pressure on the dam in the region where the transmissibility ratio is lower than 1.0 (Fig. 3.9). This implies that in order to reduce the transmitted pressure to the dam-layer interface it is necessary that: $\omega_l/\omega^1_r < 1$ where ω_l is the first free vibration frequency of the layer of thickness t_l given by:

$$\omega_l = \frac{\pi . C_l}{2t_l} \tag{3.24}$$

In the frequency range $\omega > \hat{\omega}$, where $\hat{\omega}$ denotes the non-zero frequency corresponding to unit transmissibility ratio, higher viscosity coefficient reduces the efficiency of the isolation. However, if the viscosity of the layer material is too low, other peak values corresponding to higher modes result in transmissibility ratios greater than 1.0. In this case, adding the viscosity to the layer is an advantage because it reduces the magnitude of the higher frequency peaks as shown in Fig. 3.9. In the case of a very low viscosity of the isolation layer material, higher frequency peaks occur according to Eqs. 3.20 and 3.21. In the limiting case of no viscosity, the period of the function $\bar{\sigma}(0,\omega)$ in terms of the circular frequency, ω, is $2\pi C_l/t_l$ during which the transmissibility ratio tends to infinity twice. As the viscosity increases, the imaginary term in the denominator of $\theta(\omega)$ is increased proportional to k for the kth higher peak which lowers the contribution of higher harmonics in the plot of the transmissibility ratio.

The critical values of the layer viscosity, η_{lc}, below which the higher harmonic effect is significant, can be obtained numerically. The variation of η_{lc} with layer characteristics is plotted in Fig. 3.10. The viscosity parameter f_l is the slope of the η_{lc} curve. The minimum value of viscosity obtained from Fig. 3.10 can be used to evaluate the minimum transmissibility of the hydrodynamic pressure to the upstream face of the dam. Figure 3.11

shows the transmissibility as a function of the frequency ratio, R_f, and its variation with the viscosity of the material in the isolation layer. The lowest transmissibility ratio corresponds to the curve with $f_l = (f_l)_{cr}$. The frequency ratio R_f can be expressed as:

$$R_f = \frac{C_l / C_w}{t_l / H} \tag{3.25}$$

The ratio $\hat{\omega}/\omega_l$ (Fig. 3.9) was found to vary in the range of 1.55 to 1.65 which is slightly different from the expected value of $\sqrt{2}$. Accordingly, for the upstream layer to reduce the hydrodynamic pressure on the dam, it is necessary that $R_f < 0.6$. For $C_w = 1440$ m/s, Eq. 3.25 indicates that:

$$C_l = \left(\frac{E_l}{\rho_l}\right)^{1/2} < 860 \left(\frac{t_l}{H}\right) \tag{3.26}$$

The upperbound value for the elasticity modulus to specific density ratio (E_l / ρ_l) for the isolation layer limits the selection of the material to very soft substances in the range of foams or similar materials. The reason for this is the low frequency range of interest for hydrodynamic isolation.

3.3.3 Numerical Study

The layer thickness and material properties contribute to the reduction of the hydrodynamic effects as an isolation medium. Figs. 3.12a to 3.12d show the amount of response reduction with respect to the frequency ratio R_f, for the layer with completely reflective surface (α_l=1.0). Fig. 3.12a indicates the amount of reduction of the fundamental peak of the dam crest acceleration. Fig. 3.12b shows the percentage reduction of the mean

value of the crest displacement over a 20s period. Although the maximum displacement of the dam crest is also reduced due to the effect of isolation, the mean value over a period of time is selected for comparison purposes because it provides a more reliable measure of response reduction. The reduction in the maximum tensile stresses in the dam due to the isolation is shown in Figs. 3.12c and 3.12d. The response reductions for the case of a layer with a partially reflective surface ($\alpha_l = 2/3$) are shown in Fig. 3.13.

The frequency response function of the crest acceleration for the two limiting cases of full reservoir with no isolation layer and dam without reservoir are compared in Fig. 3.14. The presented results are based on a material of assumed $\rho_l = 1500$ kg/m^3 and $E_l = 500$ kPa. In the case of a thin isolation layer ($t_l/H = 0.01$), the response reduction of the dam is mainly dependent on the wave reflection coefficient of the surface of the isolation layer, α_l (Fig. 3.2). With lower α_l, lower hydrodynamic pressure at the fundamental frequency of the reservoir develops. As both the softness and the thickness of the isolation layer is increased (lower R_f in Fig. 3.13a, $t_l/H = 0.02$ in Fig. 3.14), the peak of the acceleration response approaches the peak of the no-reservoir case with larger magnitude. It appears that for low value of α_l, softer isolation layer reduces the amount of reduction of the peak frequency response value of the dam crest acceleration (Fig. 3.13a). In terms of overall crest response as well as developed stresses in the dam, however, this does not necessarily result in a lower response reduction. A major factor is the ratio of the dominant frequency of the input earthquake to ω'_c. Fig. 3.15 shows the frequency spectrum of the S69E component of the 1952 Taft earthquake. From the figure, the dominant frequency of the record is in the vicinity of 14 rad/s. Since the fundamental frequency of the dam without the reservoir ($\omega'_s = 25.03$ rad/s) is farther away from the dominant ground motion frequency than the coupled frequency with full reservoir ($\omega'_c = 19.25$ rad/s), a thicker and softer isolation layer results

in more reduction of the maximum tensile stress in the dam and the crest displacement as shown in Figs. 3.12 and 3.13.

A soft isolation layer with low value of R_f, suppresses the effect of reservoir in the overall response function of the dam-reservoir system and shifts the fundamental frequency of the system from the coupled frequency of ω'_c to the fundamental frequency of the concrete dam without the reservoir, ω'_s as shown in Figs. 3.16a and 3.16b. The direction of the frequency shift is in accordance with the experimental results of As'kov *et al.* (1992) and Gellis *et al.* (1992). As the isolation layer becomes softer and thicker, the two separate peaks at ω'_c and ω'_s get closer to each other and eventually form a single peak at ω'_s (Fig. 3.14). Although this effect suppresses the fundamental peak of the reservoir to a considerable extent, higher-frequency peaks of the structure spectrum become significant. The effects of the thickness and material type of the isolation layer are presented in Fig. 3.17. For a given type of the isolation material, a thicker layer results in higher reduction of the dam response. The effect of the layer thickness is more significant for lower values of $1/C_l$.

The amount of reduction of the maximum tensile stresses in the dam near the heel and at the downstream side of its cross section is more than 60% for $R_f < 0.1$ (Figs. 3.12 and 3.13). It follows that provided ω_l is less that 10% of ω'_r, the dam is essentially isolated from the dynamic effect of the impounded water. This conclusion can also be made by examining Fig. 3.11.

Based on the results of the analysis, a guideline for the design of the isolation layer may be suggested. The isolation layer can be designed on the basis of the expected predominant frequency content of the ground motion at the dam site and coupled frequency of the dam-reservoir system. The objective is to shift the dam-reservoir coupled frequency away from the frequency range associated with a high seismic energy. The range of variation

for the material properties can be obtained from Figs. 3.17 to 3.19 together with Eq. 3.26. The performance index for selection of the material is its equivalent travelling speed of dilatational waves denoted as C_l. According to Eq. 3.26, a combination of the material density and modulus can be chosen for a given thickness of the isolation layer.

3.3.4 Practical Considerations

Material

At the low frequency range needed for the hydroseismic isolation, only very soft materials provide effective isolation. Foams and other soft polymers may be regarded as the practical categories of appropriate materials. This can be observed in Fig 3.18 where various materials are mapped according to the performance index E/ρ. As shown in the figure, the E/ρ ratio of the elastomer materials including rubber is very close to the appropriate range according to Eq. 3.26. The ranges of various mechanical properties of foams and elastomers are also shown in Fig. 3.19. On the basis of the available ranges of material properties and based on the criterion given by Eq. 3.26, the design of the appropriate isolation foam material can be made. The ranges of mass density and modulus of elasticity of the isolation material considered in the numerical example are shaded in Fig. 3.19. As a practical example, for H=100 m, $t_l = 2.5$ m, $\rho_l = 1300$ kg/m^3 and $E_l = 0.5$ MPa Eq. 3.26 yields: $(E_l/\rho_l)^{1/2} = 19.6$ m/s and $860(t_l/H) = 21.5$ m/s and therefore, condition 3.26 is satisfied. Table 3.1 includes some information about the mechanical properties of rubber materials.

The amount of response reduction is dependent on the damping of the isolation layer. The damping parameter considered in the present analysis is a theoretical value that takes into consideration the decay of the pressure amplitude across the thickness of the layer. A

realistic value for the equivalent damping coefficient of a specific selected material should be determined by experimental measurements within the appropriate frequency range. A practical solution for a soft isolation layer can be in the form of a composite layer made of a soft core placed inside a stiff external crust which faces the reservoir. This upstream crust can be supported on the dam upstream face at properly designed spans such that it can resist the hydrostatic pressure with negligible deformation.

Location

The isolation layer can be installed at the upstream face of the dam either attached to its surface or at a short distance away from the dam. If the layer is not attached to the dam, it may be supported by a floating cap at the reservoir surface and moored to the dam for stability. The supporting pontoon cap and attachment system have to be designed for the effect of floods, floating debris and fluctuations of the water surface level due to the reservoir operation. In the present study, the isolation layer was assumed to be attached to the upstream face of the dam.

3.4 CONCLUSIONS

The effect of a partially absorptive boundary at the dam-reservoir interface on the amount of response reduction of a concrete gravity dam when subjected to earthquake is examined. The commonly used boundary condition for the interface of the dam and reservoir is modified to account for the effect of the relative impedance of the solid boundary to water in addition to the effect of the structural flexibility of the dam. Based on the results of the analysis, the following conclusions are reached:

1. The use of an absorptive layer attached to the upstream face of the dam, in the form of hydrodynamic isolation, provides an effective means of reducing seismic response of concrete gravity dams. With an absorptive layer at the upstream side of the concrete dam, the anticipated seismic stresses in the dam may be reduced.
2. The amount of reduction in the hydrodynamic pressure transmitted to the dam depends on the softness and thickness of the absorptive layer as well as on the reflection coefficient of its surface. The layer thickness and softness influence the dissipation of the transmitted pressure across the layer.
3. In the case where the reservoir is limited at its upstream end, hydrodynamic isolation is more effective in reducing the response of the dam. The reservoir length effects are noticeable for reservoir length/height ratio, $L/H < 2$ with more response reduction for lower L/H values.
4. It is concluded that the foam or polymer isolation layer provides an alternative system to the air curtain scheme in seismic response reduction of concrete dams. With the proper design of the isolation layer, it appears possible to suppress the effect of the reservoir without increasing the peak response amplitude at the higher frequencies of the dam-reservoir system.

5. It is possible to include the proposed system in the design of new dams as well as the rehabilitation of existing dam structures.

Table 3.1 - Properties of low-stiffness elastomers (rubber) (from CMS 2.0)

Property	Range of Variation
Density (kg/m^3)	850 - 1340
Bulk Modulus (MPa)	1500 - 2000
Compressive Strength (MPa)	10 - 30
Elastic Limit (MPa)	5 - 15
Poisson's Ratio	0.495 - 0.499
Shear Modulus (MPa)	0.2 - 1.0
Tensile Strength (MPa)	5 - 15
Young's Modulus (MPa)	0.5 - 3
Price (£/kg , 1975)	0.45 - 1.5

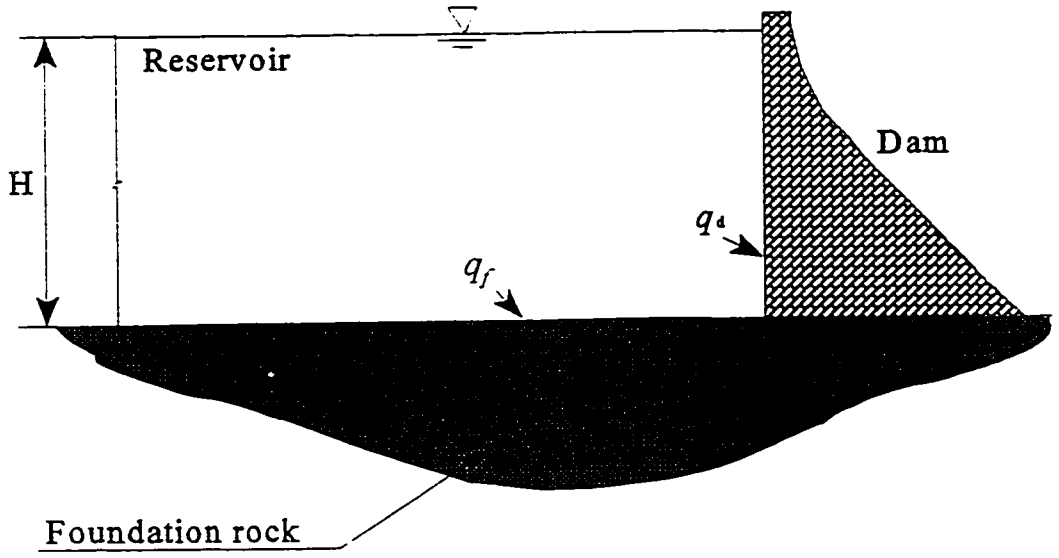

Fig. 3.1 Reservoir with a partially absorptive interface with the dam

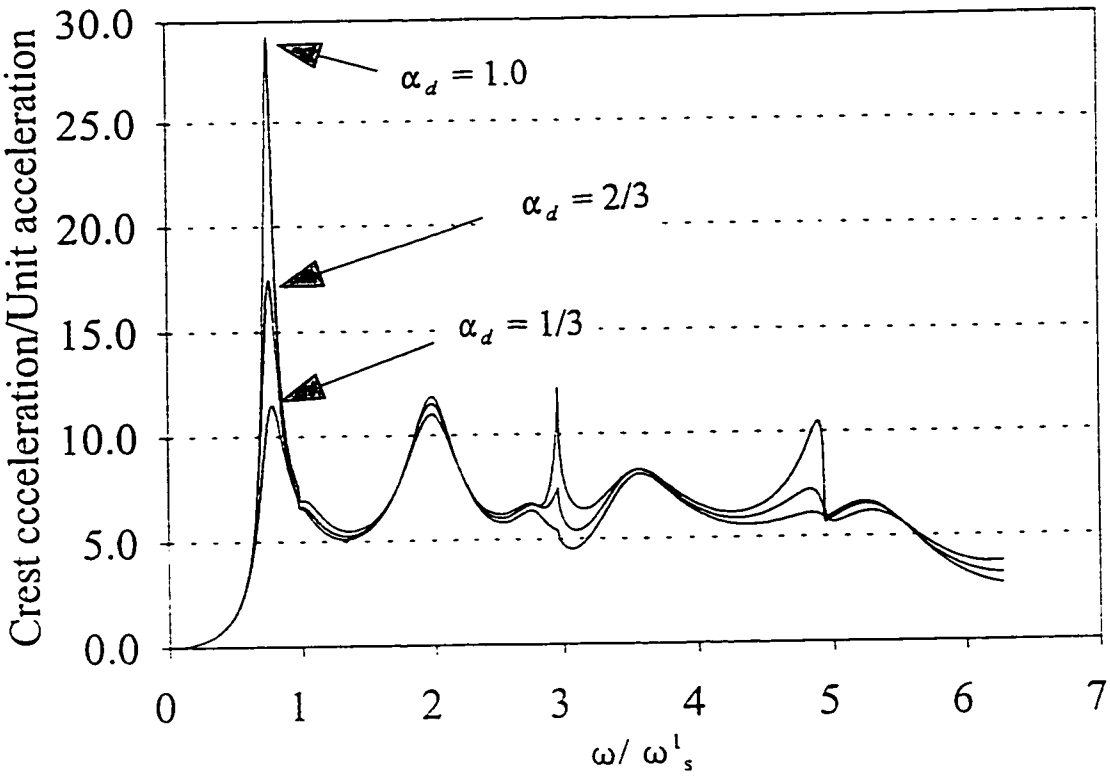

Fig. 3.2 Crest acceleration response of a dam with a partially absorptive upstream face and impounding an infinite-length reservoir

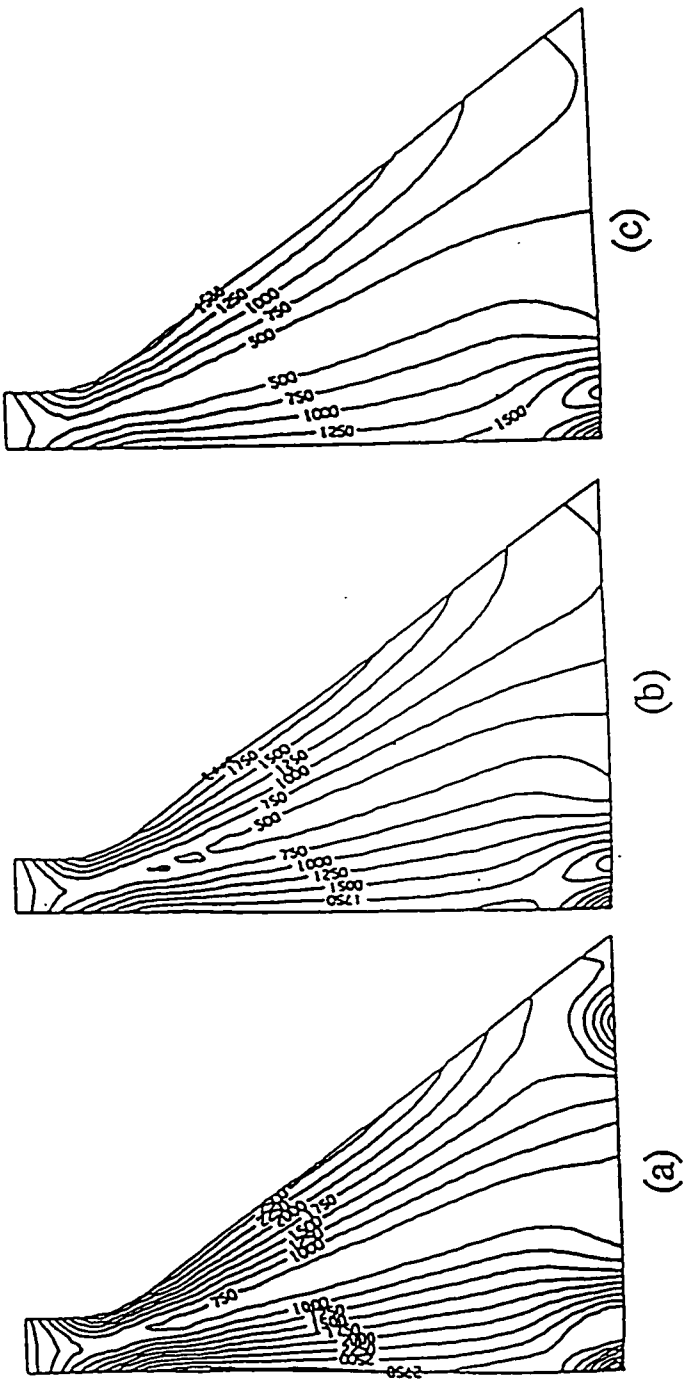

Fig. 3.3 Maximum tensile stress contours (in kPa) in the dam with a thin isolation layer for different reflection coefficients, α_b, at the upstream face: (a) $\alpha_d = 1.0$, (b) $\alpha_d = 2/3$, (c) $\alpha_d = 1/3$

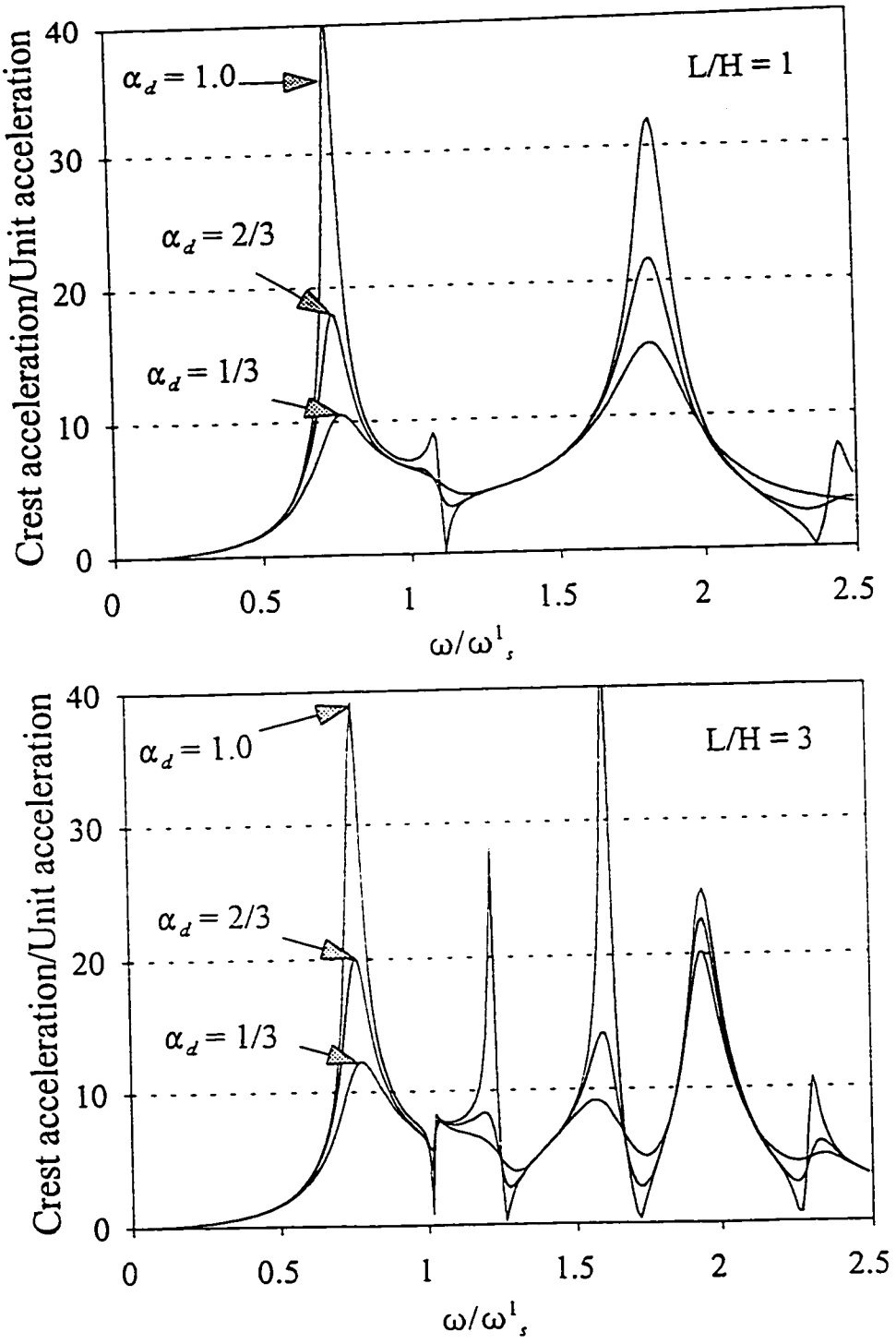

Fig. 3.4 Reduction in the response of the dam with a partially absorptive upstream face subjected to horizontal ground motion - simplified solution

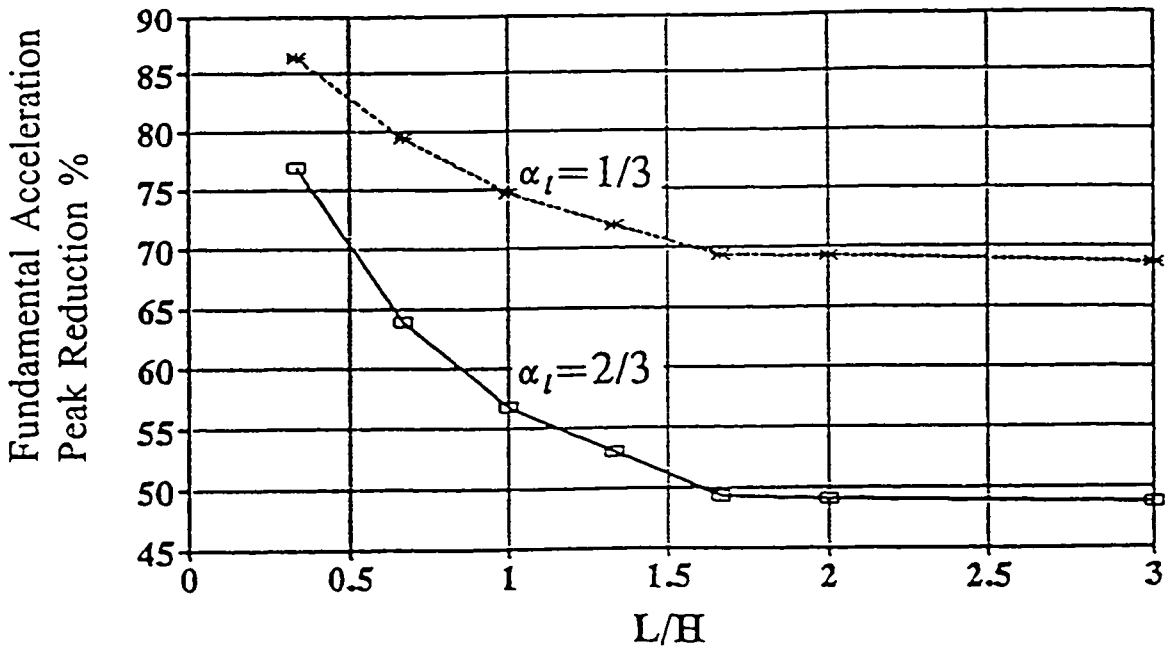

Fig. 3.5 Reservoir length effect on the response reduction of the dam with a partially absorptive upstream face subjected to horizontal ground motion - simplified solution

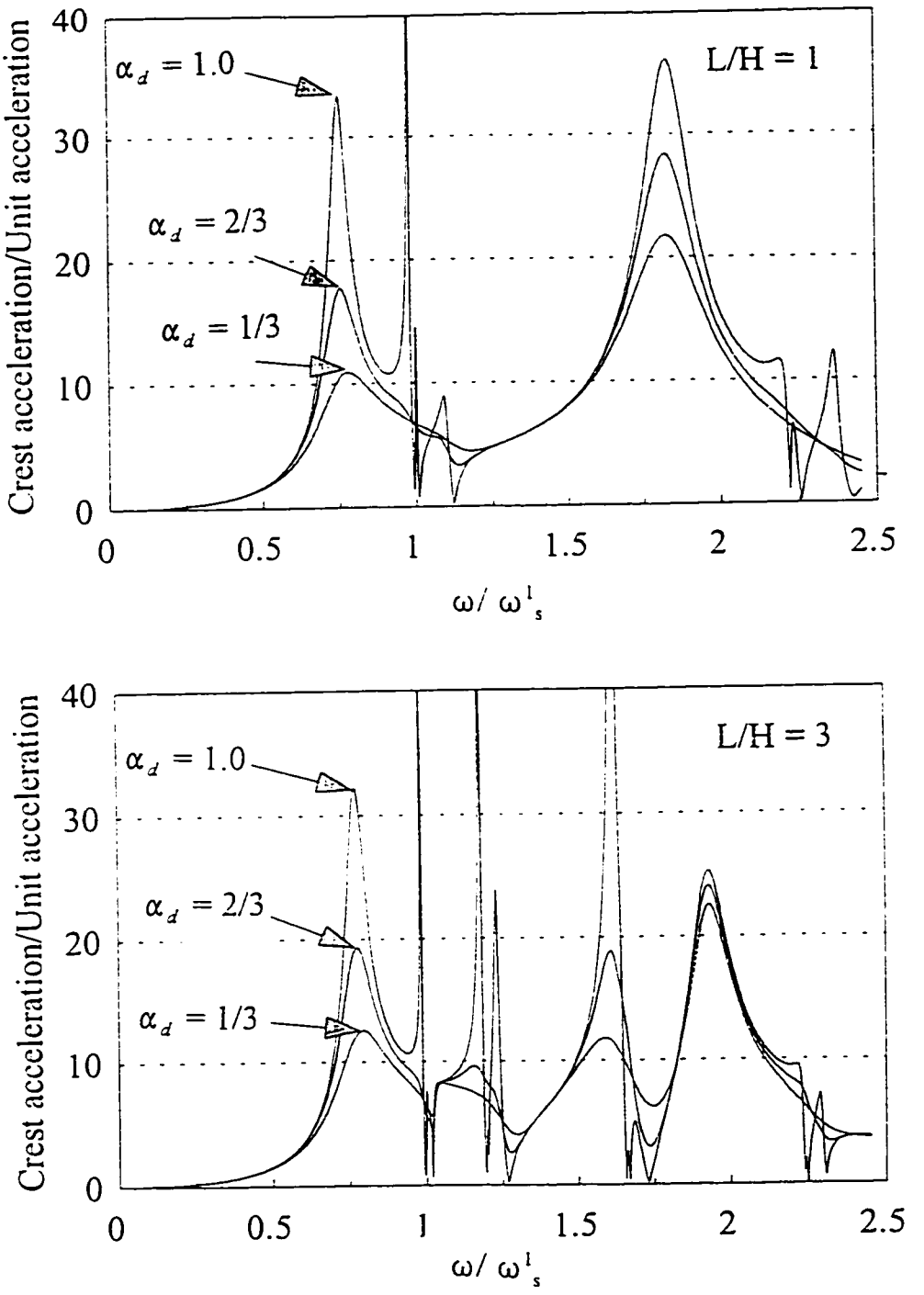

Fig. 3.6 Reduction in the response of the dam with a partially absorptive upstream face subjected to horizontal ground motion - finite element solution

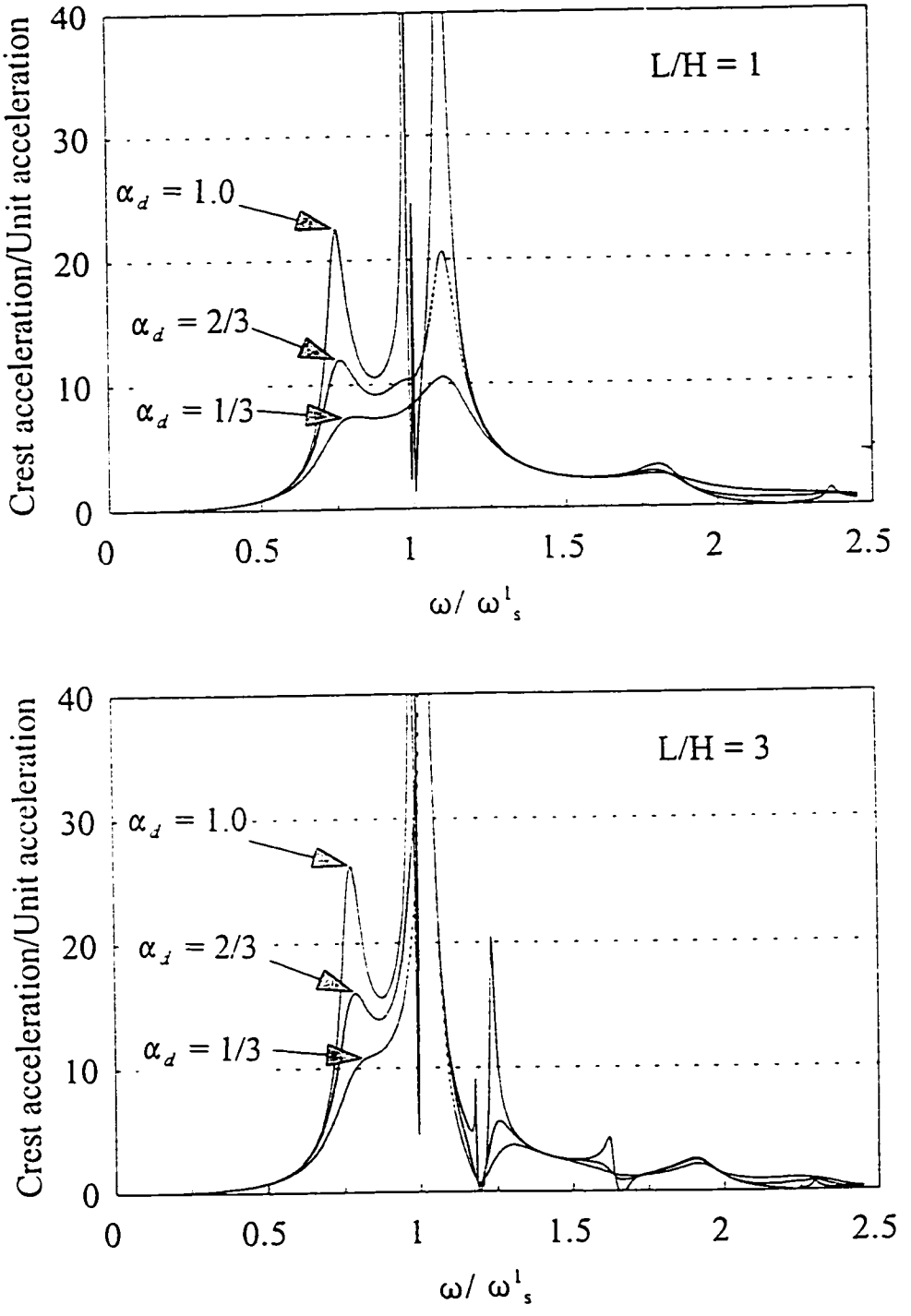

Fig. 3.7 Reduction in the response of the dam with a partially absorptive upstream face subjected to vertical ground motion - finite element solution

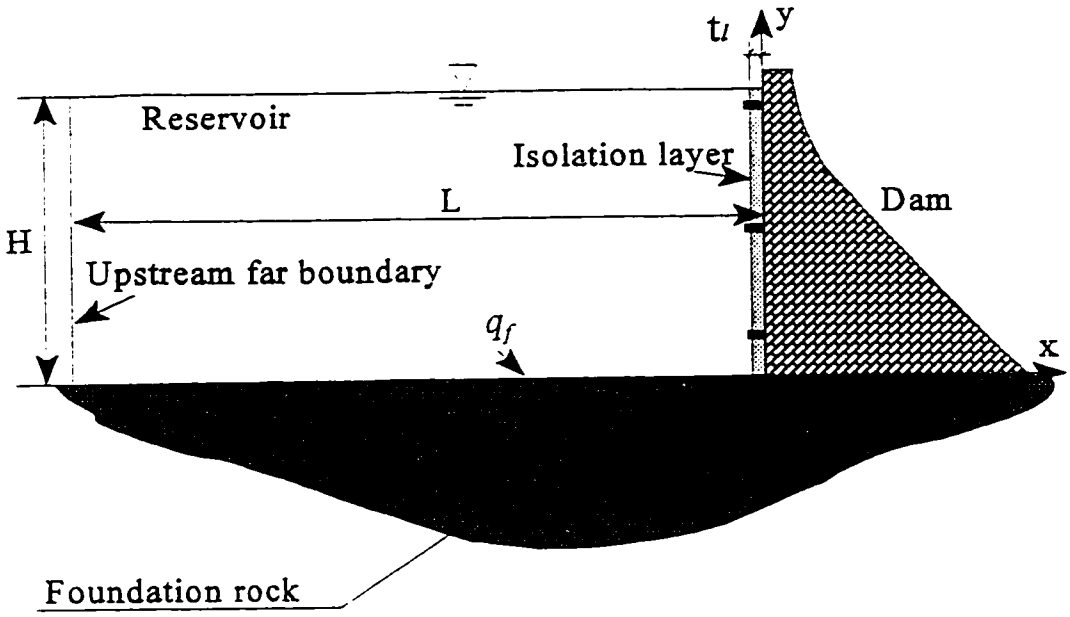

Fig. 3.8 Schematic of an isolated concrete gravity dam with a finite length reservoir

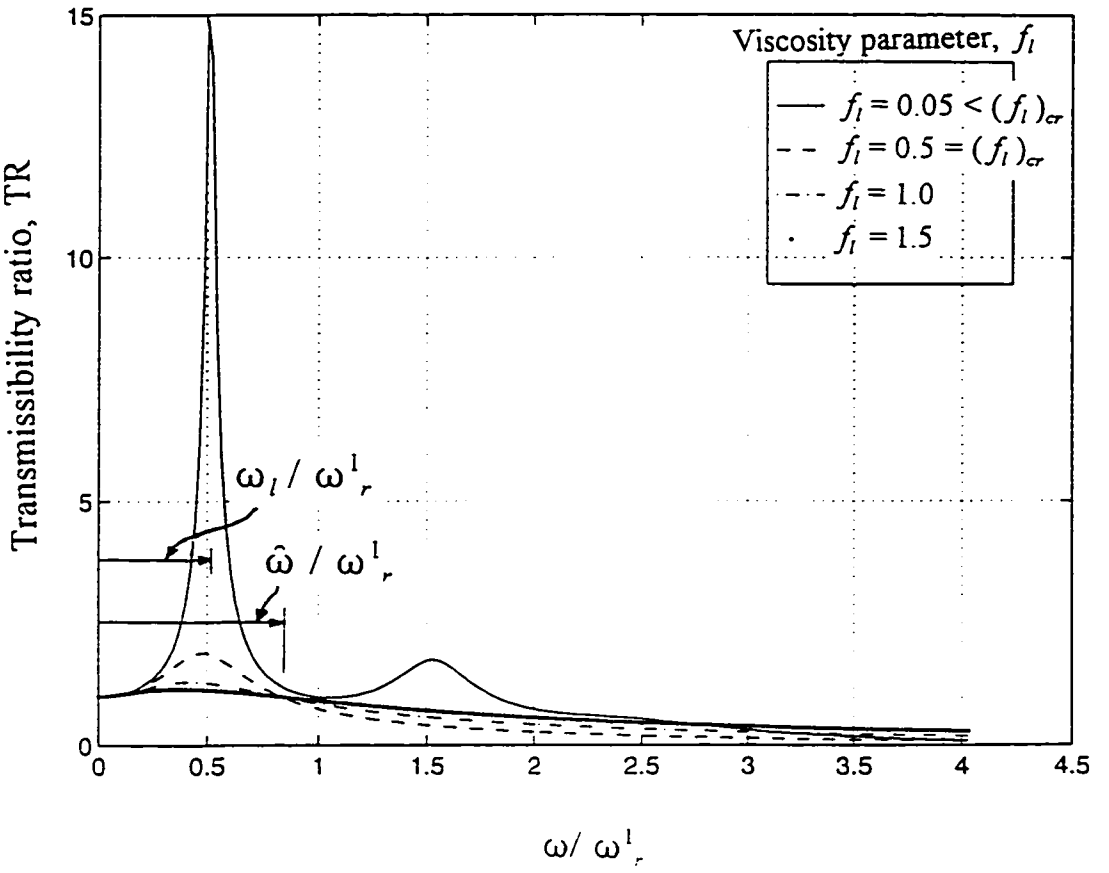

Fig. 3.9 Variation of the transmissibility ratio of the hydrodynamic pressure across the isolation layer with the frequency of excitation

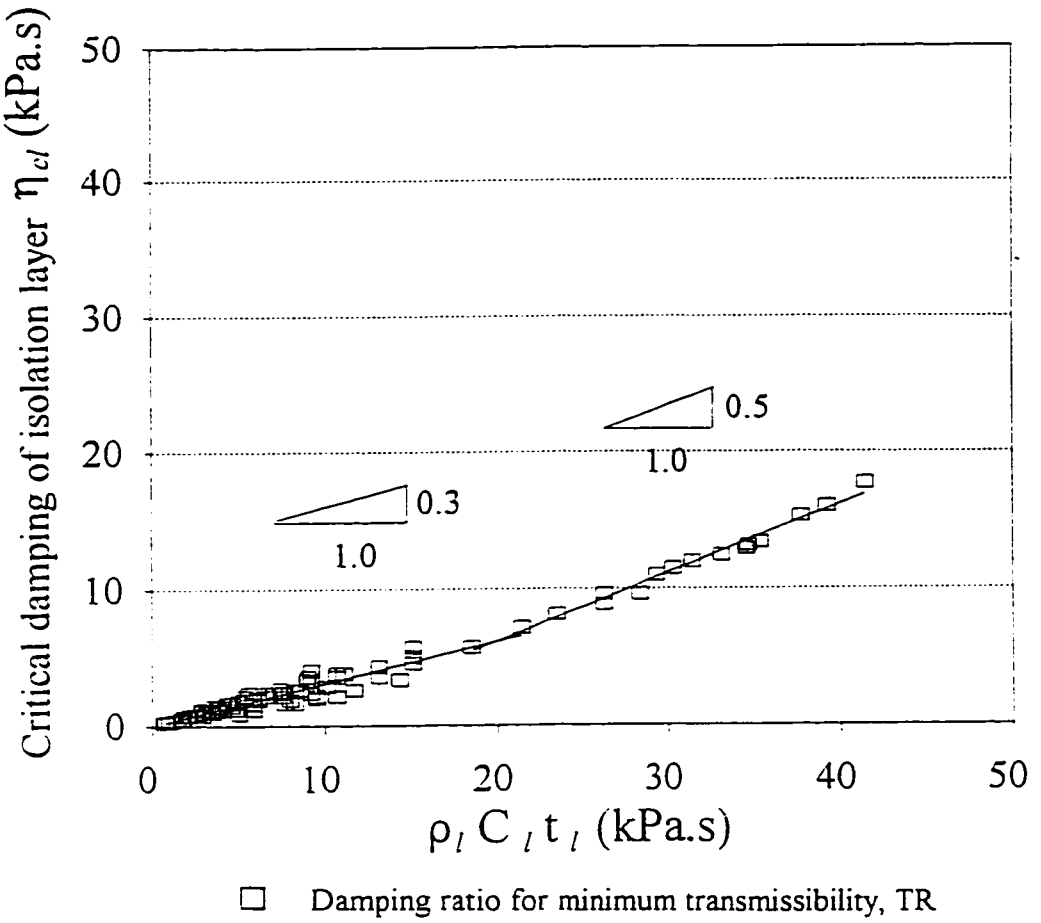

Fig. 3.10 Variation of the critical damping with characteristics of the isolation layer

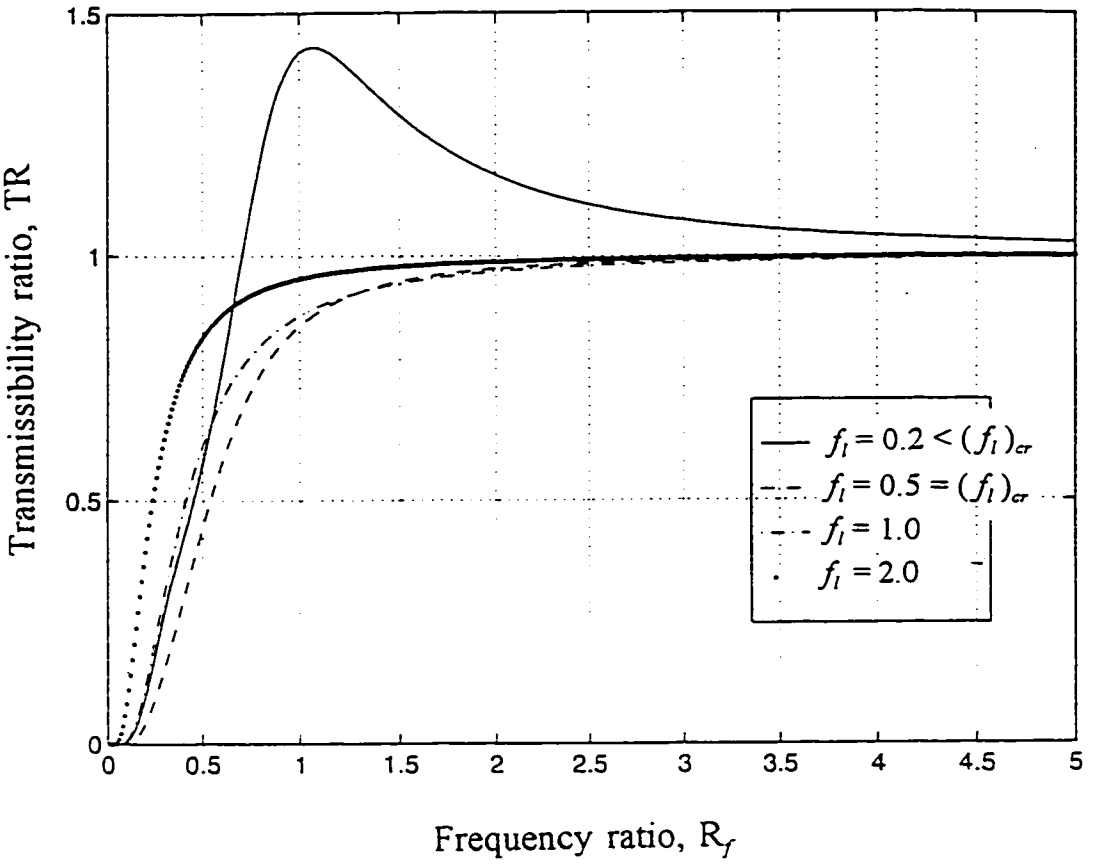

Fig. 3.11 Variation of the transmissibility ratio of the hydrodynamic pressure across the isolation layer with the frequency ratio, R_f

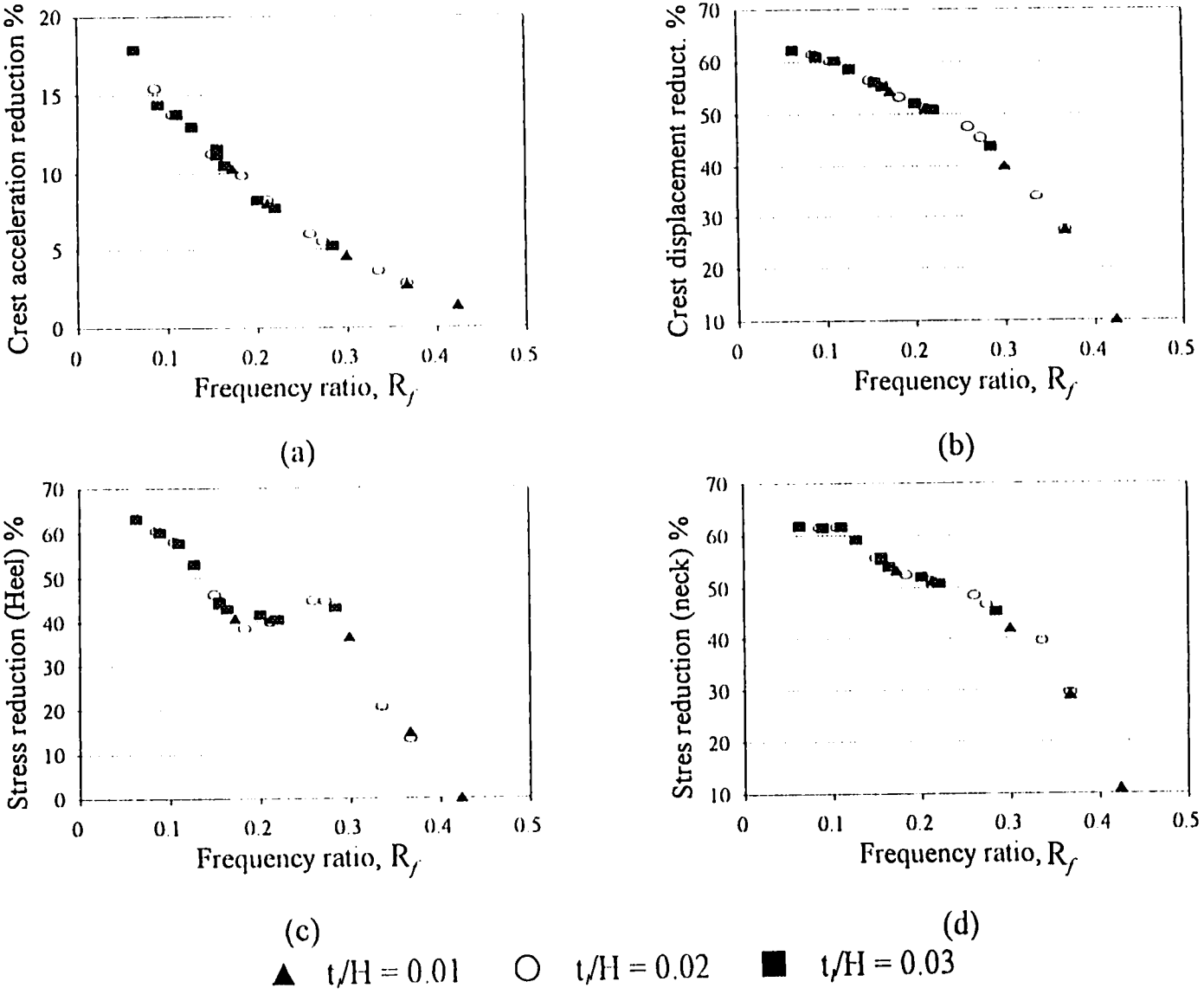

Fig. 3.12 Response reduction in concrete gravity dam with a completely reflective isolation layer (α_I= 1.0)

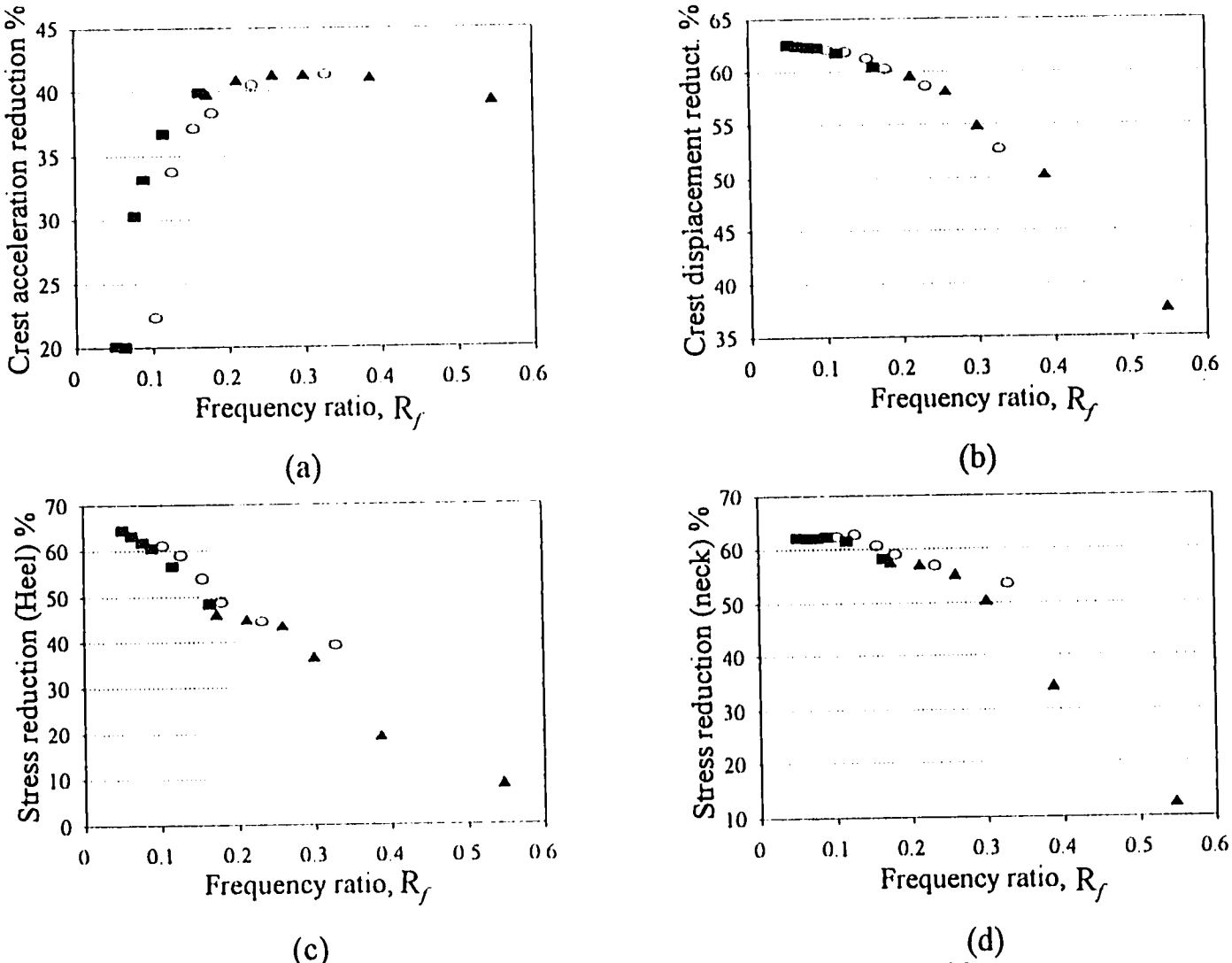

Fig. 3.13 Response reduction in concrete gravity dam with a partially reflective isolation layer (α_l = 2/3)

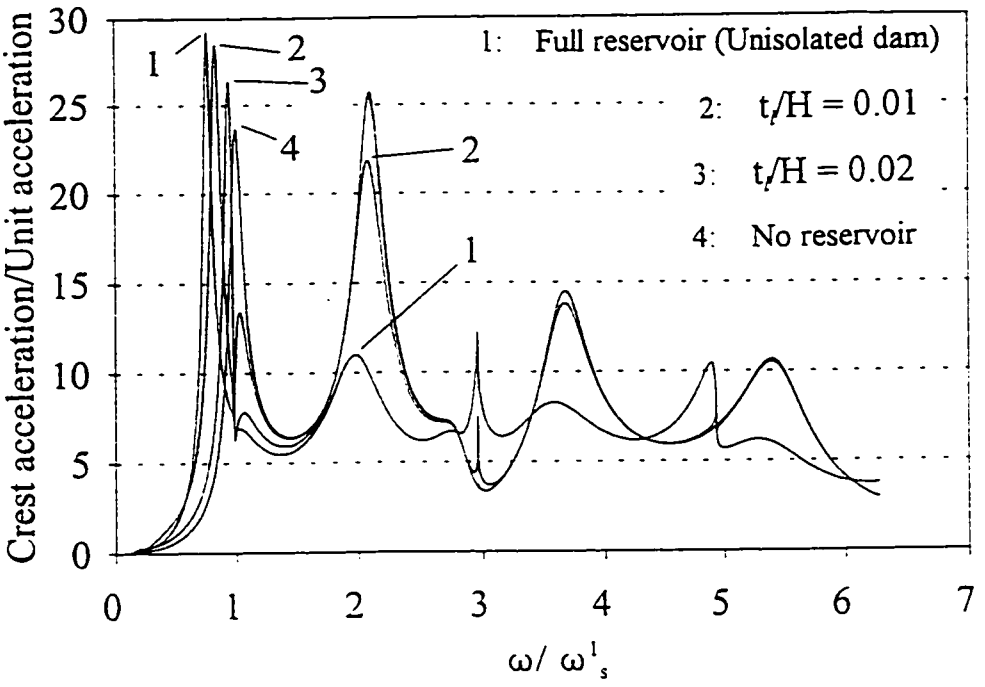

Fig. 3.14 Frequency response function of the crest acceleration for different conditions at the upstream face of the dam

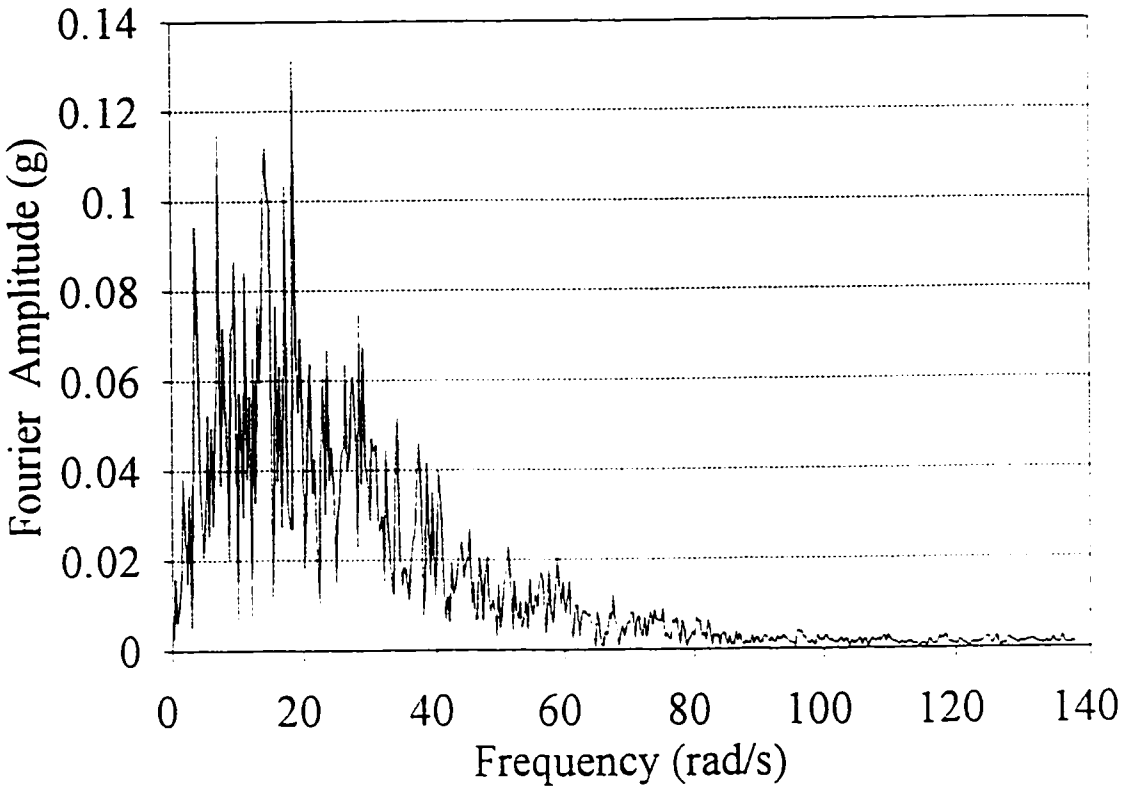

Fig. 3.15 Frequency spectrum of the S69E component at Taft Lincoln School Tunnel, 1952 Kern County earthquake

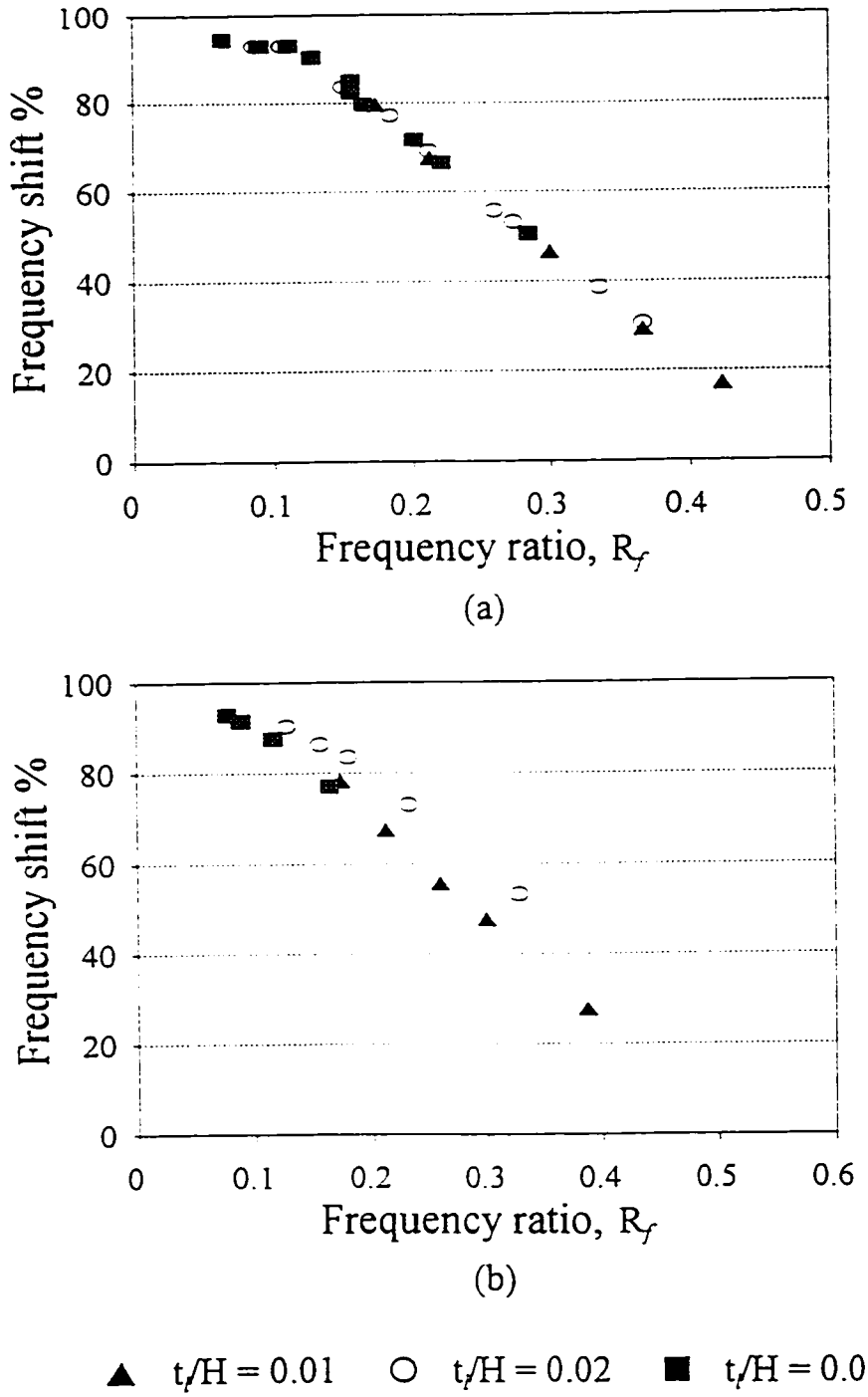

Fig. 3.16 Variation of the frequency shift of the fundamental peak of the dam response with the frequency ratio, R_f: (a) $\alpha_l = 1.0$ (b) $\alpha_l = 2/3$

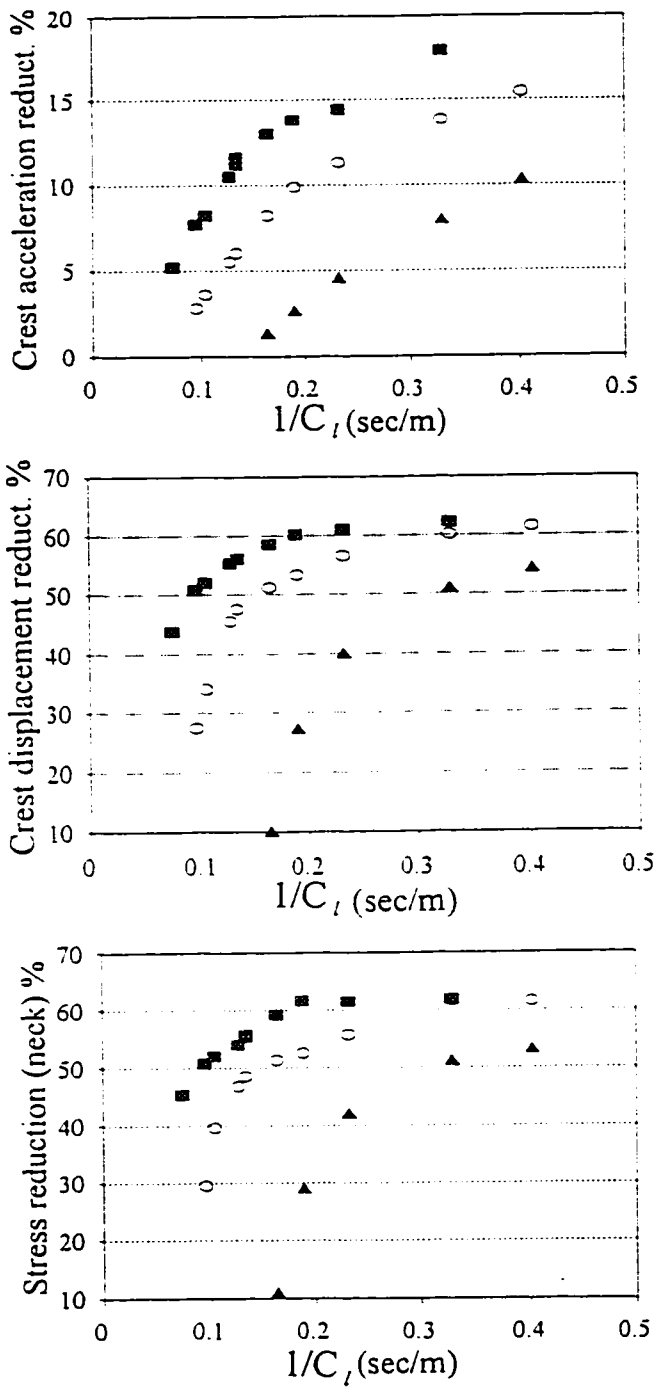

Fig. 3.17 Effects of the isolation material and layer thickness on the response reduction of the concrete gravity dam

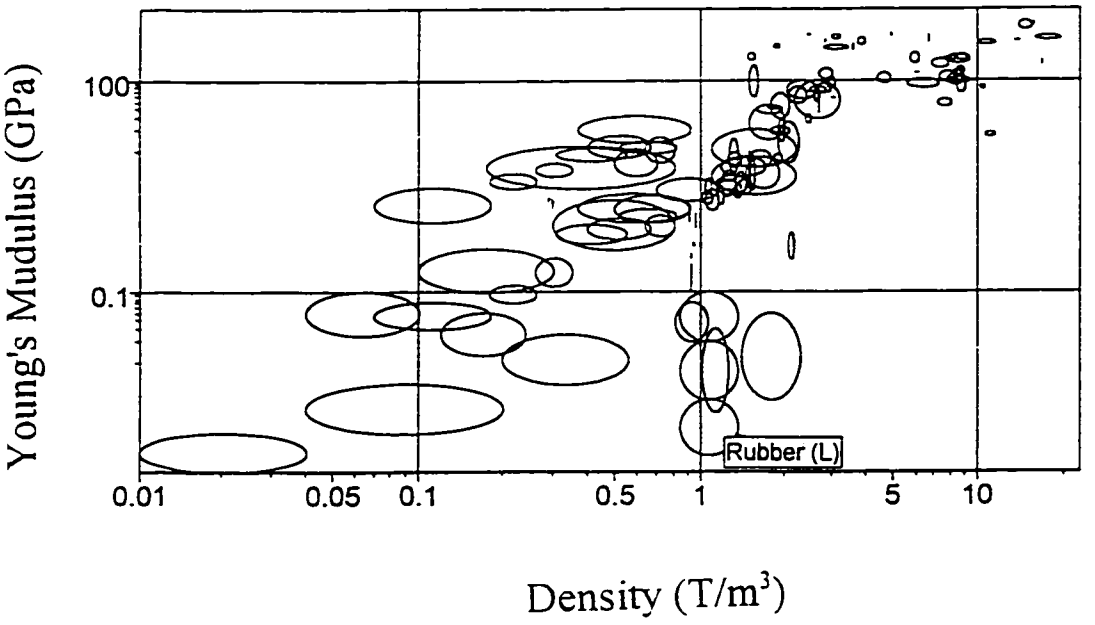

Fig. 3.18 Variation of modulus of elasticity with density of materials (from Cambridge Material Selection - CMS 2.0)

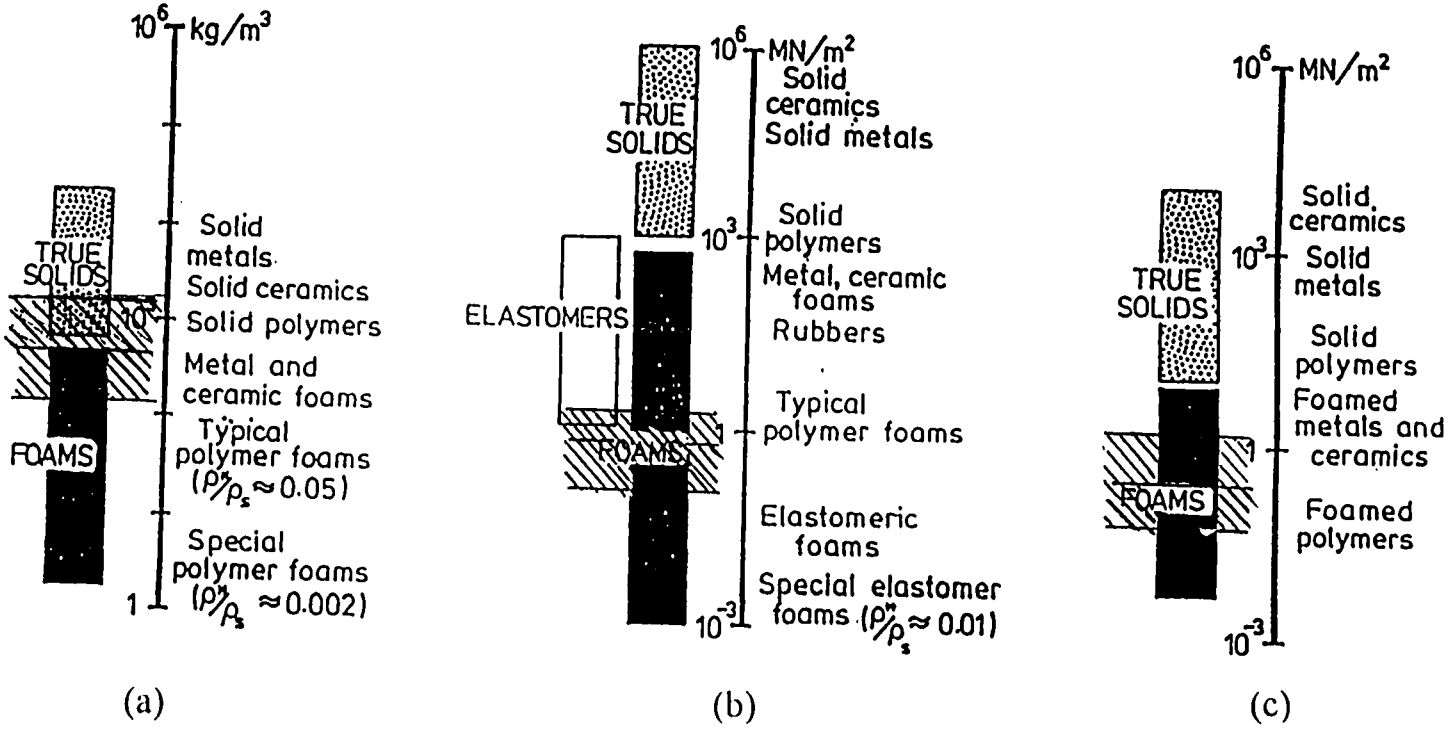

Fig. 3.19 Mechanical properties of polymer materials: (a) Density (b) Modulus of elasticity and (c) Compressive strength (After Gibson and Ashby 1988)

CHAPTER 4

RESERVOIR WITH PARTIALLY ABSORPTIVE BOUNDARIES

4.1 INTRODUCTION

In the previous chapters, analytical models were developed to examine the effects of the absorption of hydrodynamic pressure waves at individual sections of the reservoir boundary. The study was limited to the special case of a rectangular-shape reservoir where a theoretical solution for the associated boundary value problem can be obtained. For the case of a reservoir of arbitrary shape, the hydrodynamic pressure may only be obtained by the numerical solution of the governing equation subject to the specified boundary conditions. In addition, there is no closed-form solution available for the case of a rectangular-shaped reservoir of compressible water with a partially absorptive interface with the flexible dam when the dam-reservoir system is subjected to vertical ground motion. The case of a reservoir with a partially absorptive interface with the dam under horizontal ground motion is addressed in section 3.2 of the present study.

In this chapter, a general case of the boundary value problem for the hydrodynamic pressure in the reservoir is addressed. A reservoir of any arbitrary shape and absorptive boundaries is modelled in two dimensions. Both horizontal and vertical ground motion components are included in the analysis.

4.2 THE BOUNDARY VALUE PROBLEM OF THE RESERVOIR

4.2.1 Governing Equations

The hydrodynamic pressure developed during the small-amplitude vibration of the inviscid reservoir water is obtained from the solution of the two-dimensional Helmholz equation (Eq. 3.1):

$$\frac{\partial^2 P}{\partial x^2} + \frac{\partial^2 P}{\partial y^2} + \frac{\omega^2}{C_w^2} = 0$$

The solution of the governing partial differential equation is subject to the following boundary conditions:

- along the solid boundaries:

$$\frac{\partial P}{\partial n}(s,\omega) - D(\omega) P(s,\omega) = -\rho_w \ddot{u}_n(s) \qquad (4.1)$$

- at the reservoir free surface:

$$P(x,H,\omega) = 0 \qquad (4.2)$$

where ω is the frequency of excitation, $P(x,y,\omega)$ is the amplitude of the steady-state hydrodynamic pressure and ρ_w is the density of water. The depth of the reservoir water is denoted by H. The local coordinate along the reservoir solid boundary and the inward normal direction into the fluid are denoted by s and n, respectively. The normal acceleration of the reservoir boundary is denoted by $\ddot{u}_n(s)$. $D(\omega)$ is a complex-valued, frequency dependent function which represents the refraction of incoming pressure waves to the reservoir surrounding boundary. Along the absorptive part of the reservoir boundary,

the function $D(\omega)$ reduces to:

$$D(\omega) = i\omega q \tag{4.3}$$

where q is the absorption coefficient of the boundary. The function $D(\omega)$ contributes to the added damping of the dam-reservoir system. The two-dimensional model of the reservoir with absorptive boundaries is shown in Fig. 4.1. Although the approach is general and is applicable to a reservoir of any arbitrary shape, for simplicity a rectangular reservoir is assumed in the present study. The absorption coefficients of the dam-reservoir interface, reservoir bottom and the reservoir upstream far-end are denoted by q_d, q_b, q_u, respectively. The symbols δ_{xl} and δ_{yl}, $l = x, y$ in Fig. 4.1 are the Kronecker delta. The reservoir is assumed to be of limited length. In the analysis, the following assumptions are adopted:

* The impounded water is assumed compressible and inviscid.
* The effect of surface waves is neglected.
* The depth of water is assumed equal to the height of the dam.
* The dam is considered to be flexible; its deformation is approximated using its first few modes of vibration.
* The foundation of the dam and the reservoir is semi-infinite and elastic.

4.2.2 Reservoir Upstream Boundary Condition

The boundary condition at the far end of the finite-length reservoir model ($x = L$) can be expressed as:

$$\frac{\partial P}{\partial x}(L,y,\omega) - i\omega q_u P(L,y,\omega) = -\rho_w \tag{4.4}$$

where q_u is the absorption coefficient of the far end boundary which is obtained as:

$$q_u = \frac{1}{C_w}\left(\frac{1-\alpha_u}{1+\alpha_u}\right) \tag{4.5}$$

where C_w is the travelling speed of the compression wave in water and α_u is the reflection coefficient of the far end boundary. For the case of a stationary far end boundary, the right hand side of Eq. 4.4 is zero as is shown in Fig. 4.1. The excitation of the reservoir far boundary can also be included in the procedure. In the present study, however, the effects of the motion of the far end of the reservoir are excluded. The effect of different input ground motions at the dam and far end boundaries of the reservoir has been examined in a few past studies (Newmark and Rosenblueth 1971, Aviles and Sanches-Sesma 1989, Baumber 1993).

In the case of an infinitely long reservoir model, the partial absorption boundary condition at the far end may be replaced by an appropriate condition for the radiation of pressure waves to the upstream far field. In the present study, the limited reservoir far end boundary condition is chosen so as to investigate the effects of reservoir aspect ratio on the monolith response. However, radiation conditions proposed by Sommerfeld (Zienkiewicz *et al.* 1977) and Sharan (1992) are examined to verify the results of the hydrodynamic response of a truncated finite element model of the reservoir with the available closed-form solution for a semi-infinite fluid domain under horizontal excitation (Fenves and Chopra 1984a).

The radiation condition in the truncated model of an infinite length reservoir can be considered as a special case of the refracting boundary condition with no reflection of waves to the reservoir from the truncated boundary. If the striking waves are assumed to be completely absorbed at the far end boundary, the reflection coefficient, α_u, is set to zero and

Eq. 4.4 reduces to the Sommerfeld boundary condition:

$$\frac{\partial P}{\partial x}(L,y,\omega) - \frac{i\omega}{C_w} P(L,y,\omega) = 0 \tag{4.6}$$

In Eq. 4.6, the function $D(\omega)$ equals to:

$$D(\omega) = \frac{i\omega}{C_w} \tag{4.7}$$

The basic assumption involved in Sommerfeld boundary condition is that the striking pressure waves at the truncated boundary are planar and normal to the boundary. For a general irregular shape of the near field of the reservoir, this needs a long uniform channel to be included in the discretized model of the reservoir. In the present study, a radiation condition proposed by Sharan (1992) is also examined in the truncated model of the semi-infinite reservoir to investigate the performance of an alternative radiation condition in a dam-reservoir model which includes a deformable dam and an absorptive reservoir bottom. Sharan radiation condition is expressed as:

$$\frac{\partial P}{\partial x}(L,y,\omega) = \frac{\kappa_1(\omega)}{H} P(L,y,\omega) \tag{4.8}$$

where

$$\kappa_1(\omega) = \sqrt{\zeta_1^2 - (\frac{\omega H}{C_w})^2} \tag{4.9}$$

The parameter $\kappa_1(\omega)$ in Eq. 4.9 is expressed in terms of the first eigenvalue of the

impounded water, ζ_1, in the series expansion of the hydrodynamic pressure response in the form:

$$P(x,y,\omega) = \sum_{n=1}^{\infty} \mathcal{F}_n(y,\omega,\zeta_n)\, e^{\kappa_n x/H} \tag{4.10}$$

In Eq. 4.10, $\mathcal{F}_n$ is a function of the complex value ${}_n\zeta$ and the elastic and geometrical properties of the dam-reservoir system in the near field. The eigenvalue ζ_1 is the first complex root of the equation

$$e^{2i\zeta_n} = \frac{\omega q_f H - \zeta_n}{\omega q_f H + \zeta_n} \tag{4.11}$$

where q_f is the absorption coefficient of the reservoir foundation. The function $D(\omega)$ in this case takes the form:

$$D(\omega) = \frac{1}{H}\kappa_1(\omega) \tag{4.12}$$

For the case $\zeta_n = 0$, Eq. 4.8 reduces to Sommerfeld boundary condition (Eq. 4.6).

4.3 THE SOLUTION TECHNIQUE

A computer program for dynamic analysis of dams (DAD-96) is developed for the case of concrete gravity dams of finite reservoir with absorptive boundaries. The numerical solution technique utilized in DAD-96 is an adapted version of the computer program EAGD-84 developed by Fenves and Chopra (1984b). The program EAGD-84 is a versatile program which includes the effects of the structure and foundation flexibility as well as water compressibility. The program is based on the theoretical solution for the special case of an infinitely long, rectangular-shaped reservoir. The only absorbing boundary included in the program is the reservoir bottom where an approximate reflection coefficient, α_b, accounts for the effects of this boundary on the monolith structural response. The reservoir-foundation boundary is addressed in chapter two where the proposed analytical model includes the effect of a layered reservoir foundation. It is concluded that the proposed model is a more realistic representation of the bottom boundary and leads to a more reliable selection of the reflection coefficient.

The closed-form solution of the hydrodynamic pressure under vertical ground motion currently used in the EAGD program (Fenves and Chopra 1984a and 1984b) does not account for any variation of the reflection coefficient, the reservoir depth and the boundary conditions along the streamwise direction. The solution is based on the special case of a one dimensional, vertical excitation of the reservoir with the assumption of a completely reflective boundary at the upstream face of the dam. In the case of an isolated dam with a soft layer at its upstream face, the interface of the dam and the reservoir is partially absorptive. With a more general boundary condition at this boundary, the current closed-form solution for the resulting hydrodynamic pressure is not valid.

In order to enhance the ability of the program DAD-96 to apply to a general

reservoir shape and set of boundary conditions, a finite element program was developed for the computation of the required hydrodynamic terms in the reservoir. The finite element procedure outlined by Hall and Chopra (1980) was chosen for this purpose. The developed computer code was incorporated into the DAD-96 program to replace the related routines based on the closed-form solution for the reservoir used in EAGD-84 approach. The output of the developed finite element routine includes the frequency dependent hydrodynamic terms due to the vibration of the dam by a specified number of monolith's modes of vibration as well as excitation of the reservoir bottom boundary. The output terms of the finite element routine are input to the main program to formulate the frequency dependent sets of equations of the dam-reservoir-foundation system.

In the finite element model, one-dimensional damper elements are included to account for the refraction of the impinging waves at the finite-length reservoir bottom and end boundaries. The damper elements are two-noded and coincide with one side of the four-noded, isoparametric elements of the fluid domain at the vicinity of the solid boundaries. Variation of the wave reflection coefficient at different sections of the surrounding reservoir boundary can be readily accommodated using the above damper elements. The dynamic loading from the reservoir surrounding boundary is also introduced through one-dimensional, two-noded boundary elements.

4.4 VERIFICATION OF THE SOLUTION PROCEDURE

The developed finite element program is examined for the validity of the resulting outputs before it is applied to the case studies. The verification procedure includes comparing the results of the hydrodynamic terms and the structural response of the dam with the cases where theoretical solutions are available. The results of parametric studies are also presented which include the effects of the reservoir mesh refinement, the number of structural modes of vibration as well as the effects of foundation flexibility and absorption of hydrodynamic pressures at the reservoir boundaries.

4.4.1 Hydrodynamic Pressure in the Reservoir

Comparison with theoretical solutions

Fig. 4.2 shows a rectangular-shaped reservoir subjected to a unit-amplitude, time-harmonic vertical ground motion. The bottom of the reservoir is partly reflective with the reflection coefficient, α_b and is under uniform excitation. The presented case is the simplest model for which a closed-form theoretical solution is available. The solution for the resulting hydrodynamic pressure in the reservoir is given as (Fenves and Chopra 1984a):

$$P_0^y(0,y,\omega) = \frac{\rho_w C_w}{\omega} \frac{1}{\cos\frac{\omega H}{C_w} + iq_f C_w \sin\frac{\omega H}{C_w}} \sin\frac{\omega(H-y)}{C_w} \qquad (4.13)$$

where y is the vertical coordinate which is measured upward from the reservoir bottom.

A rectangular, 100 m deep reservoir is considered in the analysis. The mesh width representing the column of water, a, subjected to vertical excitation is taken as 10 m. Fig. 4.3 shows comparison of theoretical predictions of the frequency response of the

hydrodynamic pressure with the response obtained utilizing the finite element procedure for a set of selected values for the bottom boundary reflection coefficient, α_b. In the figure, the absolute value of the hydrodynamic pressure normalized to the maximum hydrostatic pressure ($|P_{dyn}| / P_{st}$) is plotted vs the normalized frequency of the input ground motion. The fundamental frequency of the reservoir is denoted by ω'_r. It is concluded that the results of the finite element solution are in good agreement with the theoretical solution for different values of the reflection coefficient for the reservoir bottom. The only difference between figures 4.3a and 4.3b is an expected slight frequency shift of the response peaks to higher frequencies in the results of the finite element solution. The finite element discretization of the reservoir is based on a linear variation of the hydrodynamic pressure along the sides of the finite elements. This linear approximation makes the resulting reservoir model to be *stiffer* than the corresponding theoretical model. Consequently, the associated natural frequencies of the reservoir are slightly higher (negligible difference for the fundamental frequency and 0.7% higher for the second resonance frequency) than the ones obtained based on the theoretical approach.

The theoretical solution for the hydrodynamic pressure in Eq. 4.2 is based on the assumption of a completely reflective boundary at the upstream face of the rigid dam and a finite amplitude of pressure at the far field. The above conditions form a special case of solution for the resulting hydrodynamic pressure which is virtually independent of the spatial coordinate in the horizontal direction. As a result, the solution is independent of the reservoir length-to-depth ratio as verified by the finite element procedure (Fig. 4.4).

For the case where the reservoir is subjected to horizontal excitation, the theoretical solution is based on a series expansion of the reservoir eigenvectors (Fenves and Chopra 1984a). For the case of a rigid dam, the expression for the hydrodynamic pressure in the

reservoir, $P_0^x(x,y,\omega)$, can be expressed in the form of Eq. 4.10 where:

$$\mathcal{F}_n(y,\omega,\zeta_n) = -2\rho H \frac{\zeta_n^2(\omega)}{H[\zeta_n^2(\omega) - (\omega q_f)^2] + i(\omega q_f)} \frac{I_{0n}(\omega)}{[\zeta_n^2(\omega) - \omega^2/C_w^2]^{1/2}} \Lambda_n(y,\omega) \tag{4.14}$$

in which $\Lambda_n(y,\omega)$ and $I_{0n}(\omega)$ are given by Eqs. 3.11 and 3.12, respectively. The rest of the parameters are as defined in section 3.2.1. The distribution of the hydrodynamic pressure along the dam height is obtained by evaluating Eq. 4.10 at the dam upstream face ($x = 0$).

Fig. 4.5a shows the response of the hydrodynamic force on rigid dam subjected to the harmonic horizontal excitation for the case where α_b varies between 0.0 and 1.0. Figure 4.6a shows the corresponding set of response results under vertical ground motion. The reservoir length to depth ratio is L/H = 5. In the above figures, the hydrodynamic force on the dam normalized to the hydrostatic force ($|F_{dyn}|/F_{st}$) for unit width of the monolith is plotted vs the normalized frequency of the input ground motion. The undulatory characteristic of the response curve for $\alpha_b = 1.0$ in Fig. 4.5a is due to the effect of reflected waves from the far boundary. The influence of the reflection coefficient of the reservoir bottom, α_b, is represented by different curves in the figure. The results shown in Figs. 4.5a and 4.6a are in good agreement with the results of the theoretical solution given by Fenves and Chopra (1984a) for both horizontal and vertical ground motions (Figs. 4.5b and 4.6b). The frequency response function for the hydrodynamic force on the rigid dam subjected to the horizontal ground motion is virtually independent of the length of the truncated reservoir model for sufficiently large L/H ratios (say, L/H $\geq$ 5). However, for the case of completely reflective bottom boundary ($\alpha_b = 1.0$) the number of additional peaks in the hydrodynamic response of the limited length reservoir increases with the L/H ratio in

the finite element model of the reservoir (cf. Figs. 4.5a and 4.7).

The effect of the far boundary on the number of additional response peaks is illustrated in Fig. 4.8. The responses of the hydrodynamic force on the rigid dam when subjected to horizontal ground motion are shown for the cases of a completely reflective ($\alpha_u = 1.0$) and a completely absorptive ($\alpha_u = 0.0$) far boundary. The response peaks associated with reservoir vertical modes are less affected by the refraction of pressure waves at the far boundary in comparison to the significant suppression of the additional peaks due to the horizontal modes of the finite-length reservoir. This suppression effect is more significant for a lower L/H ratio as shown in Fig. 4.8. In Fig. 4.8, the dam-reservoir boundary and the bottom of the reservoir are assumed to be completely reflective.

For the case of vertical ground motion, a completely reflective far boundary and dam-reservoir boundary ($\alpha_u = \alpha_d = 1.0$) result in a special solution for the hydrodynamic pressure similar to the one given by Fenves and Chopra (1984a) for the case of an infinitely long reservoir. This solution is virtually independent of the horizontal coordinate. The response of the hydrodynamic force on the dam remains unchanged for different L/H ratios and no additional peaks due to the horizontal modes appear (Figs. 4.9 and 4.10). The hydrodynamic response is the same as the curve corresponding to $\alpha_b = 1.0$ in Fig. 4.6a. In Fig 4.9, the dam-reservoir boundary and the bottom of the reservoir are assumed as completely reflective.

When the reservoir far boundary is assumed absorptive, the problem is two-dimensional and additional peaks due to the finite length of the reservoir appear (Fig. 4.9). The number of additional peaks increase with L/H ratio similar to the case of horizontal excitation. For partially absorptive reservoir sides ($\alpha_u < 1.0$ and $\alpha_d < 1.0$), the slope of the frequency response function of the hydrodynamic pressure, $\partial P(x,y,\omega)/\partial n$, at the dam and far end boundaries is non-zero (Fig. 4.1). Accordingly, the special case of the one-

dimensional response of the impounded water with completely reflective boundaries at its sides is replaced by a two-dimensional reservoir response which includes coupling effect of horizontal and vertical modes. The coupled horizontal modes are less significant for the symmetric case of $\alpha_u = \alpha_d < 1.0$ (Fig. 4.10) as compared to the non-symmetric case of $\alpha_u \neq \alpha_d$ (Fig. 4.9) where a stronger two-dimensional behaviour is expected from the reservoir. From Fig. 4.10 it can be concluded that the absorption effect of the reservoir side boundaries is more significant for a lower L/H ratio. This conclusion is in agreement with the results of studies including an absorptive dam-reservoir interface in section 3.2.2.

In Figs. 4.9 and 4.10 , there is a slight frequency shift in the hydrodynamic response of the reservoir subjected to vertical ground motion as the reflection coefficients of its side boundaries are decreased. This behaviour is opposite to the direction of the frequency shift of the response peaks in Fig. 4.6 which represents a typical trend in the response of the systems subjected to the harmonic loading. In Fig. 4.6, as the reflection coefficient, α_b, decreases, the reservoir substructure remains unchanged except for an increased damping ratio which results in a lower value for the response peak and a slightly lower resonance frequency. In Figs. 4.9 and 4.10 , as the reflection coefficients of the reservoir sides decrease, the behaviour of the impounded water excited by the uniform vertical ground motion becomes more two-dimensional which leads to higher frequencies of free vibration for the resulting system. Nevertheless, the lower reflection coefficients along the reservoir boundaries reduce the response peaks of the system as compared to the case of completely reflective boundaries at the sides.

Mesh refinement analysis

In order to select an appropriate mesh size for the finite element analysis of the dam-

reservoir system, a study is made on the effects of the mesh size on the hydrodynamic pressure response in the reservoir. The main factor in selecting the mesh refinement for computation of the response of the hydrodynamic pressure is the maximum frequency of harmonic excitation included in the analysis. According to Lysmer and Kuhlemeyer (1969), the characteristic size of a finite element in the solution of a wave propagation problem in a continuum should be limited to one twelfth of the minimum wave length considered in the analysis. In this study, the upper bound cut-off frequency in the closed-form solution of the hydrodynamic pressure is selected as $f = 25$ Hz. The frequency interval $0 \leq f \leq 25$ Hz covers the significant part of the seismic frequency range in earthquake response analysis of the structures. The results of the analysis within this frequency range are comparable with those reported by other researchers (Fenves and Chopra 1984a and 1985).

The wavelength of pressure waves in water associated with the frequency of $f = 25$ Hz is obtained as: $\lambda = C_w / f = 1420/25 = 57$ m which suggests a characteristic size of $a = 5$ m for the finite element mesh. Table 4.1 shows the relationship between the maximum excitation frequency included in the analysis in terms of the reservoir eigenfrequencies and the corresponding characteristic length of the finite element mesh.

The margin of error associated with the selection of a coarser mesh size is investigated. The results of the response of the hydrodynamic pressure at the reservoir bottom and the hydrodynamic force on a rigid dam subject to a harmonic vertical ground motion are presented in Figs. 4.11 and 4.12, respectively. Two different mesh sizes of $a = 5$ and 10 m equivalent to $a = 0.05$ H and $a = 0.10$ H are used where H denotes the depth of the reservoir. The results of the hydrodynamic response remain virtually unaffected by the reservoir mesh size for the frequency range of $\omega \leq 4\omega'_r$. The above frequency interval includes the first two peaks of the frequency response of the reservoir. Results of a case study

in section 4.4.2 show that maximum stresses in the dam do not significantly change by including more than the first two reservoir mode shapes in the analysis. Consequently, for the application of stress analysis of the dam and according to the criterion proposed by Lysmer and Kuhlemeyer, the mesh size of $a = 10\ m$ ($a = 0.10$ H) corresponding to including the first two reservoir mode shapes in the analysis is used towards a resulting saving in the computation time.

4.4.2 Structural Response of the Dam

Comparison with theoretical solutions

Figs. 4.13 and 4.14 show the finite element discretizations of the two-dimensional model of the reservoir with aspect ratios of L/H=2 and L/H=5, respectively. The one-dimensional loading and damping elements at the reservoir surrounding boundary are also shown in the above figures. Fig. 4.14 includes two different mesh sizes of the reservoir model. Fig. 4.14a contains a uniform mesh identical to the mesh shown in Fig. 4.13 for L/H=2 which is extended to the length of 5H. A different finite element discretization for the case of L/H=5 is considered as shown in Fig. 4.14b to reduce the number of elements in the fluid domain. The number of fluid quadrilateral elements in Fig. 4.14b is reduced to 216 compared with 360 elements in the uniform mesh shown in Fig. 4.14a. The number of one-dimensional loading and damping elements are also reduced from 42 and 54 to 30 and 42 elements, respectively. The loading elements are considered along the dam-reservoir interface and the reservoir bottom. The damping elements are included over the entire solid boundary of the reservoir model.

The structural response of the dam impounding the reservoir of L/H=5 for the two discretization models shown in Fig. 4.14 are compared to examine the margin of error

associated with replacing the uniform finite element mesh with a mesh with fewer number of elements. Fig. 4.15 shows a comparison of the crest acceleration response of the dam subjected to horizontal ground motion using the above two reservoir models. The acceleration of the dam crest is calculated for the unit input acceleration to the model. Maximum tensile stresses at locations of the dam monolith that are more prone to crack initiation are shown in Table 4.2. The finite element discretization of the dam monolith together with the elements with the highest stresses across the monolith section are shown in Fig. 4.16. The locations of the elements of maximum tensile stress in Fig. 4.16 are in accordance with the reported evidence of crack locations in the dams that have undergone severe ground motions (Pekau 1991, Ahmadi 1992).

The selected ground motion is the longitudinal component of Nahanni earthquake in Northwest territories, Canada on December 23, 1985 with the PGA of 1.1g recorded at Iverson (Naumoski *et al.* 1988). The 1985 Nahanni ground motion record is selected as one of the available strong ground motion records in Canada with high frequency content. It is expected that the conclusions based on the above mentioned record are also valid for the records with lower peak values. The Nahanni accelerogram has a PGA/PGV ratio (Peak acceleration in g's to maximum velocity in m/s) of 2.38. The record is scaled to the PGA of 0.35g for the analysis so that the maximum stresses remain within the uncracked range of the material behaviour. The selection basis for the mechanical strength of the monolith concrete is discussed in Chapter 5. The scaled record of Nahanni earthquake is shown in Fig. 4.17.

The foundation of the dam is assumed as rigid and the reflection coefficients of the reservoir bottom and the far boundary are chosen as $\alpha_b = 0.9$ and $\alpha_u = 0.0$, respectively. The structural response of the dam is approximated using its first six mode shapes. The effects

of hydrostatic loading and the weight of the monolith are included in the computation of the stresses.

According to Fig. 4.15 and Table 4.2, the results of the dam crest acceleration response and developed stresses in the dam are virtually unchanged after replacing the uniform mesh shown in Fig. 4.14a with the nonuniform mesh of Fig. 4.14b. It is concluded that the selected finite element discretization shown in Fig. 4.14b can be satisfactorily used for further analysis of the reservoir model with L/H = 5. The number and size of transition elements are appropriately selected so as not to develop noticeable spurious reflections within the fluid domain (Celep and Bažant 1983).

Seismic response of short-period structures, such as concrete gravity dams, is essentially due to the fundamental mode of vibration. Accordingly, The response of the dam based on the fundamental mode is studied here as the initial step of the solution procedure verification with regard to the structural behaviour of the dam. Fig. 4.18 shows the crest acceleration response of the dam monolith on rigid foundation under horizontal excitation using the fundamental mode of the dam for the approximation of the structural response. The finite element solution results corresponding to different L/H ratios are compared with the response of the dam impounding an infinitely long reservoir based on a closed-form solution for the hydrodynamic pressure. The curves corresponding to the closed-form solution for the case of an infinitely long reservoir ($L/H \to \infty$) shown in Fig. 4.18 are in good agreement with the closed-form solution curves given by Fenves and Chopra (Curves 1 and 3 in Fig. 4.19). Two main parameters governing the structural response of the dam are identified. These are the reservoir-to-monolith frequency ratio and the wave reflection coefficient of the reservoir bottom materials, α_b. A third parameter is the depth of the impounded water to dam height, H/H_s. However, this parameter is not included in the present analysis by assuming full

reservoir condition, $H/H_s=1.0$. The reservoir-to-monolith frequency ratio, Ω_r, is defined as:

$$\Omega_r = \frac{\omega_r^1}{\omega_s^1} \tag{4.15}$$

where ω^1_s is the fundamental frequency of the dam monolith on rigid foundation. The results in Fig. 4.18 are given for two different values of $\alpha_b = 1.0$ and $\alpha_b = 0.5$, respectively. For the cases presented in Fig. 4.18, $\Omega_r = 22.305/24.325 = 0.92$. For this reason, the fundamental frequency peaks for the case of infinite reservoir ($L/H \rightarrow \infty$) in Fig. 4.18 are slightly different from the peak values for the frequency ratio of $\Omega_r = 1.0$ given by Fenves and Chopra (Fig. 4.19).

According to Fig. 4.18, the results of the structural response of the dam impounding a finite length reservoir model with aspect ratios shown in the figure and radiation condition at the truncated boundary are similar to the results for the case of an infinitely long reservoir subjected to horizontal ground motion. The agreement is satisfactory for both cases of $\alpha_b = 1.0$ and $\alpha_b = 0.5$ at the reservoir bottom as two extreme cases of practical situations.

For the case of vertical excitation, there is a noticeable difference between the two cases of the closed-form solution of an infinite reservoir and the finite element solution of the truncated reservoir model. Sommerfeld radiation condition requires that the radiating boundary should be sufficiently far from the source of excitation. When the dam-reservoir system is subjected to horizontal ground motion, the harmonic excitation of the rectangular-shaped reservoir originates from the monolith's vibration. Therefore, for a sufficiently long reservoir model (e.g., $L/H \geq 2$) the absorptive boundary condition with $\alpha_u = 0.0$ leads to a satisfactory agreement with the solution for the case of the infinite-length reservoir. In the case of vertical component, the excitation of the reservoir is introduced along the entire

reservoir bottom which extends as far as the truncated end of the fluid model. In this case, the absorption boundary condition does not satisfactorily represent the radiation of pressure waves to the far field because the absorptive boundary is not sufficiently far from the exciting boundary. Accordingly, applying the absorption boundary condition or the equivalent Sommerfeld radiation condition leads to erroneous results for crest acceleration response of the dam subjected to the vertical ground motion. In a reservoir model with absorptive far end boundary, the geometric ratio between the loading length of the reservoir boundary at the bottom, L, to the length of its absorptive part at the far end, H, when subjected to uniform vertical ground motion is larger for a higher L/H ratio. In this case where the far boundary is modelled with Sommerfeld radiation condition, the fundamental peak of the monolith response is unrealistically larger for a higher L/H ratio of the reservoir model.

In Fig. 4.20, curve 2 shows the calculated response of the dam when the far end boundary of the reservoir under vertical ground motion is modelled using the Sommerfeld boundary condition. Comparison between curve 2 and curve 1 (which is based on the closed-form solution of the infinite-length reservoir) reveals that Sommerfeld boundary condition is not a valid model for radiation of the pressure waves to the upstream far end under uniform vertical excitation of the reservoir bottom boundary. However, in the case where only a part of the reservoir bottom adjacent to the dam is assumed as the exciting boundary of the reservoir under vertical ground motion, the result of the crest acceleration response approaches the corresponding result for the case of a theoretically infinite reservoir (Curves 3 and 4 in Fig. 4.20).

In the case of partial excitation of the reservoir bottom under vertical ground motion, horizontally travelling waves similar to the case of horizontal excitation of the reservoir

develop in the impounded water. The response function of the hydrodynamic pressure in the reservoir is similar to the response function in the case of horizontal ground motion. In the case of a short excited part of the reservoir bottom to the total length of reservoir model, L_e/L, close agreement with the closed-form solution is obtained. This is because the excited boundary becomes sufficiently far from the radiating boundary. The case of partial excitation of the reservoir bottom appears to be more realistic compared with the uniform excitation throughout the bottom boundary (Hall 1986). However, the part of the reservoir bottom boundary subjected to vertical excitation in the model should be long enough so that the response of the dam for the two cases of truncated and infinite length reservoir models are comparable. In the case study shown in Fig. 4.20, the calculated response of the dam using the finite element model for the reservoir with L/H=5 coincides with the response obtained based on the closed-form solution of the infinite-length reservoir when $L_e/H=1$ (Curve 4 in Fig. 4.20). This result suggests a characteristic length equal to the reservoir depth as the minimum loading length of the reservoir bottom boundary under vertical ground motion. For a shorter loading length, the dam response will be substantially reduced (Curve 5 in Fig. 4.20 and Hall 1986). The numerical results may vary to some extent for different models of the dam-reservoir systems. However, the general conclusions regarding the performance of Sommerfeld boundary condition under uniform vertical ground motion and the length of the loading bottom boundary in the finite element analysis of the reservoir remain valid.

The frequency response functions of the crest acceleration under horizontal ground motion including ten Ritz vectors are shown in Fig. 4.21. Compared with the results of Fig. 4.18 when only the fundamental mode shape of the dam was included, there is a difference between the results of the truncated and the infinite-length reservoir models in the higher frequency range. The difference is significant in the vicinity of the second resonance

frequency of the reservoir. This is in accordance with the reported drawback of the Sommerfeld radiation condition in some previous studies (Humar and Roufaiel 1983, Sharan 1984 and Humar 1984). Also, from Fig. 4.21 it is apparent that increasing the length of the reservoir model does not lead to an improvement in the result of the dam response as indicated by Humar and Roufaiel (1983).

A different boundary condition proposed by Sharan (1992) is also examined to model the truncated far end boundary of the reservoir. Fig. 4.22 shows the crest acceleration response of the dam with a truncated reservoir model where the curtailed boundary is modelled using Sommerfeld and Sharan (1992) boundary conditions (Eqs. 4.6 and 4.8, respectively). The results of the acceleration response for the case of the infinite-length model based on the closed-form solution of Eqs. 4.10 and 4.14 are also shown for comparison. The dam foundation is assumed rigid. Sharan boundary condition (Eq. 4.8) is proposed as a model for the radiation of pressure waves when the reservoir bottom is absorptive. The reflection coefficient of the reservoir bottom is taken as $\alpha_b = 0.5$. Sharan radiation condition is claimed to have satisfactory performance for short truncated reservoir models (Sharan 1992). The results in Fig. 4.22 are presented for the range of reservoir aspect ratios from L/H=1 to L/H=10. The first six Ritz vectors are included for the structural response of the dam. According to Fig. 4.22, the above two radiation conditions coincide for the case of L/H $\geq$5 (Figs. 4.22b and 4.22c). However, there is a significant difference between the two numerical results and the closed-form solution in the frequency range of $1.5 < \omega/\omega^1_r < 3.5$ regardless of the reservoir length to depth ratio. The above discrepancy in the results of the radiation conditions is reported by Sharan (1984) and Humar and Roufaiel (1983) for the case of Sommerfeld radiation condition (Eq. 4.6) and by Sharan (1992) for the condition given by Eq. 4.8.

For the case of L/H = 1, on the other hand, there is a significant difference between the results of the dam response using Sharan boundary condition and the closed-form solution throughout the frequency range shown in the Figs. 4.22 and 4.23. Although by increasing the L/H ratio of the truncated reservoir model the results of the acceleration response of the dam crest approach the corresponding results for the case of the infinite-length reservoir, the difference is remarkable even for a large value of L/H=10 (Figs. 4.22 and 4.23). For the case of L/H=10, the difference is mainly limited to the frequency range $1.5 < \omega/\omega'_r < 3.5$ similar to what is reported by Sharan (1991 and 1992); However, the L/H ratio of the reservoir truncated model is much larger than the ratio used in the above references.

Results of Fig. 4.23 confirm that Sommerfeld boundary condition is less dependent on the variation of the L/H ratio (Humar and Roufaiel 1983 and Sharan 1984) compared with Sharan radiation condition.

Equation 4.8 is based on the closed-form solution for the hydrodynamic pressure in the reservoir under horizontal excitation (Eqs. 4.10 and 4.14). The closed-form solution is expressed in terms of series expansion of the eigenvectors of the reservoir model. The boundary condition in Eq. 4.8 is derived on the grounds that the second and higher terms in the series expansion are negligible for a relatively large value of L/H ratio. Figures 4.24 and 4.25 show the plots of the real and imaginary parts of the eigenvalues ζ_n and κ_n for n = 1,2. Based on the magnitudes and variations of these eigenvalues with the normalized frequency, ω/ω'_r, the assumption of neglecting the higher terms regardless of the dominant frequency of excitation is not justified for low L/H ratios.

Based on the above analysis, Sommerfeld boundary condition is chosen as the radiation condition which gives the results for the hydrodynamic response of the truncated

reservoir models that are comparable with the response obtained using the closed-form solution for infinite-length reservoir.

Effect of mesh refinement on the structural response

The finite element approach developed in this study requires a long solution time. To make the analysis more efficient, it is of interest to investigate the optimum number of parameters that should be included in the analysis procedure. The main analysis factors include the refinement of the finite element mesh of the reservoir and the number of Ritz vectors to represent the structural response of the dam. According to the results of section 4.4.1, the mesh refinement can be decided upon based on the number of reservoir mode shapes that are sufficient to be included in the analysis. The criteria adopted in the present study to decide on the number of reservoir eigenvectors are based on the maximum developed stresses in the monolith together with the frequency response of the crest acceleration.

A dam 91.5 m high with base width of 72.0 m is analyzed. The modulus of elasticity of the dam concrete is taken as 20700 MPa. Figure 4.26 shows the finite element discretizations of the dam-reservoir system using reservoir mesh sizes of a = 4.6 m and a = 9.1 m, respectively. The reservoir aspect ratio of L/H=1 is considered so as to reduce the number of finite elements in the reservoir model to a minimum.

The crest acceleration response of the dam for the above two discretized models is shown in Fig. 4.27. The calculated maximum stresses in the dam based on the above two numerical models are presented in Table 4.3. The foundation of the dam is assumed rigid and the reflection coefficients of the reservoir bottom and far end boundaries are taken as $\alpha_b = \alpha_u = 0.9$, respectively. The average of the calculated stress values at the Gauss points

of four neighbouring elements in the fine mesh is compared with the corresponding element in the coarse mesh as shown in Fig. 4.26. The stress time history responses at the kink of the downstream slope (elements 31,32,39 and 40) and the heel of the dam (elements 145,146,153 and 154) are shown in Fig. 4.28. The results of acceleration response shown in Fig. 4.27 and 4.28 together with the values of the stresses in the dam presented in Table 4.3 indicate that the calculated structural response of the dam does not change significantly by replacing the finite element mesh size of $a = 4.6$ m with the coarser mesh size of $a = 9.1$ m. According to Table 4.1, the use of the coarser mesh size of $a = 9.1$ m is equivalent to including only the first two mode shapes of the reservoir in the analysis. This result is in accordance with the conclusion reached in section 4.4.1 (Fig. 4.12).

Minimum Number of Ritz Vectors

A series of parametric studies is conducted to investigate the appropriate number of Ritz vectors (NTRZ) for the case of a finite element solution of a limited length reservoir. The main factors included in the study are presented in Table 4.4. The results of the frequency response of the crest acceleration for different analysis cases are plotted in Figs. 4.29 to 4.34. In the above figures, the excitation frequency is normalized with respect to the fundamental frequency of the dam-foundation system with an empty reservoir, ω^1_s. The value of ω^1_s is selected because it is independent of the reservoir boundary conditions in the parametric study. The corresponding values of ω^1_s for the cases of rigid and flexible foundation rock ($E_f = E_c = 20700$ MPa) are 24.305 and 18.634 rad/s, respectively.

Figure 4.29a shows the comparison of the monolith's crest acceleration response using selected numbers of Ritz vectors, NRTZ, for the structural approximation. The dam is assumed to rest on a flexible foundation with modulus of elasticity $E_f = E_c$. The reservoir

length is twice its depth and the reflection coefficients of the reservoir bottom and far side are taken as $\alpha_b = \alpha_u = 0.9$, respectively. Three values of Ritz vectors (3, 6 and 10) are included to approximate the deflection of the dam. In Fig. 4.29a, the curves associated with 6 and 10 Ritz vectors coincide satisfactorily within the frequency range $\omega \leq 4\omega^1_s$. The curve using 3 Ritz vectors approximately matches the fundamental peak of the response using larger number of Ritz vectors but does not satisfactorily capture the higher frequency peaks. Figure 4.29b shows similar results for the case of a longer reservoir with L/H=5.

In the case of rigid foundation rock (Fig. 4.30), the frequency response of the dam crest acceleration calculated using 3 Ritz vectors shows a better agreement with the curve using 10 Ritz vectors over a wider frequency range compared with the case of flexible foundation. This agrees with the observations reported by Fenves and Chopra (1984a). Figures 4.31 and 4.32 show the corresponding results of the above study for the case of $\alpha_b = \alpha_u = 0.5$. The results shown in Figs. 4.29 to 4.32 indicate that the amplitudes of the frequency response peaks do not significantly vary with the increase of the reservoir length to depth ratio from L/H = 2 to L/H = 5 regardless of the number of Ritz vectors used in the analysis. This conclusion is in accordance with the results of the reservoir length effect discussed in section 3.2.2 based on the closed-form solution for the hydrodynamic pressure (Fig. 3.5).

The crest acceleration response results for the case of a dam-reservoir system subjected to vertical ground motion is presented in Figs. 4.33 and 4.34. The general conclusions for the case of horizontal ground motion are also valid for uniform vertical excitation of the dam-reservoir system. Comparison of Figs. 4.29 and 4.33 indicates that for the case of a dam on flexible foundation, a larger number of dam mode shapes is needed for reasonable accuracy of its structural response in the higher frequency range ($\omega \geq 6\omega^1_s$)

when the dam-reservoir system is subjected to the vertical ground motion compared to the horizontal component. In the present numerical example, $\omega^1_s = 18.634$ rad/s and therefore: $\omega \geq 6 \times 18.634 = 112$ rad/s or $f \geq 18$ Hz. This frequency is in the higher range of the dominant earthquake frequencies and therefore of little concern.

The stress in the dam is the important parameter in the design and safety assessment of dam structures. Accordingly, the effect of the number of Ritz vectors on the magnitude and location of the maximum principal stresses developed in the dam monolith is studied. Table 4.5 contains the calculated maximum principal stresses in the monolith during the first 12 seconds of the Nahanni horizontal ground motion for the cases of the flexible and rigid dam foundation, respectively. For the vertical excitation of the dam-reservoir system, the Nahanni accelerogram is applied in the vertical direction. Similar results for the vertical input ground motion are given in Table 4.6. In Tables 4.5 and 4.6, the reflection coefficients of the reservoir bottom and far end boundary are taken as $\alpha_b = \alpha_u = 0.9$, respectively.

Results of Tables 4.5 and 4.6 indicate that the location of the calculated maximum stress in the cross section of the dam monolith may be different based on the number of Ritz vectors included in the analysis. The above issue is a concern regarding the proper design of the dam monolith. A possible solution is to consider the envelope of the maximum stress values at different locations within the monolith cross section based on various numbers of Ritz vectors in the analysis. The selected number of Ritz vectors in the analysis depends on the foundation flexibility and the frequency content of the input ground motion. A higher number of Ritz vectors is included in the analysis for a stiffer foundation and a higher dominant frequency of the design ground motion.

4.5 CONCLUSIONS

A finite element program (DAD-96) is developed to calculate the dynamic response of gravity dams impounding a finite-length reservoir with absorptive boundaries. The reservoir model is two-dimensional and can be of any arbitrary shape. The dam can have vertical or inclined upstream face and subjected to both horizontal and vertical ground motion components. The performance of the program is tested and verified by comparing the results of the hydrodynamic response of the reservoir and structural response of the dam with the available closed-form solutions for special reservoir geometry and boundary conditions. The developed hydrodynamic pressure at the bottom of a rectangular shaped reservoir and the total hydrodyamic force on the vertical upstream face of a typical gravity dam are selected for comparison. The structural response of the dam is characterized by the frequency response of the crest acceleration.

The response of the reservoir model with different length to depth ratios under harmonic horizontal and vertical excitations is studied. It is concluded that the response of an infinitely long reservoir under horizontal ground motion can be satisfactorily modelled using the Sommerfeld boundary condition at the far end boundary of a sufficiently long truncated reservoir model. The response of the truncated model confirms the existence of some discrepancies with the closed-form solution in the vicinity of the second resonant frequency of the impounded water reported in some former studies (Humar and Roufaiel 1983, Sharan 1984 and Humar 1984). It is shown that modelling the truncated far end boundary using the Sommerfeld boundary condition under vertical ground motion does not lead to satisfactory results. However, for the case where a part of the reservoir bottom boundary was subjected to vertical excitation ($L_e/H = 1$), the use of the Sommerfeld boundary condition resulted in better agreement with the closed-form solution of the

structural response of the dam impounding an infinitely long reservoir and subjected to vertical ground motion.

A series of studies are conducted to determine the appropriate values for the important parameters governing the response of the dam-reservoir model. The refinement of the finite element mesh and the number of Ritz vectors for approximating the dynamic response of the dam are selected as the main study parameters. For the example dam-reservoir system studied in this chapter, a minimum number of six Ritz vectors for the dam model together with the finite element mesh size of smaller than $a = 0.1$ H was needed for satisfactory results of the calculated stress in the dam for various conditions of the foundation flexibility, ground motion components and reflection coefficients of the reservoir boundaries. It was shown that the mesh size of $a = 0.1$ H is equivalent to including the second free vibration frequency of the reservoir in the response computation of the dam-reservoir system.

Table 4.1. Relationship between the number of reservoir mode shapes in the analysis and the size of the finite element mesh

Reservoir mode shape in vertical direction (n)	Frequency f (Hz)	Mesh size $a = \lambda/12$ (m)
1	3.5	33
2	11	11
3	18	7
4	25	5

Table 4.2. Maximum tensile stresses in the dam monolith subjected to the horizontal component of Nahanni earthquake using different reservoir mesh sizes shown in Fig. 4.14 (values in MPa)

Element #	Uniform Mesh	Non-Uniform Mesh
13	3.93	3.95
16	3.97	3.96
45	1.64	1.64

Table 4.3. Calculated maximum tensile stresses in the dam based on the finite element models shown in Fig. 4.26.

Location		Fine mesh			Coarse Mesh		Error %
		Element #	Stress (MPa)	Average (MPa)	Element #	Stress (MPa)	
Neck	Up-stream	25	4.55	3.70	9	3.53	4.6
		26	3.19				
		33	4.24				
		34	2.83				
	Down-stream	31	3.81	4.16	12	4.04	2.9
		32	5.42				
		39	3.48				
		40	3.93				
Heel		145	2.08	1.77	37	1.73	2.3
		146	1.38				
		153	2.32				
		154	1.29				

Table 4.4 Study parameters in the finite element analysis of the dam-reservoir system

Description	Variants
Ground Motion Component	H and V
L/H	2 and 5
Foundation Flexibility, E_f / E_c	1 and ∞
α_d	1.0
α_b	0.5 and 0.9
α_u	0.5 and 0.9
Number of Ritz vectors (NRTZ)	3, 6 and 10

Table 4.5. Maximum principal stresses in a dam monolith subjected to horizontal ground motion based on different numbers of Ritz vectors (NRTZ)

L/H	Foundation Condition E_f/E_c	NRTZ	Maximum Tension,σ_{max} (MPa)	Elem. No.	Maximum Compression,σ_{min} (MPa)	Elem. No.
2	1	3	1.71	16	-1.55	16
		6	1.68	16	-1.46	13
		10	1.69	16	-1.47	13
	∞	3	5.00	16	-5.31	16
		6	4.61	16	-5.10	16
		10	4.63	16	-5.15	16
5	1	3	1.73	16	-1.75	16
		6	1.48	16	-1.27	13
		10	1.51	16	-1.30	13
	∞	3	5.10	16	-5.07	16
		6	4.87	16	-4.77	16
		10	4.90	16	-4.77	16

Table 4.6. Maximum principal stresses in a dam monolith subjected to vertical ground motion based on different numbers of Ritz vectors (NRTZ)

L/H	Foundation Condition E_f/E_c	NRTZ	Maximum Tension,σ_{max} (MPa)	Elem. No.	Maximum Compression,σ_{min} (MPa)	Elem. No.
2	1	3	1.31	13	-1.53	16
		6	1.20	13	-1.19	16
		10	1.17	13	-1.19	16
	∞	3	4.76	16	-4.47	16
		6	4.34	16	-4.20	16
		10	4.34	16	-4.23	16
5	1	3	1.55	16	-1.61	16
		6	1.27	16	-1.20	13
		10	1.26	16	-1.25	13
	∞	3	5.15	16	-4.92	16
		6	4.83	16	-4.45	16
		10	4.84	16	-4.47	16

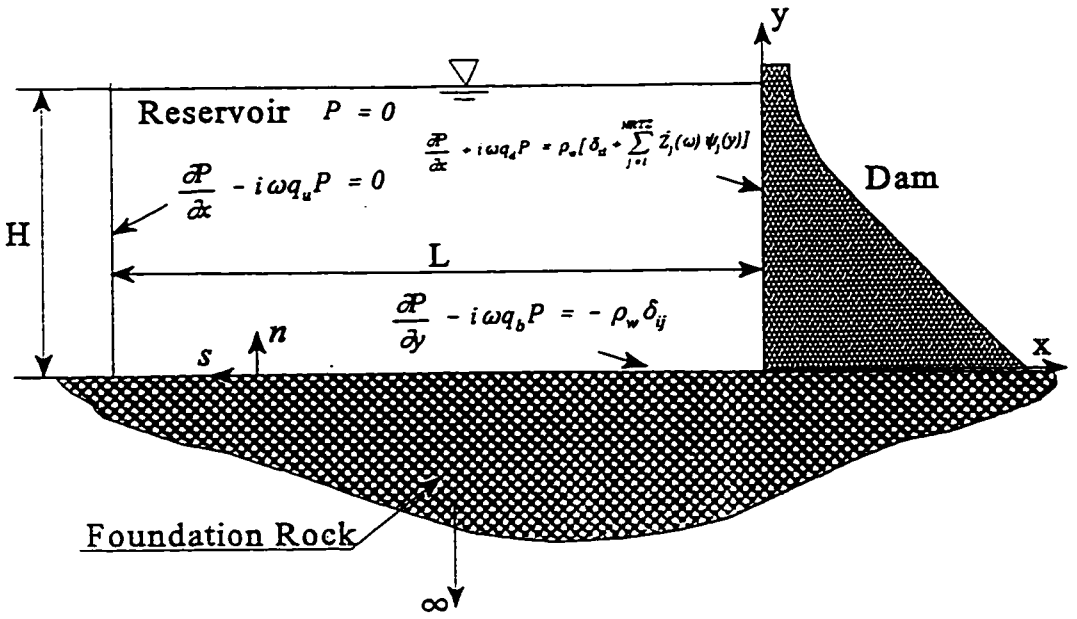

Fig. 4.1 Two-dimensional dam-reservoir model with absorptive boundaries

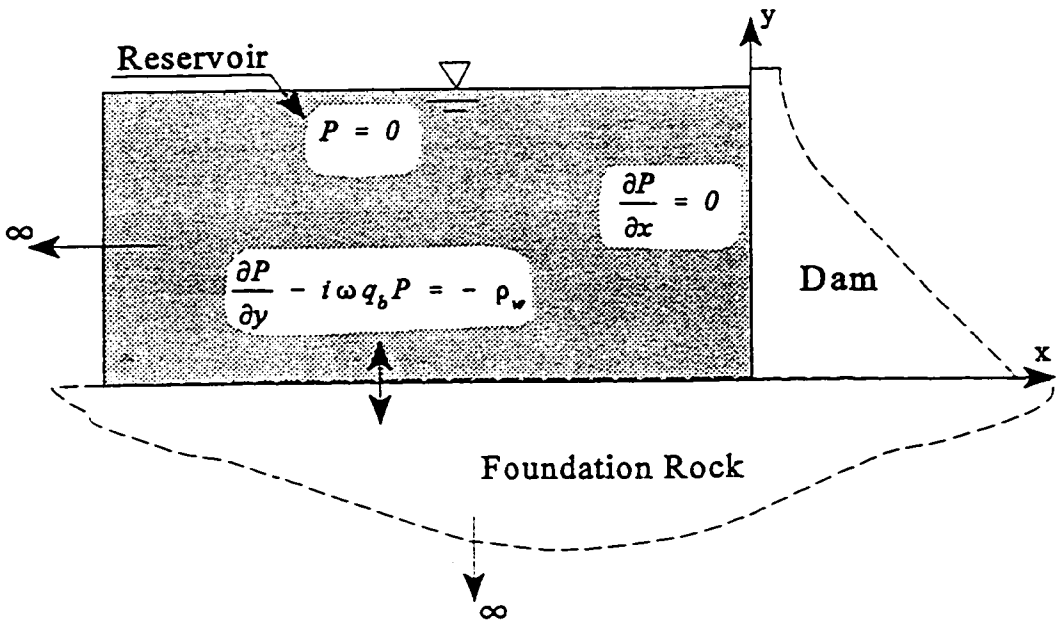

Fig. 4.2 Infinite-length reservoir with an absorptive bottom subjected to uniform vertical excitation

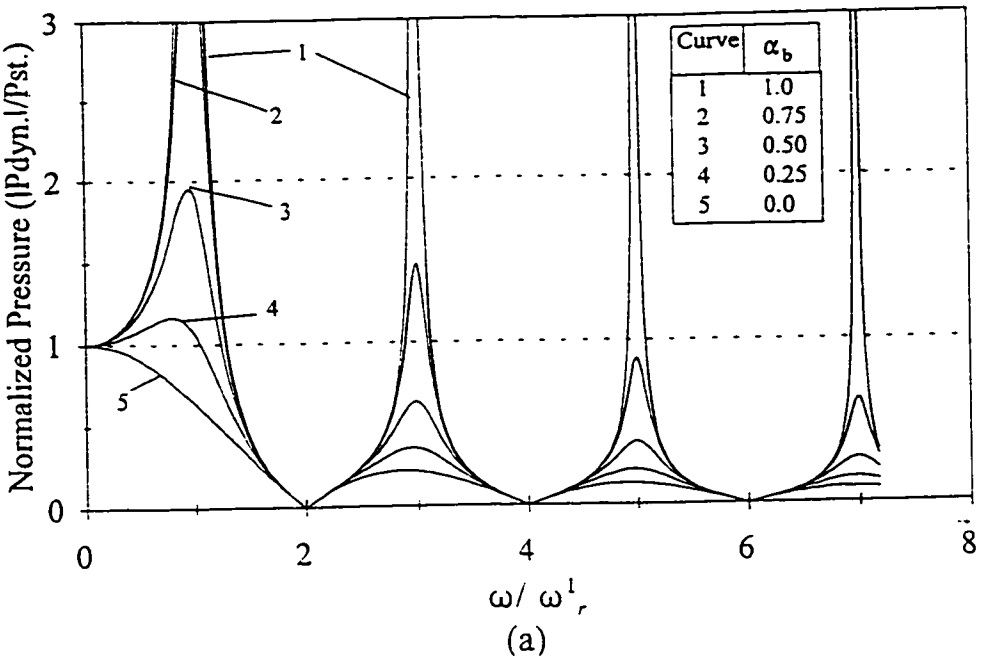

(a)

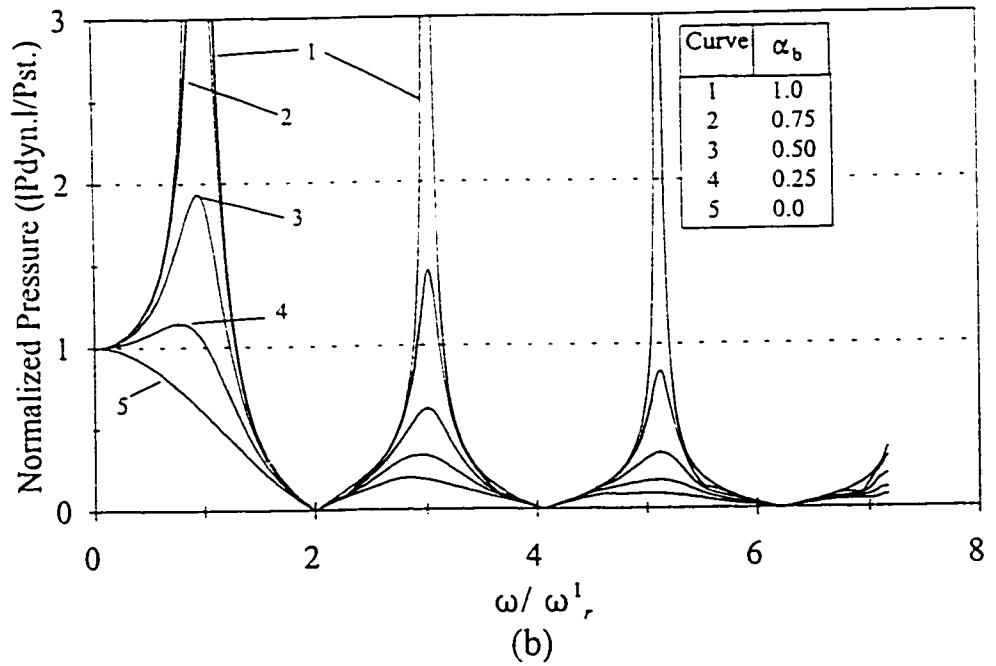

(b)

Fig. 4.3 Frequency response of the hydrodynamic pressure at the reservoir bottom due to vertical excitation: (a) Theoretical solution (b) Finite Element solution (Mesh width, $a = 10\ m$)

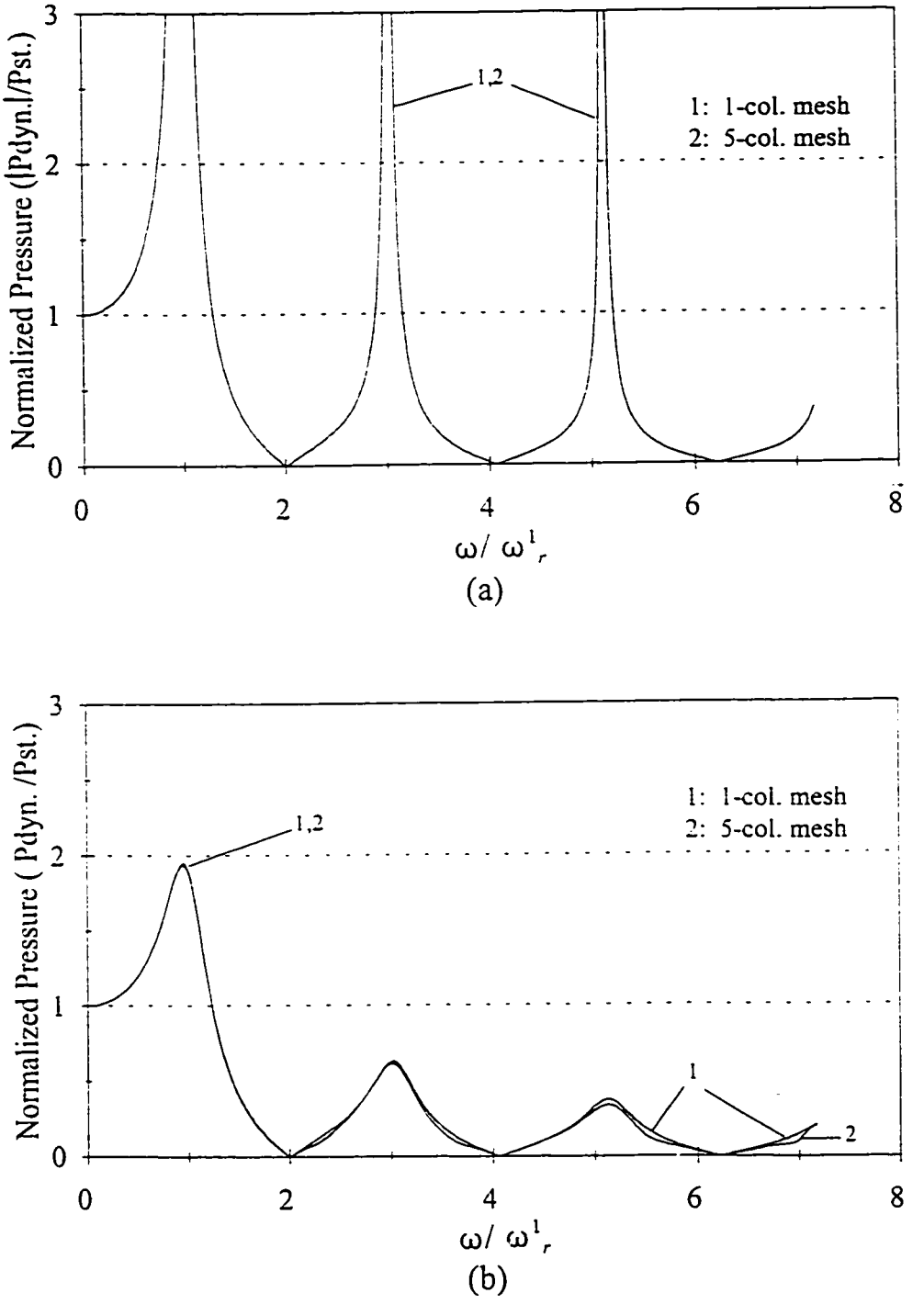

Fig. 4.4 Effect of the length of the reservoir mesh on the response of hydrodynamic pressure for different values of reflection coefficients (Mesh column width = 10 *m*) (a) $\alpha_b = 1.0$ (b) $\alpha_b = 0.5$

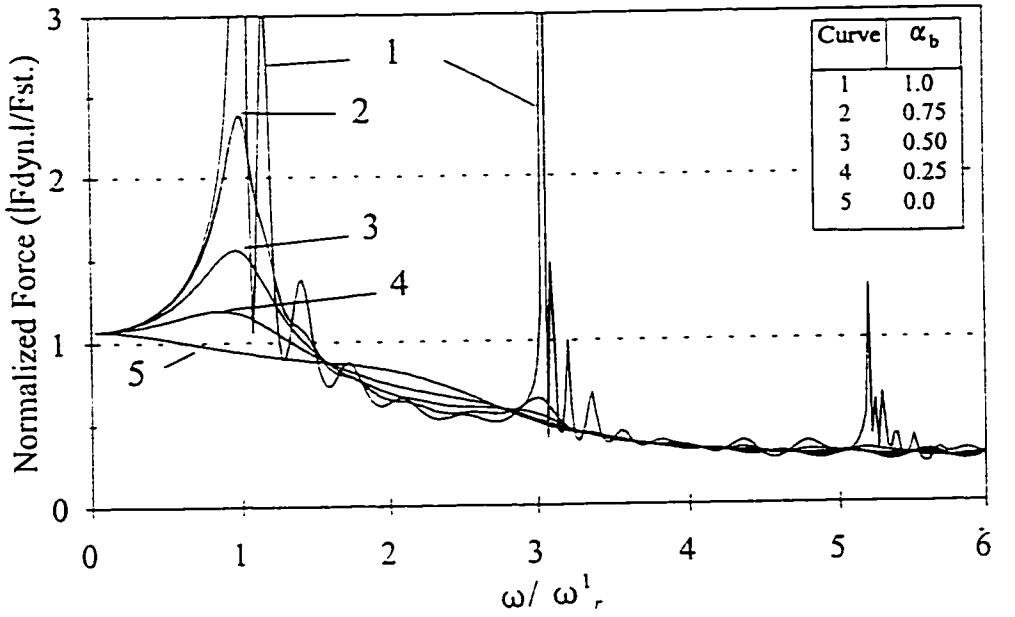

(a)

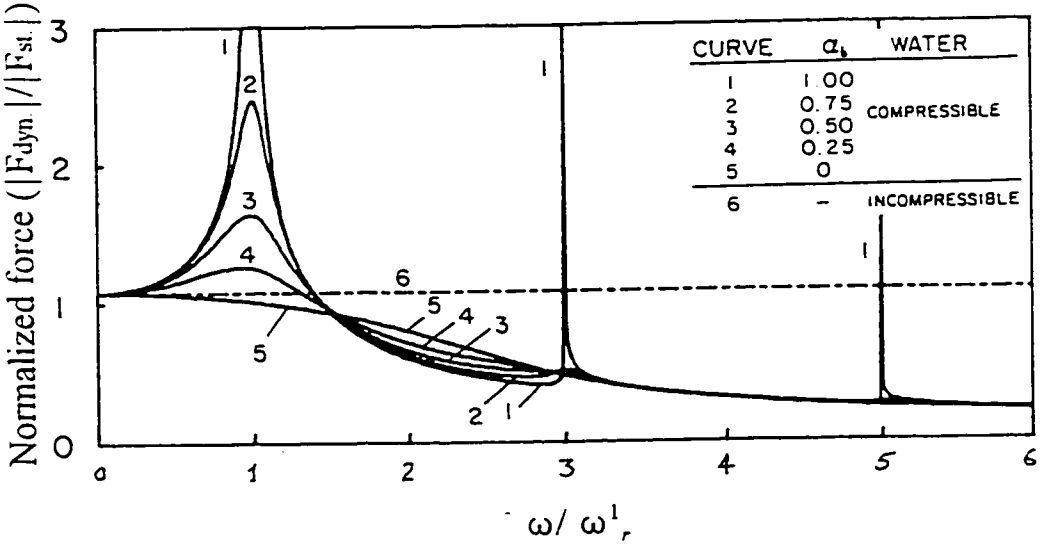

(b)

Fig. 4.5 Response of the hydrodynamic force on rigid dam subjected to harmonic horizontal ground motion for different reflection coefficients at the reservoir bottom: (a) Finite Element Solution (L/H=5) (b) Theoretical Solution (After Fenves and Chopra 1984a).

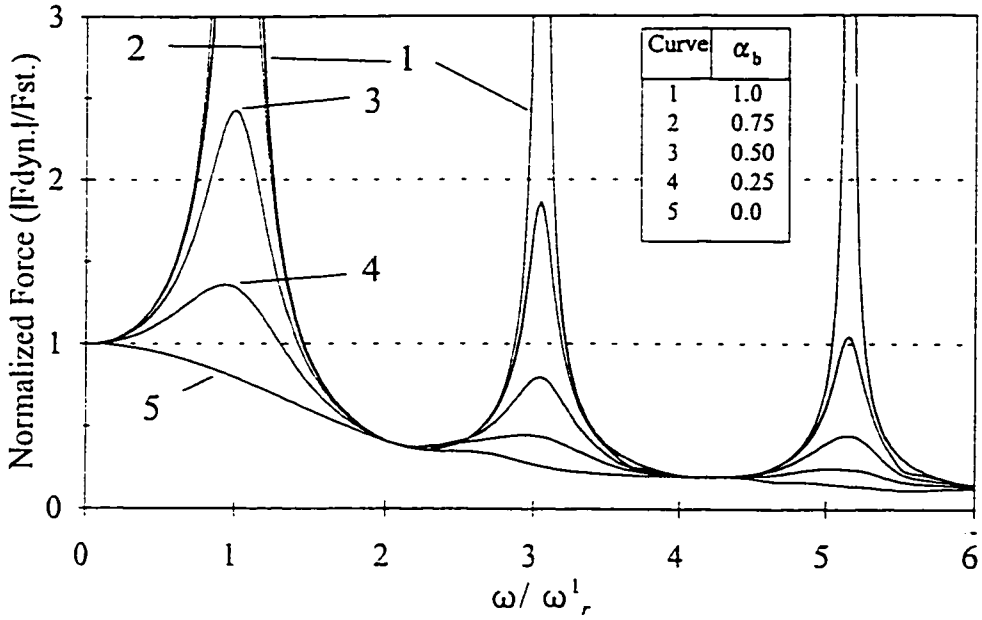

(a)

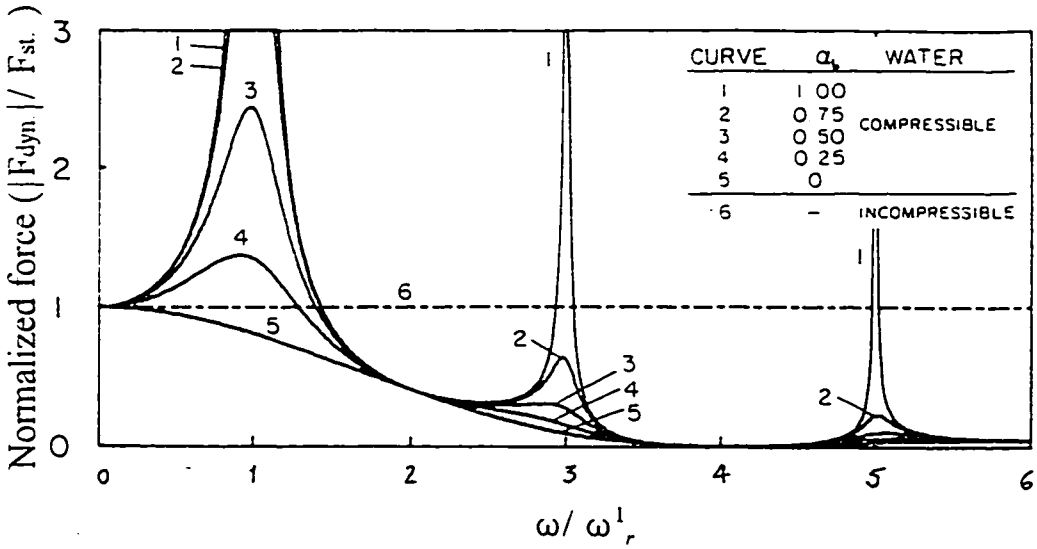

(b)

Fig. 4.6 Response of the hydrodynamic force on rigid dam subjected to harmonic vertical ground motion for different reflection coefficients at the reservoir bottom: (a) Finite Element Solution (L/H=5) (b) Theoretical Solution (After Fenves and Chopra 1984a).

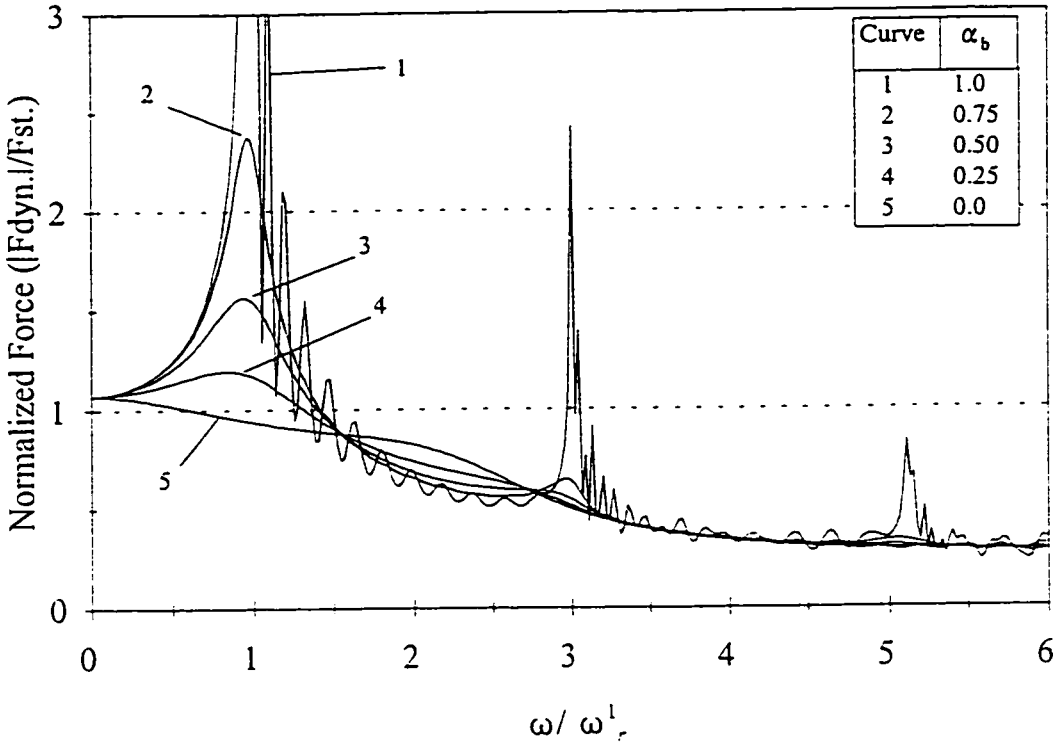

Fig. 4.7 Response of the hydrodynamic force on rigid dam subjected to horizontal excitation for a long reservoir (L/H=10)

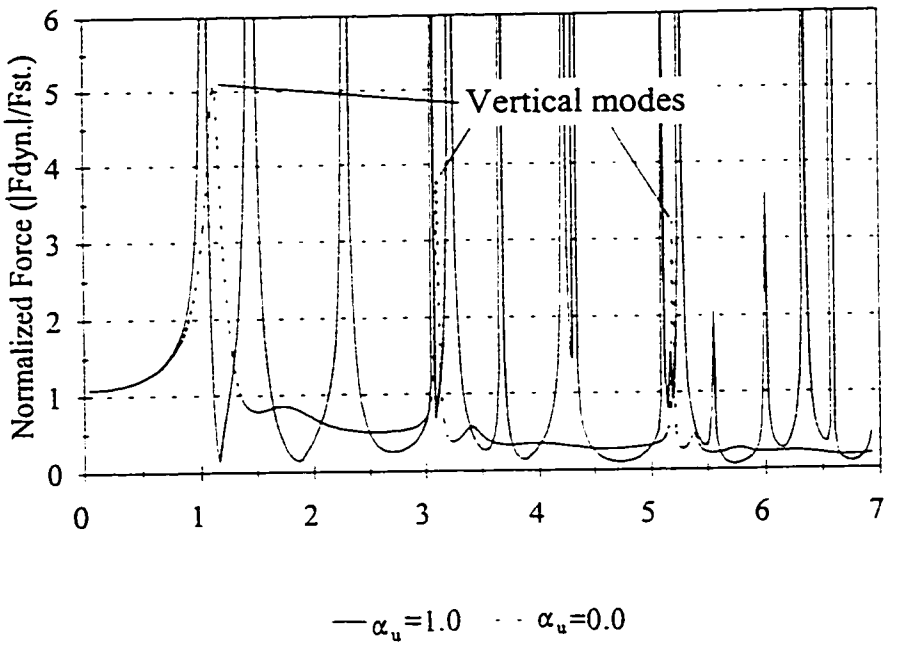

— α_u=1.0 · · α_u=0.0

(a)

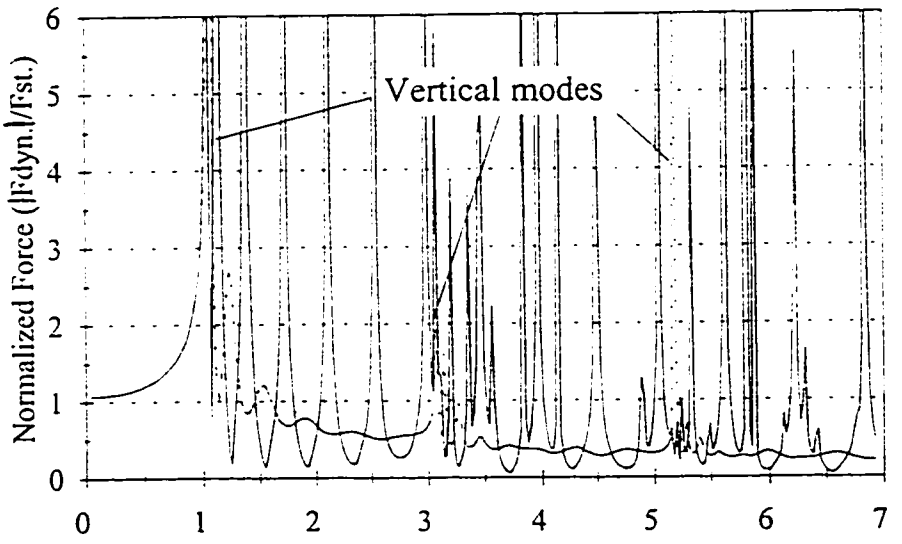

— α_u=1.0 · · α_u=0.0

(b)

Fig. 4.8 Effect of the absorption of pressure waves at the far end of the reservoir on the response of the hydrodynamic force on rigid dam subjected to horizontal ground motion ($\alpha_b = \alpha_d = 1.0$): (a) L/H=2 (b) L/H=5

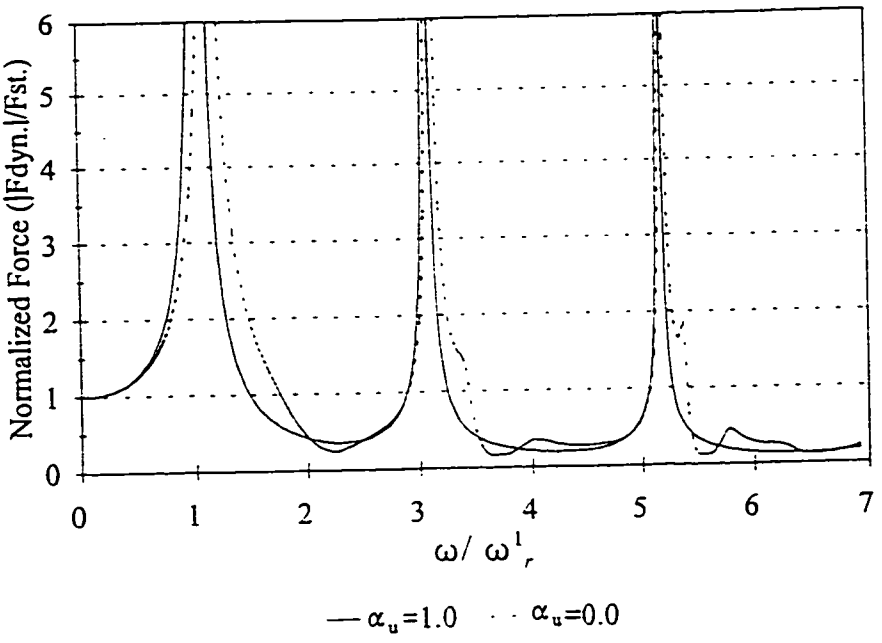

(a)

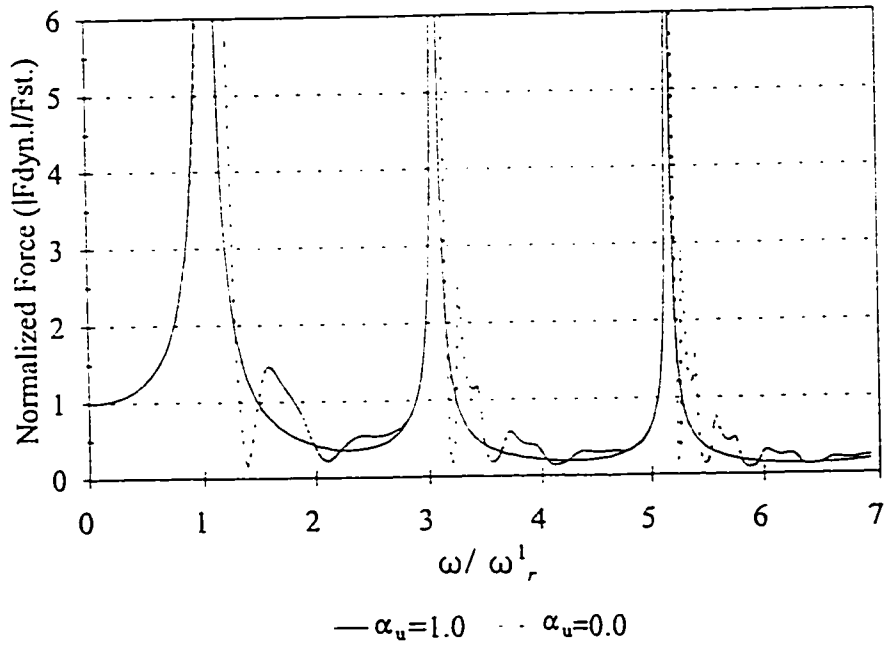

(b)

Fig. 4.9 Effect of the absorption of pressure waves at the far end of the reservoir on the response of the hydrodynamic force on rigid dam subjected to vertical ground motion ($\alpha_b = \alpha_d = 1.0$): (a) L/H=2 (b) L/H=5

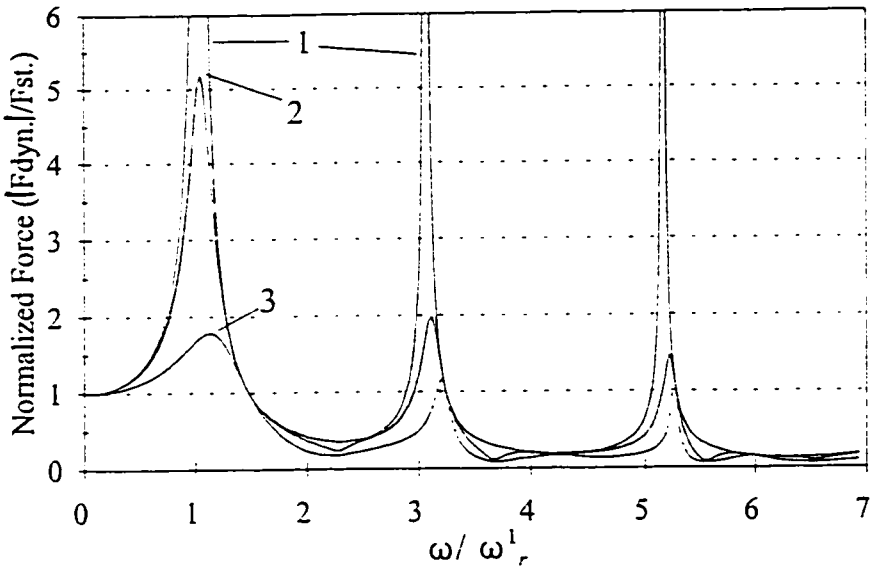

(a)

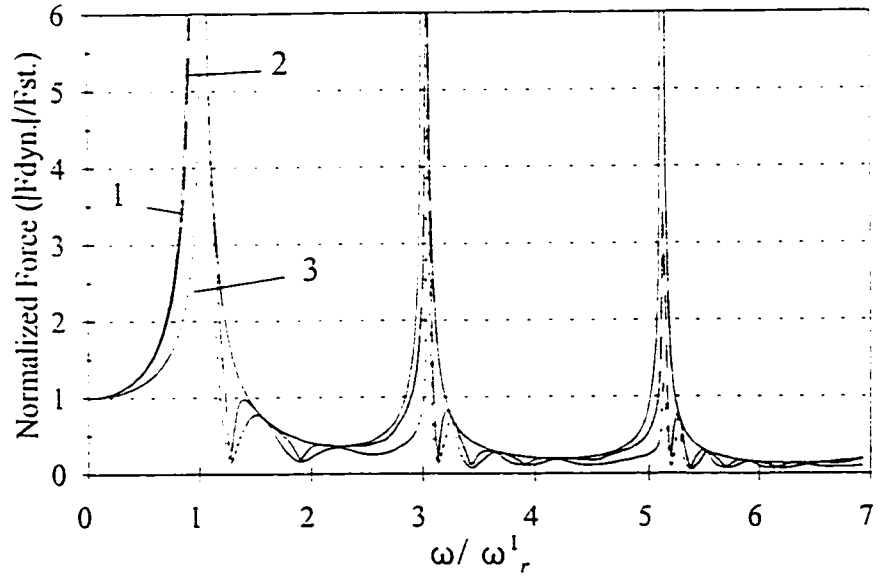

1: $\alpha_u = \alpha_d = 1.0$ 2: $\alpha_u = \alpha_d = 0.5$ 3: $\alpha_u = \alpha_d = 0.0$

(b)

Fig. 4.10 Response of the hydrodynamic force on rigid dam to vertical ground motion for different reflection coefficients at the reservoir sides ($\alpha_b = 1.0$): (a) L/H=2 (b) L/H=5

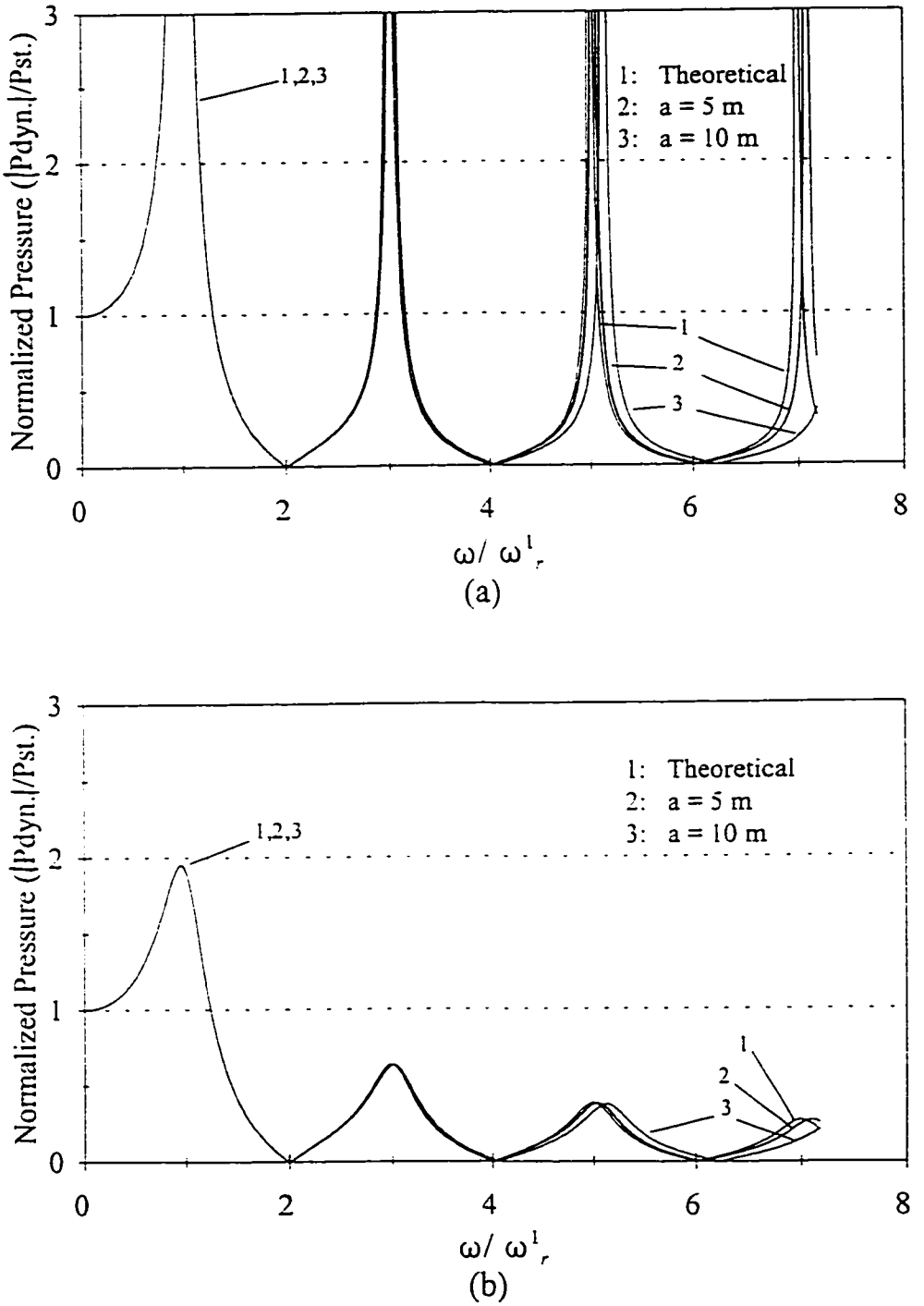

Fig. 4.11 Effect of the reservoir mesh refinement on the response of the hydrodynamic pressure at the reservoir bottom when subjected to vertical excitation: (a) $\alpha_b = 1.0$ (b) $\alpha_b = 0.5$

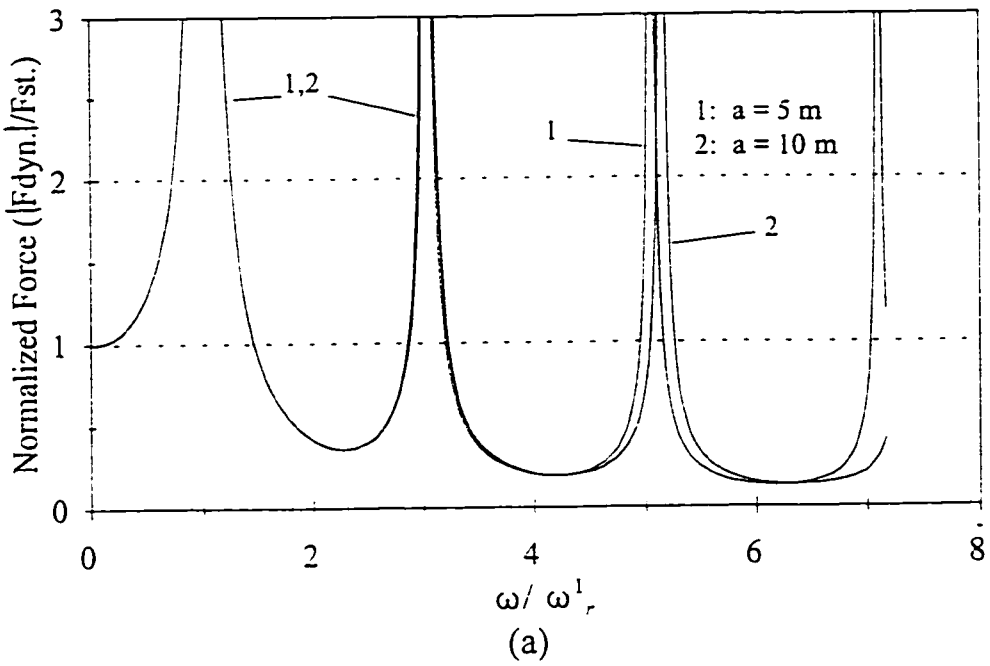

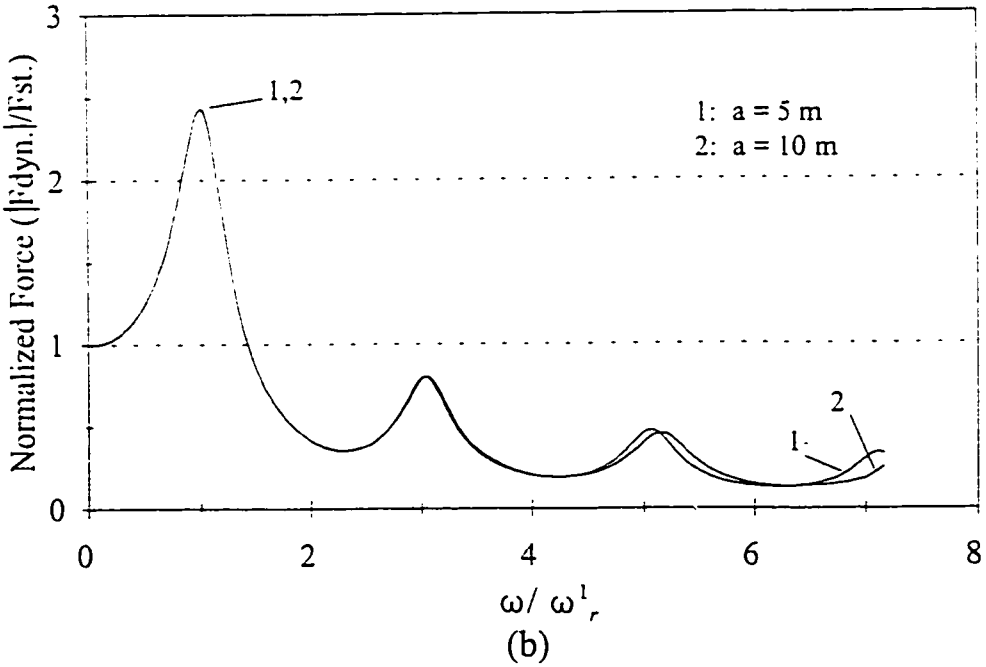

Fig. 4.12 Effect of the reservoir mesh refinement on the response of the hydrodynamic force on rigid dam subjected to vertical excitation: (a) $\alpha_b = 1.0$ (b) $\alpha_b = 0.5$

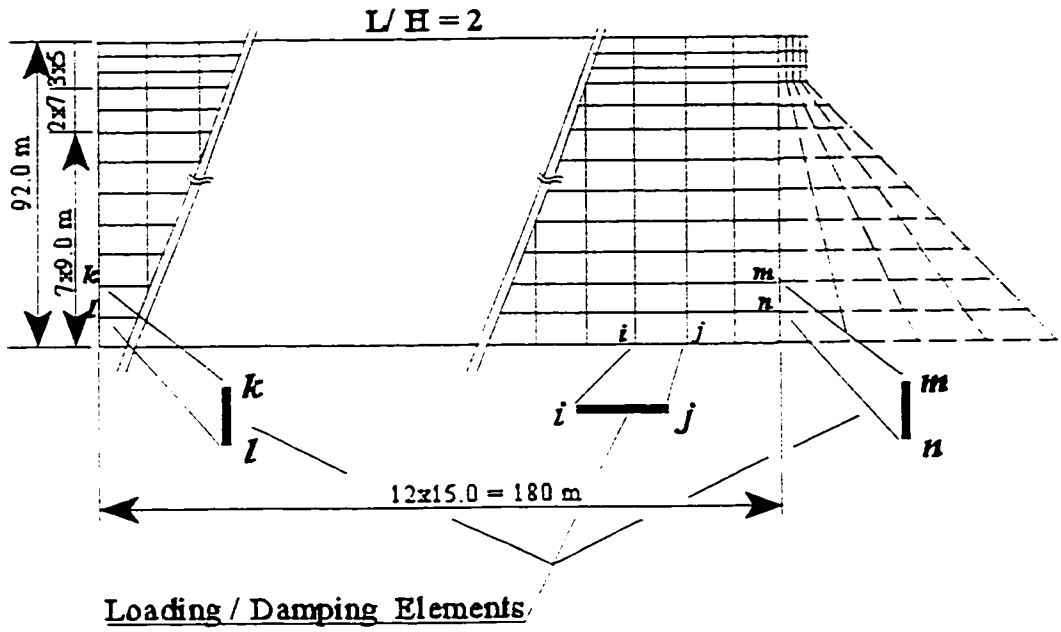

Fig. 4.13 Finite element model of the dam-reservoir system with L/H = 2

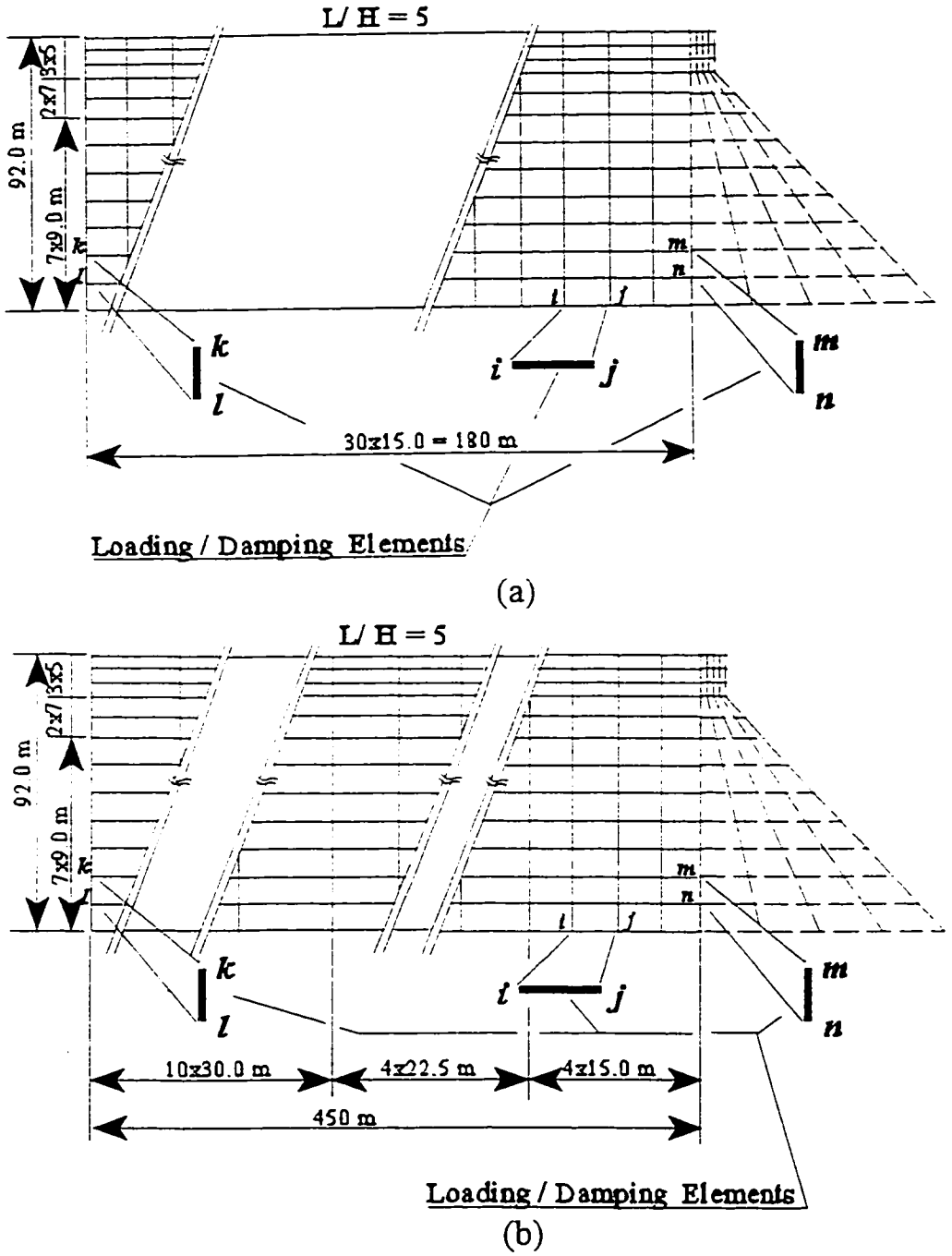

Fig. 4.14 Finite element model of the dam-reservoir system with L/H=5: (a) Uniform mesh (b) Non-uniform mesh

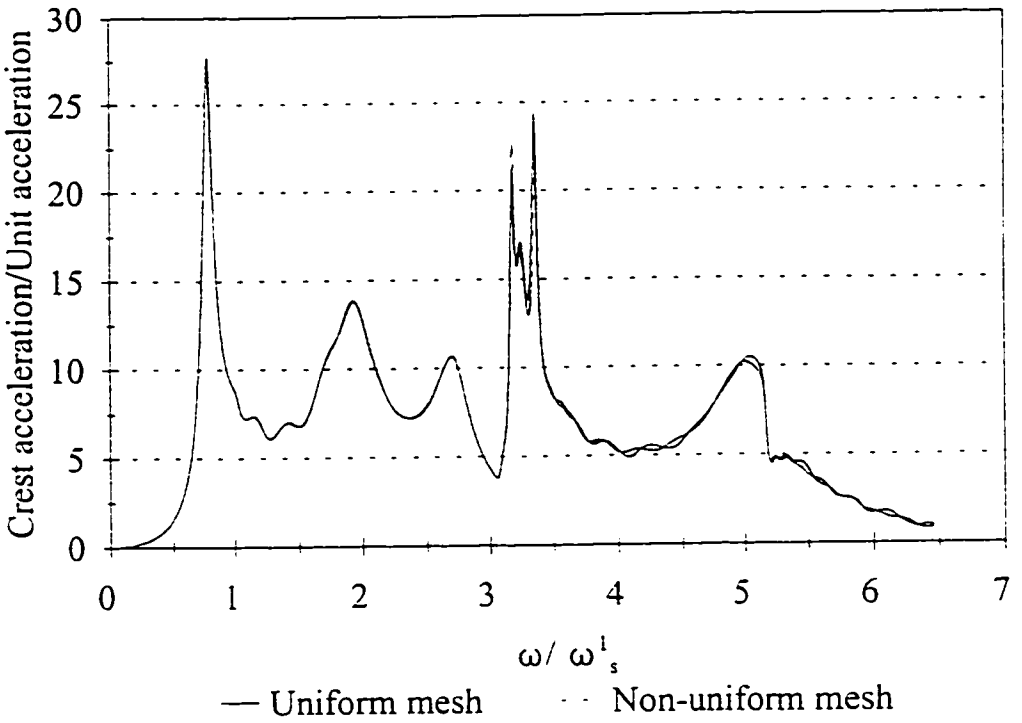

Fig. 4.15 Response of the monolith crest acceleration based on the reservoir mesh models shown in Fig. 4.14

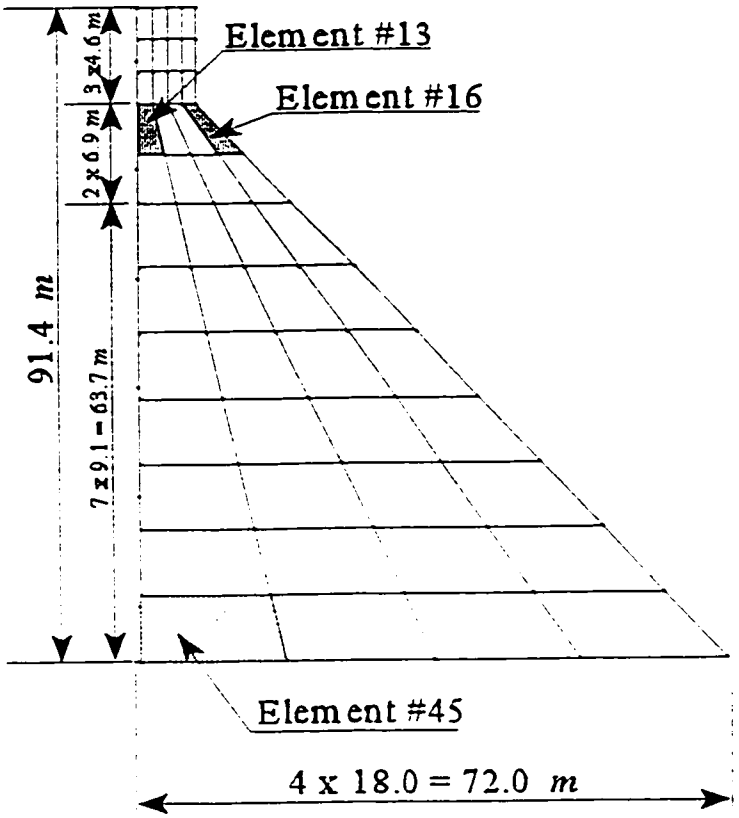

Fig. 4.16 Finite element discretization of the dam monolith (48 elements) indicating elements of maximum principal stress

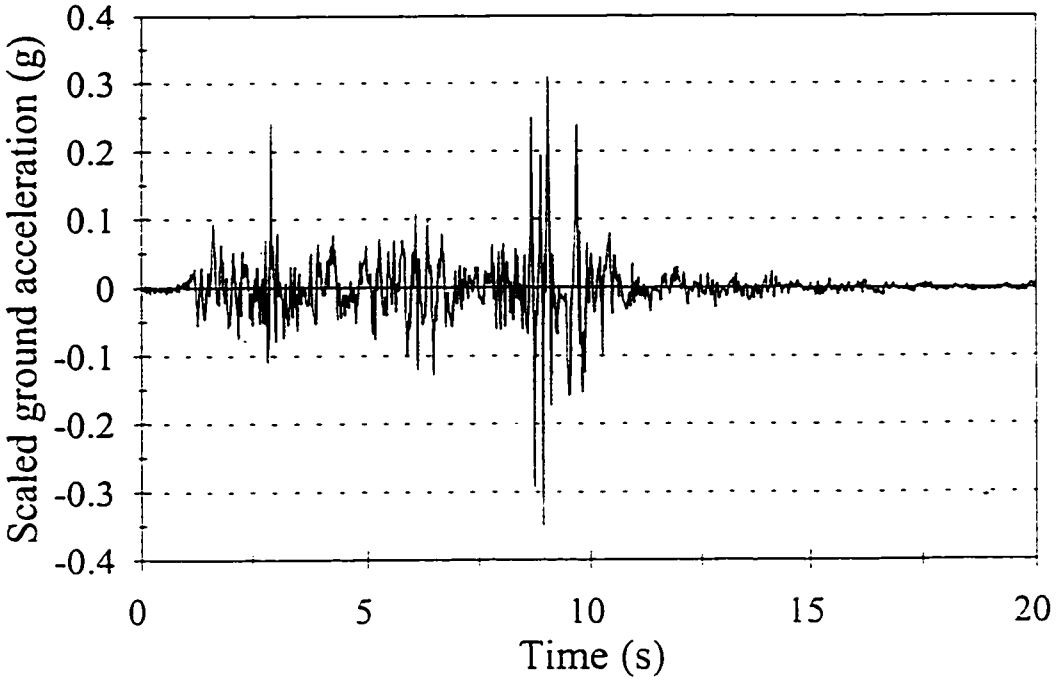

Fig. 4.17 The accelerogram of the 1985 Nahanni earthquake, Iverson record (Naumoski *et al.* 1988)- scaled to 0.35g.

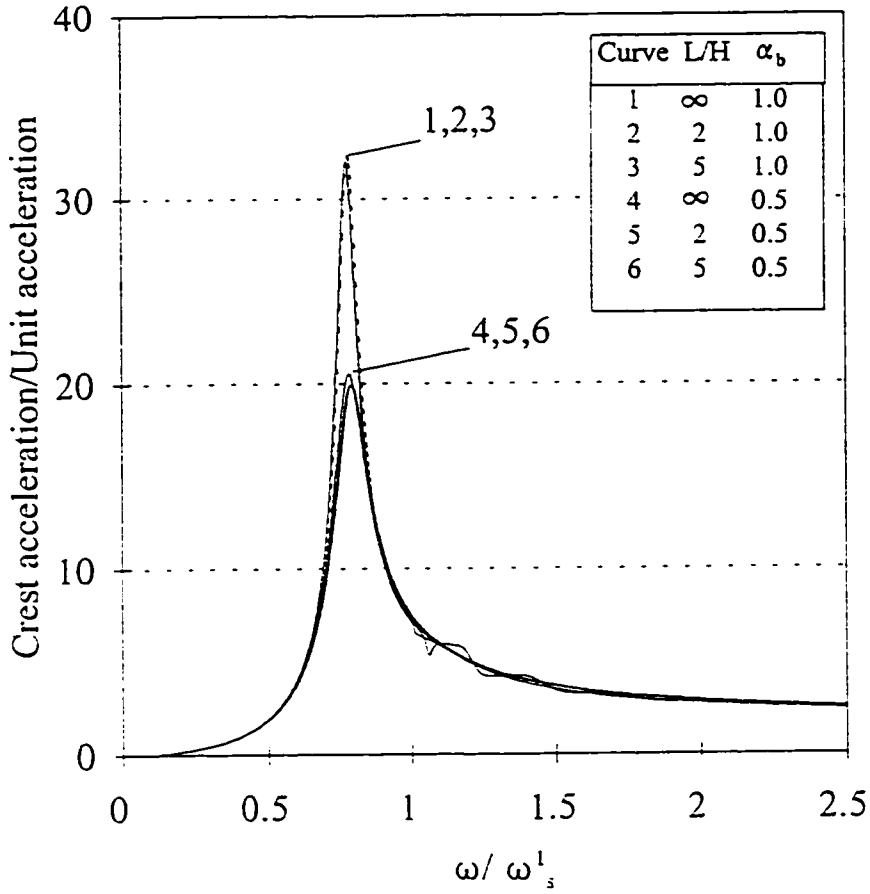

Fig. 4.18 Crest acceleration response of a dam on rigid foundation with one Ritz vector approximation and Sommerfeld radiation condition at the reservoir far end boundary under horizontal ground motion - comparison of the finite element solution with the theoretical solution for the infinite-length reservoir

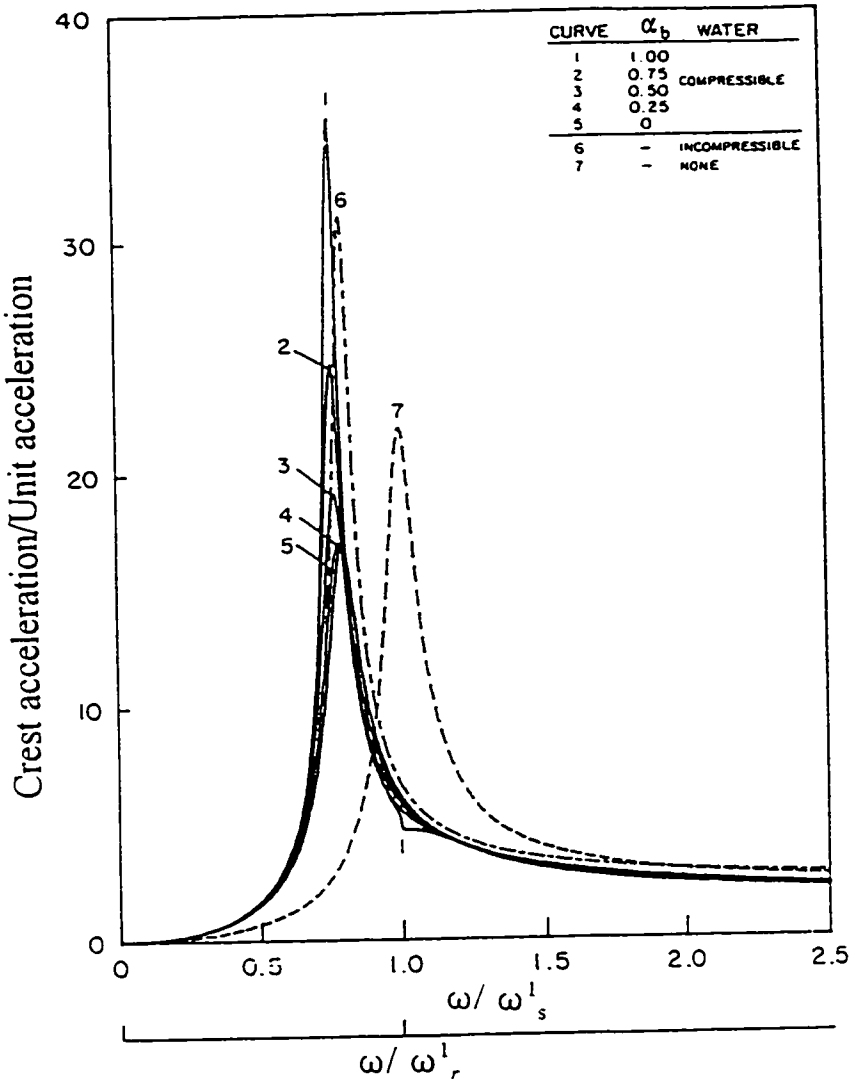

Fig. 4.19 Crest acceleration response of a dam on rigid foundation with one Ritz vector approximation under horizontal ground motion (Ω_r = 1.0) - Theoretical solution (After Fenves and Chopra 1984a)

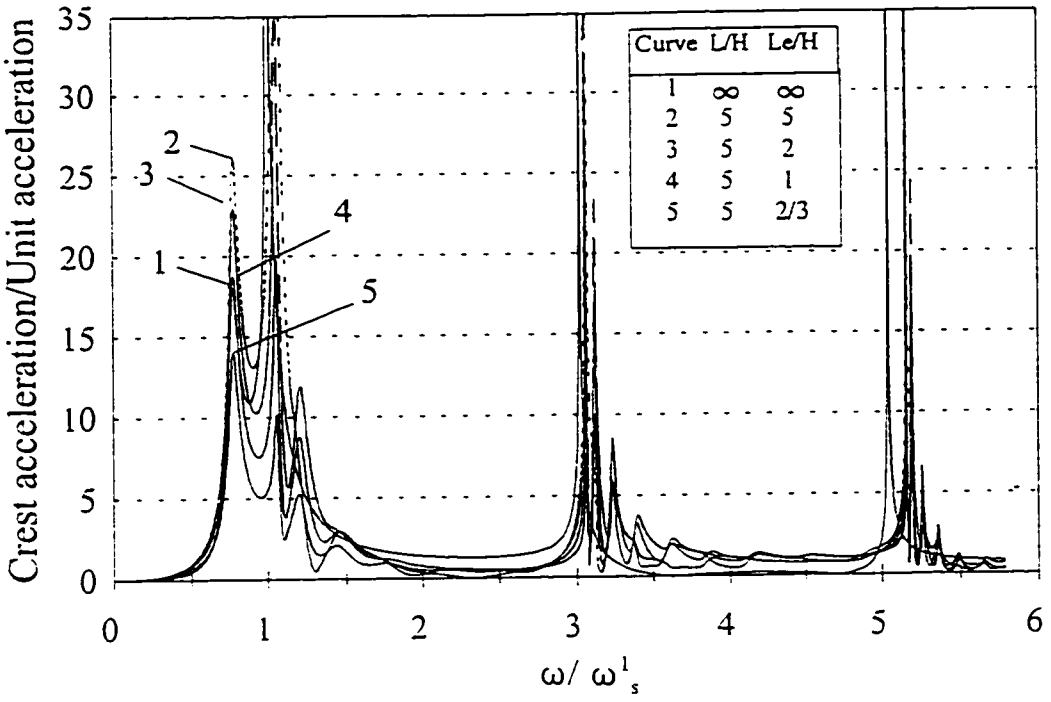

Fig. 4.20 Crest acceleration response of a dam on rigid foundation under vertical ground motion for various excitation length, L_e, at the reservoir bottom

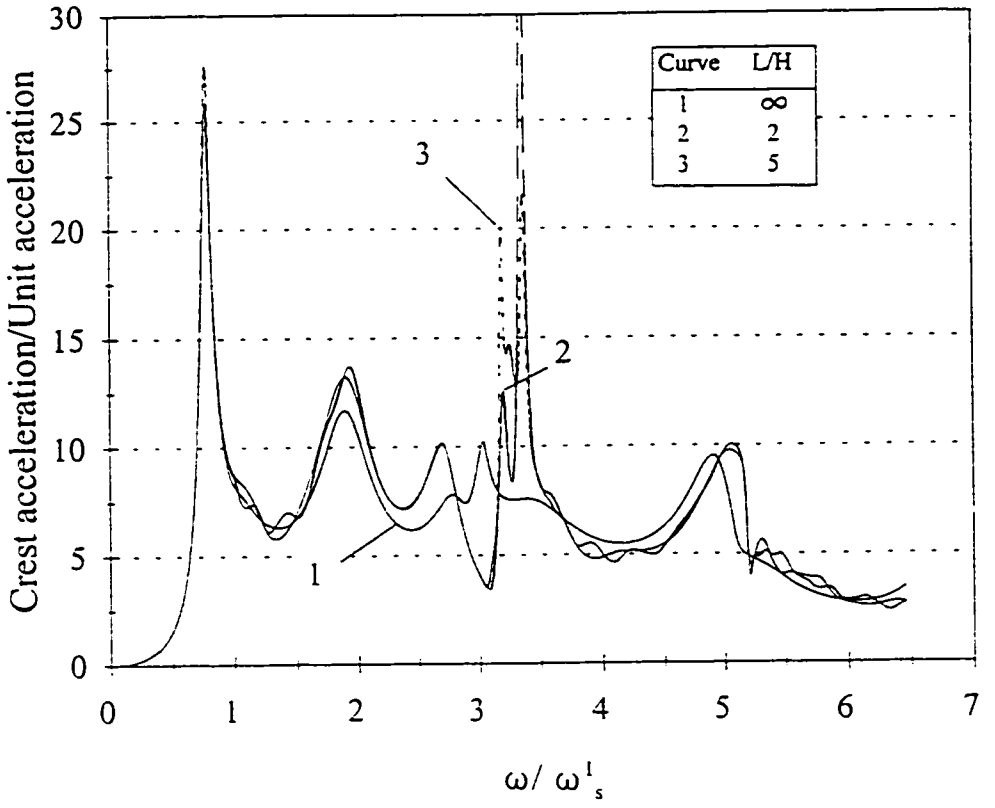

Fig. 4.21 Crest acceleration response of the dam on rigid foundation with ten Ritz vector approximation under horizontal ground motion ($\alpha_b = 0.9$ and $\alpha_u = 0.0$)

a)

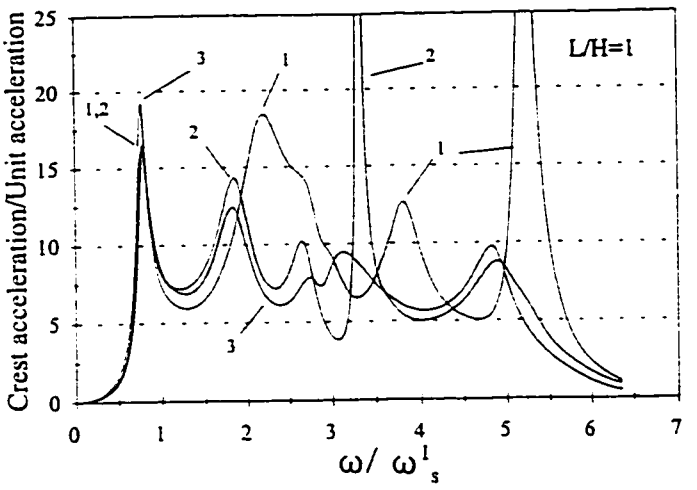

b)

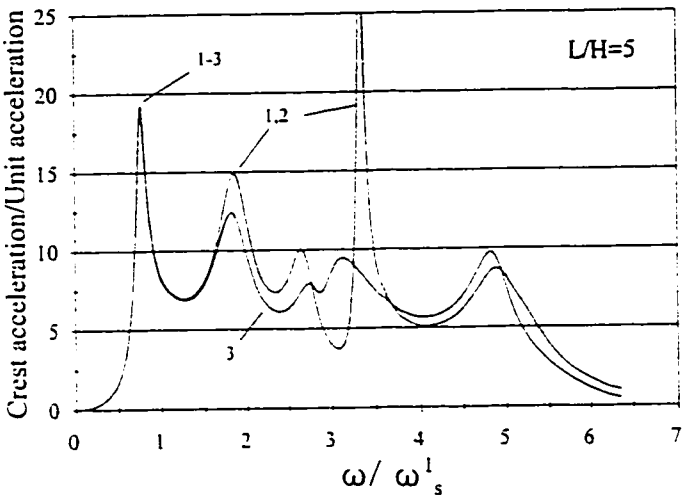

c)

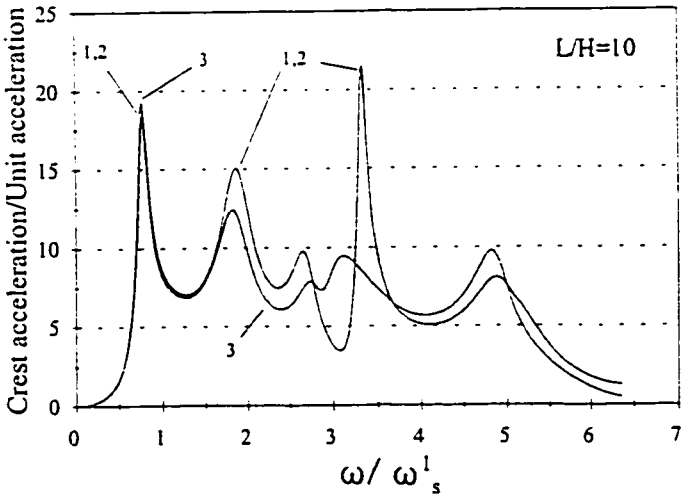

Fig. 4.22 Comparison of the crest acceleration response of the dam using Sommerfeld and Sharan boundary conditions with the closed-form solution of the infinite-length reservoir: 1) Sharan 2) Sommerfeld 3) infinite-length reservoir

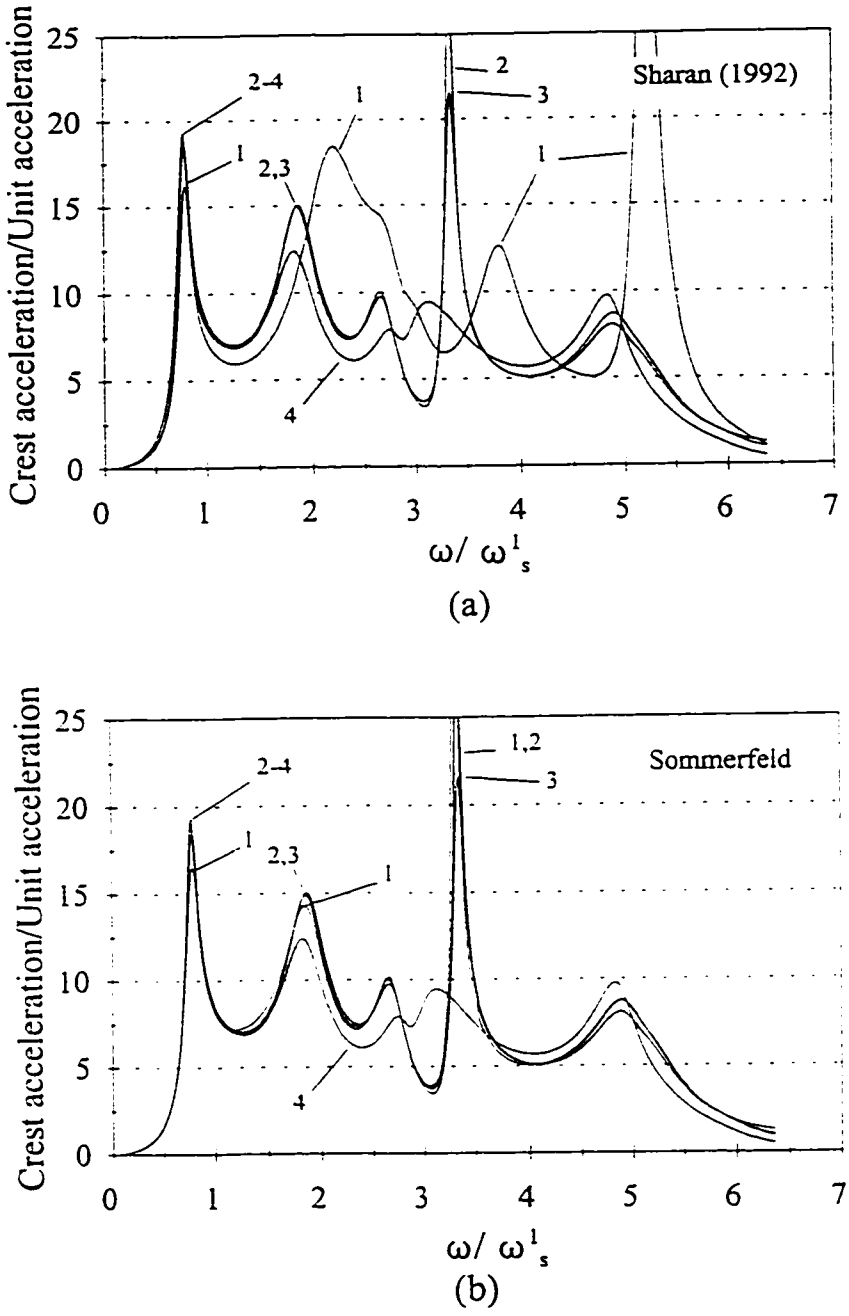

Fig. 4.23 Comparison of the crest acceleration response of the dam using Sommerfeld and Sharan boundary conditions with the closed-form solution of the infinite-length reservoir: 1) L/H=1 2) L/H=5 3) L/H=10 4) infinite-length reservoir

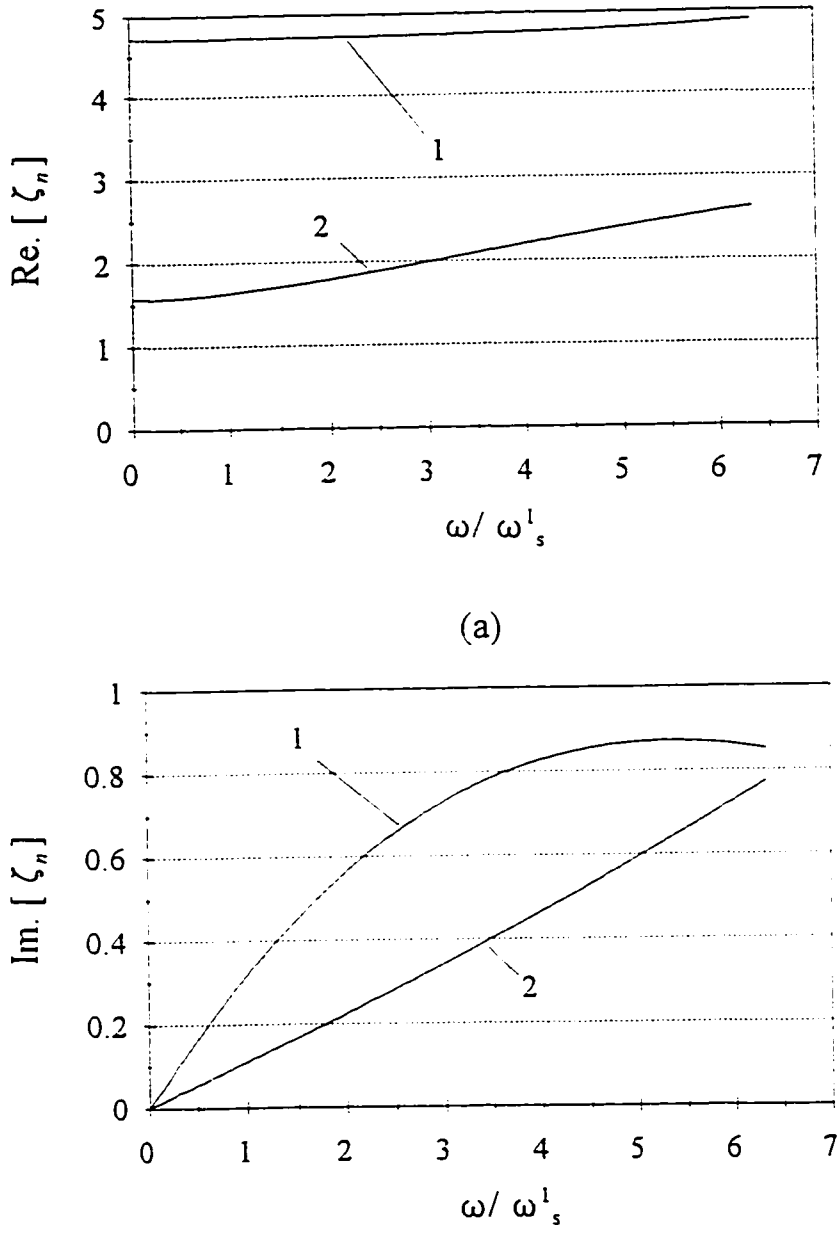

Fig. 4.24 Variation of ζ_n (Eq. 4.11) with frequency: (a) Real part of ζ_n (b) Imaginary part of ζ_n

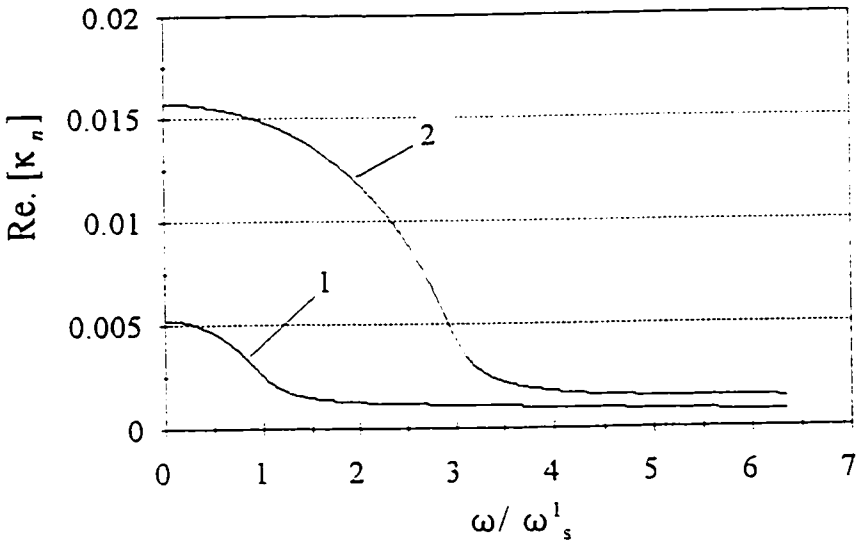

(a)

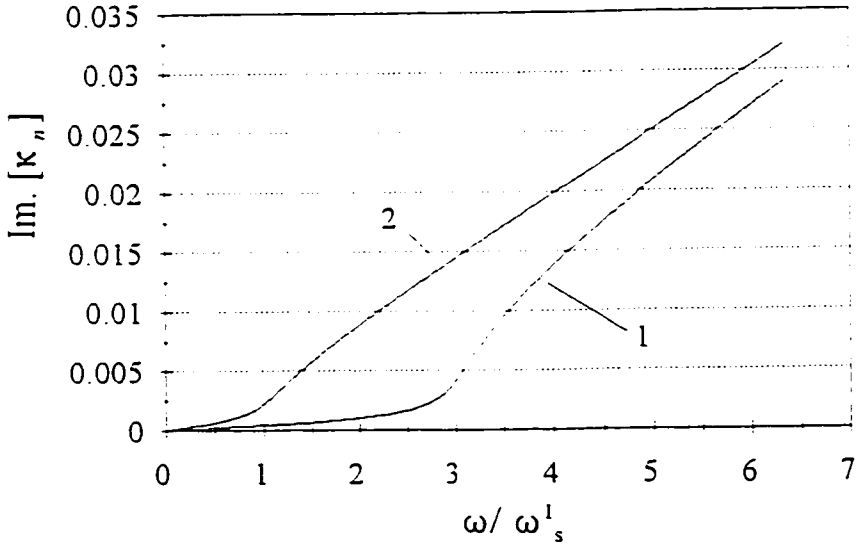

(b)

1) κ_1 2) κ_2

Fig. 4.25 Variation of κ_n (Eq. 4.9) with frequency: (a) Real part of κ_n (b) Imaginary part of κ_n

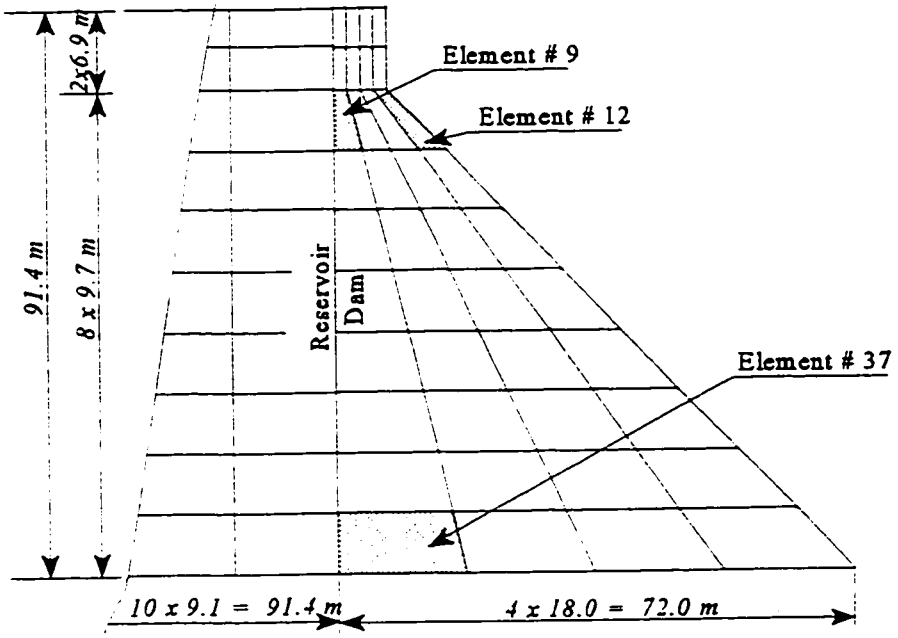

(a)

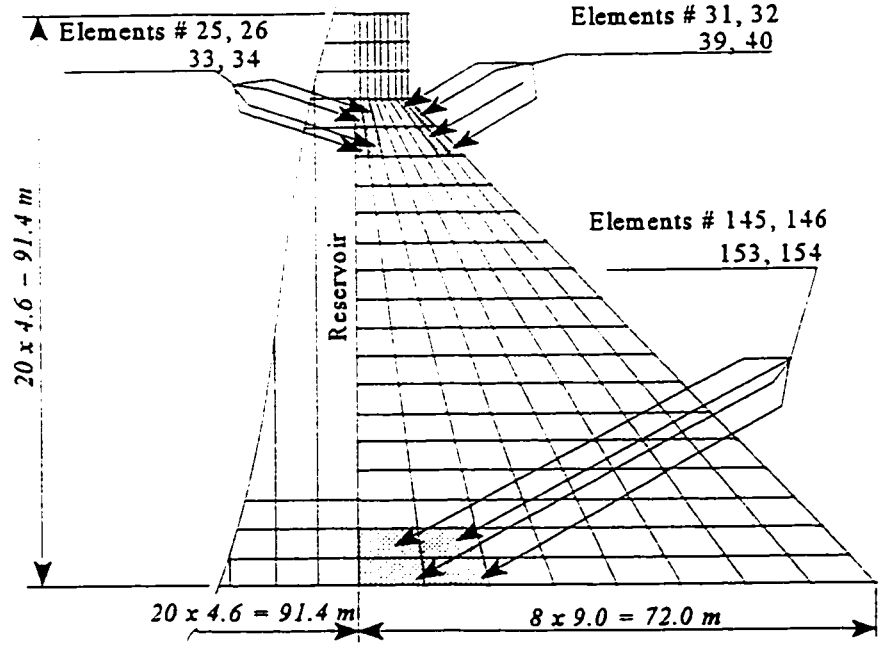

(b)

Fig. 4.26 Finite element models of the dam-reservoir system with different mesh refinements (40 and 160 elements, respectively) and indicating elements of maximum principal stress

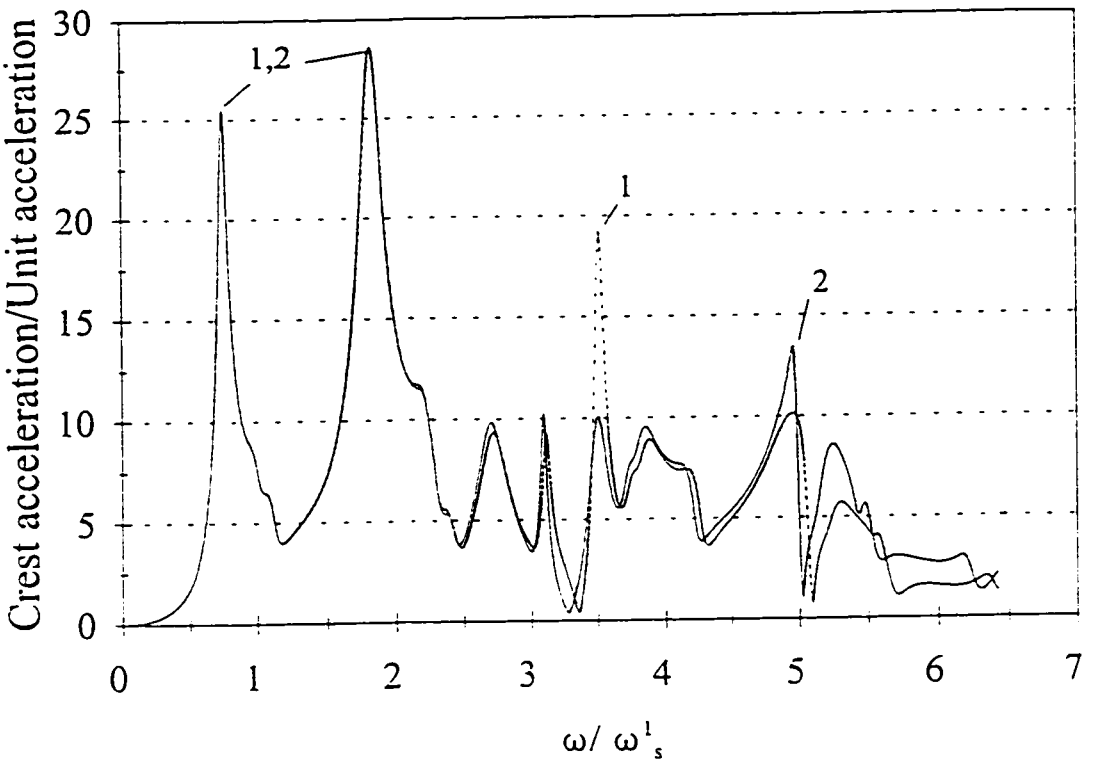

Fig. 4.27 Crest acceleration response of the dam for the finite element models shown in Fig. 4.26: (1) Coarse mesh (2) Fine mesh

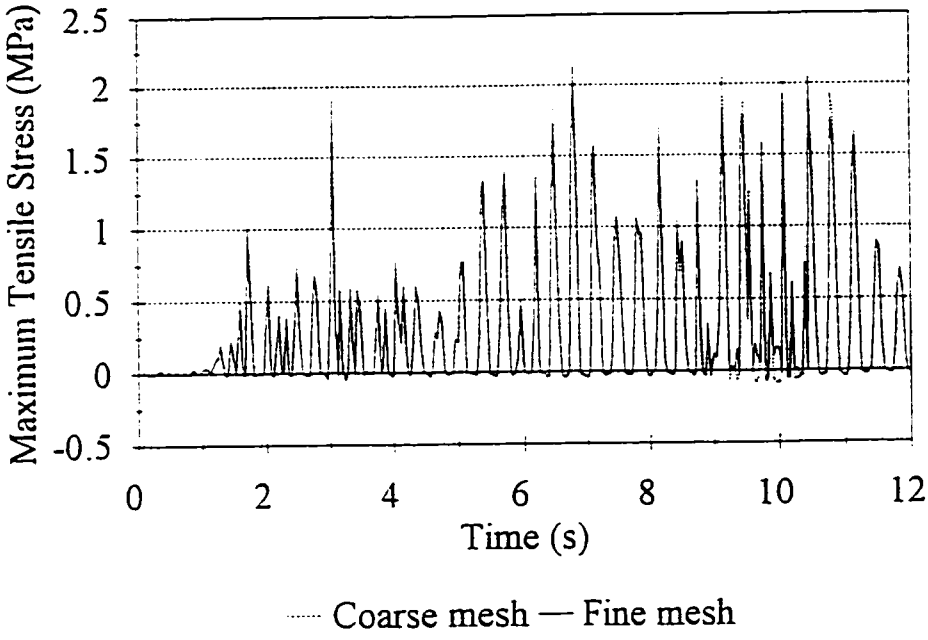

(a)

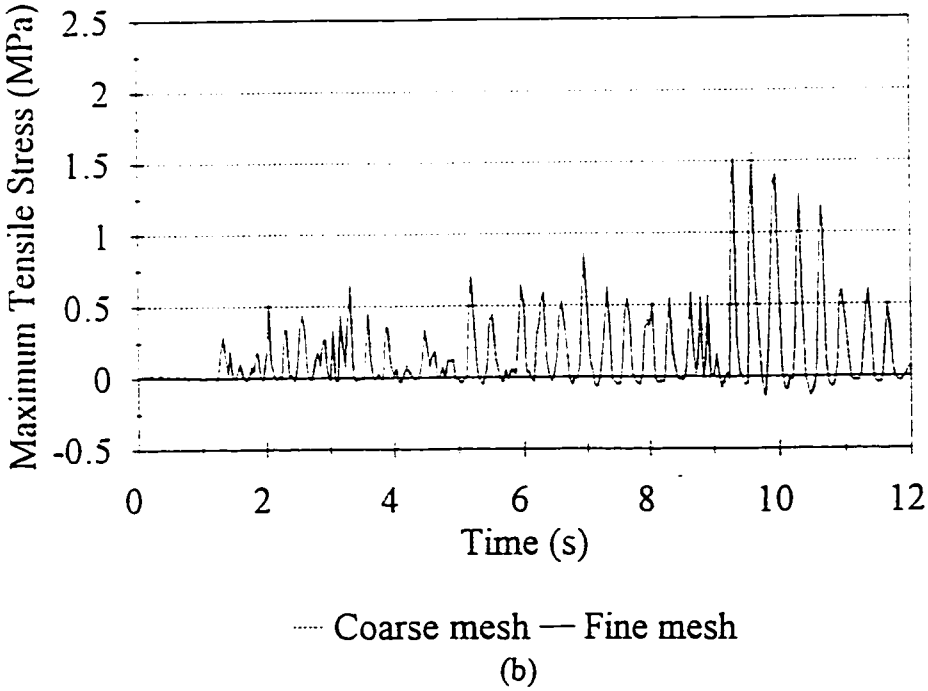

(b)

Fig. 4.28 Time-history response of the maximum tensile stresses in the dam for the finite elements shown in Fig. 4.26 (results of the fine mesh are averaged for four adjacent elements): (a) Downstream neck (b) Heel

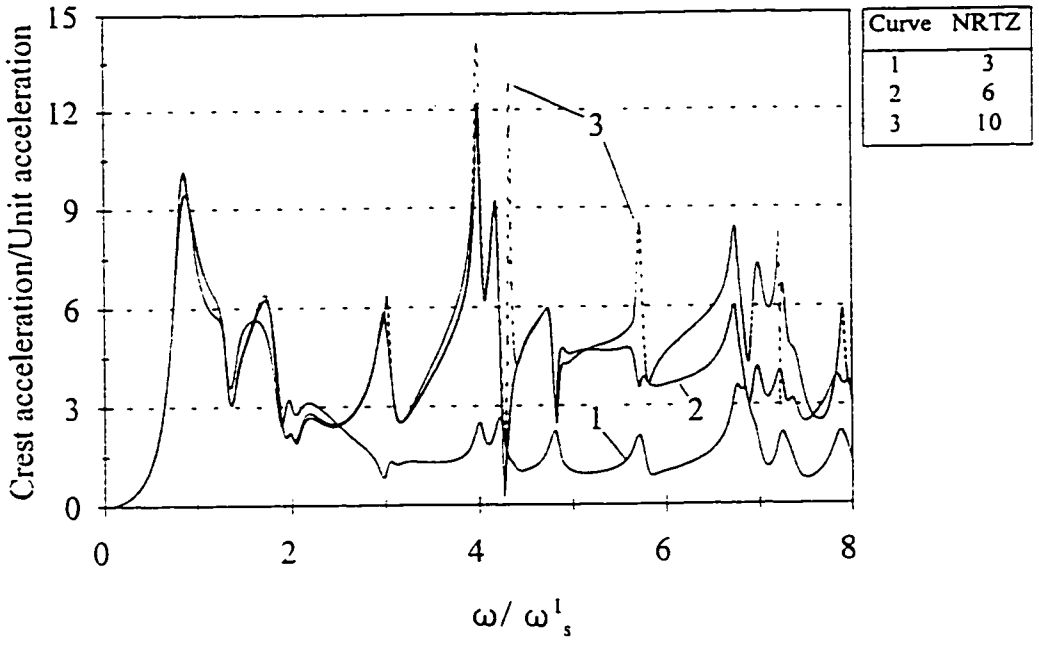

(a)

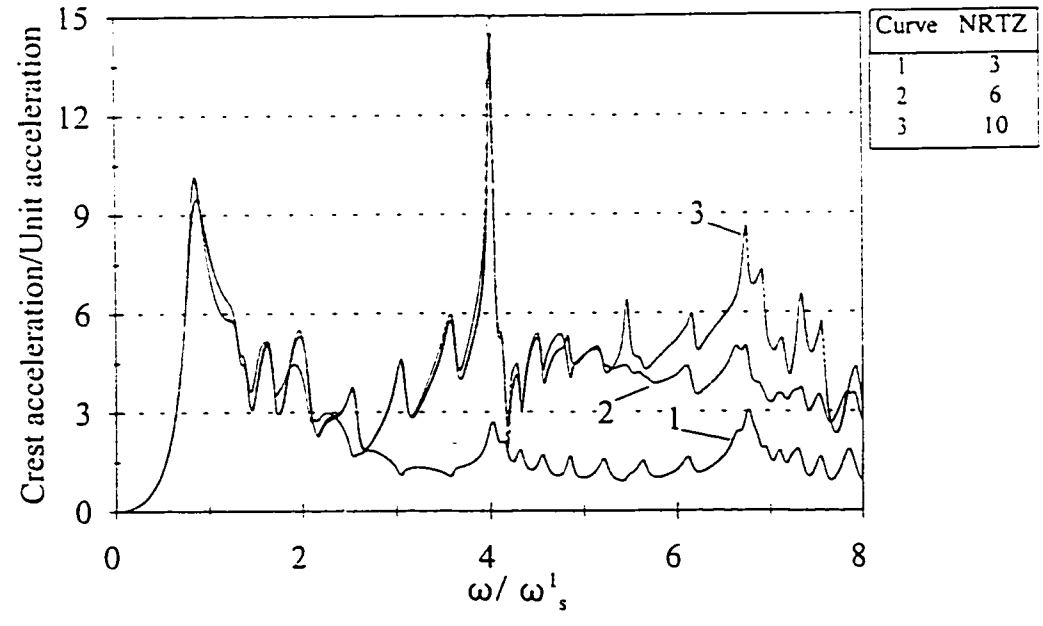

(b)

Fig. 4.29 Effect of the number of Ritz vectors on the response of the crest acceleration of a dam on flexible foundation subjected to horizontal excitation ($E_s = E_f = 20700$ MPa, $\alpha_b = \alpha_u = 0.9$) (a) L/H=2 (b) L/H = 5

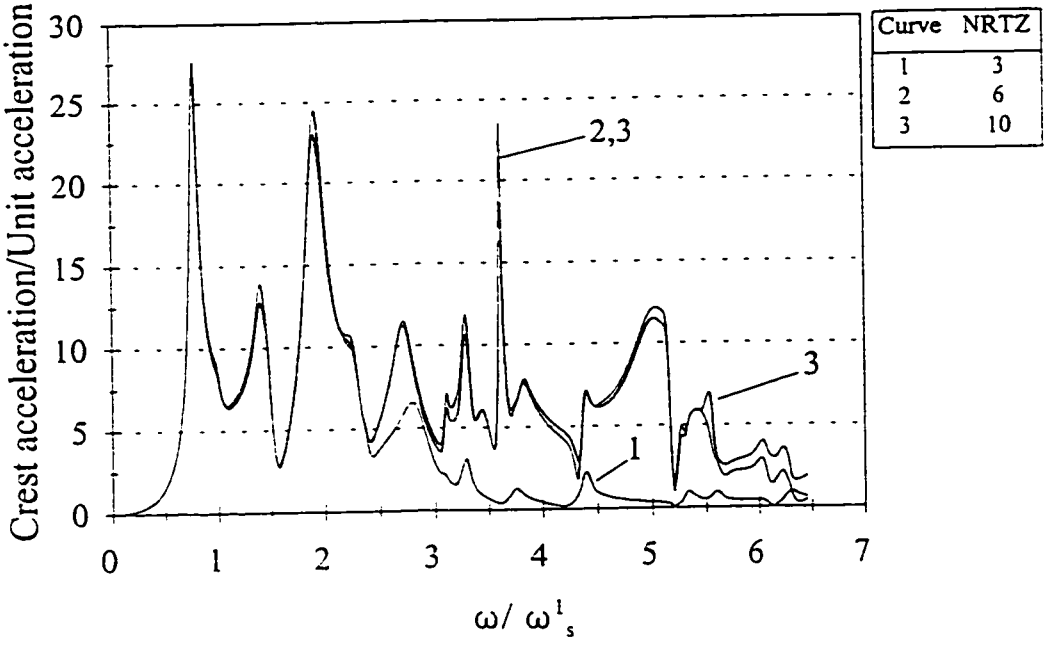

(a)

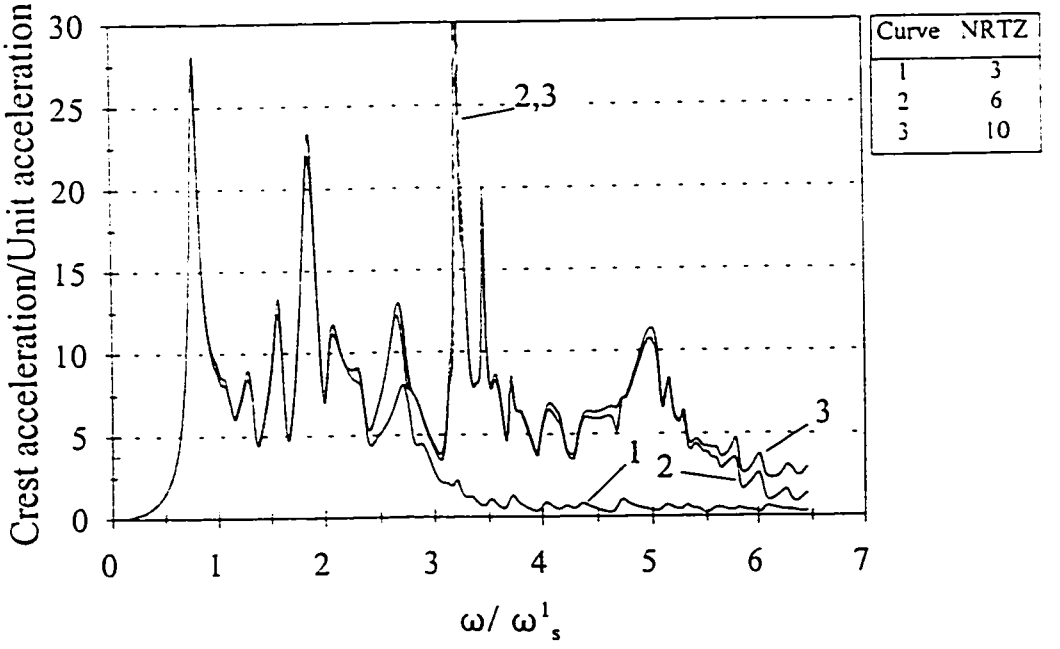

(b)

Fig. 4.30 Effect of the number of Ritz vectors on the response of the crest acceleration of a dam on rigid foundation subjected to horizontal excitation ($\alpha_b = \alpha_u = 0.9$) (a) L/H=2 (b) L/H = 5

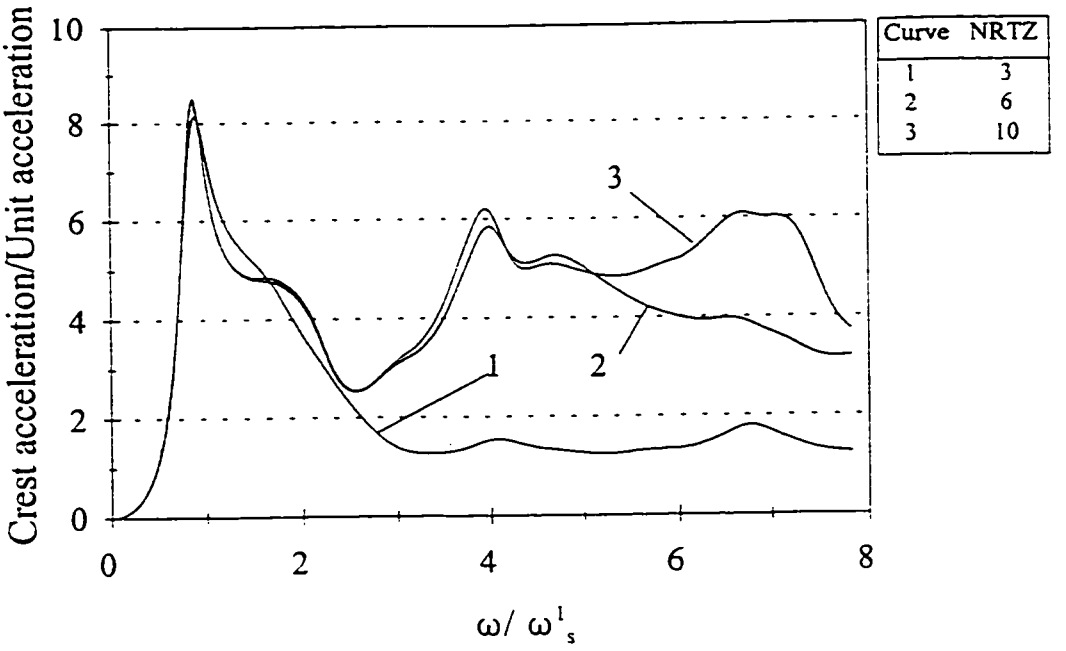

(a)

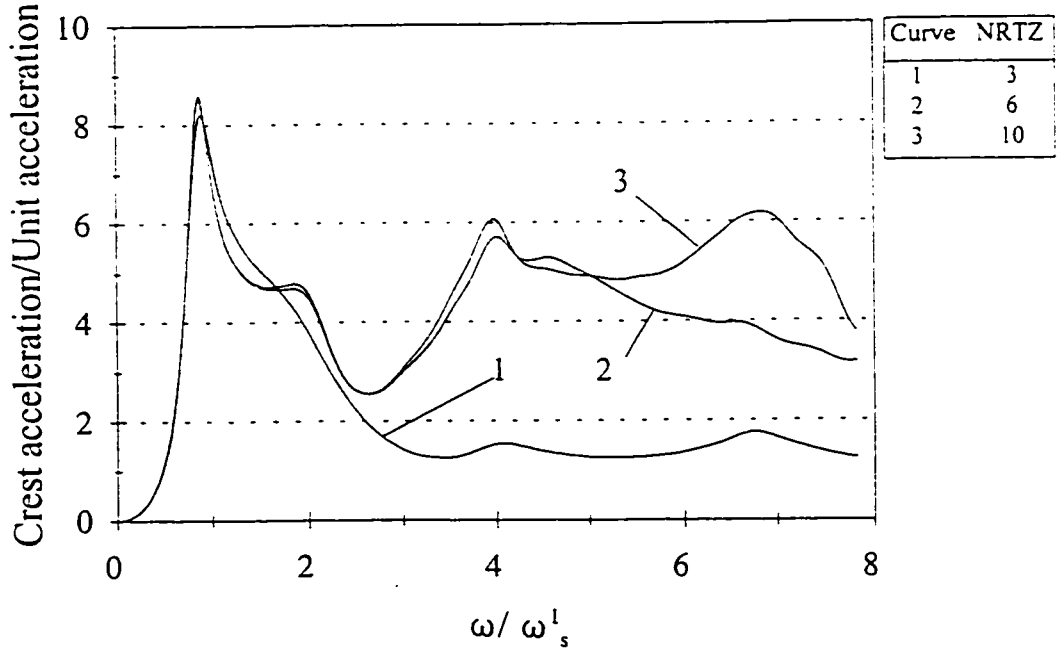

(b)

Fig. 4.31 Effect of the number of Ritz vectors on the response of the crest acceleration of a dam on flexible foundation subjected to horizontal excitation ($E_s = E_f = 20700$ MPa, $\alpha_b = \alpha_u = 0.5$) (a) L/H=2 (b) L/H = 5

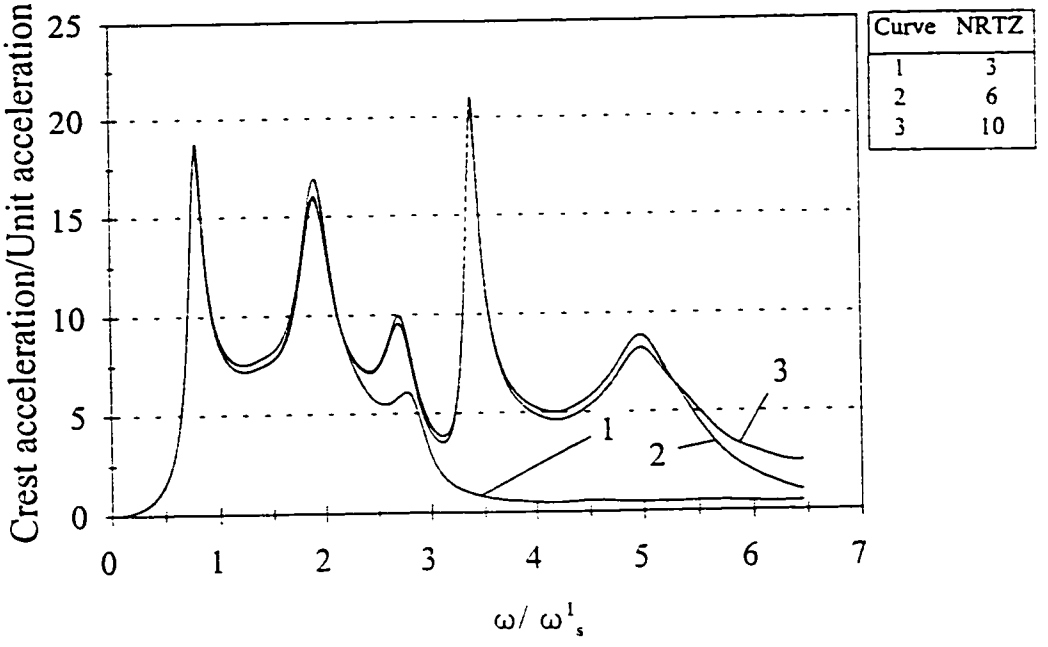

(a)

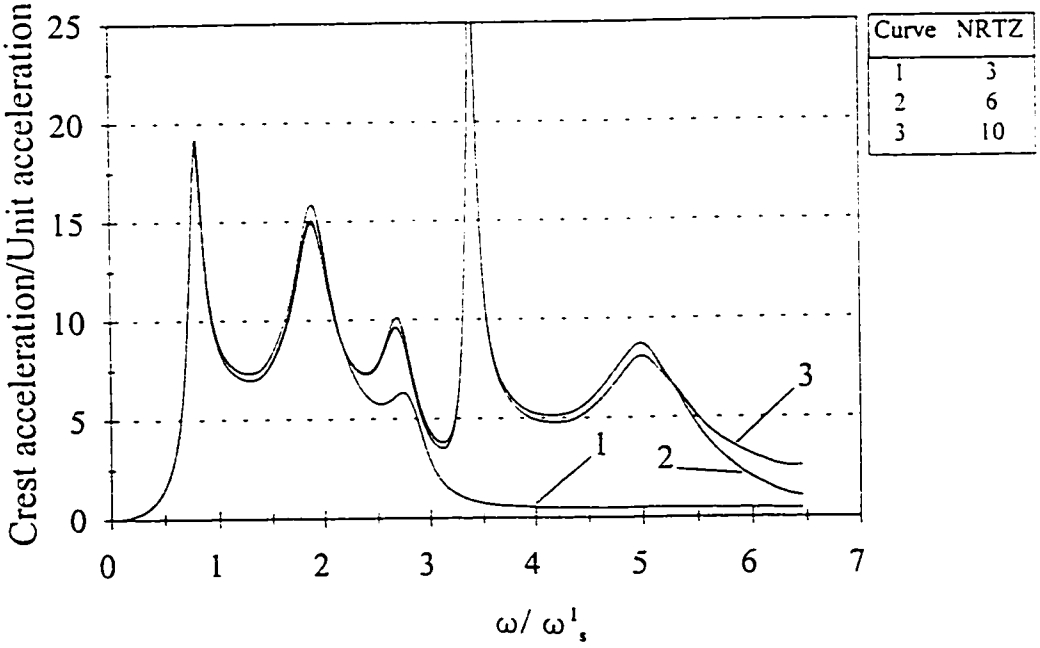

(b)

Fig. 4.32 Effect of the number of Ritz vectors on the response of the crest acceleration of a dam on rigid foundation subjected to horizontal excitation ($\alpha_b = \alpha_u = 0.5$) (a) L/H=2 (b) L/H = 5

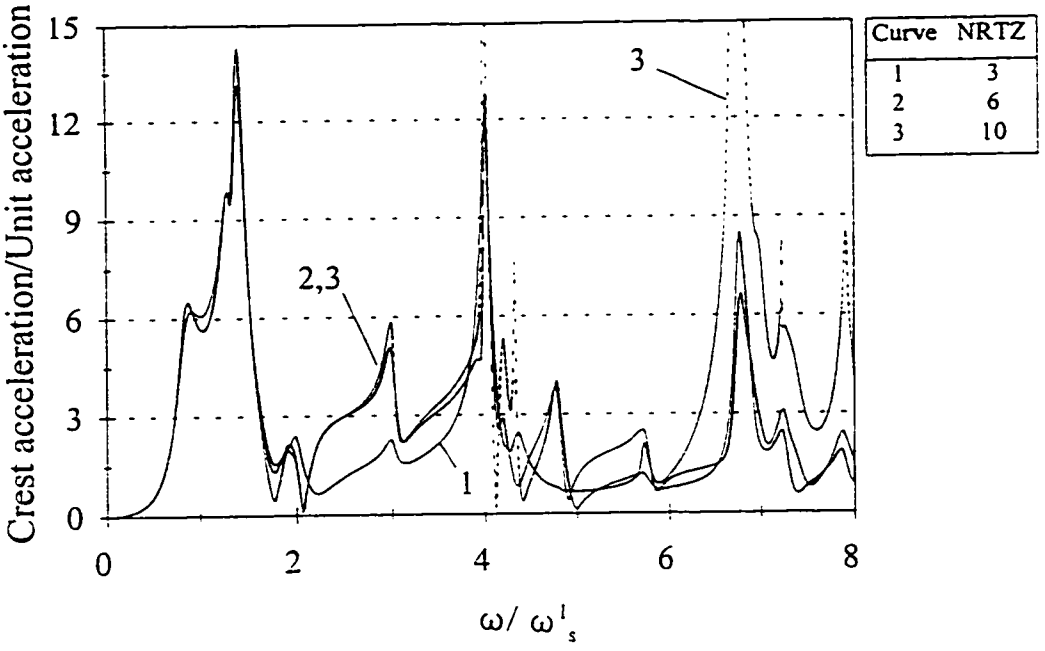

(a)

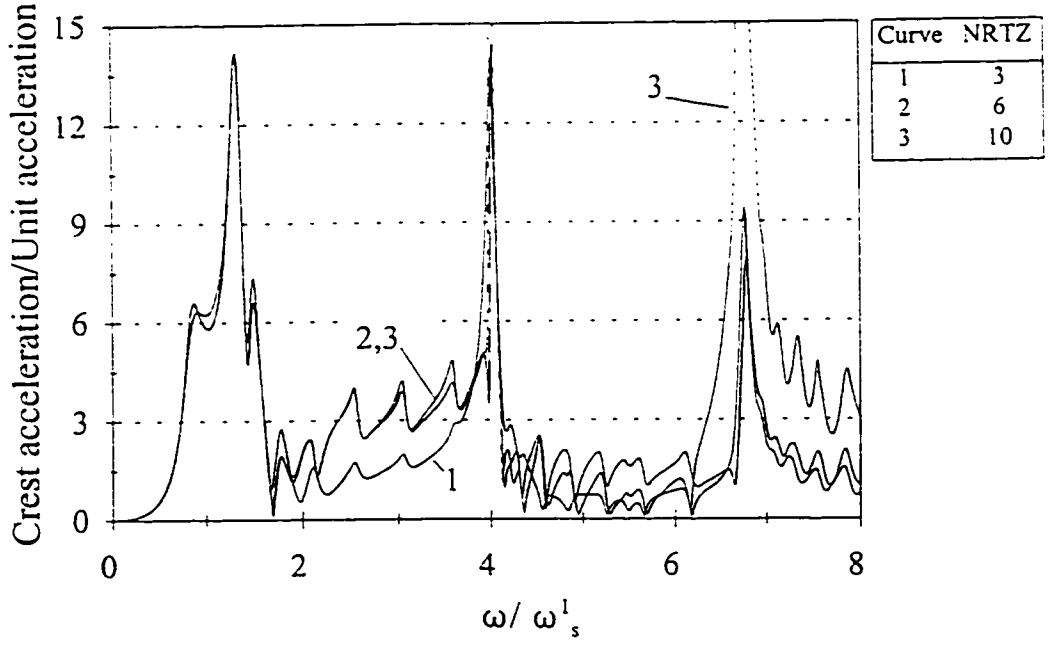

(b)

Fig. 4.33 Effect of the number of Ritz vectors on the response of the crest acceleration of a dam on flexible foundation subjected to vertical excitation ($E_s = E_f = 20700$ MPa, $\alpha_b = \alpha_u = 0.9$) (a) L/H=2 (b) L/H = 5

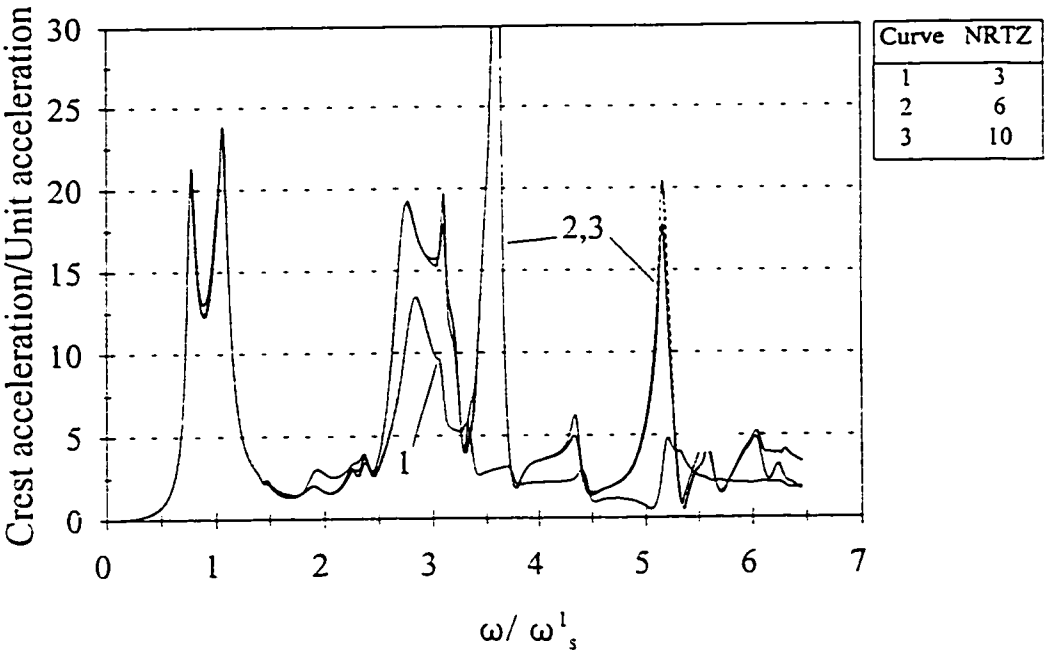

(a)

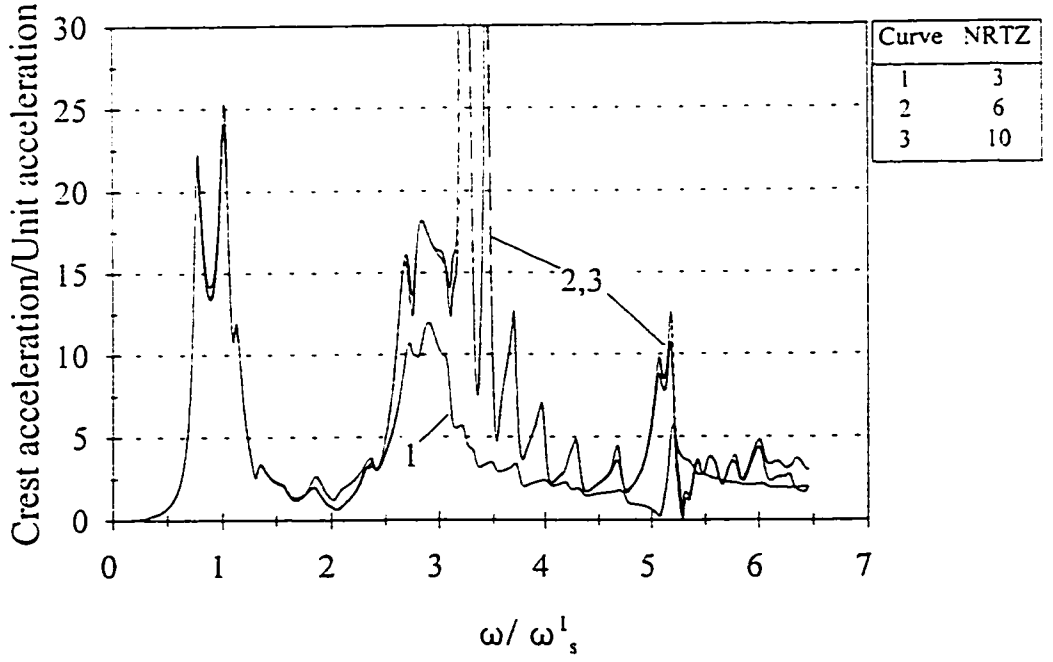

(b)

Fig. 4.34 Effect of the number of Ritz vectors on the response of the crest acceleration of a dam on rigid foundation subjected to vertical excitation ($\alpha_b = \alpha_u = 0.9$) (a) L/H=2 (b) L/H = 5

CHAPTER 5

STRESS ANALYSIS

5.1 INTRODUCTION

Earthquake response of a concrete dam is typically represented by the time history response of displacements and developed stresses in the structure. The stress time history contains valuable information concerning the response of the structure during the dynamic loading of the ground motion. However, the entire time variation of the stresses is not utilized in the design and safety evaluation of concrete dams. The instantaneous maximum values of principal stresses in the monolith cross section are normally used in evaluating the possibility of crack initiation and in conducting seismic design of the concrete dam. However, the local maximum stress values do not represent the overall state of stress in the dam cross section. The variation of developed stresses with time at several locations within the dam cross section is an important parameter in the post-cracking behaviour of the concrete dam when subjected to strong earthquake ground motion.

In this chapter, a measure of the dynamic response of concrete gravity dams is proposed in an attempt to include the effects of the stress time history and the variation of the stress magnitude over the cross section of the dam when subjected to ground motion and the hydrodynamic loading from the adjacent reservoir. Parametric studies on the effect of different zones of the reservoir surrounding boundary on the developed stresses in the dam

are conducted. These studies include the reservoir bottom absorption effects based on the model proposed in Chapter 2 as well as the influence of hydrodynamic isolation of the dam discussed in Chapter 3.

5.2 MEASURE OF DYNAMIC RESPONSE

5.2.1 Stress Time History Response

The maximum stresses in a dam subjected to several earthquake records are not sufficient for a reliable comparison of the effects of different input ground motions on seismic response of concrete dams. Comparing the entire time history response of the stresses at different locations in the dam cross section is difficult and is not an efficient design approach. An illustrative example is provided to compare the effect of different input ground motions on the stress time history response of a concrete gravity dam.

A 91.44 m high dam with a vertical upstream face and a downstream slope of 0.8:1 is considered (Fig. 5.1). The selected geometry of the dam is typical for many concrete gravity dams. A survey of the geometrical data of several gravity dams in the United States is presented in Table 5.1. The concrete dam is discretized using 48 isoparametric four-noded finite elements and is assumed in the plane stress condition. The foundation of the dam is assumed rigid and the reservoir bottom is considered as completely reflective. The impounded water is assumed compressible. The speed of the travelling pressure wave is taken as $C_w = 1440$ m/s. The depth of the reservoir is taken equal to the height of the dam. The modulus of elasticity and Poisson's ratio of concrete are assumed as $E_c = 20{,}700$ MPa and 0.2, respectively.

Figure 5.2a shows the time history responses of the maximum principal tensile stress at the neck of the dam when subjected to two different ground motions. The ground motion records are the 1970 Lytle Creek S25W and the 1971 San Fernando N90E earthquakes, respectively. The above records are denoted by HH6 and HI7 in Tables 5.2 and 5.3, respectively. Both ground motions are selected from records of California earthquakes with

nearly equal peak ground acceleration (PGA) values. The PGA of the 1970 Lytle Creek (S25W component) and the 1971 San Fernando (N90E component) ground accelerations are $0.20\,g$ and $0.21g$, respectively. The two ground acceleration records cause almost identical maximum peak tensile stress at the neck of the dam. However, the stress time history response due to the San Fernando earthquake with larger number of significant peaks appears to be the more critical of the two responses.

Another example is shown in Fig. 5.2b where the stress response at the upstream neck of the dam for the two cases of the 1966 Parkfield N85E (record HH1) and the 1952 Taft S69E (record HI2) ground motion records, are compared. The stress response due to the Parkfield earthquake is significant for a short period of time between $4 \le t \le 6$ seconds. The stress magnitude becomes immediately negligible after $t = 6\,s$. The maximum peak of the stress response to Taft ground motion is lower than the maximum stress peak due to the Parkfield earthquake. However, the stress response due to the Taft earthquake shows considerably longer fluctuations with a significant magnitude. The extent of crack propagation in the concrete dam under severe ground motion is significantly influenced by the number of strong peaks of the stress response after the crack is already initiated.

The above examples illustrate that the maximum stress at a specific point of the dam cross section does not adequately indicate the critical case of response to the applied dynamic loading. In other words, it is not possible to judge which case of loading is more critical for the dam.

5.2.2 Proposed Measure of Dynamic Response

The instantaneous maximum principal stress value at a point in the cross section of the dam is replaced by a quantity that represents the varying magnitude of the stress response during the earthquake ground motion. The norm of the principal stress can be written in the form:

$$\hat{I}_\sigma = \int_0^{t_d} | \sigma_1^t(t) | \, dt \tag{5.1}$$

where t_d is the duration of time for which the response analysis is made and $\sigma^t_1(t)$ is the time variation of the maximum principal stress at a given point in the cross section of the dam. The right hand side of expression 5.1 contains the time variation of stress including the effects of all significant stress peaks other than the maximum value in the response history. The definition of $\hat{I}_\sigma$ in Eq. 5.1 is a special case of the *Lebesgue* norm in the form:

$$\| w \|_p = [\int_0^t | w(\tau) |^p \, d\tau]^{1/p} < \infty \tag{5.2}$$

The Lebesgue norm (L_p - norm or $\| \cdot \|_p$) is calculated for the function $w(\tau)$ defined over the interval [0,t]. For the case of $p = 1$, Eq. 5.2 reduces to the L_1-norm of the function $w(\tau)$ as defined in Eq. 5.1. Since concrete is weaker in tension, the tensile stress in the monolith is monitored during the earthquake loading. The maximum principal stress at the heel of a dam monolith subjected to earthquake ground motion may remain compressive when the weight of the structure is included in the analysis. For tensile stress, the stress norm defined in Eq. 5.1 is modified as:

$$I_{\sigma} = \int_{0}^{t_d} \sigma_1^t(t)\,dt \qquad , \quad for\ \sigma_1^t(t) \geq 0 \tag{5.3}$$

The condition set in Eq. 5.3 is to ensure that only the tensile stress in concrete is included under different loading conditions.

The stress function $\sigma^t_1(t)$ varies at different selected points in the cross sectional area of the dam monolith. A weighted average of the stress norm over the cross section of the monolith is an indicator of the overall state of stress in the dam cross section. In a four-noded finite element discretization of the monolith cross section, the stresses are calculated at the geometrical centres of the elements. The computed stresses are assumed uniform over the element and can be interpreted as the average of the stresses across the area of the corresponding finite element. The same reasoning can be extended to other types of finite elements with some modifications. To change the stress into a force, both sides of Eq. 5.3 are multiplied by the element area of the finite element j, A_j (Fig. 5.1) in the form:

$$I_{Fj} = A_j \cdot \left(\int_{0}^{t_d} \sigma_1^t(t)\,dt \right)_j$$

The right hand side product has the dimension of momentum and its summation over the total number of the finite elements is analogous to a measure of the total momentum (or the equivalent impact) received by the concrete dam due to the input ground motion. The summation of the momentum over the entire monolith is written as:

$$S_I = \sum_{j=1}^{N} A_j \cdot \left(\int_{0}^{t_d} \sigma_1^t(t)\,dt \right)_j \qquad , \quad for\ \sigma_1^t(t) \geq 0 \tag{5.4}$$

where the total number of finite elements in the dam model is denoted by N. The summation given in Eq. 5.4 represents a measure of the response of the dam to the seismic loading and not just the maximum values of the calculated stresses at the specific points of the monolith cross section.

The parameter S_I is referred to as the *pseudo-impact* to the concrete dam. The prefix *pseudo* refers to the fact that the area of the finite element is different from the area on which the principal tensile stress $\sigma^t_1(t)$ is acting. The pseudo-impact parameter is normalized to a nondimensional form as:

$$SF = \frac{1}{t_S} \sum_{J=1}^{N} \frac{A_j}{A_T} \cdot \int_0^{t_d} \frac{\sigma^t_{1j}(t)}{f_r} dt \qquad for \quad \sigma^t_1(t) \geq 0 \qquad (5.5)$$

where A_T is the total area of the finite elements over which the stress norm is averaged which is the total area of the monolith, f_r is the tensile strength of concrete and t_S is the duration of strong ground motion. The parameter SF is the *Stress Factor* of the dam cross section and represents an overall measure of the state of stress in the dam structure. The definition of SF is based on the elastic behaviour of the material and does not include the post-cracking behaviour of the concrete dam.

Beside the area under the curve of the stress time history response as noted in Eq. 5.1, an important factor in comparing the effects of different earthquake records on the monolith response is the frequency of stress fluctuations. The significant part of the seismic loading is normally limited to a small fraction of the total recorded duration. The dominant frequency of stress variation in the dam is basically the coupled fundamental frequency ω^1_c for the case of full reservoir and the fundamental frequency of the dam-foundation system

for the case where the reservoir is empty. The dam-reservoir system is significantly affected only by dynamic loadings with dominant frequencies in the vicinity of the fundamental frequency of the system. Accordingly, the frequency of the stress variation in the dam subjected to various ground accelerations does not significantly change as is observed in Fig. 5.2.

5.3 CORRELATION STUDIES

5.3.1 Intensity of the Input Ground Motion

The applicability of the proposed stress factor in seismic response analysis of dams is verified by examining its correlation with the intensity scales of the input ground motion. Three different measures of the ground motion intensity are considered. The intensity measures include the peak ground acceleration, PGA, the spectral intensity, SI and the energy-based definition of ground motion intensity, I_E, given by Arias (1970). The peak ground acceleration of the recorded earthquake partly represents the severity of the ground motion specially for short-period structures. Therefore, it is included in the correlation studies for comparison purposes. The spectral intensity, SI, is defined by Housner (Arias 1969) as:

$$SI(\xi) = \int_{0.1}^{2.5} S_v(\xi,T)\ dT \tag{5.6}$$

where ξ and T are the viscous damping ratio and the period of the equivalent single degree of freedom (SDOF) system of the structure, respectively. The pseudo-relative velocity $S_v(\xi,T)$ is given by:

$$S_V(\xi,T) = \max_t \left| \frac{T_d}{T} \int_0^t \ddot{u}_g(\tau) \exp\left[-\frac{2\pi}{T}\xi(t-\tau)\right] \sin\frac{2\pi}{T_d}(t-\tau)\, d\tau \right| \tag{5.7}$$

where $T_d = T(1-\xi^2)^{-1/2}$ denotes the damped vibration period of the structure and $\ddot{u}_g(\tau)$ is the recorded ground acceleration. The limits of integration in Eq. 5.6 are chosen based on the range of the natural periods of common buildings. The spectral intensity approach is widely used in spectral analysis of structures. For dam analysis, however, the range of interest is in lower free vibration periods. The period range representing the limits of

integration in the formulation of the spectral intensity for dams is taken as $0.05 \leq T \leq 0.5\ s$ which is equivalent to the frequency range of $2.0 \leq f \leq 20\ Hz$. This range of integration is more appropriate for the analysis of concrete gravity dams. The damping ratio in Eq. 5.6 is chosen as $\xi = 0.20$ for the analysis of ordinary structures (Arias 1969). The damping ratio is selected on the basis of the expected energy dissipating mechanisms in joints and connections between various structural and non-structural elements in buildings. Such mechanisms do not exist in concrete dams. For this reason, it is more appropriate to assume a lower damping ratio in the analysis. The conservative value of $\xi = 0.05$ is assumed for the monolith's damping ratio.

A different definition for the intensity of ground motion is given by Arias (1969) as:

$$I_E(\xi) = \frac{\cos^{-1}(\xi)}{g\sqrt{1-\xi^2}} \int_0^{t_T} \ddot{u}_g^2(t)\,dt \tag{5.8}$$

where t_T is the total duration of earthquake and g is the gravitational acceleration. The definition of $I_E(\xi)$ is based on the concept of energy dissipation in a viscously damped harmonic oscillator. The intensity $I_E(\xi)$ in Eq. 5.8 is a quadratic function of the input ground acceleration, $\ddot{u}_g(t)$. A modified intensity formulation is proposed utilizing the L_2-norm of the ground acceleration in the form:

$$I_{EQ}(\xi) = \frac{\cos^{-1}(\xi)}{g\sqrt{1-\xi^2}} \left(\int_0^{t_T} \ddot{u}_g^2(t)\,dt \right)^{1/2} \tag{5.9}$$

The modified earthquake intensity, $I_{EQ}(\xi)$, is a linear function of the ground acceleration and therefore is consistent with the peak ground acceleration, PGA, and the spectral intensity, SI, of the ground motion.

A set of 27 records of horizontal components and 24 records of vertical components is used in the correlation study of the proposed stress factor with the intensity measures of the ground motion. The data for the selected ground motion records are presented in Tables 5.2 to 5.5. The earthquake records are denoted alpha-numerically for convenient reference. The first letter denotes the component of the record (horizontal or vertical) followed by a letter indicating its PGA/PGV ratio category (H-high and I-intermediate). The parameter PGV denotes the peak ground velocity of the recorded ground motion. The PGA and PGV values in the PGA/PGV ratio are substituted in terms of the gravitational acceleration, g, and m/s, respectively. The records of horizontal components are categorized based on their PGA/PGV ratios (Naumoski *et al.*, 1988). The plots of horizontal ground acceleration records with high (PGA/PGV > 1.2) and intermediate (0.8 < PGA/PGV < 1.2) PGA/PGV ratio are presented in Appendix I. The records of horizontal components with high and intermediate PGA/PGV ratios are selected in the analysis of the gravity dam example due to the high fundamental frequency of the structure. A similar classification is not available for records of vertical components. However, the records of vertical components generally contain high frequency contents and therefore are included in the correlation study. The plots of vertical ground acceleration records corresponding to the horizontal high and intermediate PGA/PGV ratio classification are presented in Appendix II. The ground acceleration records in Appendices I and II are presented within the same duration of 30 seconds for horizontal components and 20 seconds for vertical components so that the plots of the recorded ground motions are visually comparable. In order to evaluate the effect of severe earthquakes on the state of stress in concrete gravity dams, some of the actual earthquake records are scaled by a factor of 3. The resulting set of ground motion data includes a wide range of peak ground accelerations and earthquake intensities which are used in the correlation studies.

5.3.2 Duration of the Input Ground Motion

The response of the dam subjected to various ground motions is calculated for an identical duration of $t_d = 10\,s$. The selected part of the ground motion records also includes the significant part of the accelerograms with duration of 10 seconds. In general, the duration of strong ground motion, t_S, is different from the arbitrarily selected duration of response computation, t_d, in Eq. 5.5. The duration time, $_St$, is an application-based definition and was found to be different for the two categories of the PGA/PGV ratio. The duration of the strong motion part of the record was found to be generally longer for the case of the intermediate PGA/PGV ratio category compared with the corresponding duration for the records with high PGA/PGV ratio. The significant duration of the ground motion is reported to be dependent on the frequency characteristics of the recorded earthquake (Novikova and Trifunac 1994). For simplicity, the significant duration of the ground motion in Eq. 5.5 was arbitrarily taken as $t_S = 1s$ in the correlation studies so as to exclude the effect of the definition of the ground motion duration on the variations of the stress factor.

5.3.3 Tensile Strength of the Monolith Concrete

The calculated tensile stresses over the cross section of the dam are compared with an indicator of the tensile strength of the mass concrete. This limiting value depends on the testing method as well as on the origin of the concrete sample. The tested tensile strength of the cores taken from a number of concrete dams are reported to be lower than the values taken from laboratory samples due to the drying shrinkage and surface cracking of the core samples from the dam concrete (Jansen 1988). The results of the splitting tension tests on core samples of a few existing concrete dams are reported to be generally higher than the results obtained using the direct tension test. The splitting test measures the tensile strength of the concrete at a predefined plane within the sample whereas the tensile fracture occurs

at the weakest plane of the entire specimen under the direct tension test. The results of the splitting tests are also found to be less scattered due to transportation and storage problems and are more reliable as the true tensile strength of concrete (Jansen 1988).

The calculated stresses in the dam also depend on the adopted simplifying assumptions. The linearly elastic model for the concrete with a constant modulus of elasticity results in an overestimation of the evaluated stresses in the dam. The developed stress for a given strain level in a more realistic, nonlinear model for the concrete is lower than the predicted value based on linear analysis. This difference becomes significant at higher stress levels near the ultimate strength of the concrete. An *apparent* tensile strength is defined to compensate for the difference between the linear assumption and the true behaviour of the concrete. Raphael (1984) presented the following expressions for the tensile strength of mass concrete as a function of its compressive strength:

- *Actual static* tensile strength:

$$f_{as} = 1.7 f_c^{2/3} \tag{5.10}$$

- *Apparent static* tensile strength:

$$f_{as} = 2.3 f_c^{2/3} \tag{5.11}$$

- *Actual dynamic* tensile strength:

$$f_{ad} = 2.6 f_c^{2/3} \tag{5.12}$$

- *Apparent dynamic* tensile strength:

$$f_{ad} = 3.4 f_c^{2/3} \tag{5.13}$$

where f_c is the compressive strength of concrete in psi. In the present study, the apparent

dynamic tensile strength, f_{pd}, is used as the cracking limit for the calculated tensile stresses in the dam. The compressive strength of concrete is taken as 27.6 MPa (4000 psi) which yields $f_{pd} = 5.9$ MPa (857 psi) for the tensile strength of the concrete.

The magnitude of the calculated principal tensile stress in nearly all the elements over the cross sectional area of the dam can theoretically reach the f_{pd} value during the main shock of the excitation, t_S, when the dam is subjected to a severe input ground motion. The stress is assumed negligible during the excitation time apart from the main shock period. The magnitude of the stress factor of a dam monolith subjected to a severe earthquake approaches unity based on Eq. 5.5. The summation in Eq. 5.5 is zero for the structure at rest. Therefore, the expected range of variation of the stress factor, SF, is:

$$0 \leq SF \leq 1 \tag{5.14}$$

The stress factor, SF, provides a measure of the state of the principal tensile stress in the dam under dynamic loading. It is based on the time variation of the stress response which includes the effects of the significant stress peaks other than the maximum value. The stress factor is a linear operator on the stress function $\sigma'_1(t)$. Accordingly, it is directly proportional to the intensity of the ground motion which makes it consistent with the idea of Spectral Intensity proposed by Housner (Arias 1969). The stress factor is also based on the tensile stress magnitudes over the entire cross sectional area of the dam monolith. Therefore, it is a *global*, single-valued parameter that can be used to study and compare the effects of different input ground motions on the dam as is discussed in the next section.

5.4 DISCUSSION OF RESULTS

5.4.1 Intensity Measures

The correlations between the maximum principal tensile stresses in the dam cross section, $(\sigma'_1)_{max}$, and the intensity measures of the input ground motions are presented for horizontal ground motion in Figs. 5.3 and 5.4 and for vertical ground motion in Figs. 5.5 and 5.6. The maximum stress values are shown for both the neck (Figs. 5.3 and 5.5) and the heel (Figs. 5.4 and 5.6) of the dam and are normalized with the apparent dynamic tensile strength of the concrete, f_{pd}. The dynamic response of the structure in Figs. 5.3 to 5.6 does not include the hydrostatic loading or the weight of the monolith. From figures 5.3 to 5.6 it is concluded that the PGA of the input earthquake record is an acceptable measure of the ground motion intensity for concrete gravity dams. The results of correlation between $(\sigma'_1)_{max}$ and PGA of the input excitation are nearly as good as the corresponding results for the spectral intensity, SI and the modified Arias intensity, I_{EQ}. The reason is that concrete gravity dams are generally short period structures. Consequently, the effect of higher modes of the structure are less significant and therefore, there is a direct proportionality between the magnitudes of the applied ground acceleration and the maximum developed stress at a given point in the dam.

The concept of spectral intensity introduced by Housner with modified limits of the period range and viscous damping ratio proves to be applicable for seismic analysis of gravity dams. Housner's idea was to propose a measure of ground motion intensity which is directly proportional to the maximum developed stresses in the structure (Arias 1969). Figures 5.3 to 5.6 show such a relationship for maximum principal stresses in the dam with the spectral intensity of the ground acceleration. The correlation is quite acceptable at both monitoring locations within the dam cross section (namely, the neck and the heel) subjected to both horizontal and vertical components of the input ground motion.

5.4.2 Stress Factor due to Horizontal and Vertical Ground Motions

The correlations of the tensile stress factor, SF, with the ground motion intensities are shown in Figs. 5.7 and 5.8 for the horizontal and vertical ground motion records, respectively. The response shown in Figs. 5.7 and 5.8 does not include the hydrostatic pressure or the weight of the monolith. The calculated intensity measures of the selected horizontal and vertical components are presented in Tables 5.6 and 5.7, respectively. The PGA and SI intensities of the ground motion records depend on the determined maximum values and do not vary with the duration of response calculation, t_d ,provided that t_d includes the significant part of the strong motion in the earthquake record. The Arias intensity of the earthquake record depends on the duration time included in the response calculation according to Eqs. 5.8 and 5.9. The adequacy of the calculation time of $t_d = 10\ s$ is verified by calculating the modified Arias intensity (Eq. 5.9) for a longer duration of $t_d = 20\ s$. The modified Arias intensity almost remains unchanged after including the insignificant part of the ground motion records up to $t_d = 20\ s$ for almost all the accelerograms presented in Tables 5.6 and 5.7. The intensity calculations for $t_d = 20s$ are performed for the earthquakes with the available record of duration longer than 20 *s*. The vertical ground motion records in Tables 5.4 and 5.5 are named according to the PGA/PGV classification of the horizontal components. The vertical component records are classified based on their own PGA/PGV ratio in the results of the correlation studies for the vertical ground motions. An arbitrary value of 1.6 is chosen to separate the vertical records based on their available PGA/PGV ratios into an intermediate and a high category. The limit of 1.6 for the PGA/PGV ratio is slightly higher than the corresponding value of 1.2 for the horizontal ground motion records suggested by Naumoski *et al.* (1988).

The correlations of the maximum tensile stress , $(\sigma'_1)_{max}$, and the stress factor, SF, with the intensities of the horizontal and vertical ground motion components including the effects

of the hydrostatic loading and the weight of the structure, are presented in Figs. 5.9 to 5.14. By comparing the variations of the maximum tensile stress and the stress factor with the intensity of the ground motion in Figs. 5.3 to 5.14, the following conclusions are reached:

1) The stress factor, SF, shows generally good correlations with all the included intensity measures of the ground motions and proves to be a valid parameter in comparing the effects of different earthquake records on the overall structural response of gravity dams.

2) The stress factor of the monolith cross section under horizontal ground motion shows a noticeable dependence on the PGA/PGV ratio of the input earthquake (Fig. 5.7). The overall state of tensile stress over the entire monolith cross section is generally higher when the dam is subjected to a record with intermediate PGA/PGV ratio based on the values of the stress factor in Fig. 5.7. The peak ground velocity of the input earthquake is an indicator of the energy conveyed to the structure. The amount of the input energy of the ground motion for a given PGA is expected to be higher for a record in the intermediate PGA/PGV category compared with the energy of a record with high PGA/PGV ratio. Examination of the response spectra of the horizontal component records (Naumoski *et al.* 1988) reveals that there is no significant difference in the spectral amplitudes between the two PGA/PGV ratio categories in the vicinity of the fundamental frequency of the dam-reservoir model (ω^1_c = 20 rad/s). Therefore, records in the high and intermediate PGA/PGV ratio categories have different effects on the dam-reservoir model based on their energy rather than their frequency contents.

The dependence of the dam response on the PGA/PGV characteristic of the ground motion is not present in the variation of the maximum tensile stress at a point within the monolith cross section (Figs. 5.3 to 5.6). The results of the maximum

tensile stresses at both the heel and the neck of the dam show an independent variation with the PGA/PGV ratio of the input ground motion. The dependence of the stress factor on the PGA/PGV ratio of the ground motion record is less significant when the dam-reservoir system is subjected to vertical excitation. The reason is partly due to the fact that vertical ground motion categories in the present study are arbitrarily set. More investigation is needed for the classification of the vertical component records based on their PGA/PGV ratios.

3) Comparison of Figs. 5.7 and 5.13 indicates that the tensile stress factor is significantly influenced by the hydrostatic loading and the weight of the dam. The difference between the two cases of loading is pronounced when the dam is subjected to vertical ground motion (Figs. 5.8 and 5.14). This difference is not indicated in the plots of maximum tensile stress at a given point of the dam cross section (cf. Figs. 5.5 and 5.6 with Figs. 5.11 and 5.12). The reason is that the additional tensile stresses at the heel and (to a less extent) at the neck of the dam due to the effect of the hydrostatic loading are counteracted by the imposed compression due to the weight of the monolith. However, the redistribution of the stresses across the cross sectional area of the monolith due to the weight and hydrostatic loadings affects the associated stress factor as indicated in Figs. 5.13 and 5.14. It follows that the tensile stress factor is a more reliable indicator of the dam response than the maximum stress value at a point of the cross section under different load combinations.

4) The relative significance of the weight of the dam and hydrostatic force of the reservoir in the overall response of the dam can readily be assessed by comparing the corresponding stress factors for the two different load cases (Figs. 5.9 and 5.10 which neglects hydrostatic and weight loadings) and (Figs. 5.15 and 5.16 which includes the monolith weight and the hydrostatic loadings). A curve of best fit of the data of the

stress variation with the ground motion intensity under seismic loading only in Figs. 5.3 and 5.4 appear to pass through the origin. Tensile stresses develop in the dam when the hydrostatic loading is included before the dynamic loads are applied. The variation of the stress factor with the ground motion intensity appears to be asymptotic at the low-intensity range of earthquakes. This indicates nonzero tensile stresses in the monolith cross section (Figs. 5.13 and 5.14) due to the static loads only. The stress factor also shows good correlation between the stress level in the dam and all three measures of ground motion intensity for strong earthquakes. The variation of the stress factor with the ground motion intensity shows that the overall state of tensile stress in the dam is essentially governed by the effects of hydrostatic loading and the weight of the dam when PGA < 0.30g for high PGA/PGV ratio records. For the case when the dam is subjected to an intermediate PGA/PGV ratio ground motion, the range of PGA drops to < 0.15g (or equivalent intensities of the records). This represents the level of excitation below which the effect of seismic loading on the overall state of stress in the dam is negligible compared to the other sources of the loading. The same observations concerning the maximum tensile stress in the dam can be made whether or not the hydrostatic loading and dam weight is included (Figs. 5.3 to 5.6 and Figs. 5.9 to 5.12). The local maximum tensile stress vanishes without approaching a lowerbound value as the intensity of the input ground motion to the dam-reservoir model is reduced. The main reason for the above behaviour is that the maximum tensile stress is monitored at predetermined areas such as the heel and the neck of the dam. When the effects of the hydrostatic loading and the weight of the dam are included, the maximum tensile stress in the monolith shifts to the other parts of the cross section which, in general, can not be readily located. The location of the maximum tensile stress varies depending on various factors including the geometry

of the dam, the water level in the reservoir and the level of seismic excitation. However, this occurs at very low levels of earthquake intensities which are below the values of interest in design.

5) The effect of vertical ground motion is less significant when compared with the horizontal excitation when the effects of hydrostatic loading and the weight of the dam are included in the analysis. When the gravity and the hydrostatic load are included, the stress factor of the dam due to the vertical ground motion is much less than the case when these loads are not included in the analysis. The reduction in the stress factor is significant for low intensities of the input ground motion (cf. Figs. 5.8 and 5.14).

5.4.3 Influence of Ground Motion Characteristics

The time history response of maximum principal stresses at the neck of the dam due to different input ground motions are compared as shown in Fig. 5.2. It is noted that the maximum peaks of stress due to the 1970 Lytle Creek S25W (record HH6) and the 1971 San Fernando N90E (record HI7) earthquakes are identical. However, the overall time history response of the maximum stress in the dam subjected to the 1971 San Fernando N90E earthquake is more severe than the case of the Lytle Creek earthquake (Fig. 5.2a). Comparing the effects of the 1966 Parkfield N65W (record HH1) and the 1952 Taft N69E (record HI2) earthquakes on the dam response shown in Fig. 5.2b is difficult. The effects of the ground motion records on the dam response can readily be examined by comparing the corresponding stress factors. The maximum tensile stresses in the dam subjected to Lytle Creek and San Fernando earthquakes are 0.358 f_{pd} and 0.357 f_{pd}, respectively. The stress factors of the monolith due to the Lytle Creek (record HH6) and San Fernando (record HI7) ground motions are 0.177 and 0.426, respectively. Comparison of the stress factors

indicates the severe effect of San Fernando ground acceleration.

A more interesting case is the comparison between the developed stress levels in the dam when subjected to the 1966 Parkfield N65W (record HH1) and the 1952 Taft N69E (record HI2) earthquakes. The maximum tensile stresses of the dam subjected to the Parkfield and Taft earthquakes are 0.558 f_{pd} and 0.394 f_{pd}, respectively. The stress factors of the monolith model due to the 1966 Parkfield N65W (record HH1) and the 1952 Taft N69E (record HI2) ground motions are 0.277 and 0.621, respectively. Based on the corresponding stress factors, it is concluded that Taft ground motion produces higher risk level of crack initiation and propagation in the dam as compared to the Parkfield earthquake.

5.4.4 Damage Evaluation

The stress factor of the dam monolith is used to examine the extent of the overstressed part of the dam cross section. Figures 5.15 and 5.16 show the parts of the dam cross section where the calculated principal tensile stress exceeds the tensile strength of the concrete. The dam-reservoir model described in section 5.2.1 is used to obtain the results presented in Figs. 5.15 and 5.16. The results do not include the hydrostatic loading and the weight of the dam. Three different ranges of stresses are defined. The unshaded areas denote finite elements where the principal tensile stress is less than the concrete static strength: $(\sigma^t_1)_{max} < f_{as}$ where $(\sigma^t_1)_{max}$ and f_{as} denote the maximum principal tensile stress and the actual static tensile strength of the mass concrete given by Eq. 5.10, respectively. In this stress range, the concrete is uncracked. The lightly shaded finite elements indicate the parts of the dam that undergo stresses that are higher than the actual static tensile strength of the concrete but do not exceed its apparent seismic tensile strength, f_{pd} as: $f_{as} \leq (\sigma^t_1)_{max} < f_{pd}$. In this range of tensile stress, the concrete may develop some cracks. The elements of the dam which are darkly shaded indicate the parts of the dam cross section which develop

excessive tensile stresses. The tensile stress is larger than the apparent seismic tensile stress of the monolith concrete computed according to Eq. 5.13. Therefore, at these locations: $(\sigma^{t}_{1})_{max} \geq f_{pd}$. The states of stress depicted in Figs. 5.15 and 5.16 are due to the ground accelerations presented in Table 5.8. According to the Figs. 5.15 and 5.16 and Table 5.8, the stress factor of the dam appears to be an appropriate measure to evaluate the progress of overstressing in the dam cross section. The extent of the expected cracking in the dam cross section is directly proportional to the computed stress factor of the monolith cross section for both horizontal and vertical ground motion components.

The results illustrated in Figs. 5.15 and 5.16 also suggest that the stress factor of a dam can be utilized as a convenient means for optimum design of the monolith. A larger SF value with lower extent of the parts with $(\sigma^{t}_{1})_{max} \geq f_{as}$ indicates a more favourable stress distribution under a given load combination. Accordingly, the geometry of the monolith as well as the design of the mass concrete at different parts of the monolith cross section can be made such that a larger portion of the dam cross section carries the tensile stresses provided the stresses remain within the uncracked range of the dam concrete.

5.5 EFFECT OF THE RESERVOIR BOUNDARIES ON THE STRESS IN THE DAM

5.5.1 Introduction

The evaluation of the effects of the reservoir boundary conditions on the dynamic response of the dam-reservoir system in previous chapters is based on specific earthquake records. In this section, the effects of the reservoir boundary characteristics on the developed stresses in the dam are investigated when the dam is subjected to a number of different ground motion records. The study is conducted in two separate parts: First, the effect of reservoir bottom sedimentation is addressed. The characteristics of a layered reservoir bottom boundary are varied and the maximum tensile stresses in the dam are determined. The stress factors of the dam for various cases are evaluated. Secondly, the effect of hydrodynamic isolation on the tensile stresses and the stress factor of the dam is examined. The isolation layer characteristics are selected according to the results obtained in Chapter 3. The extent of response reduction due to hydrodynamic isolation of the dam when subjected to different input ground acceleration records, is investigated.

The selected dam example is that shown in Fig. 5.1. The finite element discretization of the monolith includes 48 four-noded quadrilateral elements. The dam is assumed in plane stress condition with the height of $H_s = 91.44$ m (300 ft). The modulus of elasticity of the concrete and the Poisson ratio are assumed as 21500 MPa and 0.2, respectively. The foundation rock underneath the dam is assumed rigid. However, the method is equally applicable to the case of a flexible foundation beneath the entire dam-reservoir system. For simplicity, only the dynamic component of the response of the dam is included in the analysis. The reservoir is assumed infinitely long with a constant depth equal to the height of the impounding dam ($H = H_s$).

5.5.2 Reservoir Bottom Absorption Effects on the Stresses in the Dam

Two horizontal component records from each category of high and intermediate PGA/PGV ratio are chosen. The selected ground accelerations are the HH1, HH6, HI2 and HI7 records as listed in Tables 5.2 and 5.3. The selected vertical component records are VH1 and VI9 as described in Tables 5.4 and 5.5, respectively. All the selected records are from California earthquakes in an attempt to exclude major site differences in the parametric studies. The PGA/PGV ratios of the *high* categories in both horizontal and vertical ground motion records are approximately twice the PGA/PGV ratios of the *intermediate* groups according to Tables 5.2 to 5.5. The ground acceleration records are scaled to PGA = 0.25g.

The characteristics of the reservoir bottom are varied and the dam is subjected to the selected ground accelerations. The stresses in the dam and the stress factor of the dam monolith are evaluated. The mechanical properties of the reservoir foundation are chosen to represent the practical ranges of the sedimentation and the underlying rock characteristics. The modulus of elasticity of the sediment material is chosen in the range of E_s = 360 - 1440 MPa (50 - 200 ksi) which represent typical values for soils (Bowles 1984). The damping constant b in Eq. 2.28 is taken as $b = 0.5$. The modulus of elasticity of the foundation rock is assumed as E_f = 71820 MPa (10400 ksi). The normalized thickness of the sediment layer is varied in the range of d_s/H = 0.010 - 0.075.

Figure 5.17 shows the variation of maximum tensile stress in the dam with the normalized thickness of the sediment layer when subjected to the selected horizontal ground motions. The maximum tensile stress is normalized to the apparent seismic tensile strength of mass concrete, f_{pd}. The variation of the tensile stress factor with the normalized thickness of the sediment layer is shown in Fig. 5.18. The effect of the sediment layer thickness on developed tensile stress and the stress factor of a dam subjected to vertical ground motions

is presented in Fig. 5.19. From Figs. 5.17 to 5.19, the following conclusions are reached:

1) The variation of the modulus of elasticity of the sediment material does not show significant effect on the stresses in the dam for a given rigidity of the underlying foundation rock under the same horizontal input ground motion (Fig. 5.17).

2) The dam response is reduced by increasing the thickness of the sediment layer for all the selected ground motion records. The variation of the seismic tensile stresses in the dam with the normalized thickness of the sediment layer is almost linear within the examined range of the layer thickness.

3) The amount of reduction in the response in terms of both maximum tensile stress and the stress factor of the dam due to the effect of the sediment layer varies with the input ground acceleration (Figs. 5.17 to 5.19). However, the rate of the reduction in the stress factor with increasing the thickness of the sediment layer is almost independent of the input earthquake record (Figs. 5.18 and 5.19b).

4) The maximum tensile stress in the dam does not show any dependence on the PGA/PGV ratio of the input ground motion. The stress factor, on the other hand, shows a clear dependence on the PGA/PGV ratio of the ground excitation. The examined horizontal ground motions with intermediate PGA/PGV ratio produce higher stress factors in the dam (Figs. 5.18 and 5.19). This conclusion is in accordance with the second conclusion mentioned in section 5.4.2. The examined records with intermediate PGA/PGV ratio result in higher values of the stress factor for the range of the sediment layer thickness and modulus of elasticity used in the analysis.

5) The effect of reservoir bottom characteristics on the stresses in the dam is more significant when the dam-reservoir model is subjected to vertical ground motion. Figure 5.19a shows a noticeable difference in the maximum tensile stress in the dam

when the normalized modulus of elasticity of the sediment material, E_s / E_f, is varied from 0.005 to 0.02. The same increase in E_s / E_f value does not result in observable increase in the maximum tensile stress in the dam under horizontal ground motion (Fig. 5.17). The sediment thickness also shows a significant influence on the developed stresses in the dam under vertical ground acceleration as compared to the case of horizontal excitation (Fig. 5.19). The above observations are valid for both VH1 and VI9 vertical ground motion records with considerably different PGA/PGV ratios.

The absorption effect of the sediment layer on the tensile stress in the dam when subjected to vertical excitation is examined using the set of the ground motion records listed in Tables 5.4 and 5.5. The objective is to verify the response reduction effect of the sediment mathematical model discussed in Chapter 2 using the ground motion records with various characteristics. Figure 5.20 shows the calculated reduction of the maximum principal tensile stress and the stress factor of the dam for the set of vertical ground motion records. The vertical component records are classified as high and intermediate categories based on their PGA/PGV ratio according to an arbitrary value of PGA/PGV = 1.6. The response of the dam is computed for the two cases where no sedimentation is considered at the reservoir bottom and when the a sediment layer with the thickness of $d_s/H = 0.05$ is assumed. The mechanical properties of the sediment material and the reservoir foundation are given in the figure. The results presented in Fig. 5.20 confirm that the mathematical model of the sedimented reservoir bottom shows stress reduction in the dam for all input ground motion records as compared to the case where no sediment layer is assumed. The amount of stress reduction in the dam-reservoir example subjected to different vertical component ground motions varies in the range of 10% to 40% for the maximum principal stress and in the range of 8% to 35% for the stress factor of the dam.

The amount of response reduction of the dam due to the effect of the reservoir bottom sedimentation does not show any specific variation with the peak ground acceleration of the input ground motion (Fig. 5.20).

The variations of the maximum tensile stress and the stress factor of the dam with the PGA/PGV ratio of the input earthquake are shown in Fig. 5.21. The ground motion records are scaled to PGV = 0.1 m/s. The thickness of the reservoir bottom sediment layer is taken as $d_s/H = 0.05$. The normalized maximum tensile stress shows a linear variation with the PGA/PGV ratio of the input earthquake which is independent of the PGA/PGV ratio category. This observation is in accordance with the variation of the computed maximum tensile stress in the dam with PGA of the ground motion shown in Fig. 5.5a. The reason is that for a constant PGV value, Fig. 5.21a represents the almost linear dependence of the developed stress in the dam as a type of low-period structure on the PGA of the ground motion as shown in Fig. 5.5a. The stress factor of the dam shows different trends of dependence on the PGA/PGV ratio of the ground motion input. According to Fig. 5.21b, the PGA/PGV of the records in the *intermediate* category has more significant effect on the stress factor of the dam as compared to the records of high PGA/PGV category. The stress factor increases with the PGA/PGV of the records in both categories when scaled to the same PGV value.

5.5.3 Stress Reduction With Hydrodynamic Isolation of the Dam

The performance of the hydrodynamic isolation layer when the dam-reservoir system is subjected to different earthquake excitations is investigated. The objective is to examine the effectiveness of hydrodynamic isolation in reducing the seismic response of the dam under different ground motion characteristics. The same dam-reservoir example discussed in section 5.5.2 is used in the study. The only difference is that the reservoir bottom is

assumed completely rigid with no sediment layer and $\alpha_b = 1.0$. An attached isolation layer is assumed to cover the upstream face of the dam. The thickness of the layer is assumed constant and equal to $t_l = 2.4$ m ($t_l/H = 0.025$). The density and the modulus of elasticity of the isolation material are assumed as: $\rho_l = 1300$ kg/m^3 and $E_l = 0.1$ MPa, respectively. The appropriate damping of the material is obtained using Fig. 3.9 as: $\rho_l C_l t_l = 27.9$ kPa.s and therefore: $\eta_{cl} = 0.5 \times 27.9 = 14.0$ kPa.s. Figures 5.22 and 5.23 show the variation of the maximum tensile stress and the stress factor of a dam subjected to the horizontal ground motion records listed in Tables 5.2 and 5.3, respectively. The horizontal components of the ground motion are selected for the analysis because they cause higher stresses in the dam than the vertical components. The results presented in Figs. 5.22 and 5.23 confirm the reduction effect of the hydrodynamic isolation scheme on the stress in the dam subjected to ground motion records with different intensity and frequency characteristics. The reduction effect of the hydrodynamic isolation appears to be more significant when the dam is subjected to stronger ground motion records. However, more recorded ground motions need to be examined for verification of this observation.

5.6 CONCLUSIONS

A measure of the structural response (Stress Factor) is introduced to evaluate the overall state of stress in a gravity dam monolith over a given period of time. It is shown that the introduced parameter correlates well with various measures of the input ground motion intensity and therefore, is applicable in seismic design and reliability analysis of concrete gravity dams. The maximum tensile stress and the stress factor proved useful in the evaluation of the effects of reservoir bottom sedimentation and the hydrodynamic isolation layer introduced in previous chapters on the seismic response of the dam-reservoir system.

It is concluded that the evaluation of the stress factor of the dam as a complementary design parameter provides a convenient measure in comparing the effect of different input ground motion records as well as the influence of reservoir boundary characteristics on earthquake response of the dam.

The stress factor can also be used in damage evaluation of the concrete gravity dam when subjected to severe earthquake ground motion. The stress factor is shown to be a direct measure of the expected overstressed part of the dam cross section. However, it only provides an overall indication of the state of excessive stress in the dam subjected to strong ground motion. A nonlinear analysis is needed to study the post-cracking behaviour of the dam and the extent of crack propagation over the monolith cross section.

Table 5.1 Partial list of large concrete gravity dams in the United States (Kollgaard 1988)

Dam	Year Built	Height (*m*)	Face Slope (*)		Notes
			D.stream	Upstream	
Lower Crystal Springs	1888	46.9	0.71	0.25	
Arrowrock	1915	106.7	0.67	0.05	
Elephant Butte	1916	91.7	0.83	-	
O'shaughnessy	1938	131.1	0.78	V	95.1 *m* above streambed
Shaver Lake	1927	56.4	0.71	V	
Morris	1934	100.0	0.81	0.05	
Hiwassee	1940	93.6	0.69	V	
Friant	1942	97.2	0.70	V	
Grand Coulee	1942	167.6	0.80	V	
Fontana	1944	146.3	0.76	V	140.2 *m* above streambed
Shasta	1945	183.5	0.80	V	
Hartwell	1963	73.2	0.67	V	62.2 *m* above streambed
Dworshak	1973	218.5	0.80	V	
Willow Creek	1983	53.9	0.82	V	51.5 *m* above streambed
Middle Fork	1984	37.8	0.88	-	
Galesville	1986	50.9	0.80	V	47.9 *m* above streambed
Upper Stillwater	1988	88.4	0.60	V	Roller Compacted Concrete

(*) For the cases where the dam has multiple face slopes, the main slope is listed.

Table 5.2 Records of horizontal components with High PGA/PGV ratio (Naumoski *et al.* 1988)

Rec. No.	Earthquake	Date	M	Site	Comp.	Max.Acc. PGA (g)	Max.Vel. PGV (m/s)	PGA / PGV	Site Condition
HH1	Parkfield California	Jun.27, 1966	5.6	Temblor No.2	N65W	0.269	0.145	1.9	Rock
HH2	Parkfield California	Jun.27, 1966	5.6	Cholame, Shandon No.5	N85E	0.434	0.255	1.7	Rock
HH3	San Francisco California	Mar.22, 1957	5.3	Golden Gate Park	S80E	0.105	0.046	2.3	Rock
HH4	San Francisco California	Mar.22, 1957	5.3	State Bldg., S.F.	S09E	0.085	0.051	1.7	Soil
HH5	Helena Montana	Oct.31, 1935	6.0	Carroll College	N00E	0.146	0.072	2.0	Rock
HH6	Lytle Creek	Sep.12, 1970	5.4	Wrightwood, California	S25W	0.198	0.096	2.1	Rock
HH7	Oroville California	Aug.1, 1975	5.7	Seism. Station, Oroville	N53W	0.084	0.044	1.9	Rock
HH9	San Fernando California	Feb. 9, 1971	6.4	Lake Hughes, Station 4	S21W	0.146	0.085	1.7	Rock

Table 5.2 (*Contd.*) Records of horizontal components with High PGA/PGV ratio (Naumoski *et al.* 1988)

HH11	Central Honshu, Japan	Feb.26, 1971	5.5	Yoneyama Bridge	Trans.	0.151	0.059	2.6	Soil
HH12	Near E. Coast Honshu, Japan	May 11,1972	5.8	Kushiro Central Wharf	N00E	0.146	0.06	2.4	Soil
HH13	Honshu, Japan	Apr.5, 1966	5.4	Hoshina-A	N00E	0.27	0.111	2.4	Soil
HH15	Banja Luka Yugoslavia	Aug.13,1981	6.1	Seis. Station, Banja Luka	N90W	0.074	0.032	2.3	Rock

Table 5.3 Records of horizontal components with Intermediate PGA/PGV ratio (Naumoski *et al.*1988)

Rec. No.	Earthquake	Date	M	Site	Comp.	Max.Acc .PGA (g)	Max.Vel. PGV (m/s)	PGA / PGV	Site
HI1	Imperial Valley California	May18, 1940	6.6	El Centro	S00E	0.348	0.334	1.04	Soil
HI2	Kern County California	Jul.21, 1952	7.6	Taft Lincoln School Tunnel	S69E	0.179	0.177	1.01	Rock
HI3	Kern County California	Jul.21, 1952	7.6	Taft Lincoln School Tunnel	N21E	0.156	0.157	0.99	Rock
HI4	Borrego Mtn. California	Apr.8, 1968	6.5	San Onofre SCE Power Plant	N57W	0.046	0.042	1.10	Soil
HI5	Borrego Mtn. California	Apr.8, 1968	6.5	San Onofre SCE Power Plant	N33E	0.041	0.037	1.11	Soil
HI6	San Fernando California	Feb.9, 1971	6.4	3838 Lankershim Blvd., L.A.	S90W	0.150	0.149	1.01	Rock
HI7	San Fernando California	Feb.9, 1971	6.4	Hollywd. Storag. P.E. Lot, L.A.	N90E	0.211	0.211	1.00	Soil
HI8	San Fernando California	Feb.9, 1971	6.4	3407 6th Street, L.A.	N90E	0.165	0.166	0.99	Soil
HI9	San Fernando California	Feb.9, 1971	6.4	Griffith Park observatory, L.A.	S00W	0.180	0.205	0.88	Rock

Table 5.3 (*Contd.*) Records of horizontal components with Intermediate PGA/PGV ratio (Naumoski *et al.*1988)

HI10	San Fernando California	Feb.9, 1971	6.4	234 Figueroa St., L.A.	N37E	0.199	0.167	1.19	Soil
HI11	Near E. Coast Honshu, Japan	Nov.16, 1974	6.1	Kashima Harbor Works	N00E	0.070	0.072	0.97	Soil
HI12	Near E. Coast Honshu, Japan	Aug.2, 1971	7.0	Kushiro Central Wharf	N90E	0.078	0.068	1.15	Soil
HI13	Monte Negro Yugoslavia	Apr.15, 1979	7.0	Albatros Hotel, Ulcinj	N00E	0.171	0.194	0.88	Rock
HI14	Mexico Earthquake	Sep.19, 1985	8.1	El Suchil, Guerrero Array	S00E	0.105	0.116	0.91	Rock
HI15	Mexico Earthquake	Sep.19, 1985	8.1	La Villita, Guerrero Array	N90E	0.123	0.105	1.17	Rock

Table 5.4 Records of vertical components corresponding to the horizontal components with high PGA/PGV ratio

Rec. No.	Earthquake	Date	M	Site	Max.Acc. PGA (g)	Max. Vel. PGV (m/s)	PGA / PGV
VH1	Parkfielda, CA	Jun. 27, 1966	5.6	Temblor No.2	0.132	0.04	3.30
VH2	Parkfield, CA	Jun. 27, 1966	5.6	Cholame, Shandon No.5	0.119	0.073	1.63
VH3	San Francisco, CA	Mar.22, 1957	5.3	Golden Gate Park	0.037	0.012	3.08
VH4	San Francisco, CA	Mar.22, 1957	5.3	State Bldg., S.F.	0.044	0.024	1.83
VH5	Helena Montana	Oct. 31, 1935	6.0	Carroll College	0.089	0.097	0.92
VH6	Lytle Creek	Sep. 12, 1970	5.4	Wrightwood, California	0.054	0.032	1.69
VH7	Oroville, CA	Aug. 1, 1975	5.7	Seismogr. Station, Oroville	0.115	0.049	2.35
VH8	San Fernando, CA	Feb. 9, 1971	5.7	Pacoima Dam	0.709	0.583	1.22
VH9	San Fernando, CA	Feb. 9, 1971	6.4	Lake Hughes, Station 4	0.154	0.071	2.17
VH13	Honshu, Japan	Apr. 5, 1966	5.4	Hoshina-A	0.058	0.026	2.23
VH14	Monte Negro Yugoslavia	Apr. 9, 1979	5.4	Albatros Hotel, Ulcinj	0.030		
VH15	Banja Luka Yugoslavia	Aug.13, 1981	6.1	Seismogr. Station, Banja Luka	0.044		

Table 5.5 Records of vertical components corresponding to the horizontal components with Intermediate PGA/PGV ratio

Rec. No.	Earthquake	Date	M	Site	Max.Acc. PGA (g)	Max. Vel. PGV (m/s)	PGA/PGV
VI1	Imperial Valley, CA	May18, 1940	6.6	El Centro	0.210	0.108	1.94
VI2	Kern County, CA	July 21, 1952	7.6	Taft Lincoln School Tunnel	0.105	0.067	1.57
VI41(*)	Borrego Mtn., CA	April 8, 1968	6.5	San Onofre SCE Power Plant	0.055	0.031	1.77
VI42(*)	Borrego Mtn., CA	April 8, 1968	6.5	San Onofre SCE Power Plant	0.037		
VI6	San Fernando, CA	Feb. 9, 1971	6.4	3838 Lankershim Blvd., L.A.	0.071	0.05	1.42
VI7	San Fernando, CA	Feb. 9, 1971	6.4	Hollywood Strg. P.E. Lot, L.A.	0.089	0.055	1.62
VI8	San Fernando, CA	Feb. 9, 1971	6.4	3407 6th Street, L.A.	0.057	0.088	0.65
VI9	San Fernando, CA	Feb. 9, 1971	6.4	Griffith Park Observatory, L.A.	0.123	0.073	1.68
VI10	San Fernando, CA	Feb. 9, 1971	6.4	234 Figueroa St., L.A.	0.069	0.078	0.88
VI11	Honshu, Japan	Nov.16, 1974	6.1	Kashima Harbor Works	0.039	0.02	1.95
VI13	Monte Negro Yugoslavia	Apr. 15, 1979	7.0	Albatros Hotel, Ulcinj	0.163	0.118	1.38
VI14	Mexico Earthquake	Sep. 19, 1985	8.1	El Suchil, Guerrero Array	0.051	0.06	0.85
VI15	Mexico Earthquake	Sep. 19, 1985	8.1	La Villita, Guerrero Array	0.059	0.047	1.26

(*) Record VI4 is splitted into two separate ground motion records for the analysis.

Table 5.6 Intensity measures of the selected horizontal components

Record	t_{record} (s)	t_d (s)	Ground motion Intensity			
			PGA (g)	SI (cm)	$I_{EQ} \times 10^2$ $(s)^{1/2}$	
					t_d=10s	t_d=20s
HH1	30.3	10, 20	0.269	11.9	3.0	3.0
HH2	44.0	10, 20	0.434	15.5	4.8	5.0
HH3	39.8	10, 20	0.105	3.5	1.2	1.2
HH4	40.8	10, 20	0.085	3.5	1.2	1.2
HH5	51.0	10, 20	0.146	4.3	1.5	1.5
HH6	16.8	10	0.200	6.4	2.1	--
HH7	12.4	10	0.084	2.5	1.2	--
HH9	36.9	10,20	0.146	5.1	2.3	2.4
HH11	16.9	10	0.151	4.0	1.7	--
HH12	28.0	10, 20	0.146	5.3	1.7	1.8
HH13	9.9	10	0.270	7.1	2.7	--
HH15	16.4	10	0.074	2.3	1.1	--

Table 5.6 (*Contd.*) Intensity measures of the selected horizontal components

HI1	53.7	10, 20	0.348	13.0	6.0	6.8
HI2	54.3	10, 20	0.179	7.6	3.5	3.9
HI3	54.3	10, 20	0.156	6.8	3.2	3.7
HI4	44.9	10, 20	0.046	1.6	0.8	0.8
HI5	45.1	10, 20	0.041	1.9	0.7	0.7
HI6	65.1	10, 20	0.150	5.9	2.9	2.9
HI7	79.4	10, 20	0.211	8.7	4.2	4.3
HI8	62.5	10, 20	0.165	5.1	3.0	3.2
HI9	42.9	10, 20	0.180	6.8	3.1	3.3
HI10	47.0	10, 20	0.200	8.9	3.7	3.9
HI11	29.9	10, 20	0.070	2.3	1.3	1.4
HI12	60.0	10, 20	0.078	3.2	0.3	0.4
HI13	40.3	10, 20	0.171	9.3	4.1	4.3
HI14	32.5	10	0.105	3.7	1.9	--
HI15	40.6	10	0.123	4.4	1.9	--

Table 5.7 Intensity measures of the selected vertical components

Record	t_{record} (s)	t_d (s)	Ground motion Intensity			
			PGA (g)	SI (cm)	$I_{EQ} \times 10^2$ $(s)^{1/2}$	
					t_d=10s	t_d=20s
VH1	30.4	10, 20	0.132	3.3	1.2	1.3
VH2	44.0	10, 20	0.119	4.3	2.2	2.2
VH3	39.7	10, 20	0.037	0.8	0.4	0.4
VH4	40.6	10, 20	0.044	2.0	0.6	0.6
VH5	51.0	10, 20	0.089	3.2	1.1	1.1
VH6	16.6	10	0.054	1.8	0.8	--
VH7	12.1	10	0.115	2.7	1.1	--
VH8	41.7	10, 20	0.709	27.0	10.9	11.0
VH9	37.0	10, 20	0.154	4.2	2.2	2.2
VH13	10.0	10	0.058	1.9	0.7	--
VH14	11.5	10	0.03	1.0	0.4	--
VH15	16.5	10	0.044	1.7	0.7	--

Table 5.7 (*Contd.*) Intensity measures of the selected vertical components

VI1	53.8	10, 20	0.21	4.7	3.5	3.7
VI2	54.2	10, 20	0.105	4.6	2.1	2.5
VI41	45.2	10	0.055	1.3	0.7	--
VI42	45.2	10	0.037	1.4	0.6	--
VI6	65.2	10, 20	0.071	2.9	1.6	1.7
VI7	79.5	10, 20	0.089	2.0	1.5	1.6
VI8	62.5	10, 20	0.057	2.2	1.1	1.3
VI9	43.0	10, 20	0.123	3.8	2.0	2.1
VI10	47.1	10, 20	0.069	2.4	1.2	1.3
VI11	30.0	10, 20	0.039	1.0	0.6	0.7
VI13	40.4	10, 20	0.163	6.8	3.4	3.5
VI14	32.5	10	0.051	2.5	1.1	--
VI15	40.6	10	0.059	2.7	1.2	--

Table 5.8 Ground motion and stress factor data for the stress analysis of Figs. 5.17 and 5.18.

Case No.		Ground Motion	PGA(*) (g)	Stress Factor
Horizontal	1	San Francisco, CA, 1957, S80E Golden Gate Park	0.315	0.179
	2	Helena, Montana, 1935, N00E Carroll College	0.438	0.287
	3	Lytle Creek, CA, 1970, S25W Wrightwood	0.594	0.531
	4	Parkfield, CA, 1966, N65W Temblor No.2	0.807	0.832
Vertical	1	Parkfield, CA, 1966 Cholame, Shandon No. 5	0.357	0.449
	2	San Fernando, CA, 1971 Lake Hughes, Station 4	0.462	0.491
	3	San Fernando, CA, 1971 Griffith Park Observatory, L.A.	0.369	0.511
	4	Imperial Valley, CA, 1940 El Centro	0.630	0.798

(*) The records are scaled by a factor of 3.

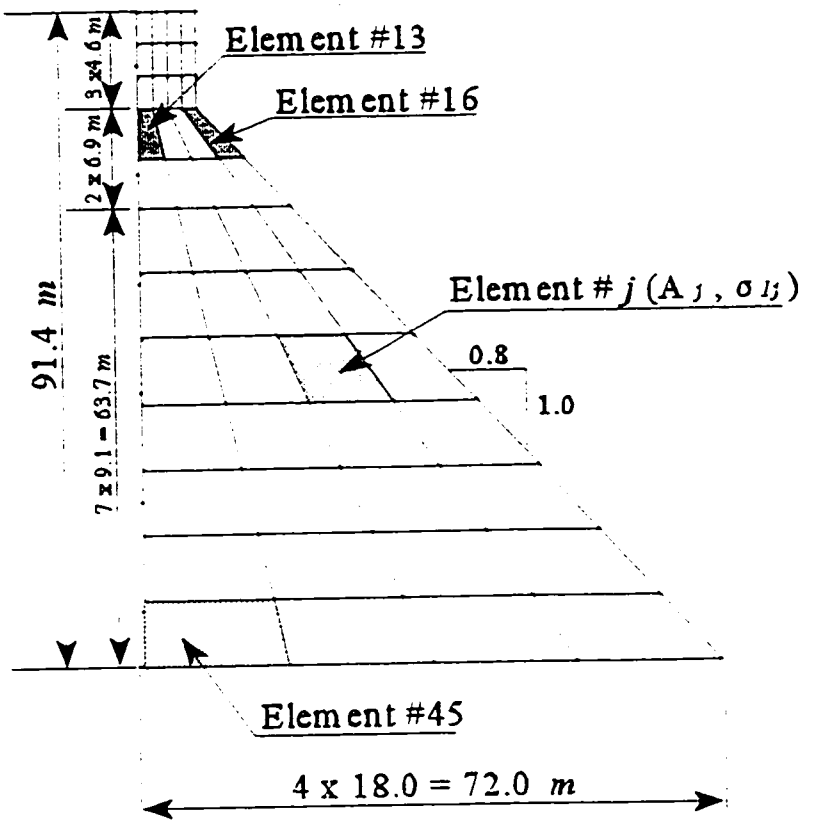

Fig. 5.1 - Finite element discretizations of the dam monolith indicating elements of maximum principal stress

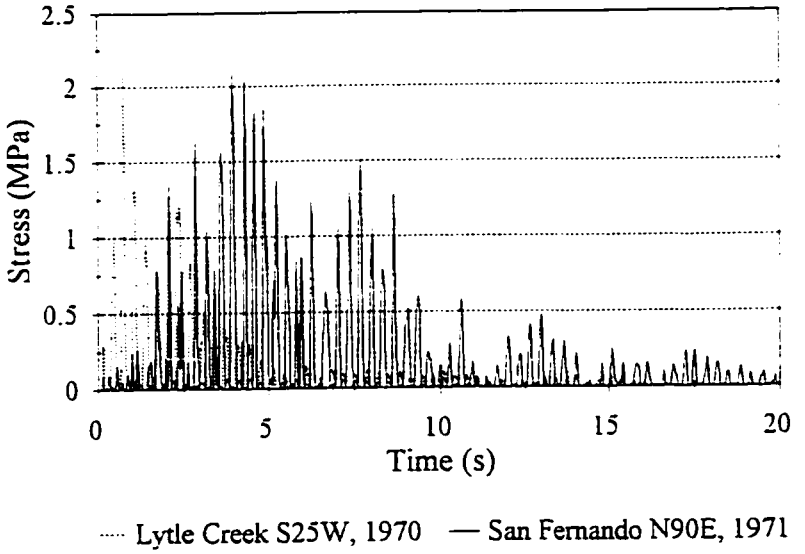

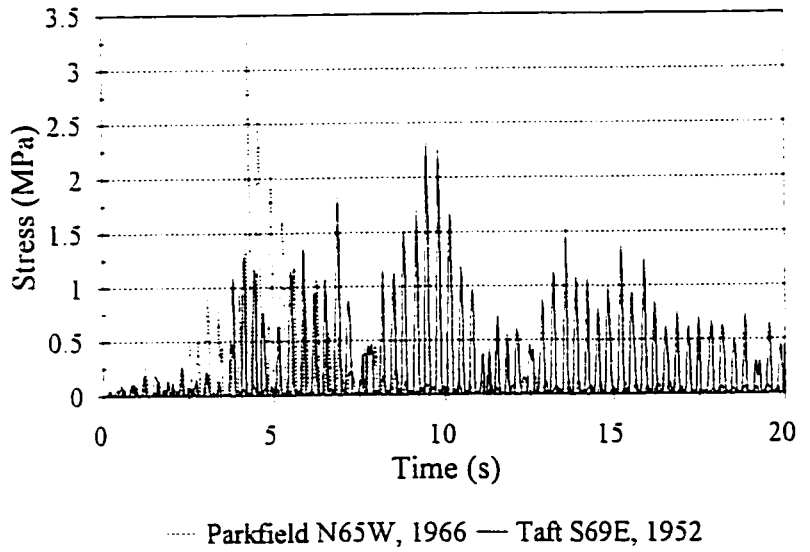

Fig. 5.2 Tensile stress time history response at the neck of the concrete dam subjected to different ground motions: (a) Identical maximum peaks (b) Different maximum peaks

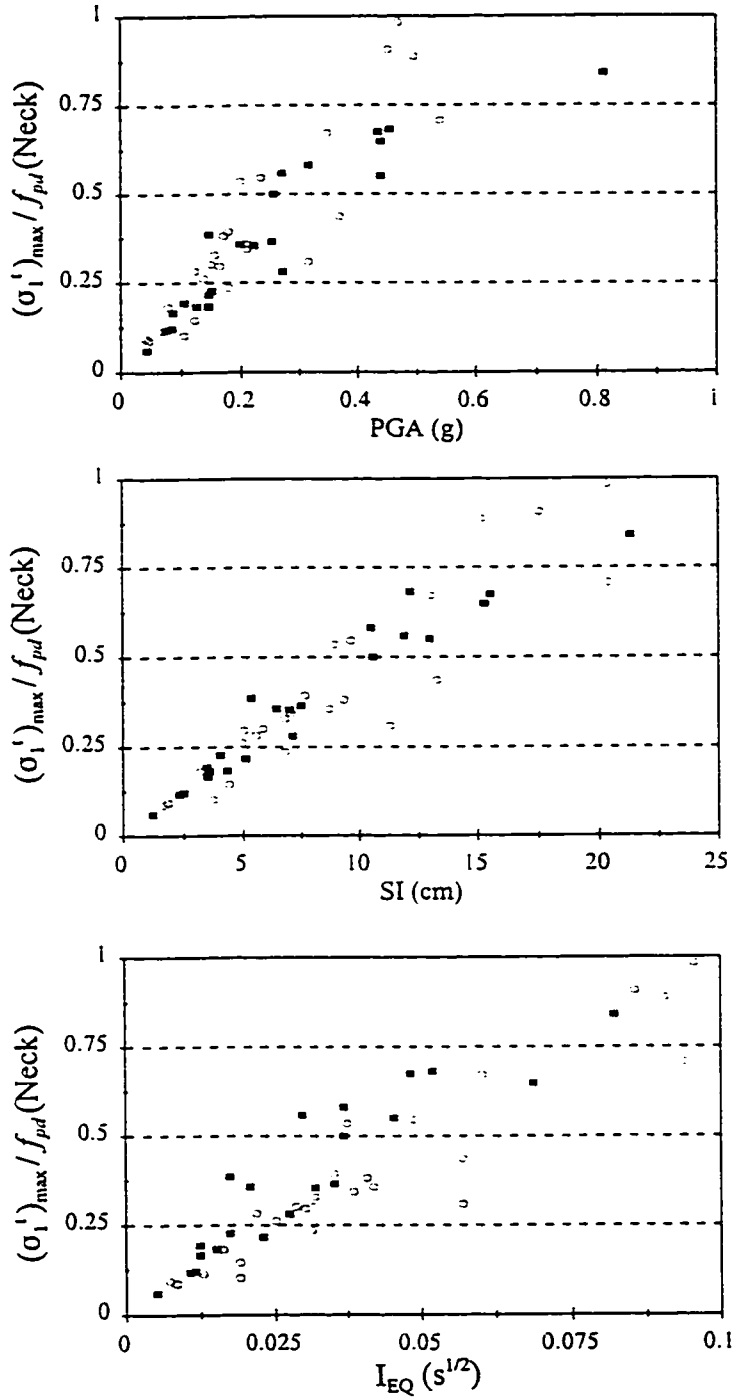

Fig. 5.3 - Correlation of the normalized maximum tensile stress at the neck of the dam with the intensities of the horizontal ground motion records (dynamic response only)

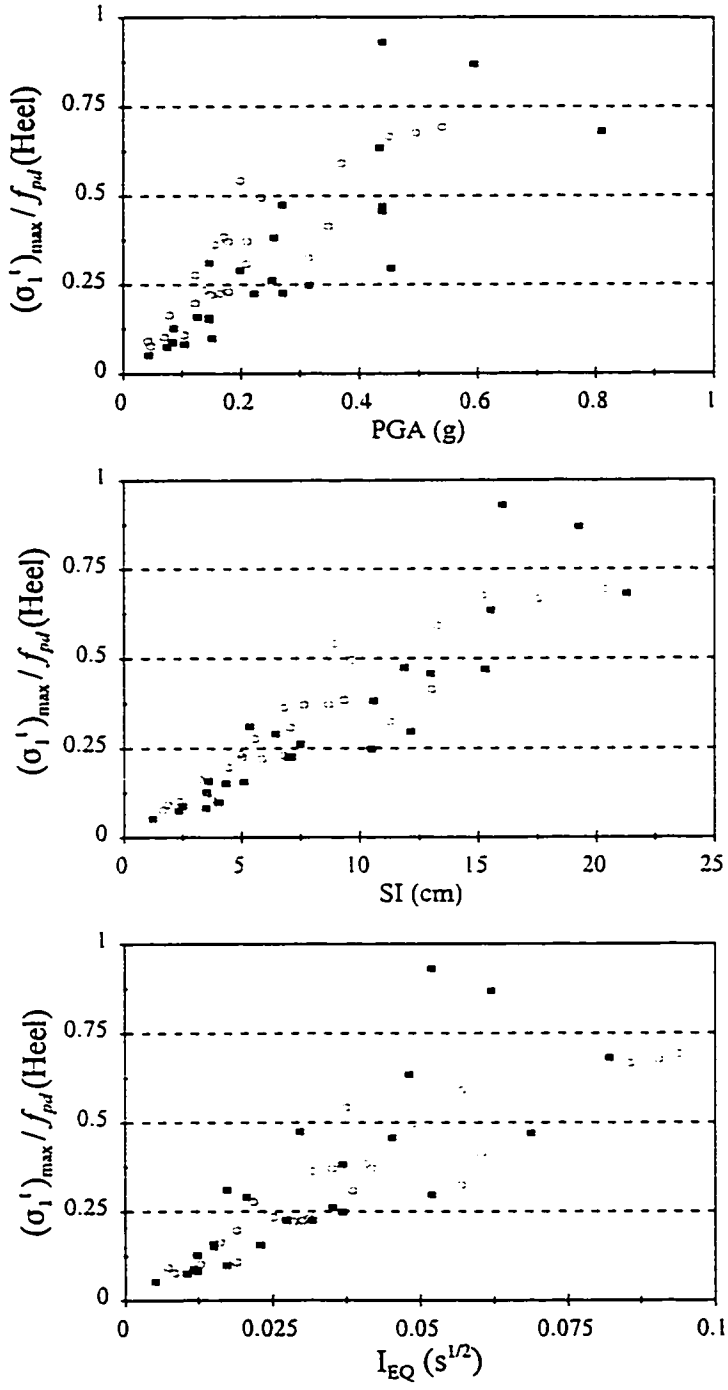

Fig. 5.4 - Correlation of the normalized maximum tensile stress at the heel of the dam with the intensities of the horizontal ground motion records (dynamic response only)

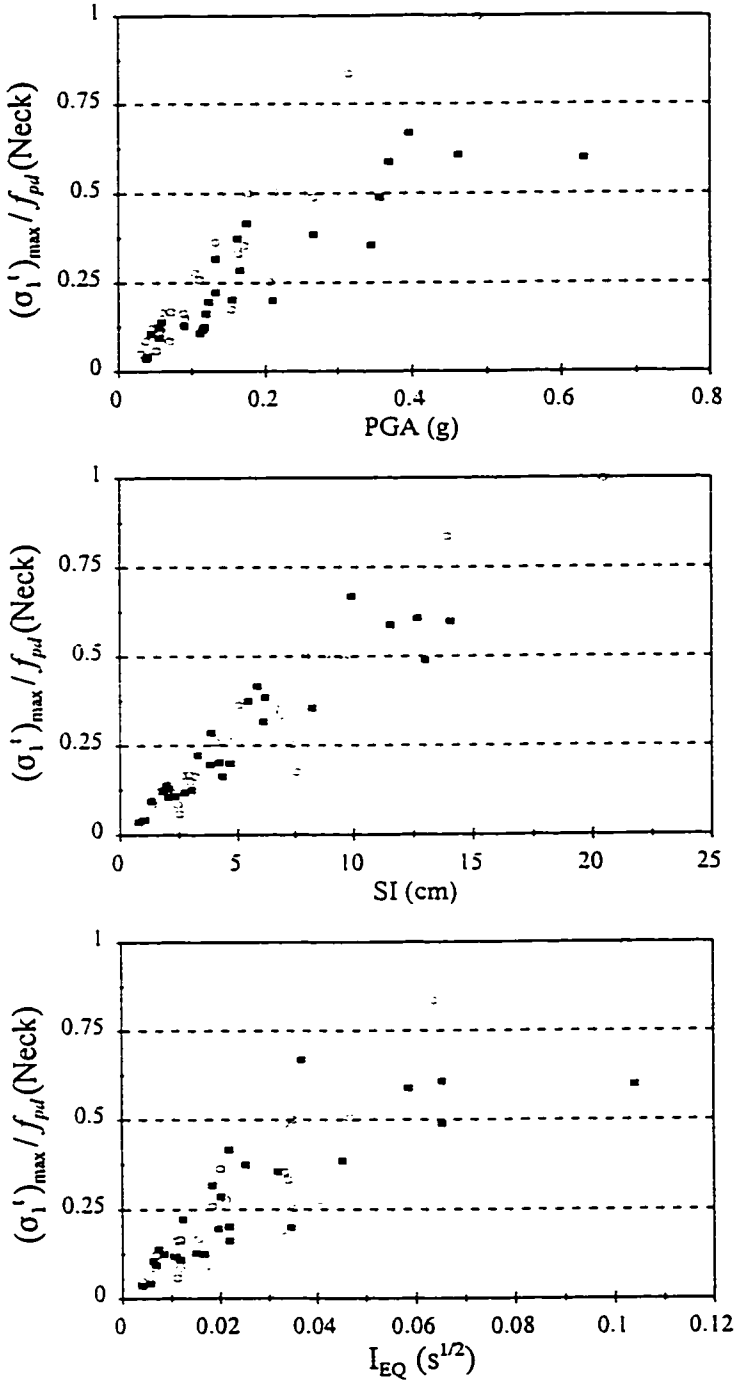

Fig. 5.5 - Correlation of the normalized maximum tensile stress at the neck of the dam with the intensities of the vertical ground motion records (dynamic response only)

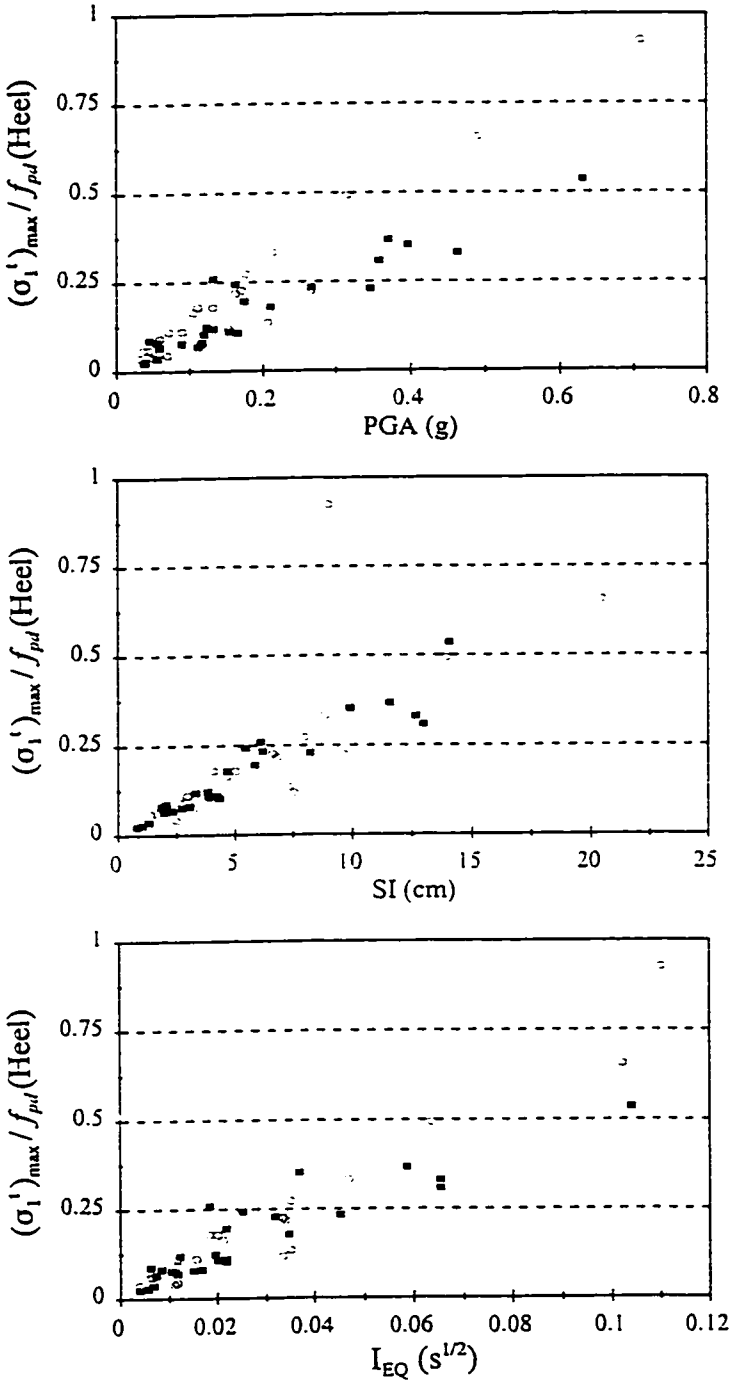

Fig. 5.6 - Correlation of the normalized maximum tensile stress at the heel of the dam with the intensities of the vertical ground motion records (dynamic response only)

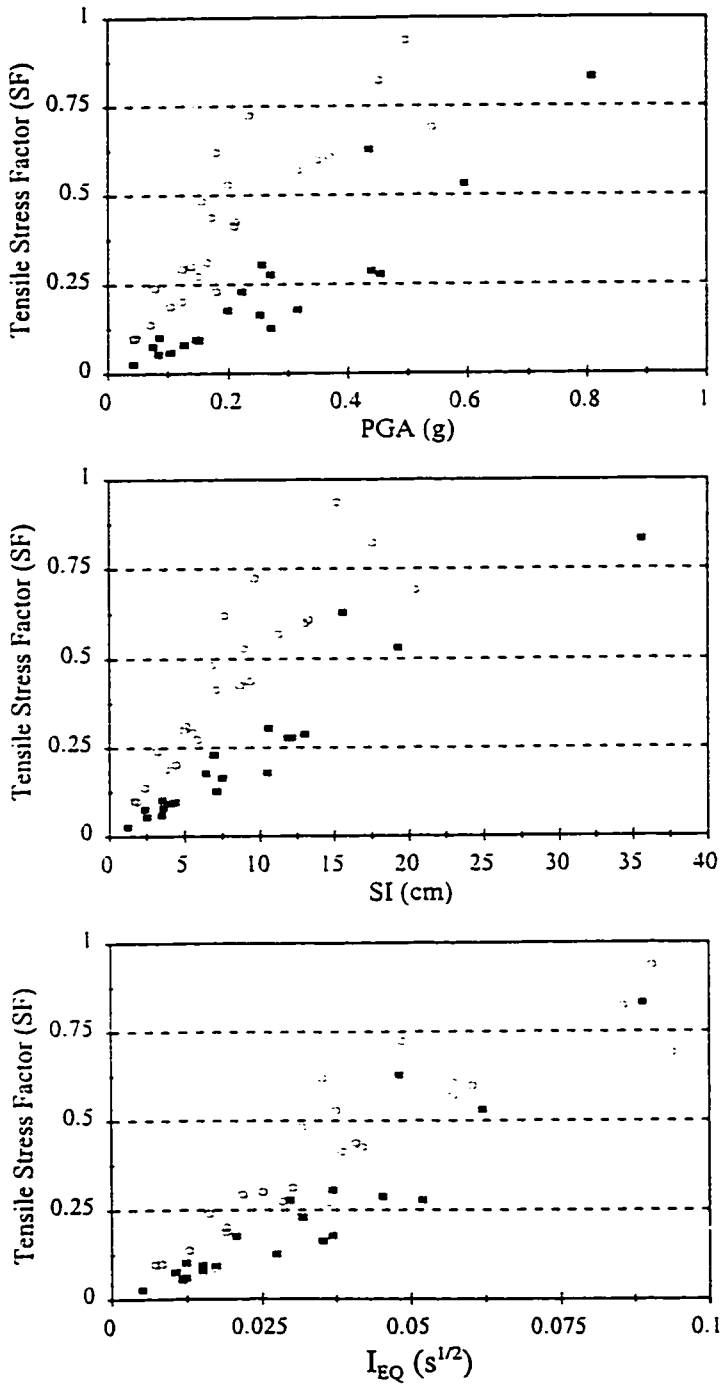

Fig. 5.7 - Correlation of the tensile stress factor (SF) of the dam with the intensities of the horizontal ground motion records (dynamic response only)

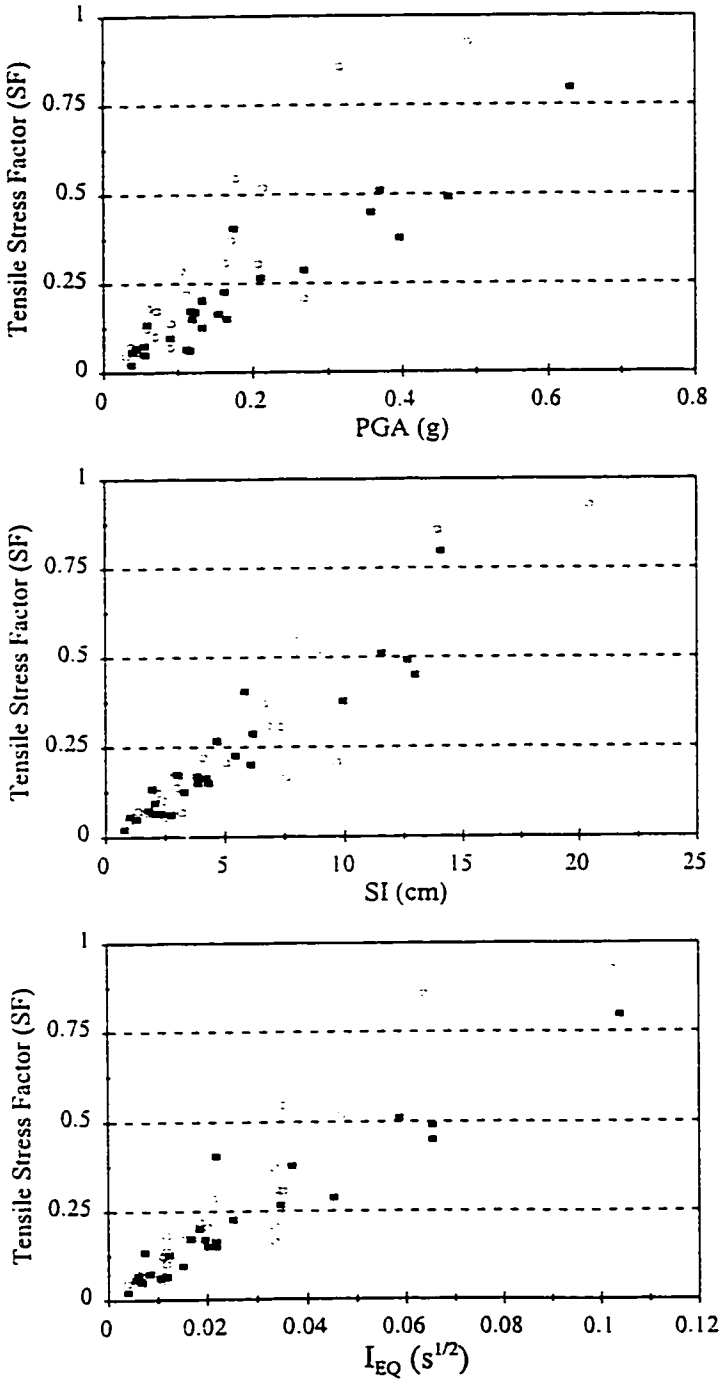

Fig. 5.8 - Correlation of the tensile stress factor (SF) of the dam with the intensities of the vertical ground motion records (dynamic response only)

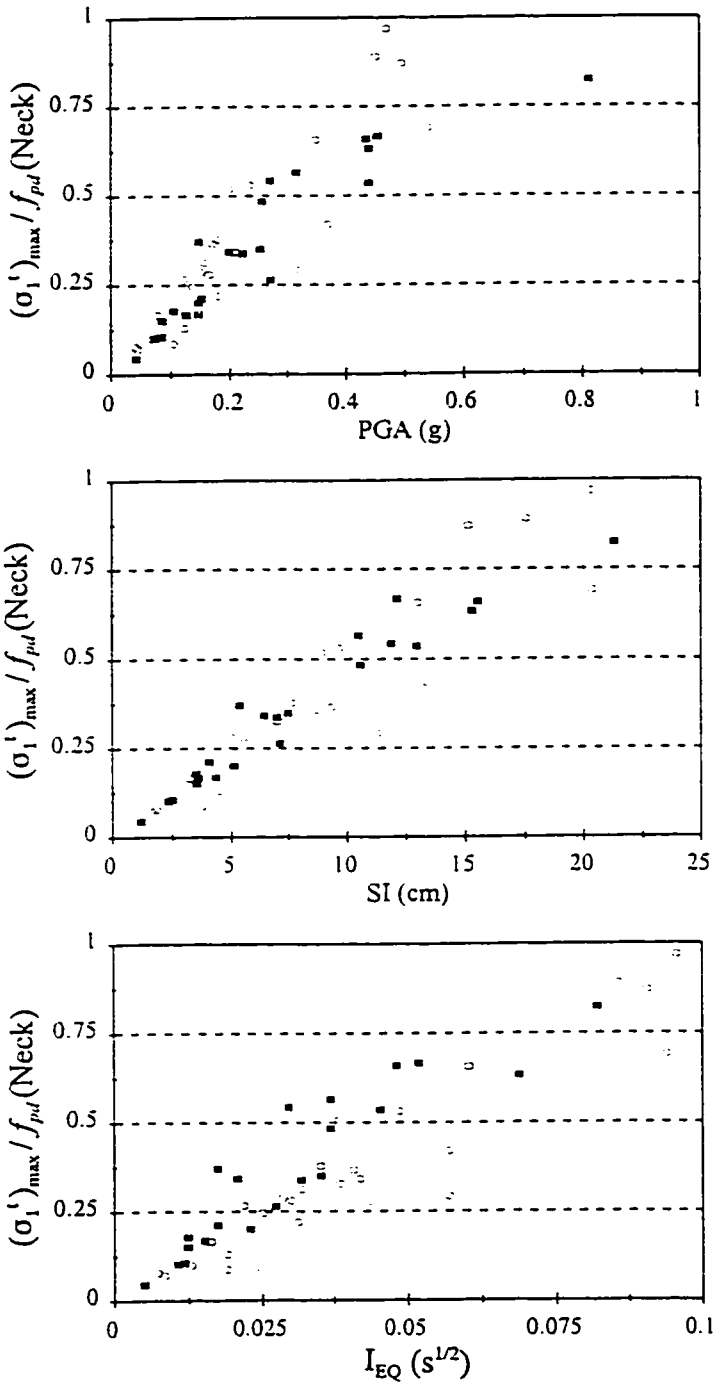

Fig. 5.9 - Correlation of the normalized tensile stress at the neck of the dam with the intensities of the horizontal ground motion records (monolith weight and hydrostatic loadings included)

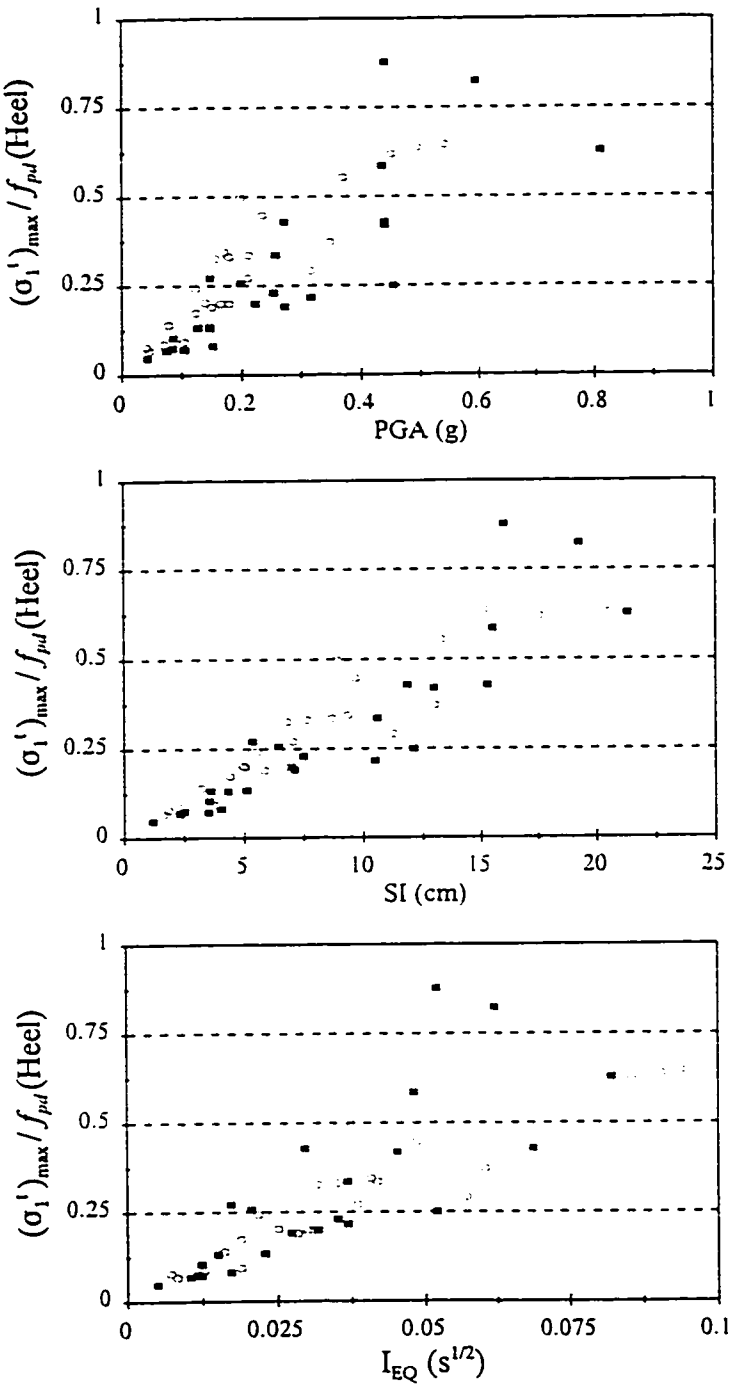

Fig. 5.10 - Correlation of the normalized tensile stress at the heel of the dam with the intensities of the horizontal ground motion records (monolith weight and hydrostatic loadings included)

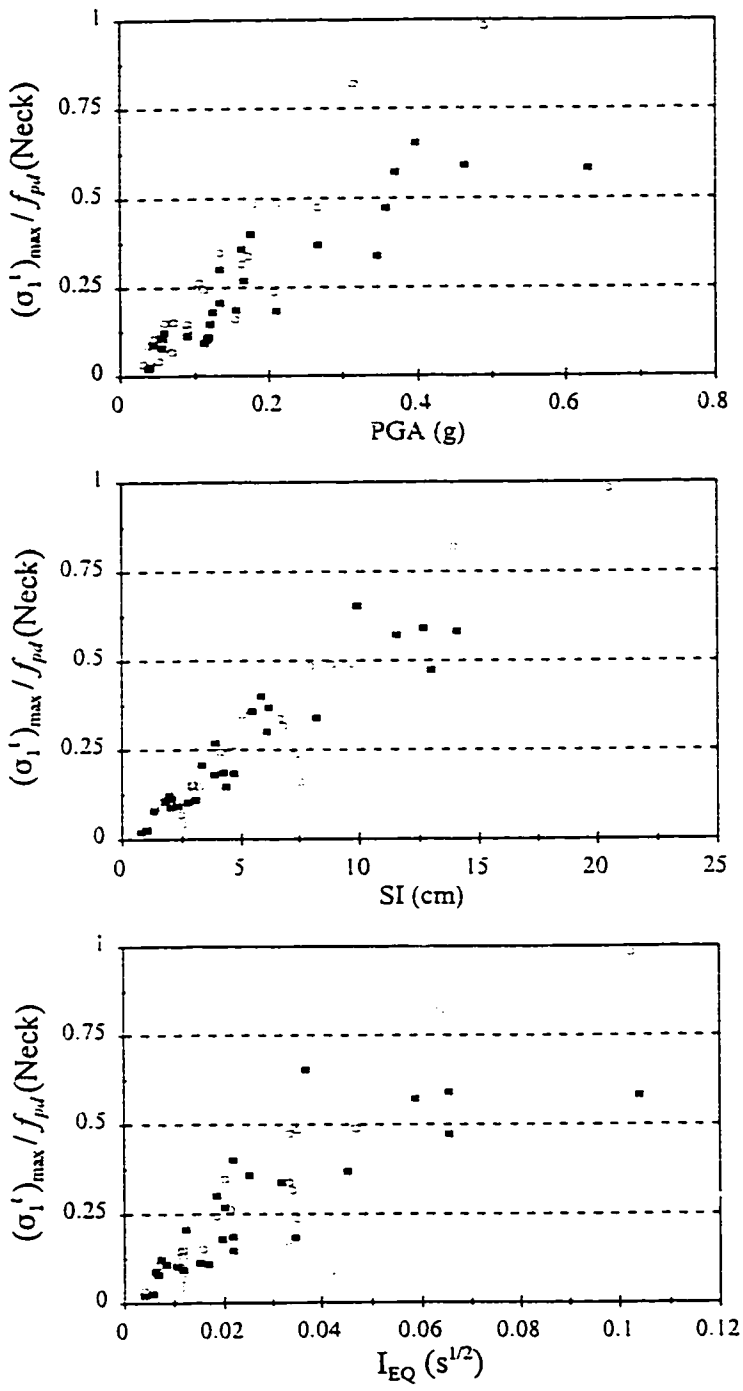

Fig. 5.11 - Correlation of the normalized tensile stress at the neck of the dam with the intensities of the vertical ground motion records (monolith weight and hydrostatic loadings included)

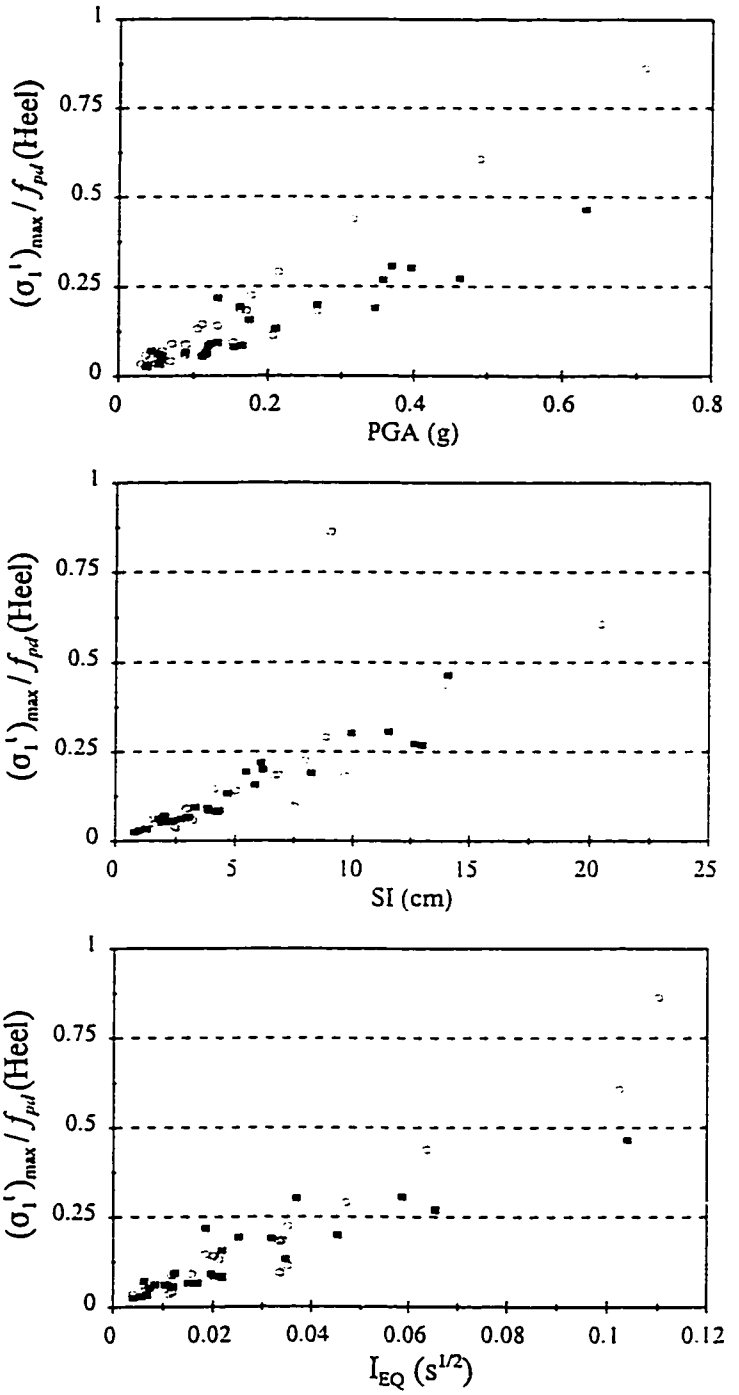

Fig. 5.12 - Correlation of the normalized tensile stress at the heel of the dam with the intensities of the vertical ground motion records (monolith weight and hydrostatic loadings included)

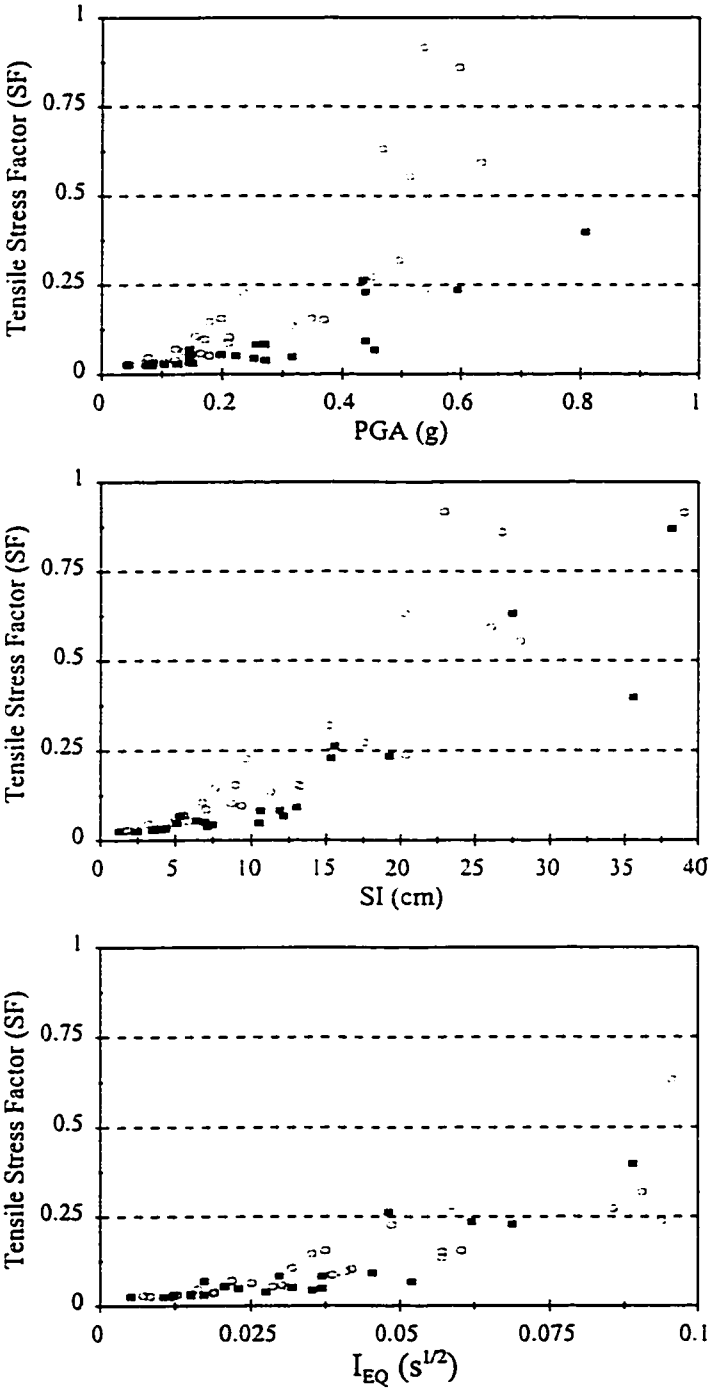

Fig. 5.13 - Correlation of the tensile stress factor of the dam with the intensities of the horizontal ground motion records (monolith weight and hydrostatic loadings included)

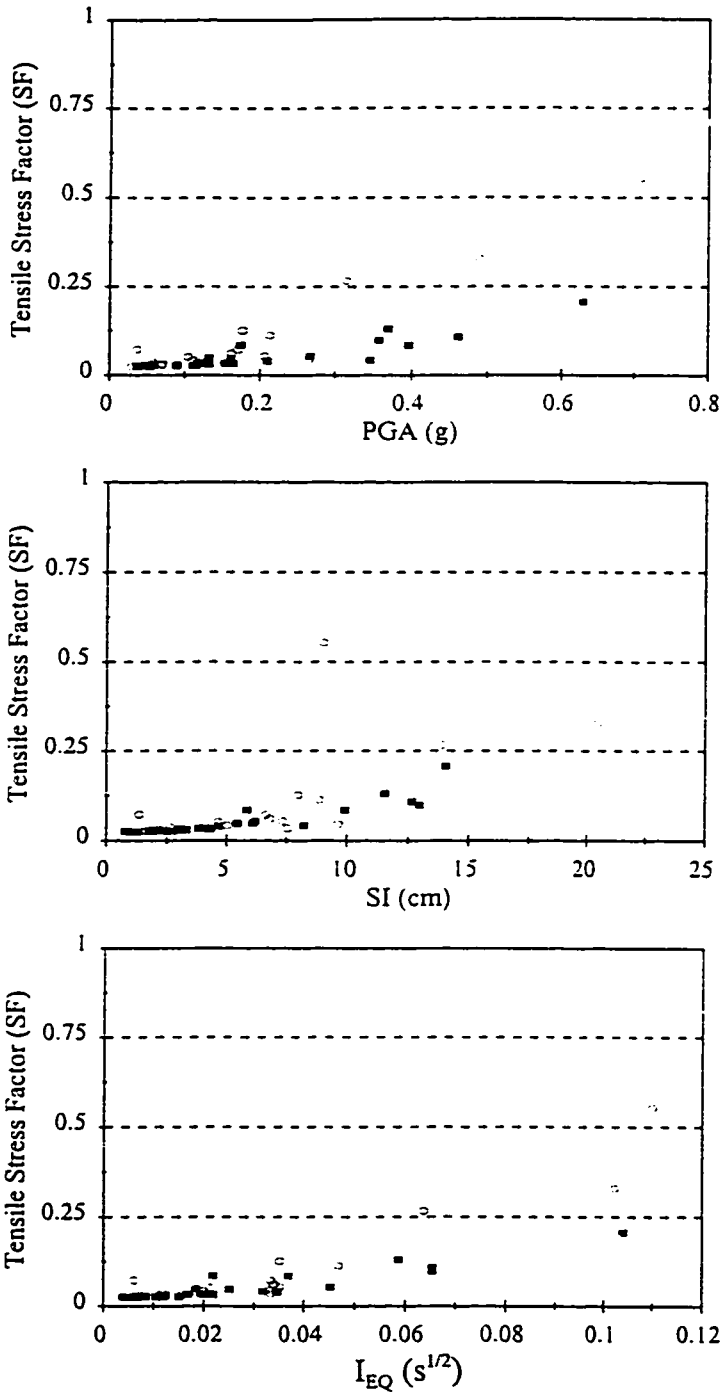

Fig. 5.14 - Correlation of the tensile stress factor of the dam with the intensities of the vertical ground motion records (monolith weight and hydrostatic loadings included)

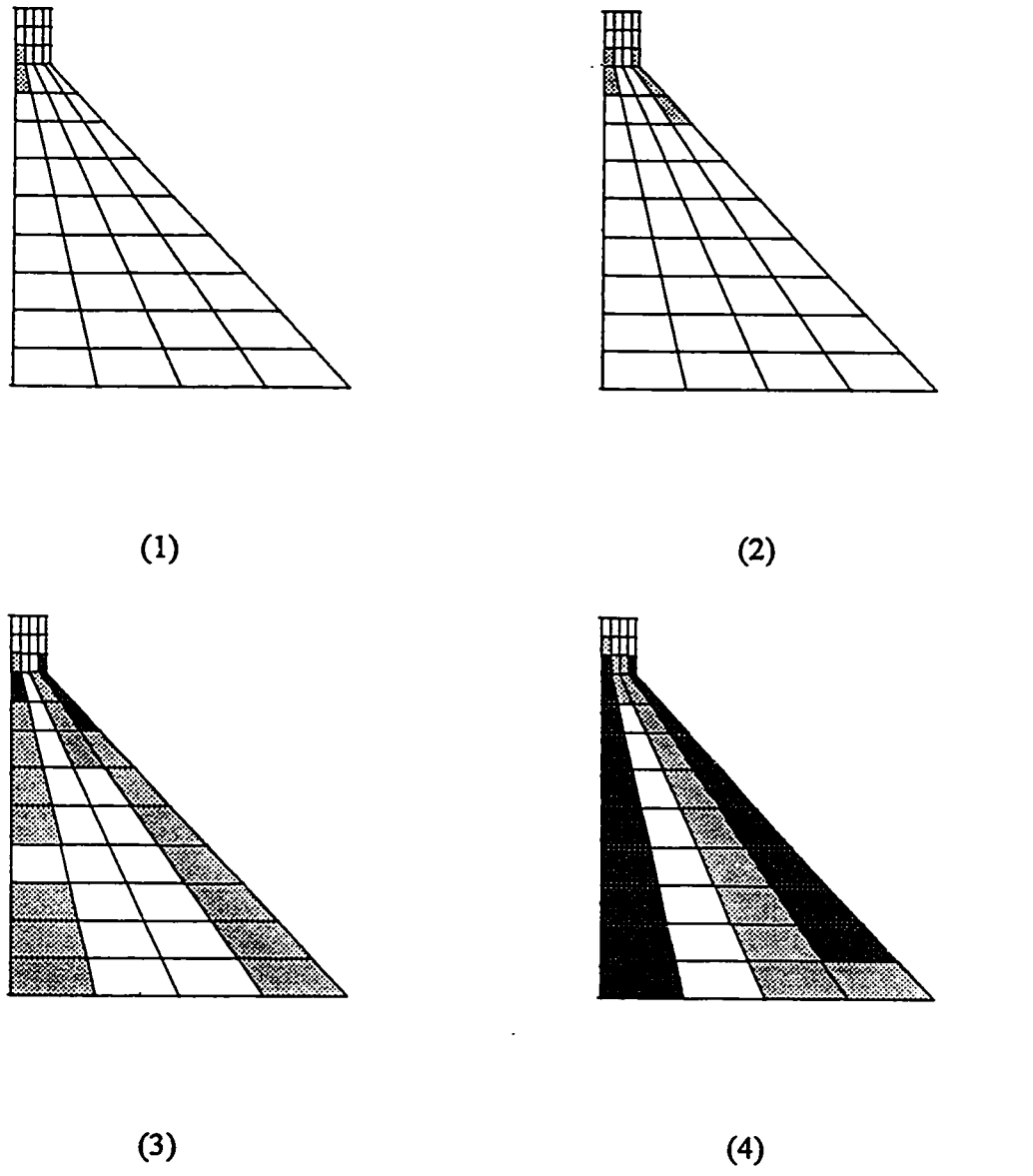

Fig. 5.15 Extension of excessive tensile stress over the cross section of the dam monolith with the increase of the stress factor (horizontal ground motions, dynamic response only). Cases numbered in the figure are described in Table 5.8.

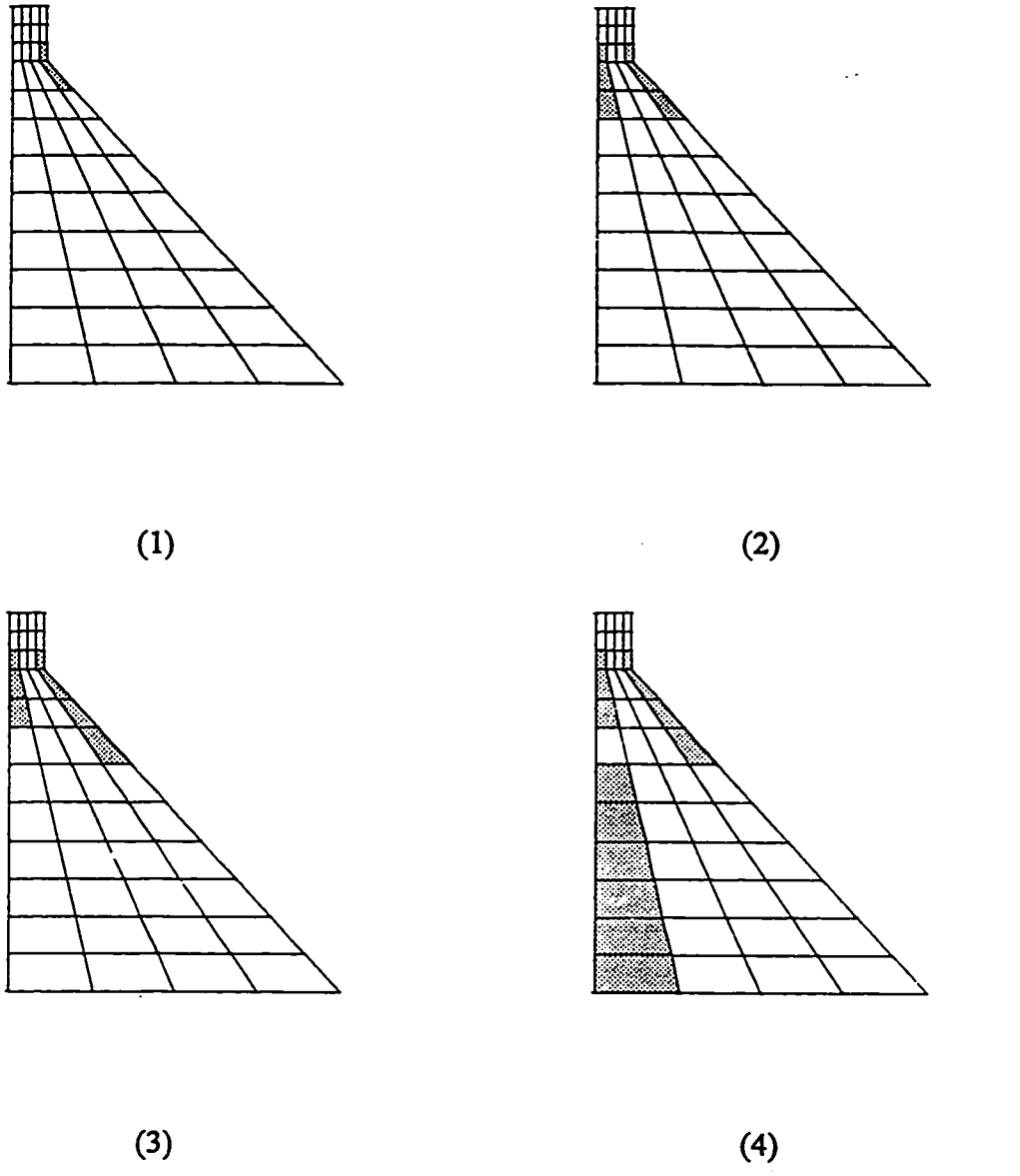

Fig. 5.16 Extension of excessive tensile stress over the cross section of the dam monolith with the increase of the stress factor (vertical ground motions, dynamic response only). Cases numbered in the figure are described in Table 5.8.

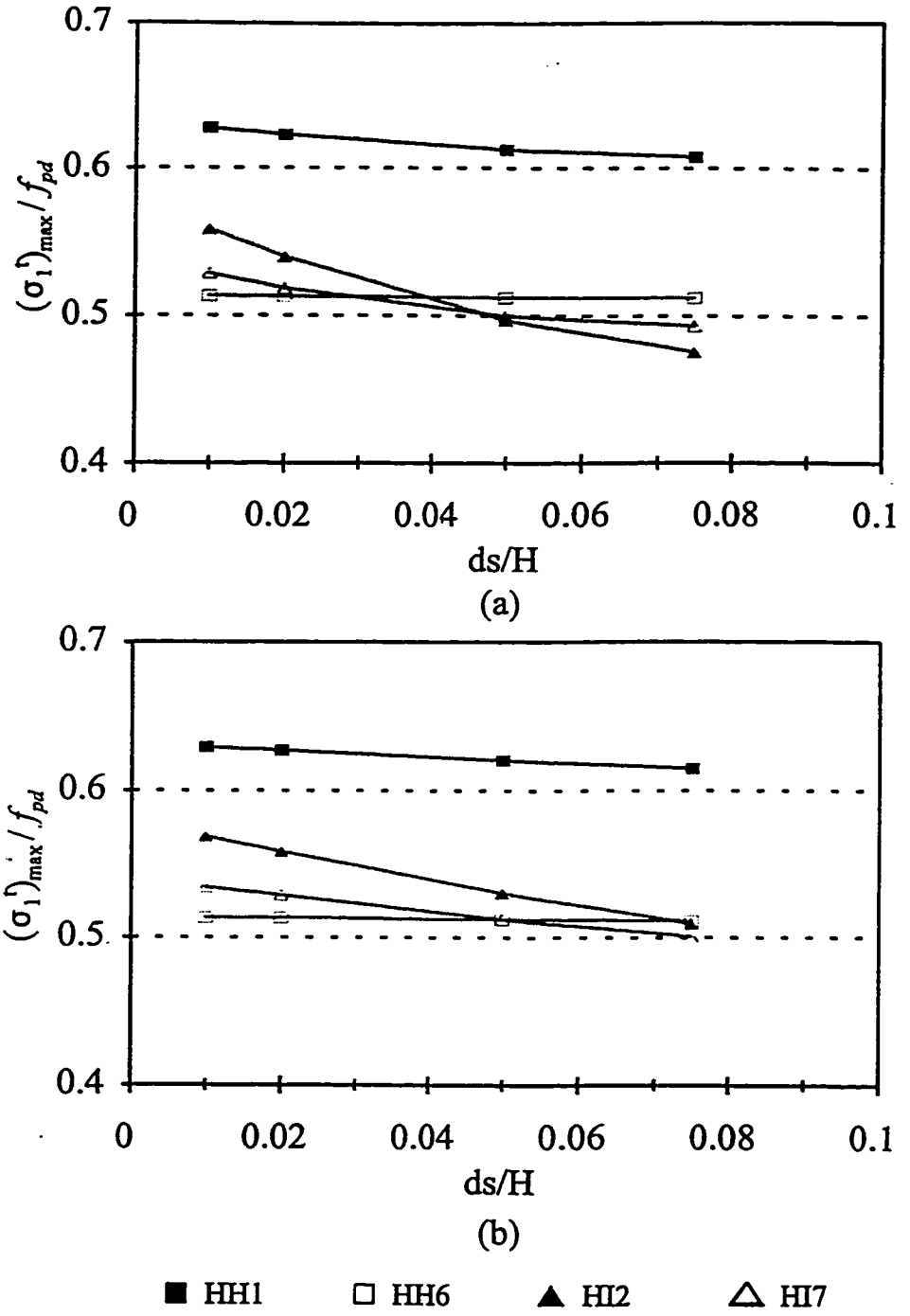

Fig. 5.17 Maximum tensile stress in the dam monolith subjected to horizontal ground accelerations HH1, HH6, HI2 and HI7 scaled to PGA = 0.25g: Reservoir foundation properties: $b = 0.50$ and $E_f = 71820$ MPa: (a) $E_s/E_f = 0.005$ (b) $E_s/E_f = 0.02$

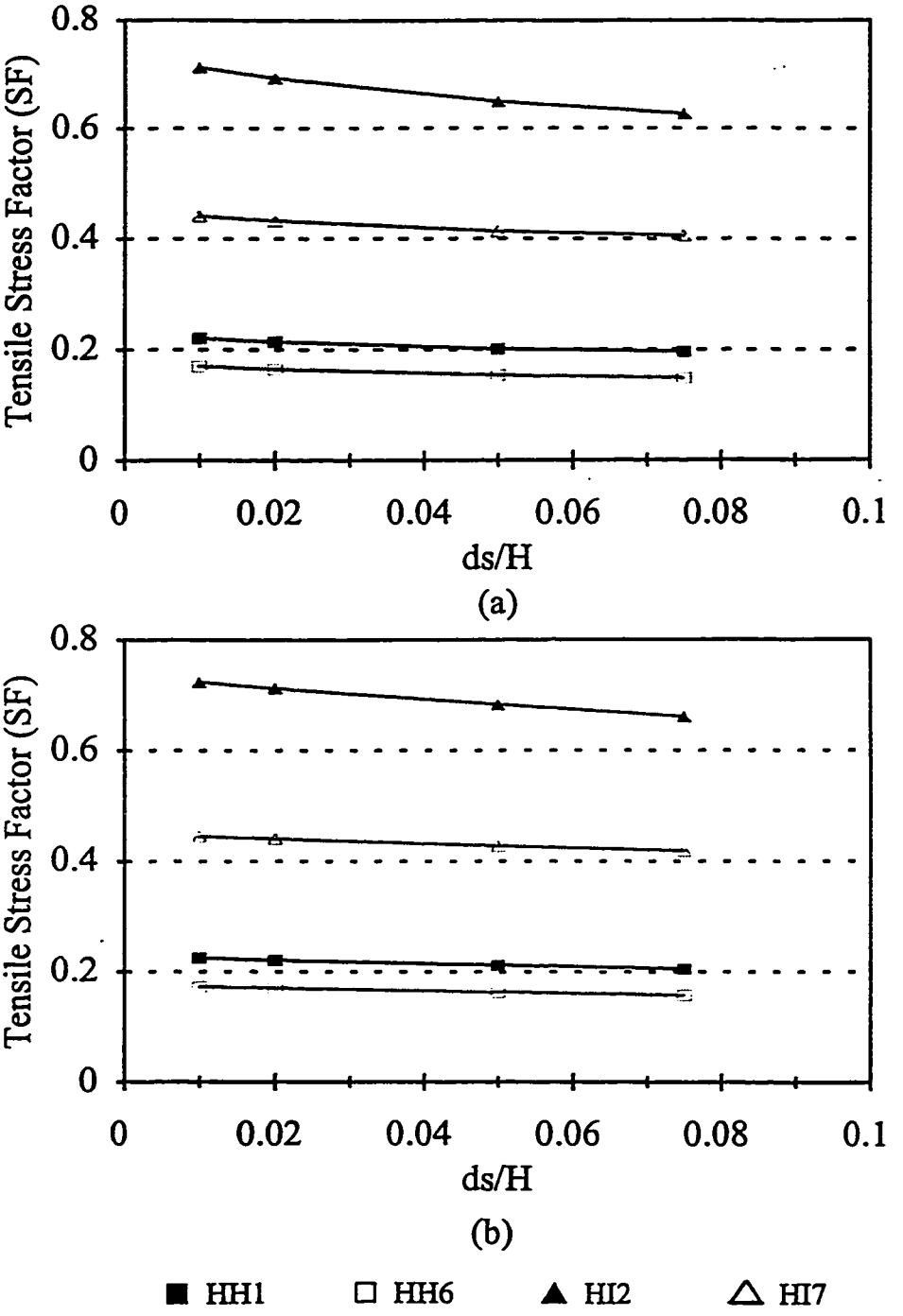

Fig. 5.18 Tensile stress factor of the dam monolith subjected to horizontal ground accelerations HH1, HH6, HI2 and HI7 scaled to PGA = 0.25g: Reservoir foundation properties: $b = 0.50$ and $E_f = 71820$ MPa: (a) $E_s/E_f = 0.005$ (b) $E_s/E_f = 0.02$

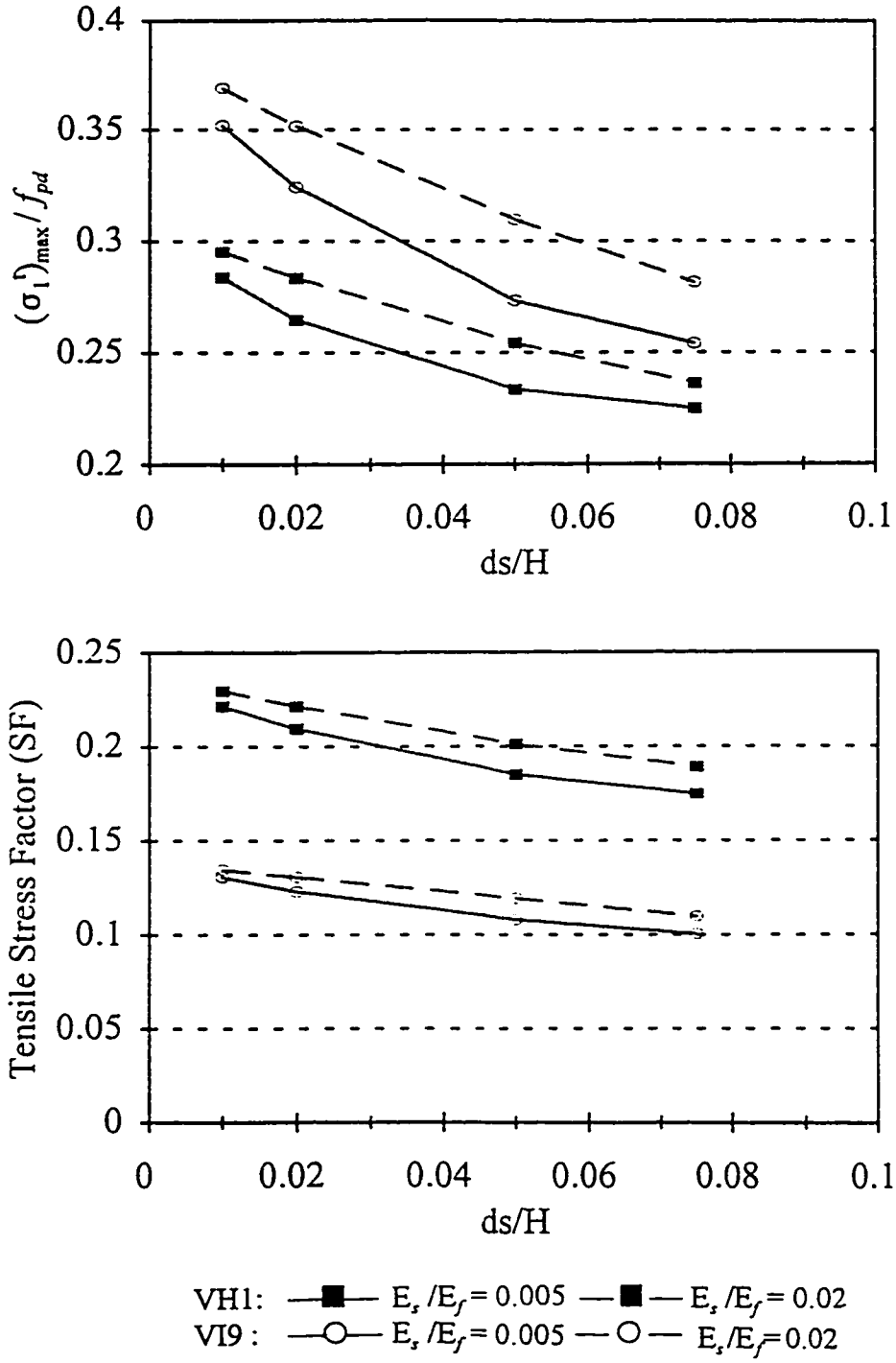

Fig. 5.19 Maximum tensile stress and tensile stress factor of the dam monolith subjected to vertical ground accelerations VH1 and VI9 scaled to PGA = 0.25g: Reservoir foundation properties: $b = 0.50$, $E_f = 71820$ MPa and $E_s/E_f = 0.005$ and 0.02

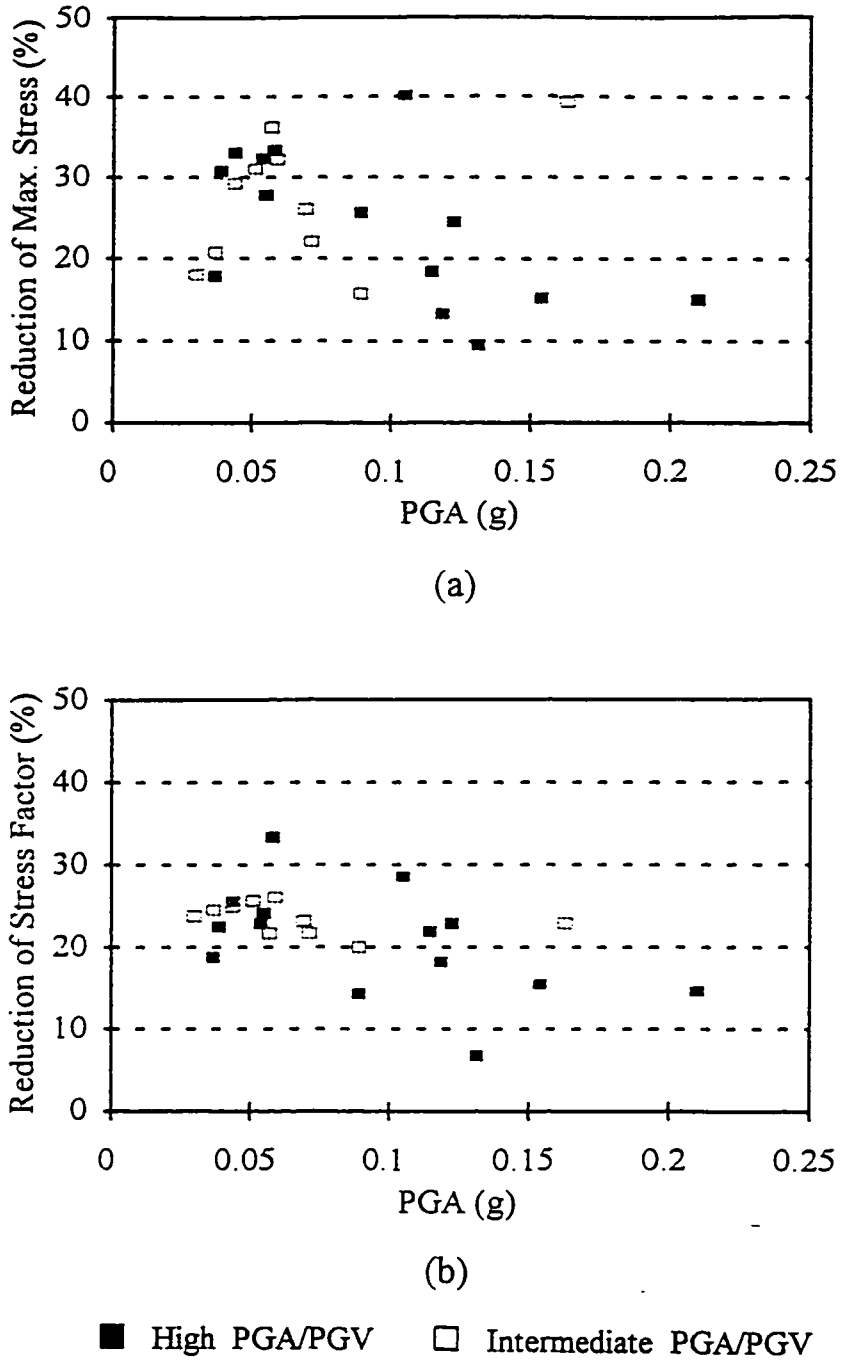

Fig. 5.20 - Absorption effect of the reservoir bottom sedimentation on the tensile stress in the dam monolith subjected to vertical ground motion (Tables 5.4 and 5.5): (a) Maximum principal stress (b) Stress Factor Reservoir foundation properties: b = 0.50, E_f = 71820 MPa and E_s/E_f = 0.005. The calculated reduction is based on the comparison of the stress in the dam for the two cases of d_s/H=0.00 and d_s/H=0.05.

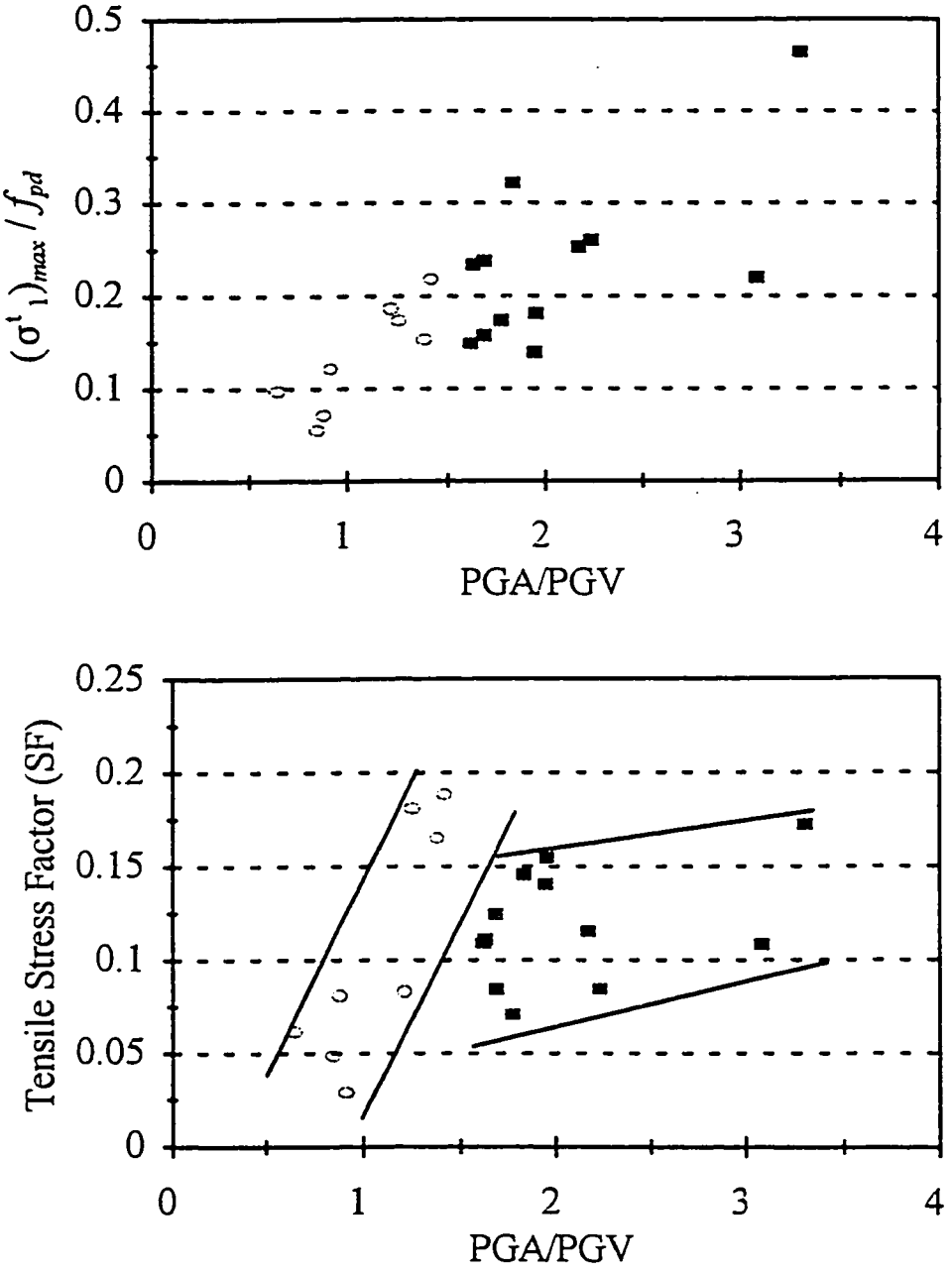

Fig. 5.21 - Maximum tensile stress and tensile stress factor of the dam monolith subjected to vertical ground accelerations scaled to PGV = 0.1 m/s : Reservoir foundation properties: b = 0.50, E_f = 71820 MPa, E_s / E_f = 0.005, d_s /H= 0.05

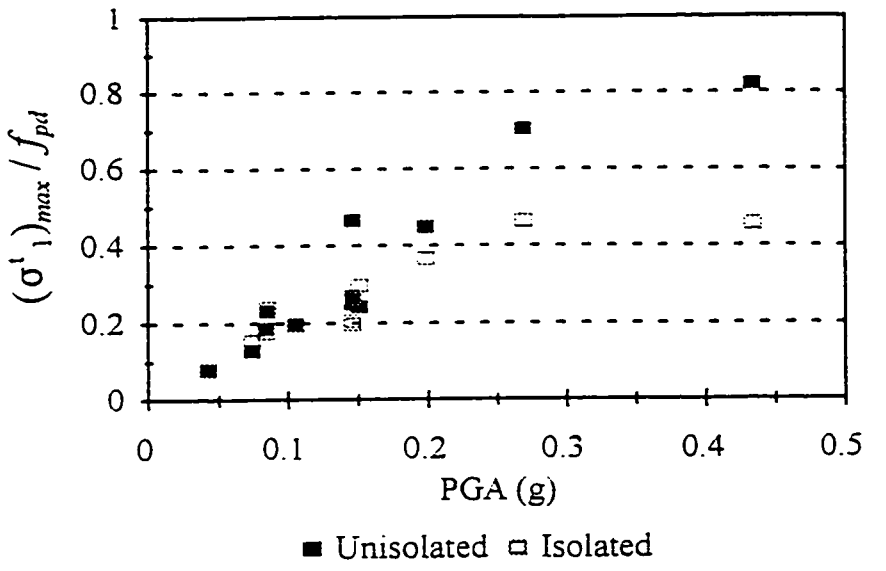

(a)

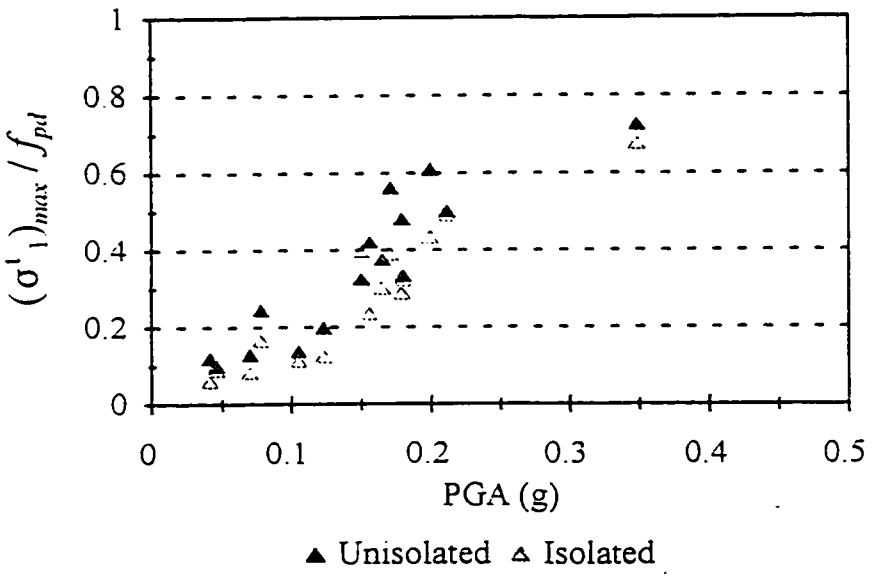

(b)

Fig. 5.22 - Normalized maximum principal tensile stress in the dam monolith subjected to horizontal ground accelerations with: (a) high PGA/PGV ratio (b) intermediate PGA/PGV ratio. Isolation layer properties: ρ_l = 1300 kg/m^3, E_l = 0.1 MPa, η_l = 14 kPa.s and t_l/H = 0.025

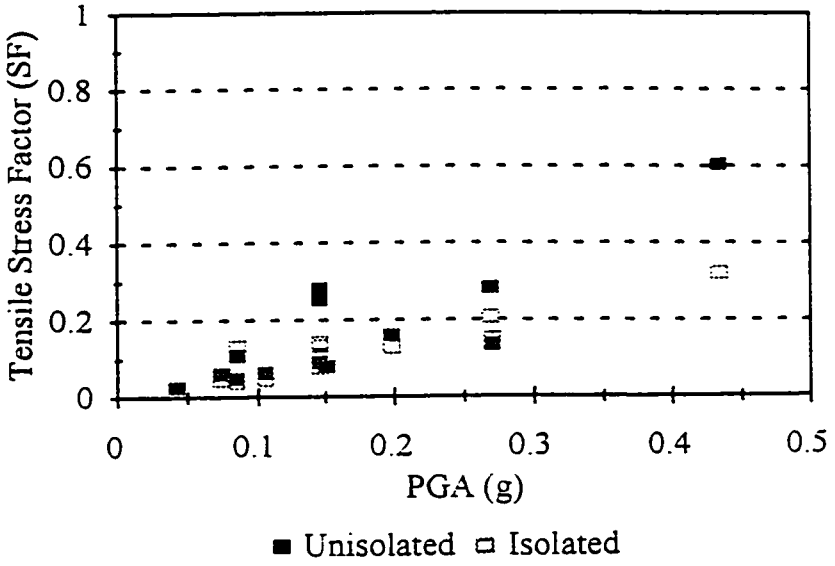

(a)

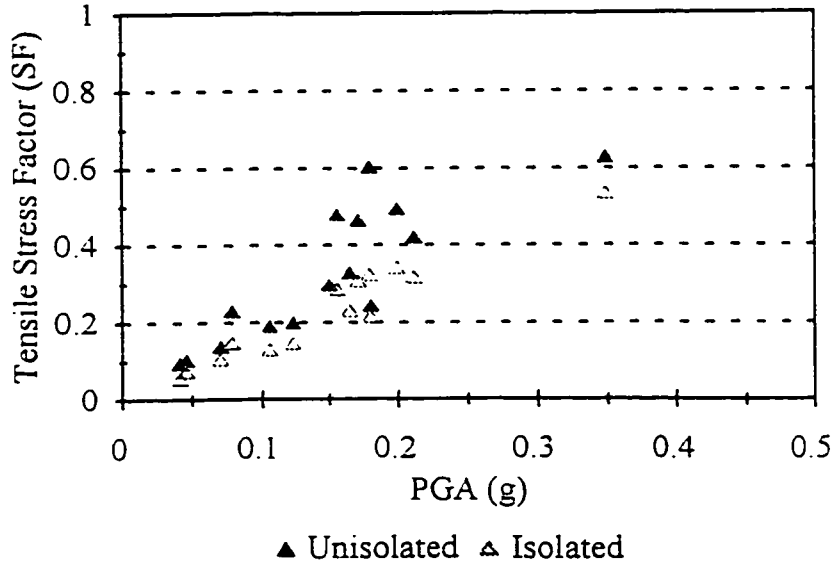

(b)

Fig. 5.23 - Tensile stress factor of the dam monolith subjected to horizontal ground accelerations with: (a) high PGA/PGV ratio (b) intermediate PGA/PGV ratio. Isolation layer properties: $\rho_l = 1300$ kg/m^3, $E_l = 0.1$ MPa, $\eta_l = 14$ kPa.s and $t_l/H = 0.025$

CHAPTER 6

CONCLUSIONS

6.1 CONTRIBUTIONS

In this thesis, the effects of the reservoir boundary conditions on the seismic response of gravity dams are investigated. The boundaries of the two-dimensional model of the reservoir include the reservoir bottom, the dam-reservoir interface boundary and the far end upstream boundary.

An analytical model is proposed for the sedimented bottom of the reservoir to account for the damping of the reflected waves into the sediment layer as well as the reflection of pressure waves from the underlying foundation rock. The effects of the mechanical properties of the sediment layer and the foundation rock on the overall reflective characteristic of the reservoir bottom boundary and the dynamic response of the dam are studied.

The response of the dam to the seismic excitation with an isolation layer at the dam-reservoir boundary is investigated. The appropriate mechanical properties of the isolation layer for an effective response reduction is determined. The amount of seismic response reduction compared with the case of an unisolated dam for a range of mechanical characteristics of the isolation layer is studied. A theoretical solution for the hydrodynamic pressure in a finite, rectangular-shaped reservoir with generally different reflection

coefficients at its boundaries subjected to horizontal ground acceleration is derived. The effect of the reservoir aspect ratio, L/H, on the performance of the isolation layer is investigated using the developed theoretical solution for the finite-length reservoir model.

A detailed analytical procedure is developed to evaluate the seismic response of a gravity dam impounding a reservoir of given length and absorptive characteristics at its boundaries. The response of the hydrodynamic pressure in the finite-length reservoir under horizontal and vertical ground accelerations is studied. The effects of a number of theoretical parameters including the number of Ritz vectors in the dam structural model, the reservoir aspect ratio, the far end boundary condition and the reflection coefficients at the reservoir boundaries on the calculated earthquake response of the dam-reservoir model are investigated.

Finally, a stress analysis is conducted to evaluate the variation of stresses in the dam monolith subjected to different ground motion records and impounding a reservoir with various boundary characteristics. A single-valued parameter, called the *stress factor*, is introduced to accommodate the stress time history and stress variation across the monolith cross section in the structural response of the dam when subjected to different earthquake ground motions. The introduced parameter is verified by examining its variations with the intensity of the input earthquakes. The studies of the effects of reservoir different boundary conditions on the seismic response of the gravity dam model are extended to include the variations of the tensile stresses and the stress factor of the dam monolith subjected to a range of ground acceleration records.

6.2 CONCLUSIONS

From the analysis conducted in the present research, the following conclusions are reached at different parts of the study:

1. The proposed model for the reservoir bottom boundary shows reasonable variations with the mechanical characteristics of the sediment layer and the underlying foundation rock and may be used to evaluate the equivalent reflection coefficient of the layered reservoir bottom in the earthquake analysis of dams.

2. The proposed model for the sedimented reservoir bottom reveals a strong dependence of the equivalent reflection coefficient of this boundary on the stiffness of the underlying foundation rock. The dependence of the reflection coefficient of the reservoir bottom on the mechanical properties of the sediment layer is more significant for the case of a very soft and dissipative sediment. The sedimentation in a newly built, deep reservoir is expected to be thin and dense under high hydrostatic pressure. The hydrodynamic pressure in such a reservoir overlying a stiff foundation is significant in the case of a seismic event due to the large reflection coefficient of the reservoir bottom boundary.

3. The results of a theoretical study shows that the seismic response of the dam can be reduced by isolating the dam from the imposed hydrodynamic pressure of the reservoir. The isolation layer reduces the hydrodynamic loading on the dam in two different ways: First, it serves as a boundary for the fluid domain with low reflection coefficient which results in lower developed hydrodynamic pressure in the reservoir

as compared to the case of an unisolated dam. Secondly, it reduces the amplitude of the transmitted pressure to the dam based on its designed mechanical characteristics. The isolation material needs to be very soft and with sufficient thickness so as to reduce the hydrodynamic pressure on the dam significantly. The appropriate mechanical properties of the isolation layer for an effective response reduction of the dam are determined in the present study. A survey is made to determine the appropriate range of materials that can be used as practical solutions for the hydrodynamic isolation of dams. The properties of rubber materials appear to be appropriate as the isolation material and can be adjusted to the required mechanical characteristics for an effective isolation scheme.

4. The effectiveness of the isolation of the dam at the dam-reservoir boundary is more significant when the dam impounds a confined reservoir at the upstream end as compared to the case of an infinitely long reservoir. The reason is that the importance of the hydrodynamic isolation at the dam-reservoir boundary increases in the absence of the radiation of pressure waves to the far-end. The reservoir length effects were negligible in the dam-reservoir model with the stationary upstream boundary when the reservoir length was selected more than twice the reservoir depth in the present study.

5. The problem of hydrodynamic pressure in the reservoir under vertical excitation with generally different boundary conditions at the dam-reservoir interface and the upstream far-end boundary can not be tackled with the available theoretical solution

for the infinitely long reservoir. The existing theoretical solution for the hydrodynamic pressure in the reservoir under vertical ground motion is in fact a one-dimensional solution which does not accommodate any variation of the boundary conditions in the horizontal direction. A finite-element program is developed to calculate the earthquake response of a gravity dam impounding a reservoir of arbitrary shape and boundary conditions. The procedure includes the boundary conditions due to hydrodynamic isolation of the dam, a solid far-end upstream boundary and a layered reservoir bottom with a constant sedimentation thickness. The results of the frequency response of the hydrodynamic force on the dam indicate that the two-dimensional response of the reservoir under uniform vertical ground motion is pronounced when the boundary conditions at the side boundaries of the two-dimensional, rectangular-shaped reservoir model are significantly different.

6. The finite element mesh refinement of the dam-reservoir model and the number of Ritz vectors in the structural response approximation of the dam should be properly chosen so as to capture the effects of higher frequency modes of the dam and the reservoir in the seismic response of the dam-reservoir model. The refinement of the finite element mesh and the number of Ritz vectors depend on the required degree of accuracy in the results as well as the selected parameter to represent the response of the dam. The increase of the mesh refinement and the number of Ritz vectors beyond a certain limit slightly alters the peak amplitude of the frequency response function of the crest acceleration while having no observable effect on the maximum stress in the dam.

7. The effects of reservoir boundary conditions on the stresses in the dam subjected to different ground motion records are studied by using an introduced index (called the stress factor) in the stress analysis. The stress factor of the monolith cross section is defined in an attempt to describe and compare the overall state of the tensile stress in the dam subjected to different earthquake ground motions using a single-valued parameter. The applicability of the introduced parameter in seismic response analysis of the gravity dams is tested by studying its variation with the intensity of the input ground motion. The stress factor showed acceptable correlations with the intensity of the selected ground motion records under different load combinations.

8. The stress factor is shown to be a valid parameter in evaluating the overstressed part of the dam cross section. The portion of the monolith cross section with excessive tensile stress grows with the increase of the stress factor. Based on this observation, the stress factor can be used as a complementary design tool for optimum design of the dam cross section.

6.3 RECOMMENDATIONS

A list of suggestions for further studies is presented below. These suggested subjects have been developed along the course of the present research work. The major recommendations include:

1. The proposed model for the sedimented reservoir bottom should be extended to include a two-dimensional behaviour of the layered foundation. However, it should be attempted to develop a model which preserves its practical applicability for design purposes without excessive number of design parameters. The two-dimensional model will include the effect of variations of the thickness of the sediment layer in the streamwise direction which has practical applications in sloped-bottom reservoirs.

2. There is little available experimental evidence on the mechanical characteristics of the sedimentation in the reservoirs of existing dams. A realistic evaluation of the reflectivity of the reservoir bottom boundary requires experimental measurements of the input parameters of the proposed mathematical model. In situ measurements provide more reliable information about the sedimented material than the laboratory tests on disturbed samples of the material.

3. The isolation layer in the present study was assumed to uniformly cover the entire upstream face of the dam monolith. There is a possibility of reducing the cost of the isolation scheme by providing the isolation layer at separate parts along the height of the dam where it can be most effective. The optimum design of the isolation scheme should be conducted based on the analysis of a proper mathematical model.

4. The three dimensional effect of the reservoir on the hydrodynamic force on the dam is expected to be significant when the reservoir banks taper towards the upstream end. The reflection of pressure waves towards the impounding dam may result in significantly higher stresses in the dam as compared to the two dimensional assumption of the fluid domain. The seismic response reduction of the hydrodynamic isolation scheme for such reservoir geometry needs to be evaluated.

5. The use of rubber materials is determined as one practical solution for the isolation scheme in this study. Laboratory tests are needed to determine their favourable material design so as to develop the required mechanical properties for an effective isolation. Their mechanical response in dynamic isolation tests needs to be evaluated.

6. The earthquake response of the isolated dam was computed with the assumption that the reservoir water is compressible. The effect of water compressibility may be negligible for the case where the impounded water subjected to ground motion is in contact with the soft isolation layer. The effect of water compressibility on the seismic response of the isolated dam needs to be investigated.

7. There is no proper boundary condition available for the frequency domain analysis of a dam-reservoir model with truncated boundary at the reservoir upstream far-end subjected to vertical ground acceleration. An appropriate boundary condition needs to be developed for reducing the size of the truncated reservoir finite element model under vertical input ground motion. A possible solution is to study the response of

the hydrodynamic pressure under vertical excitation at the truncated boundary using the results of the finite element analysis.

8. The response of the hydrodynamic pressure and the seismic response of the dam impounding a finite-length reservoir are evaluated based on the assumption of a stationary far-end solid reservoir boundary. The vibration of the upstream boundary alters the hydrodynamic pressure in the reservoir. The effect of the moving upstream boundary on the response of the dam needs to be evaluated including the effects of phase difference between the vibrations of the reservoir side boundaries, incoherence of the excitations, the travelling direction of the seismic excitation and the effects of site conditions.

9. The reservoirs of many concrete dams do not have a perfect rectangular shape. Consequently, the complexity of the reservoir shape should also be included in the analysis of a specific dam-reservoir system. A survey of the reservoir shapes of currently existing dams can be made and a set of typical geometrical groups can be defined. The results of the present study can be examined by including different geometrical shapes of the reservoirs in the analysis.

10. The stress factor of the dam proved to be a reliable complementary design parameter in evaluation of the overall stress response of the dam when subjected to ground motion. The validity of the stress factor can be further examined by including various geometrical shapes of the monolith cross section.

REFERENCES

Ahmadi, M.T., Khoshrang, Gh., Mokhtarzadeh, A. and Jalalzadeh, A., "Behaviour of a large concrete dam due to an actual maximum credible earthquake", *Proc. Tenth World Conf. Earthq. Eng.*, Madrid, vol.7, 1992, pp. 3995-4000.

Antes, H. and Von Estorff, O., "Analysis of absorption effects on the dynamic response of dam reservoir systems by BEM", *Earthq. Eng. Struct. Dyn.*, vol. 15, 1987, pp. 1023-1036.

Arias, A., "A measure of earthquake intensity", *Seismic Design of Nuclear Power Plants*, MIT Press, Cambridge, 1970, pp. 438-483.

As'kov, V.L., Kalitseva, I.S., Komarov, A.I. and Sheinin, I.S., "Physical modelling of phenomena of the interaction of hydraulic structures with water in the presence of an air curtain", *Hydrotechnical Construction*, vol. 26, no. 10, 1992, pp. 636-646.

Aviles, J. and Sanchez-Sesma, F.J., "Water pressures on rigid gravity dams with finite reservoir during earthquakes", *Earthq. Eng. Struct. Dyn.*, vol. 18, 1989, pp. 527-537.

Bakhmeteff, B.A., Discussion on "Water pressures on dams during earthquakes", *Trans. ASCE*, vol. 98, 1933, pp.460-468.

Baumber, T., "Reservoir length effects on the seismic response of concrete gravity dams", *Ph.D. Dissertation*, McMaster University, Hamilton, Ont., 1993.

Baumber, T. and Ghobarah, A., "Response of concrete gravity dam with finite reservoir to earthquake ground motion", *Proc. Seventh Can. Conf. Earthq. Eng.*, Montreal 1995, pp. 349-356.

Bettess, P., "Infinite elements", *Int. J. Num. Meth. Eng.*, vol. 11, 1977, pp. 53-64.

Bougacha, S. and Tassoulas, J.L., "Seismic analysis of gravity dams. I: Modelling of sediments", *Proc. ASCE, J. Eng. Mech.*, vol. 117, no. 8, 1991a, pp. 1826-1837.

Bougacha, S. and Tassoulas, J.L., "Seismic response of gravity dams. II: effects of sediments", *Proc. ASCE, J. Eng. Mech.*, vol. 117, no. 8, 1991b, pp. 1839-1850.

Bowles, J.E., *Foundation Analysis and Design*, McGraw-Hill, Singapore, 1984.

Brekhovskikh, L. M. and Maksimovich, L., *Fundamentals of Ocean Acoustics*, Springer Verlag , 2nd ed., Series on Wave Propagation, New York, vol. 8, 1991.

Bustamante, J.I. and Flores, A., "Water pressure on dams subjected to earthquakes", *Proc. ASCE, J. Eng. Mech. Div.*, vol. 92, no. EM5, 1966, pp. 115-127.

Cambridge Material Selection Software - CMS 2.04, 1994.

Celep, Z. and Bazant, P., "Spurious reflection of elastic waves due to gradually changing finite element size", *Int. J. Num. Meth. Eng.*, vol. 19, 1983, pp. 631-646.

Chakrabarti, P. and Chopra, A.K., "Hydrodynamic pressures and response of gravity dams to vertical earthquake component", *Earthq. Eng. Struct. Dyn.*, vol.1, 1973, pp. 325-335.

Chandrashaker, R. and Humar, J.L., "Fluid-foundation interaction in the seismic response of gravity dams," *Earthq. Eng. Struct. Dyn.*, vol. 22, 1993, pp. 1067-1084.

Cheng, A.H.-D., "Effect of sediment on earthquake-induced reservoir hydrodynamic response", *Proc. ASCE, J. Eng. Mech.*, vol. 112, no. 7, 1987, pp. 654-665.

Chopra, A.K., "Hydrodynamic pressures on dams during earthquakes", *Proc. ASCE, J. Eng. Mech. Div.*, vol. 93, no. EM6, 1967, pp. 205-223.

Chopra, A.K., "Earthquake response of concrete gravity dams", *Proc. ASCE, J. Eng. Mech. Div.*, vol. 96, no. EM4, 1970, pp. 443-454.

Chopra, A.K. and Chakrabarti, P., "The Earthquake Experience at Koyna Dam and Stresses in Concrete Gravity Dams", *Earthq. Eng. and Struct. Dyn.*, vol.1, 1972, pp. 151-164.

Chopra, A. K. and Chakrabarti, P., "Earthquake analysis of concrete gravity dams including dam-water-foundation rock interaction", *Earthq. Eng. Struct. Dyn.*, vol. 9, 1981, pp. 363-383.

Chopra, A.K., Wilson, E.L. and Farhoomand, I., "Earthquake analysis of reservoir-dam systems", *Proc. Fourth World Conf. Earthq. Eng.*, Santiago, vol. 2, B4, 1969, pp. 1-10.

Clayton, R. and Engquist, B., "Absorbing boundary conditions for acoustic and elastic wave equations", *Bull. Seism. Soc. Am.*, v. 67, no. 6, 1977, pp. 1529-1540.

Eatock Taylor, R., "A review of hydrodynamic load analysis for submerged structures excited by earthquakes", *Eng. Struct.*, vol.3, 1981, pp. 131-139.

Engquist, B. and Majda, A., "Absorbing boundary conditions for the numerical simulation of waves", *Mathematical Computation*, vol. 31, no. 139, 1977, pp.629-651.

Fenves, G.L. and Chopra, A.K., "Effects of reservoir bottom absorption on earthquake response of concrete gravity dams", *Earthq. Eng. Struct. Dyn.*, vol. 11, 1983, pp. 809-829.

Fenves, G.L. and Chopra, A.K., "Earthquake analysis and response of concrete gravity dams", *Report No. UCB/EERC-84/10*, University of California, Berkeley, 1984a.

Fenves, G.L. and Chopra, A.K., "EAGD-84, a computer program for earthquake analysis of concrete gravity dams", *Report No. UCB/EERC-84/11*, University of California, Berkeley, 1984b.

Fenves, G.L. and Chopra, A.K., "Reservoir bottom absorption effects in earthquake response of concrete gravity dams", *Proc. ASCE, J. Struct. Eng.*, vol. 111, no.3, 1985, pp. 545-562.

Galindo, M., Cervera, M. and Oliver, J., "Efficient solution schemes for fluid-structure-soil interaction problems", *Proc. Tenth World Conf. Earthq. Eng.*, Madrid, vol. 8, 1992, pp. 4651-4656.

Gellis, V.K., Kalitseva, I. S., Mel'nikov, E. P. and Sheinin, I. S., "On-Site Studies of an Experimental Air Curtain on the Dam of the Krivoporozhsk Hydroelectric Station", *Hydrotechnical Construction*, vol. 26, no. 10, 1992, pp. 647-652.

Gibson, L. J. and Ashby, M. F., *Cellular Solids* , Pergamon press, New York, 1988.

Hall, J.F., "Study of the earthquake response of Pine Flat dam", *Earthq. Eng. Struct. Dyn.*, vol. 14, 1986, pp. 281-295.

Hall, J.F. and Chopra, A.K., "Dynamic response of embankment, concrete-gravity and arch dams including hydrodynamic interaction, *Rept. UCB/EERC-80/39*, University of California, Berkeley, 1980.

Hall, J.F. and Chopra, A.K., "Two-dimensional dynamic analysis of concrete gravity and embankment dams including hydrodynamic effects", *Earthq. Eng. Struct. Dyn.*, vol. 10, 1982a, pp. 305-332.

Hall, J.F. and Chopra, A.K., "Hydrodynamic effects in the dynamic response of concrete gravity dams", *Earthq. Eng. Struct. Dyn.*, vol. 10, 1982b, pp. 333-345.

Hall, J.F., Dowling, M. J. and El-Aidi, B.,"Defensive earthquake design of concrete gravity dams", *Report No. EERL* 91-02, California Institute of technology, Pasadena, 1991.

Hall, J.F., Dowling, M. J. and El-Aidi, B.,"Defensive earthquake design of concrete gravity dams", *Dam Engineering*, vol. III, No. 4, 1992, pp. 249-264.

Hall, J.F. and El-Aidi, B., "Hydrodynamic isolation of concrete dams", Proceedings of the Seismic Eng. Struct. Congress, San Francisco, 1989, pp. 307-316.

Hamilton, E.L., "Compressional-wave attenuation in marine sediments," *Geophysics*, vol. 37, no. 4, 1972, pp. 620-646.

Hanna, Y.G. and Humar, J.L., "Boundary element analysis of fluid domain", *Proc. ASCE, J. Eng. Mech. Div.*, vol. 108, no. EM2, 1982, pp.436-450.

Hanna, Y.G. and Humar, J.L., Closure to "Boundary Element Analysis of Fluid Domain", *Proc. ASCE, J. Eng. Mech. Div.*, vol. 109, no. EM2, 1983, pp.666-667.

Hanson, M.E. and Petschek, A.G., "A boundary condition for significantly reducing boundary reflections with a Lagrangian mesh", *Journal of Computational Phyics.*, vol. 21, 1976, pp. 333-339.

Hatami, K., "A Model for Reservoir Bottom Absorption Effects in Seismic Response Analysis of Concrete Dams", 1995 Student Paper Competition, *EERI 48th Annual Meeting*, Los Angeles, CA, Feb. 1996.

Hatami, K. and Ghobarah, A., "Reduction of the Seismic Response of Concrete gravity Dams using Hydrodynamic Isolation", *Proc. Seventh Canadian Conf. Earthq. Eng.*, Montreal, 1995, pp. 333-340.

Humar, J., Closure to "Finite element analysis of reservoir vibration", *Proc. ASCE, J. Eng. Mech.*, vol. 110, no. 4, 1984, pp. 664-666.

Humar, J. and Roufaiel, M., "Finite element analysis of reservoir vibration", *Proc. ASCE, J. Eng. Mech.*, vol. 109, no. 1, 1983, pp. 215-230.

Jablonski, A.M., "Effect of location of transmitting boundary on seismic hydrodynamic pressures on gravity dams", *Proc. Fourth U.S. Nat. Conf. Earthq. Eng.*, Palm Springs, Calif., 1990, pp. 95-103.

Jansen, R.B., *Advanced Dam Engineering*, Van Nostrand - Reinhold, New York, 1988.

Kausel, E. and Tassoulas, J.L., "Transmitting boundaries: a closed-form comparison", *Bull. Seism. Soc. Am.*, v. 71, no. 1, 1981, pp. 143-159.

Kollgaard, E.B., *Development of Dam Engineering in the United States*, Pergamon Press, New York, 1988.

Leger, P. and Tinawi, R., "A bibliography on structural analysis behaviour and safety of concrete dams", *Report No. EPM/GCS-1994-17*, Ecole Polytechnique, Montreal, Quebec, 1994.

Lombardo, V.N., Mikhailov, L.P. and Semenov, I.V., "Studies and design of earthquake-resistant concrete dams", *Proc. Int. Symp. Earthq. Dams*, vol. 1, ICOLD, Beijing, China, 1987, pp. 233-241.

Lotfi, V., Roesset, M. and Tassoulas, J.L., "A technique for the analysis of the response of dams to earthquakes," *Earthq Eng. Struct. Dyn.*, vol. 15, 1987, pp. 463-490.

Lysmer, J. and Kuhlemeyer, R.L., "Finite dynamic model for infinite media", *J. Eng. Mech. Div.*, vol. 95, no. EM4, 1969, pp. 859-877.

McCann, M.W. Jr. and Shah, H.C. "Determining strong-motion duration of earthquakes", *Bull. Seism. Soc. Am.*, v. 69, no. 4, 1979, pp. 1253-1265.

Medina, F., Dominguez, J., and Tassoulas, J.L., "Response of dams to earthquakes including effects of sediments," *Proc. ASCE, J. Struct. Eng.*, vol. 116, no.11, 1990, pp. 3108-3121.

Nath, B., "Hydrodynamic pressures on high dams due to vertical earthquake motions", *Proc. Instit. Civ. Eng.*, vol. 46, 1969, pp. 413-421.

Nath, B., "Coupled hydrodynamic response of a gravity dam", *Proc. Instit. Civ. Eng.*, vol. 48, 1971, pp. 245-257.

Naumoski, N., Tso, W.K., & Heidebrecht, A.C., "A selection of representative strong motion earthquake records having different A/V ratios", *Report no. EERG/88-01*, McMaster University, Hamilton, Ont., Canada, 1988.

Newmark, N.M. and Rosenblueth, E., *Fundamentals of Earthquake Engineering*, Prentice-Hall, 1971.

Novikova, E.I. and Trifunac, M.D., "Duration of strong ground motion in terms of earthquake magnitude, epicentral distance, site conditions and site geometry", *Earthq. Eng. Struct. Dyn.*, vol. 23, 1994, pp. 1023-1043.

Pekau, O.A. and Batta, V., "Seismic crack propagation in concrete gravity dams", *Proc. Sixth Canadian Conf. Earthq. Eng.*, Toronto, 1991, pp. 197-204.

Pekau, O.A., Lingmin, F. and Chuhan, Z., "Seismic fracture of Koyna dam: Case study", *Earthq. Eng. Struct. Dyn.*, vol. 24, 1995, pp. 15-33.

Raphael, J.M., "Tensile strength of concrete", *ACI Journal*, March-April 1984, pp. 158-165.

Saini, S.S., "Coupled hydrodynamic response of a gravity dam using finite and infinite elements", *Proc. Seventh Symp. Earthq. Eng.*, Roorkee, India, 1982, pp. 45-50.

Saini, S.S., Bettess, P. and Zienkiewicz, O.C., "Coupled hydrodynamic response of concrete gravity dams using finite and infinite elements", *Earthq. Eng. Struct. Dyn.*, vol. 6, 1978, pp. 363-374.

Savinov, O.A., Sheinin, I.S., Kalitseva, I.S. and Sheinina, S.I., "Mathematical modelling and theoretical studies of problems of seismic stability of hydraulic structures with an air curtain", *Hydrotechnical Construction*, vol. 26, no. 10, 1992, pp. 631-635.

Sharan, S.K., Discussion of "Finite element analysis of reservoir vibration", *Proc. ASCE, J. Eng. Mech.*, vol. 110, no. 4, 1984, pp. 663-664.

Sharan, S.K., "Finite element analysis of unbounded and incompressible fluid domains", *Int. J. Num. Meth. Eng.*, vol. 21, 1985a, pp. 1659-1669.

Sharan, S.K., "Finite element modelling of infinite reservoirs", *Proc. ASCE, J. Eng. Mech.*, vol. 111, no. 12, 1985b, pp. 663-664.

Sharan, S.K., "Modelling of radiation damping in fluids by finite elements", *Int. J. Num. Meth. Eng.*, vol. 23, 1986, pp. 945-957.

Sharan, S.K., "A non-reflecting boundary in fluid-structure interaction", *Computers and Structures*, vol. 26, no.5, 1987a, pp. 841-846.

Sharan, S.K., "Time-domain analysis of infinite fluid vibration", *Int. J. Num. Meth. Eng.*, vol. 24, 1987b, pp. 945-958.

Sharan, S.K., "Dam-reservoir interaction during earthquake", *Proc. Sixth Canadian Conf. Earthq. Eng.*, Toronto, 1991, pp. 181-188.

Sharan, S.K., "Efficient finite element analysis of hydrodynamic pressure on dams", *Computers and Structures*, vol. 42, no.5, 1992, pp. 713-723.

Sheinin, I.S., "An air curtain for protecting hydraulic structures from seismic and blast effects", *Hydrotechnical Construction*, vol. 26, no. 10, 1992, pp. 609-615.

Shumway, G., "Sound speed and absorption studies of marine sediments by a resonant method-part II", *Geophysics*, Vol. XXV, no. 3, 1960, pp. 659-682.

Smith, W.D., "A non-reflecting plane boundary for wave propagation problems", *Journal of Computational Physics*, vol. 15, 1974, pp. 492-503.

Stuardi, J. E. and Prato, C. A. "The influence of valley shape on seismic response: Piedra del Aguila dam", *Dam Engineering*, Vol. I, No. 3, 1990, pp. 177-199.

Tsai, C.S. and Lee, G.C., "Hydrodynamic pressure on gravity dams subjected to ground motions", *Proc. ASCE, J. Eng. Mech. Div.*, vol. 115, no. 3, 1989, pp. 598-617.

Tsai, C.S. and Lee, G.C., "Semi-analytical solution for hydrodynamic pressures on dams with arbitrary upstream face considering water compressibility", *Computers and Structures*, vol. 42, no. 4, 1992, pp. 497-502.

Tsai, C.S., Lee, G.C. and Ketter, R.L., "Solution of the dam-reservoir interaction problem using a combination of FEM, BEM with particular integrals, modal analysis, and substructuring", *Engineering Analysis with Boundary Elements*, vol. 9, 1992, pp.219-232.

Valliappan, S., Zhao, C. and Wang, Y.C., "Numerical simulation of water-gravity dam-foundation system under earthquake loading", *Proc. Int. Conf. Comp. Meth. Adv. Geomech.*, vol. 2, 1991, pp. 897-892.

Westergaard, H. M., "Water pressures on dams during earthquakes", *Trans. ASCE*, vol. 98, 1933, pp. 418-433.

White, W., Valliappan, S. and Lee, I.K., "Unified boundary for finite dynamic models", *Proc. ASCE, J. Eng. Mech. Div.*, vol. 103, no. EM5, 1977, pp. 949-964.

Wylie, E.B., "Seismic response of reservoir-dam systems", *Proc. ASCE, J. Hydr. Div.*, vol. 101, no. HY3, 1975, pp. 403-419.

Zienkiewicz, O.C. and Bettes, P., "Fluid-Structure dynamic interaction and wave forces. An introduction to numerical treatment", *Int. J. Num. Meth. Eng.*, vol. 13, 1978, pp. 1-16.

Zienkiewicz, O.C., Kelly, D.W. and Bettes, P., "The Sommerfeld (radiation) condition on infinite domains and its modelling in numerical procedures", *Comp. Meth. Appl. Sci. Eng.*, vol. I, 1977, pp. 169-203.

Zienkiewicz, O.C. and Newton, R.E., "Coupled vibrations of a structure submerged in a compressible fluid", *Proc. Symp. Fin. Elem. Tech.*, Stuttgart, Germany, 1969, pp. 359-380.

Zuoxin, F., "Reservoir bottom condition and hydrodynamic pressure on dams", *Proc. Int. Symp. Earthq. Dams*, vol.1, ICOLD, Beijing, China, 1987, pp. 80-89.

APPENDIX I

RECORDS OF HORIZONTAL GROUND MOTION

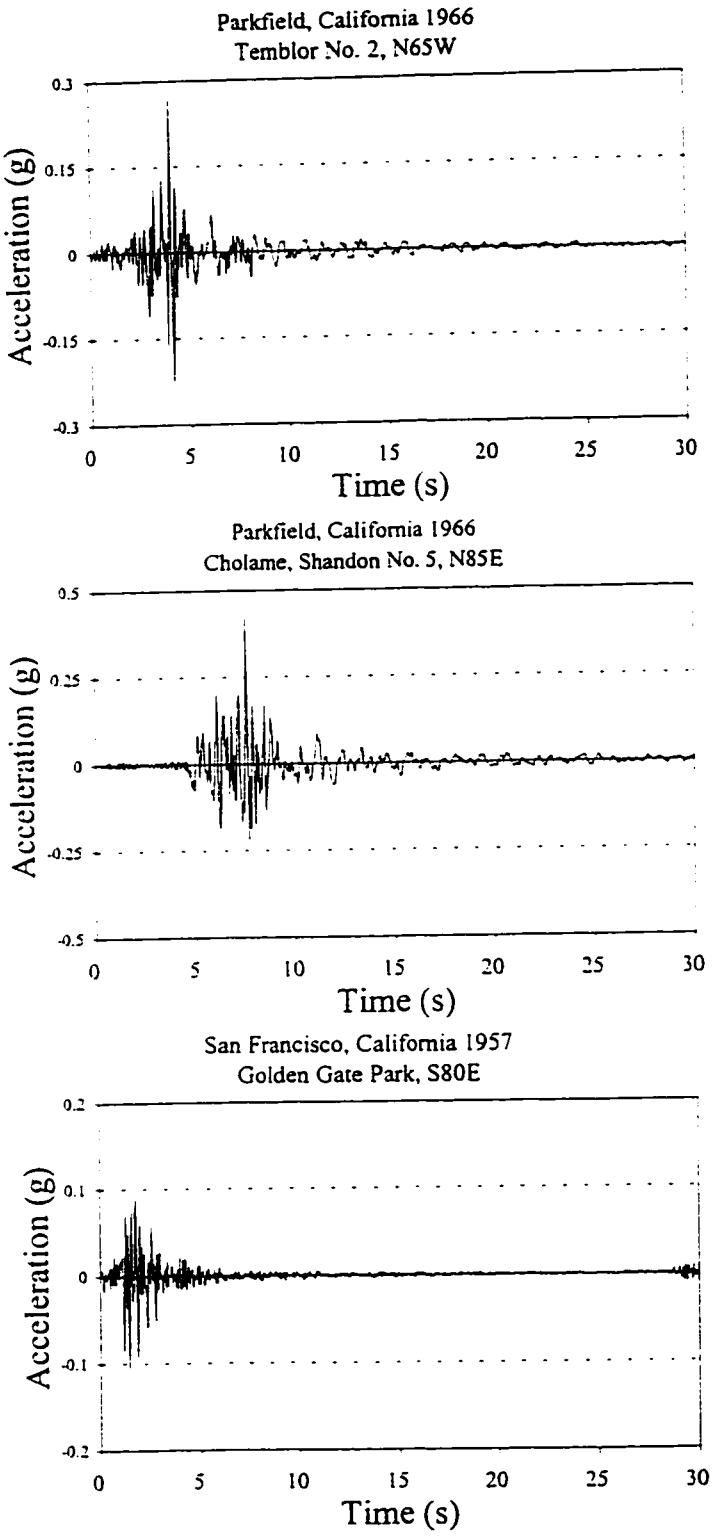

Records of horizontal components with high PGA/PGV ratio (Naumoski et al. 1988)

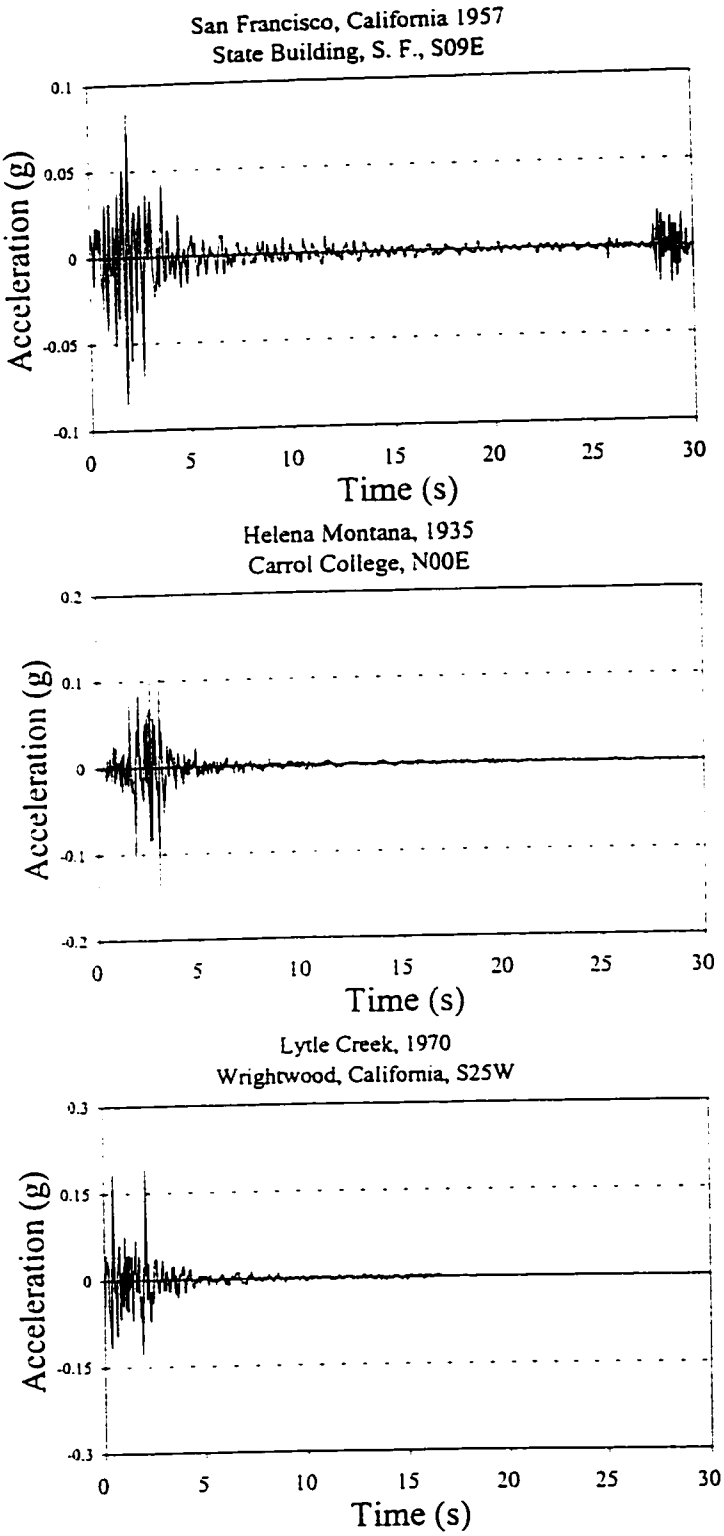

Records of horizontal components with high PGA/PGV ratio (Contd.)

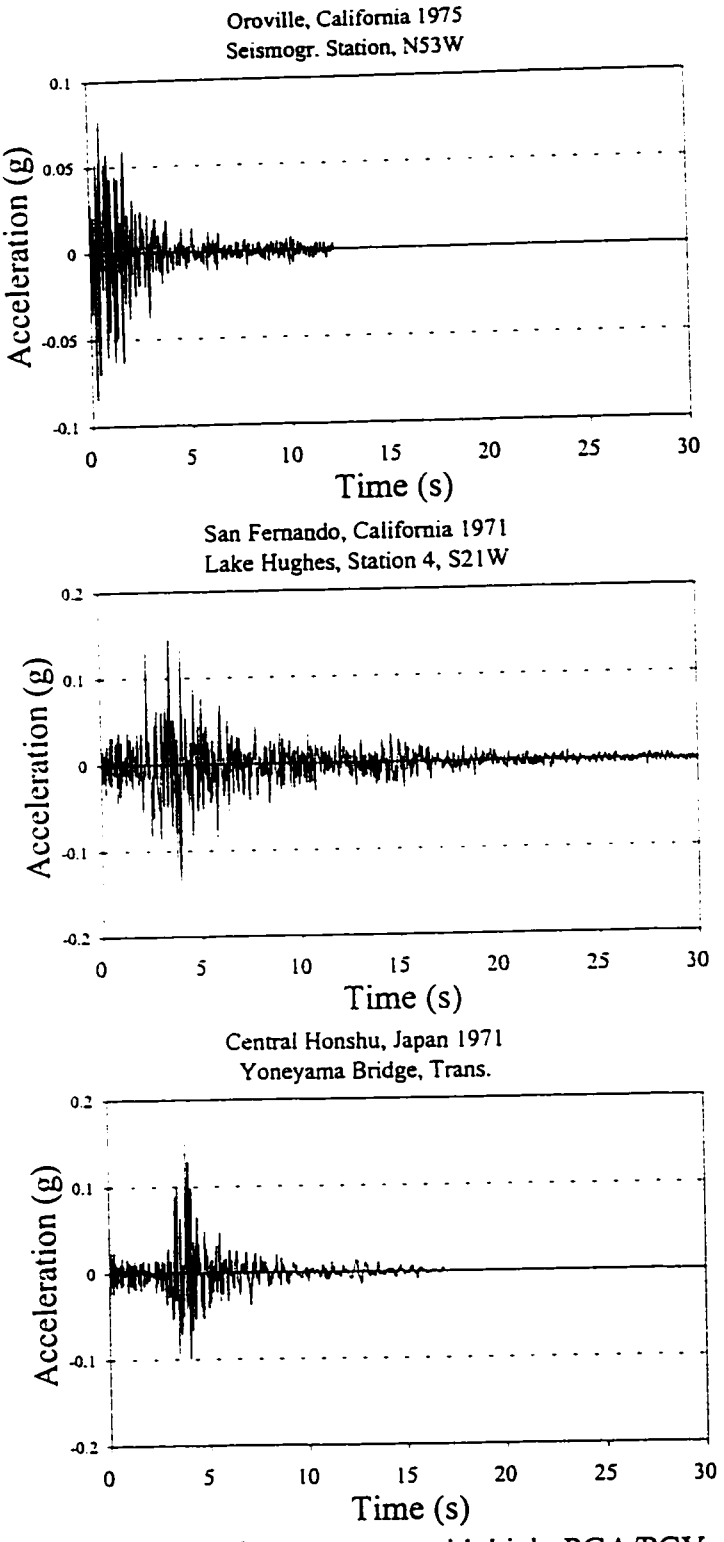

Records of horizontal components with high PGA/PGV ratio (Contd.)

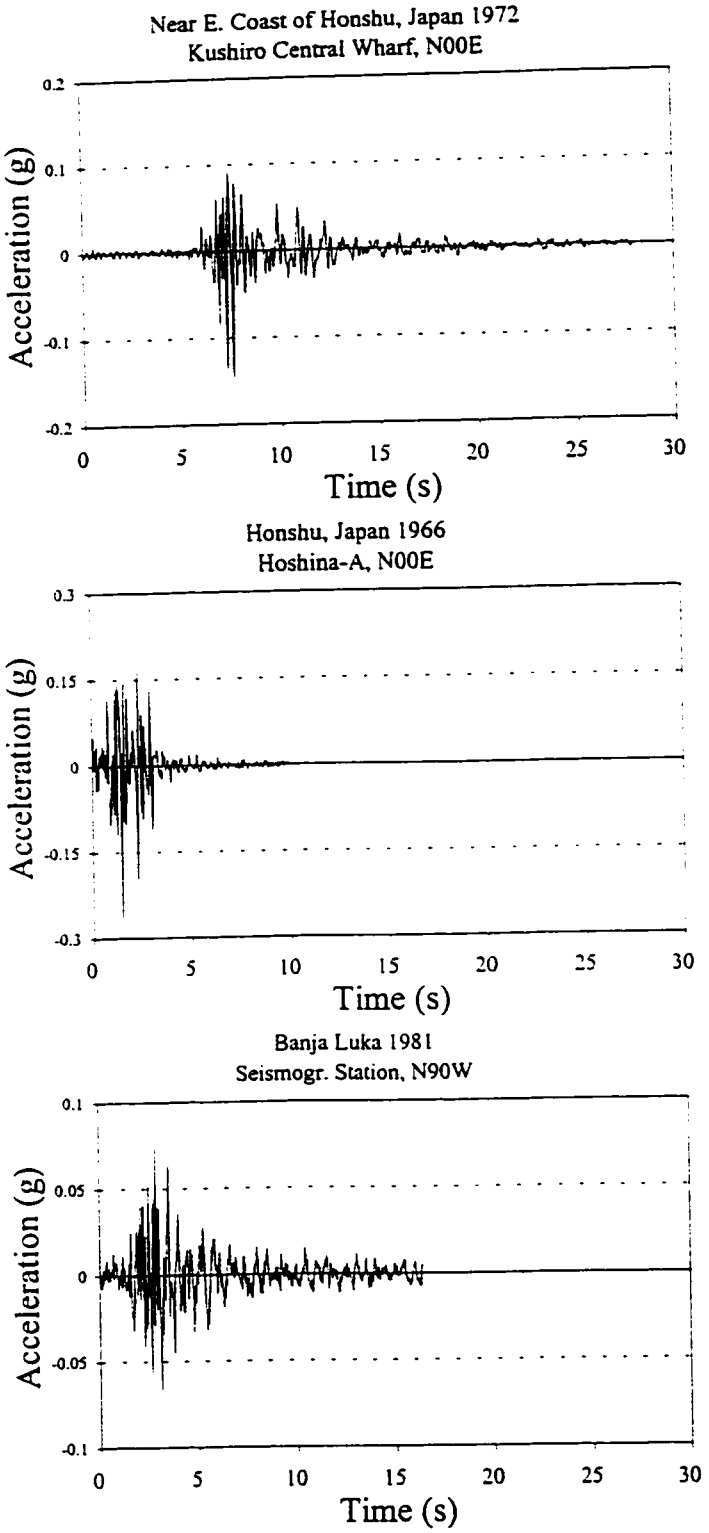

Records of horizontal components with high PGA/PGV ratio (Contd.)

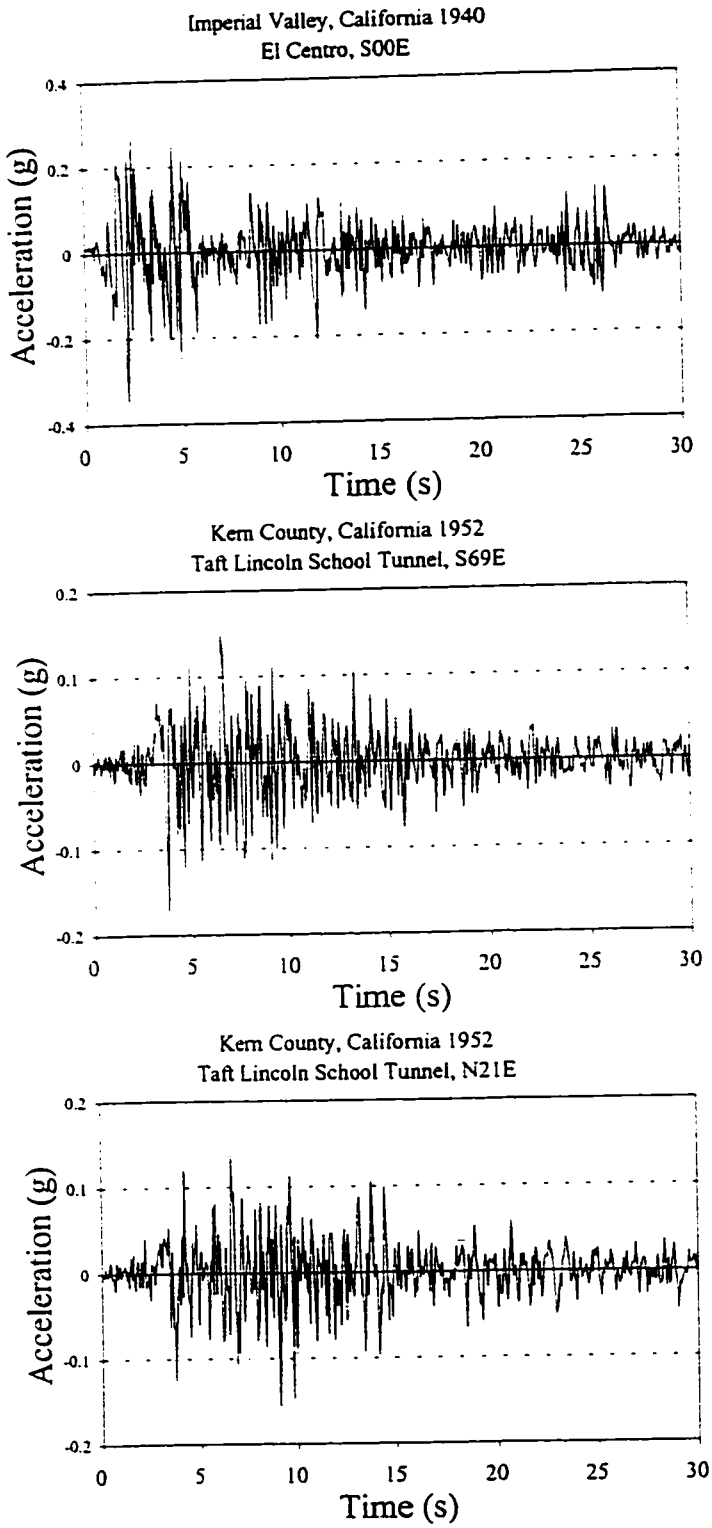

Records of horizontal components with intermediate PGA/PGV ratio (Naumoski et al. 1988)

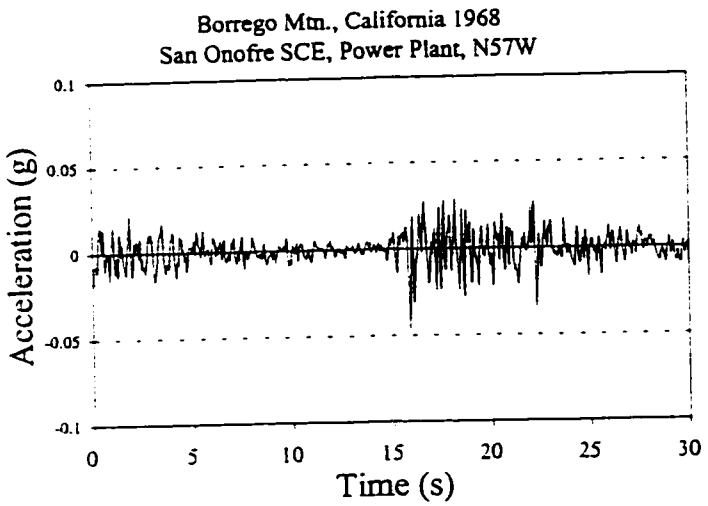

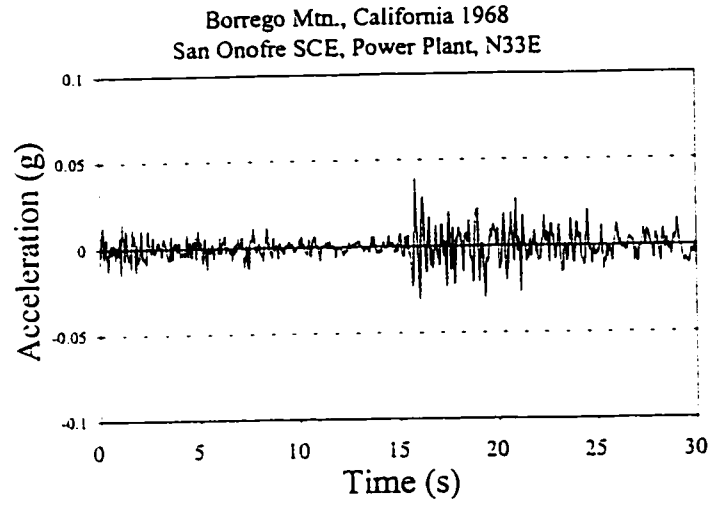

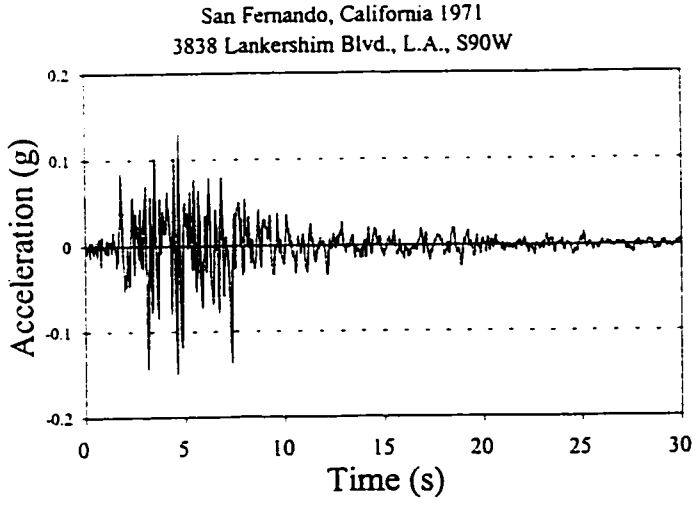

Records of horizontal components with intermediate PGA/PGV ratio (Contd.)

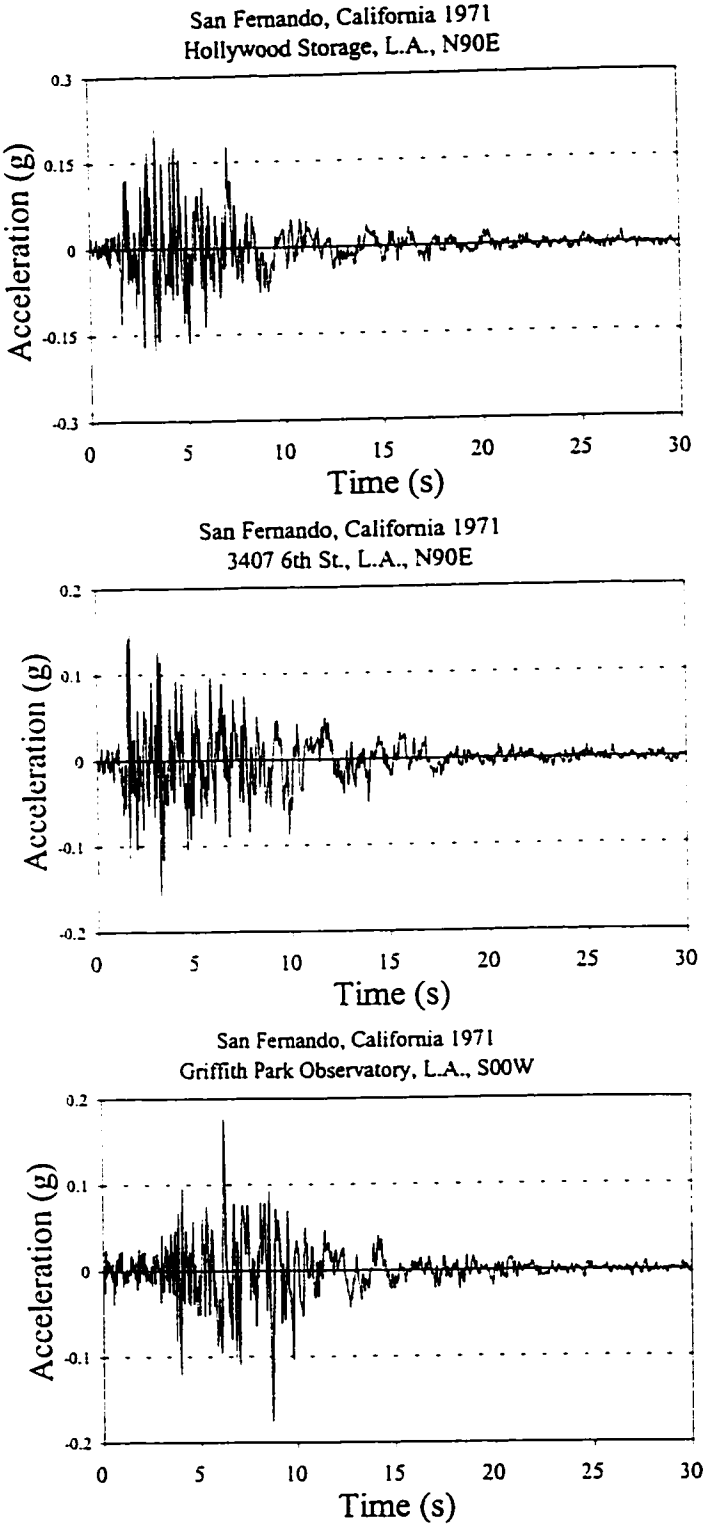

Records of horizontal components with intermediate PGA/PGV ratio (Contd.)

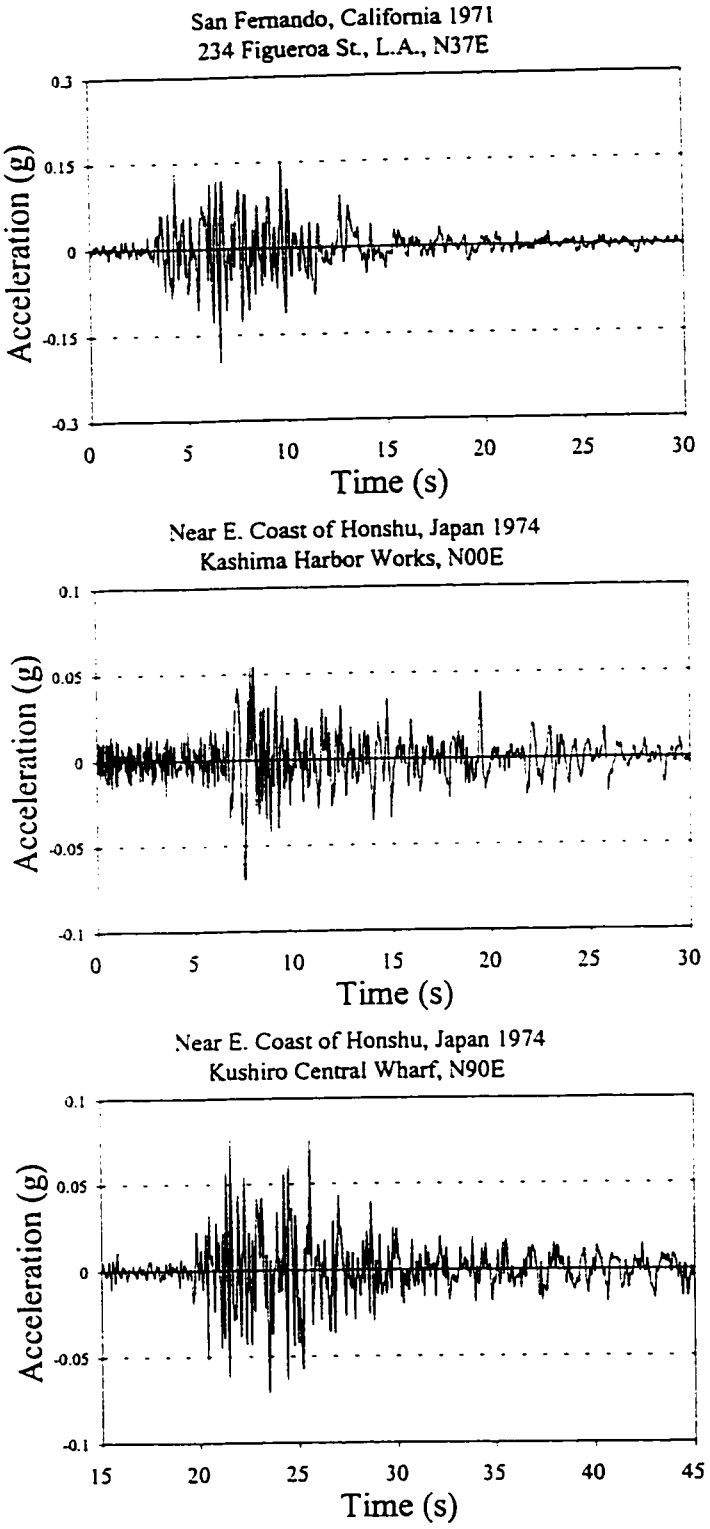

Records of horizontal components with intermediate PGA/PGV ratio (Contd.)

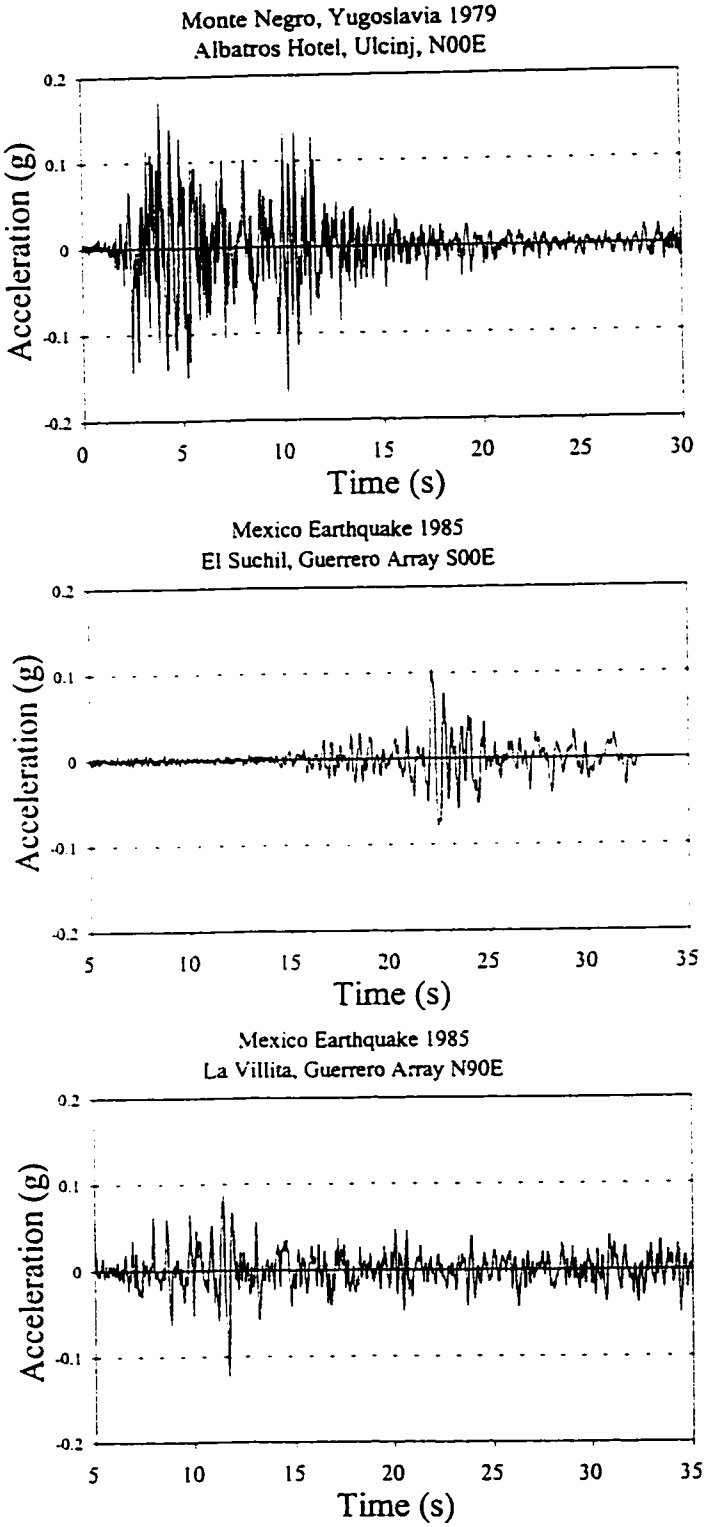

Records of horizontal components with intermediate PGA/PGV ratio (Contd.)

APPENDIX II

RECORDS OF VERTICAL GROUND MOTION

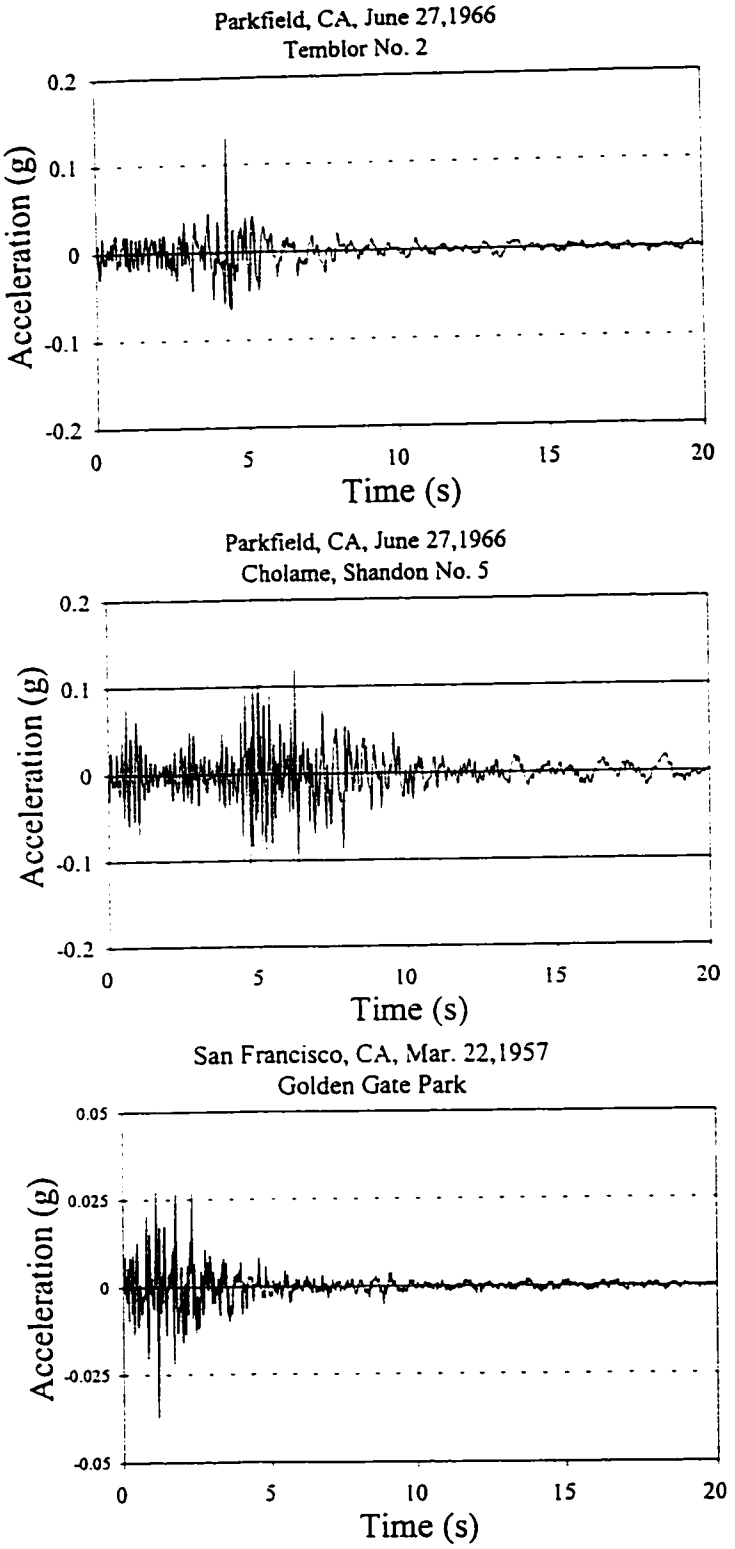

Records of vertical components corresponding to high PGA/PGV ratio horizontal components (Naumoski et al. 1988)

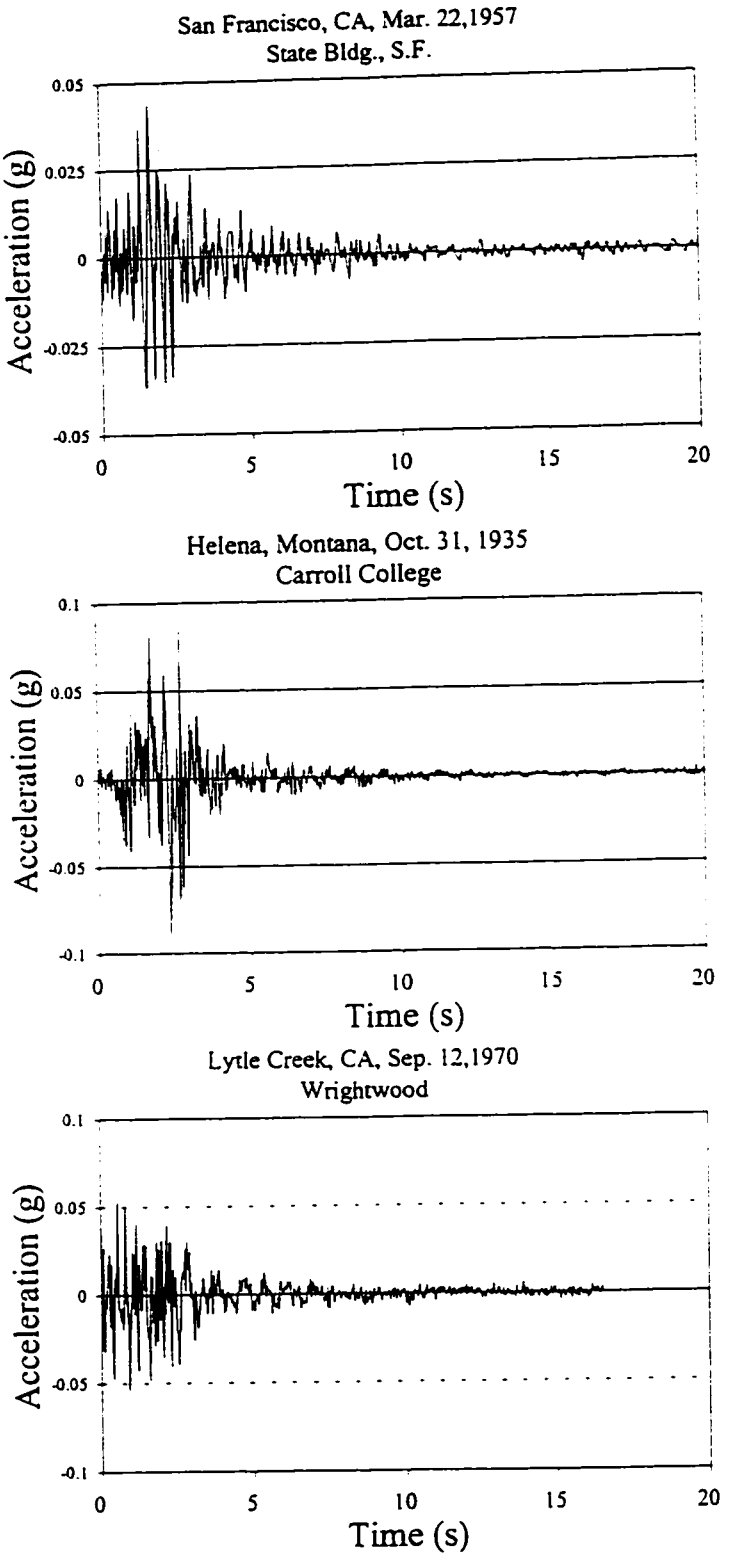

Records of vertical components corresponding to high PGA/PGV ratio horizontal components (Contd.)

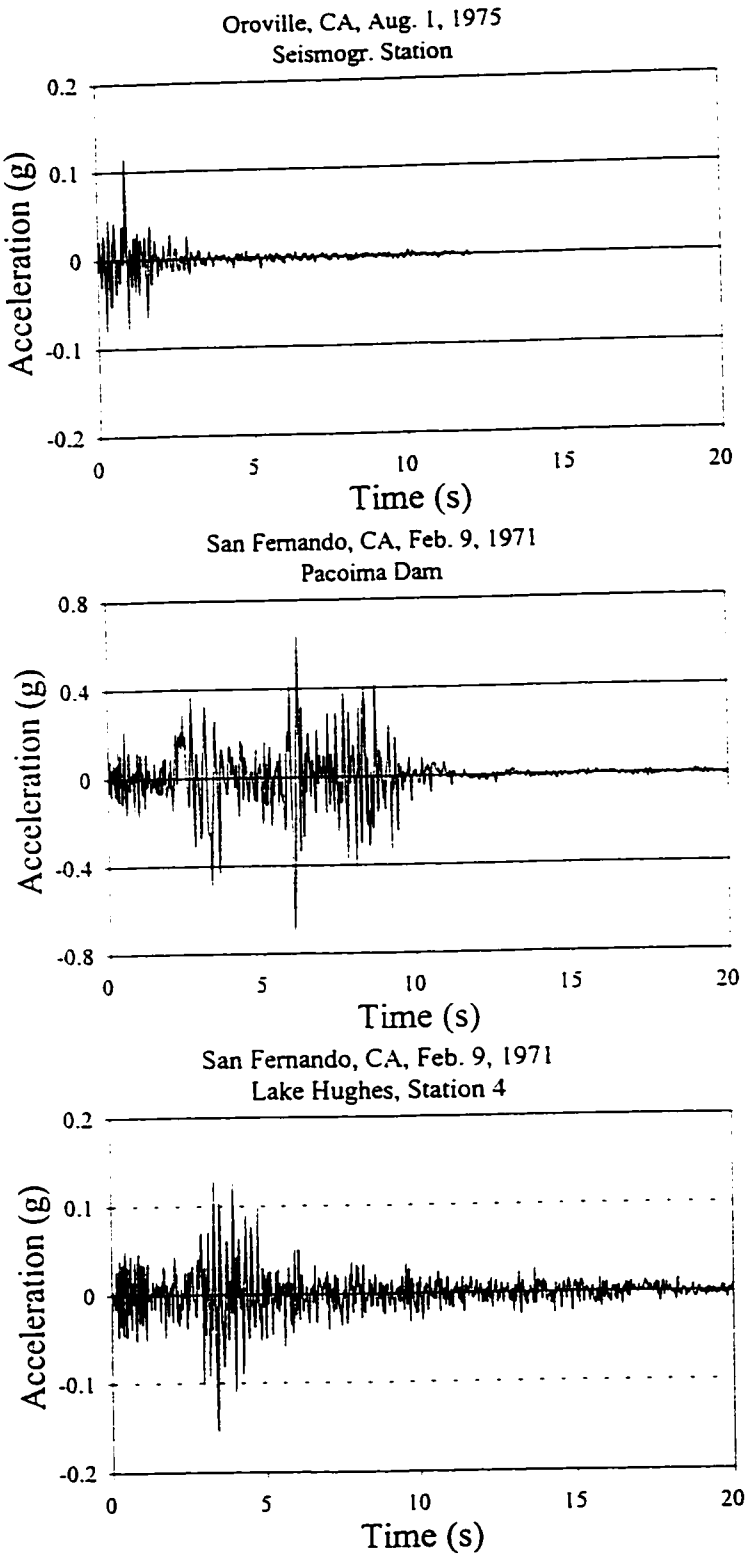

Records of vertical components corresponding to high PGA/PGV ratio horizontal components (Contd.)

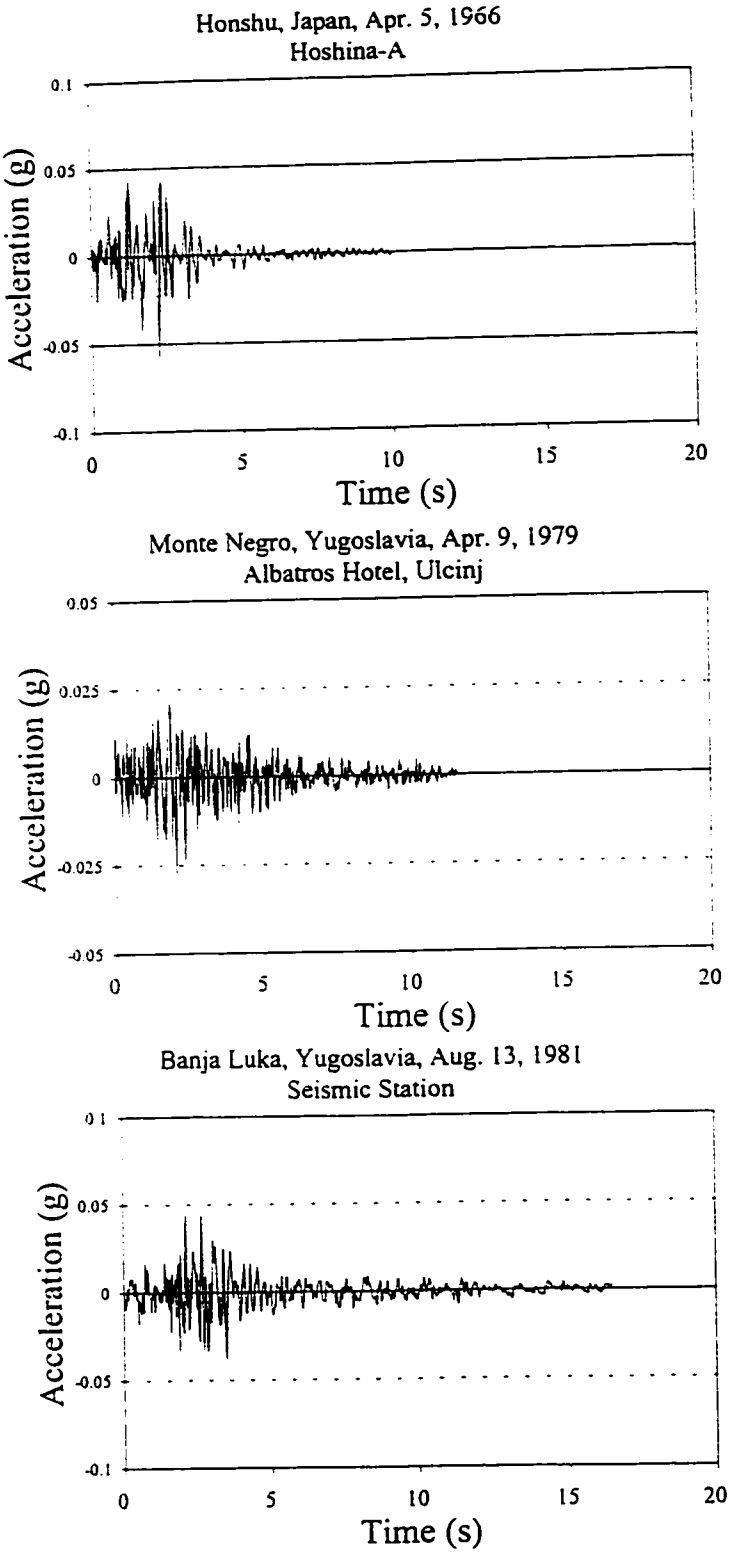

Records of vertical components corresponding to high PGA/PGV ratio horizontal components (Contd.)

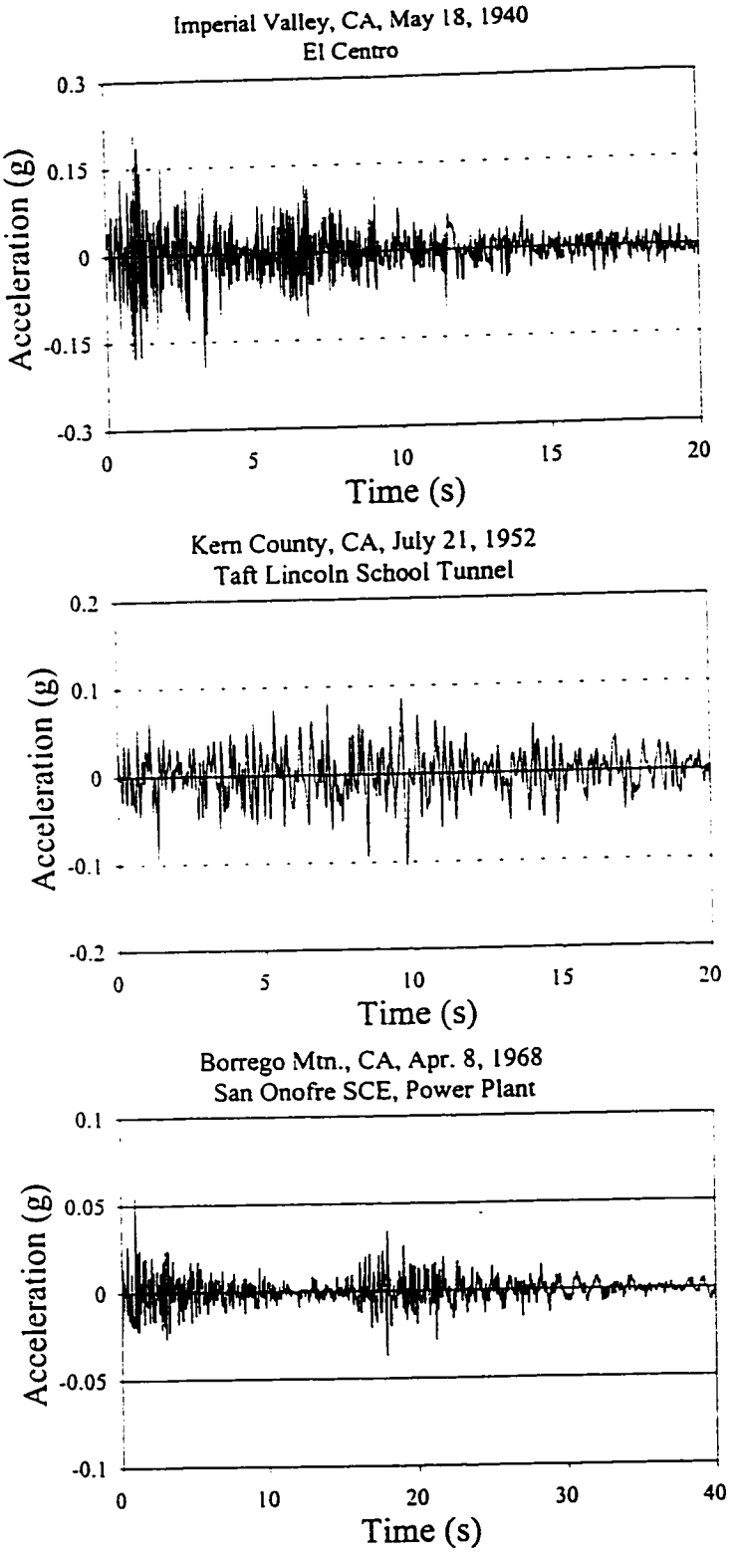

Records of vertical components corresponding to intermediate PGA/PGV ratio horizontal components (Naumoski et al. 1988)

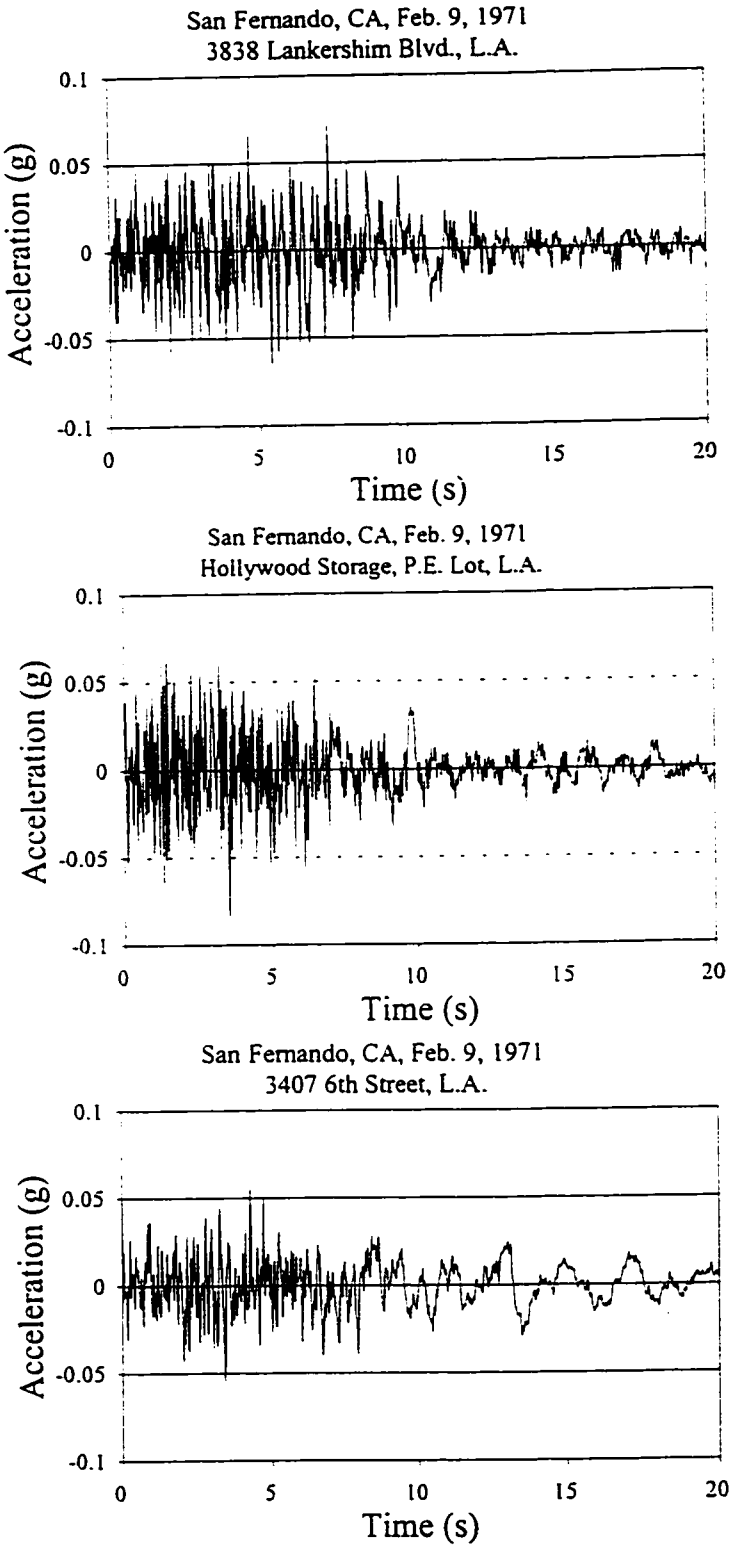

Records of vertical components corresponding to intermediate PGA/PGV ratio horizontal components (Contd.)

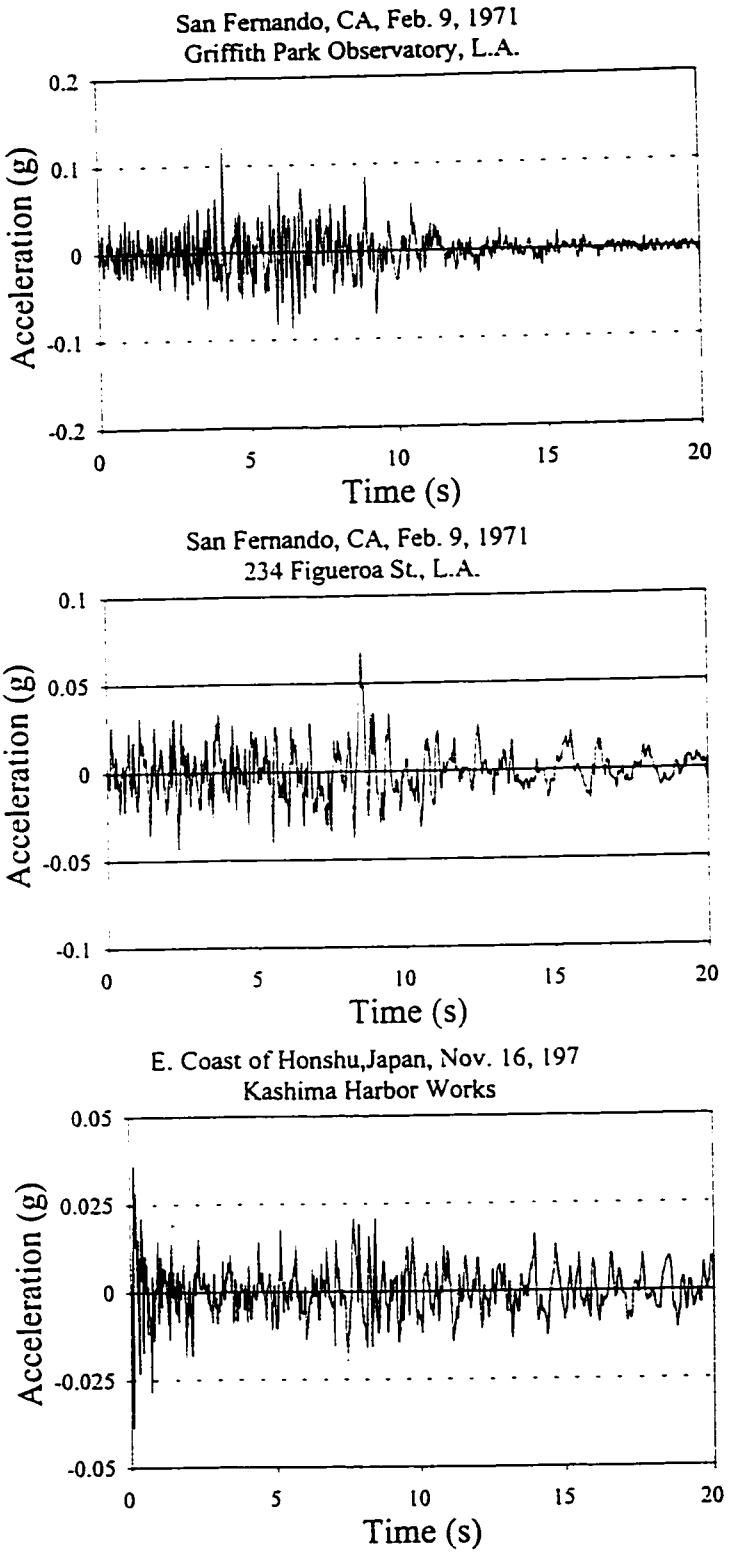

Records of vertical components corresponding to intermediate PGA/PGV ratio horizontal components (Contd.)

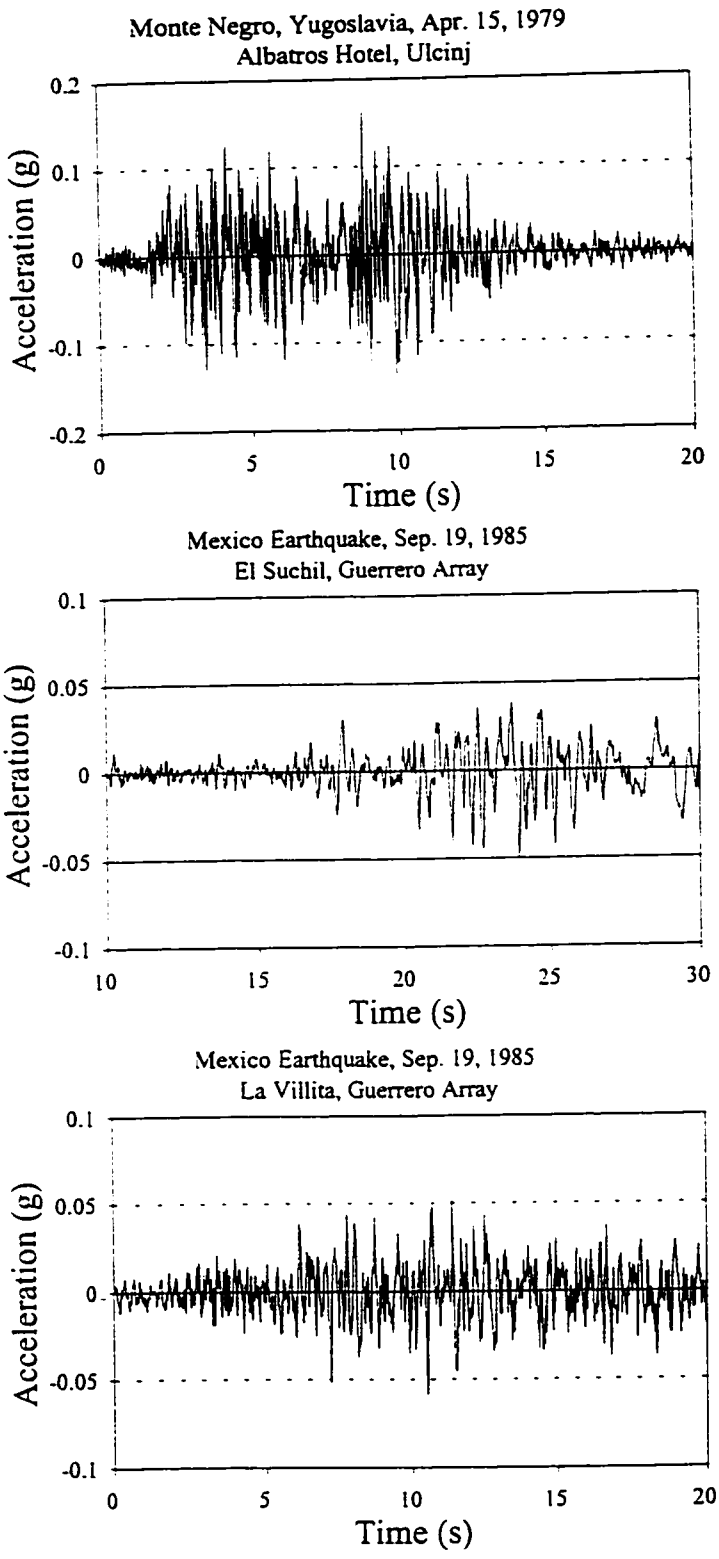

Records of vertical components corresponding to intermediate PGA/PGV ratio horizontal components (Contd.)

IMAGE EVALUATION
TEST TARGET (QA-3)

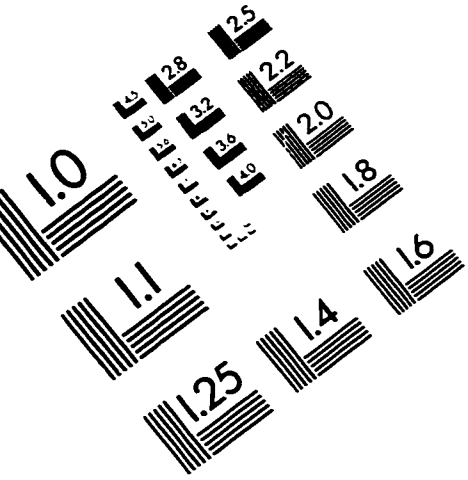

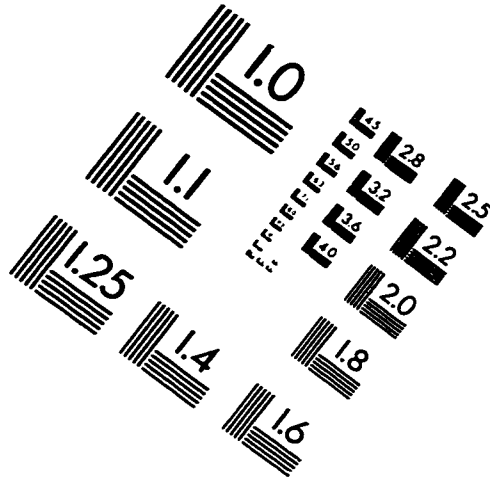

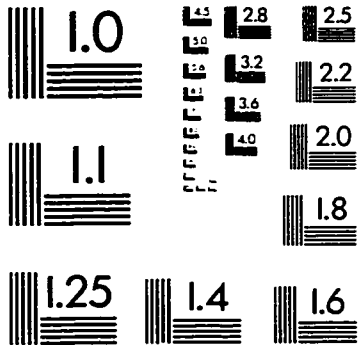

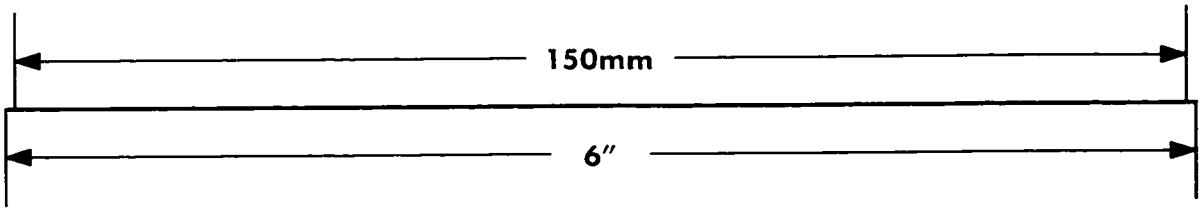

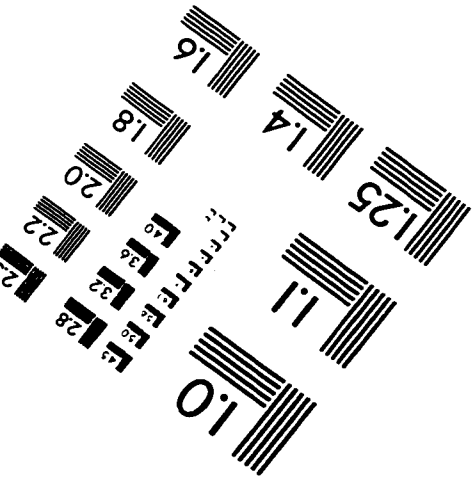

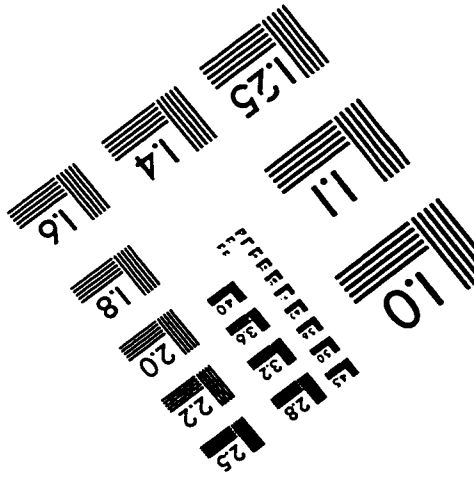

APPLIED IMAGE . Inc
1653 East Main Street
Rochester, NY 14609 USA
Phone: 716/482-0300
Fax: 716/288-5989